# Modelling the Optical Response of Multilayered Gratings Containing Liquid Crystals

*submitted by*

## Jonathan Blair Harris

*to the University of Exeter*
*as a thesis for the degree of*
*Doctor of Philosophy*
*in the Faculty of Science*

*June 1996*

*I certify that all material in this thesis which is not my own work has been identified and that no material is included for which a degree has previously been conferred upon me*

# Abstract

The primary aim of this thesis was to develop a theoretical model to describe the optical response of multilayer surface - relief gratings containing anisotropic layers, such systems being typical of real experimental cells. In the end time was available to look at doubly - periodic grating surfaces or bi - gratings, although not in the context of anisotropic materials.

The optical response of multilayer surface - relief gratings containing anisotropic layers has, up to now been the domain of the experimentalist, with no suitable theoretical model available to investigate such systems. The introduction of such a model would clearly benefit this relatively unexplored area of diffractive optics. To this end I have developed the method of Chandezon *et al.* [1982], who managed to develop a numerically robust formalism while retaining fast computation times. This particular method was chosen because first: when coupled with a scattering matrix it enables modelling of deep gratings with any number of arbitrarily thick overlayers; and second because it is conceptually simple and relatively easy to implement as a computer code.

Chandezon's method is based on a co - ordinate transformation which maps a grating surface onto a plane. The resulting Maxwell equations are more complicated than their Cartesian counterparts, but the boundary conditions across the interface are much simplified.

The chapters of this thesis introduce the formalism as applied to the most simple systems, and then progressively generalise it's application to more and more complex grating geometries, including those made with anisotropic materials. In my penultimate chapter I generalise Chandezon's method to model doubly - periodic surfaces. The final chapter summarises the work completed and outlines some further developments.

Along the way I have attempted to established the validity of the formalism via a series of tests and comparisons with experimental data. In particular the multilayer, anisotropic model is used to model a number of grating - coupled liquid crystal cells, characterising one of these in detail by fitting to experimental angle dependent reflectivity data.

## Acknowledgements

My thanks go out to the following people ...

Principally to my supervisor Dr. Trevor Preist for encompassing the combined knowledge of humanity within his head, and passing on selected bits of it to me upon request. Equally to Professor Roy Sambles for his boundless enthusiasm and uncanny intuition

To the members of the Thin Film Photonics Group: Nick Cotter for his preliminary work in this field; Emma Wood for providing experimental data and much useful advice; Scot Martin for forgetting my insults (eventually); Chris Lawrence for reminding him again; Rob Crook for endless amusement; Dave Nash likewise; Rich Watts for his sickening cheerfulness and valuable experimental contributions to this thesis; Richard Amos for stoicism in the face of endless LB; Ben Hodder for not being ashamed of his car; Matt McSweeny and Robin Stevens without whom the group will never be quite the same; also to Steve Kitson, Mike Jory, Alan Brady, Piers Andrew, Mike Linehan, Dominic Mikulin, Fuzi Yang, Lizhen Ruan, Pete Cann, and Nick Wanstal who continues the pursuit of all things groovy.

Finally to EPSRC and DRA Malvern for funding my research.

# Contents

## 1. A review of grating theory 14

## 2. The differential method of Chandezon 39

# List of figures and tables

# 1. A review of grating theory

## *1.1 An introduction to diffraction gratings*

### *1.1.1 Some basic concepts*

On the broadest level what follows is an investigation into the deviation of light by matter. Here 'deviation' encompasses the classical concepts of refraction and diffraction.

Refraction is most commonly illustrated by the change of velocity and direction suffered by a light beam crossing a plane boundary separating two media with different optical properties. On passing from one medium to another of higher optical density, the beam slows and is bent towards the normal to the material interface. As illustrated in figure 1.1 momentum in the direction parallel to the interface is conserved while the perpendicular component is altered by the overall change in velocity suffered by the light beam giving the familiar relationship that is Snell's law, namely $n_1 \sin\theta_i = n_0 \sin\theta_r$.

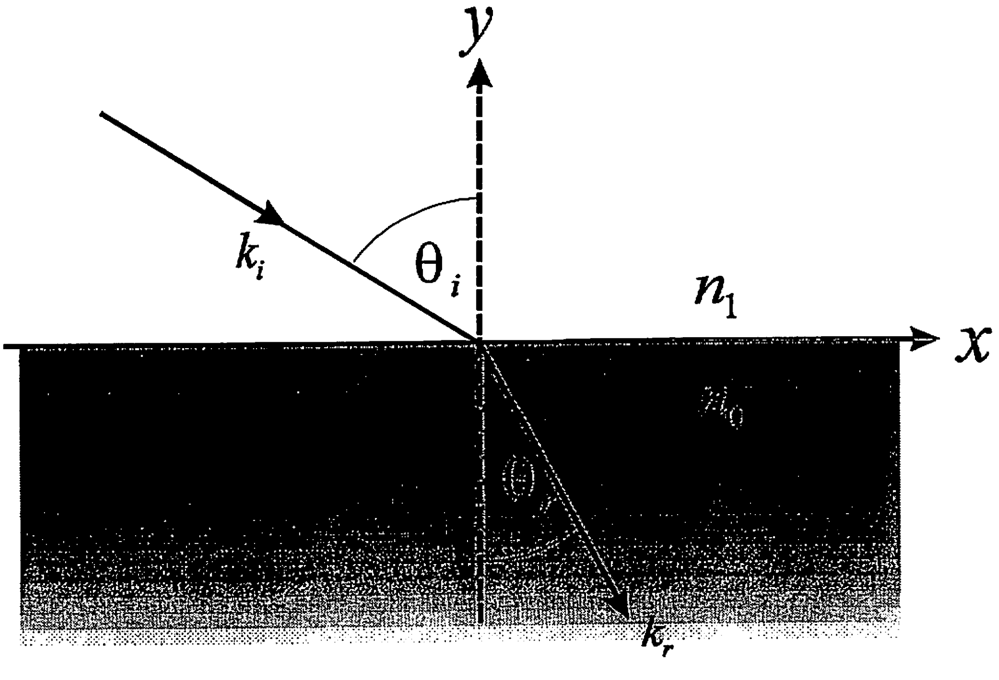

**Figure 1.1:** Momentum conservation in refraction

The second concept - diffraction, is a much more complicated issue involving the interaction of light with regions of matter whose character, be it optical density or spatial distribution, changes over distances comparable with the wavelength of that light. To illustrate this, figure 1.2 shows what is known as a phase-grating. Region 1, a semi - infinite homogeneous non - absorbing medium is separated from medium 0, which has a permittivity which is periodic in the $x$ direction, by a planar surface of constant $y$.

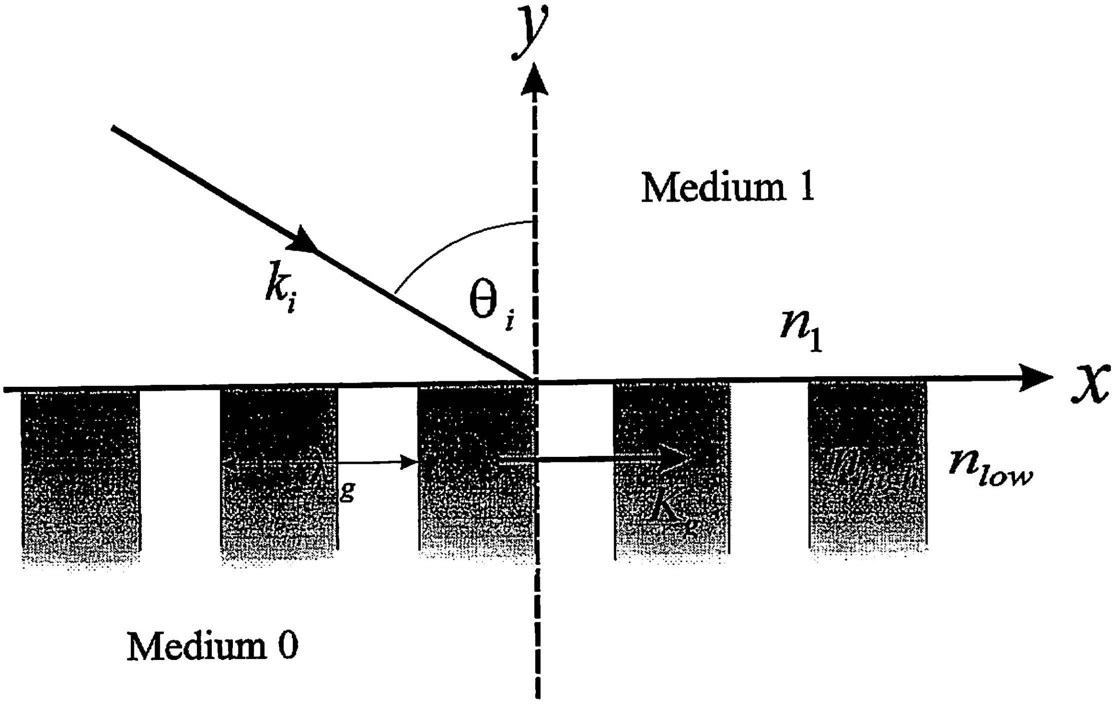

**Figure 1.2:** The phase grating

Suppose we illuminate this system from medium 1, with a monochromatic light beam whose wavelength λ is comparable to the periodicity distance $\lambda_g$ of the permittivity in medium 0. Within medium 0 light undergoes a process known as 'Bragg scattering' whereby a photon with $x$ wavevector $k_x$ may pick up or lose integer multiples of the Bragg vector - defined to lie along the direction of periodicity (the $x$ axis) and have magnitude $K=2\pi/\lambda_g$. Thus the range of $x$ momenta available to Bragg scattered photons is $k_x + mK$, $m=0, \pm1, \pm2, \dots$, with corresponding $y$ momenta $k_y$ given by

$\varepsilon_r k^2 = (k_x + mK)^2 + k_y^2$. Here $\varepsilon_r$ is the relative permittivity of the medium in question so that if, for example, we chose to look at light reflected back into medium 1, we might see a number of beams with wave vectors $K_m = (k_x + mK, k_y)$. A given beam is referred to by the number $m$ of Bragg vectors that have been added to the $x$ wavevector, so that the zeroth or specular order is that with the same $x$ wavevector as the beam incident upon the grating. Typically only a few values of $m$ centred around zero produce real $k_y$ and hence propagating waves, all other orders have complex $k_y$ and are evanescent or surface waves bound to the material interfaces.

A different type of grating is shown in figure 1.3. This is known as a surface relief grating, so called because the interface between the two media is now the periodic entity rather than the permittivity.

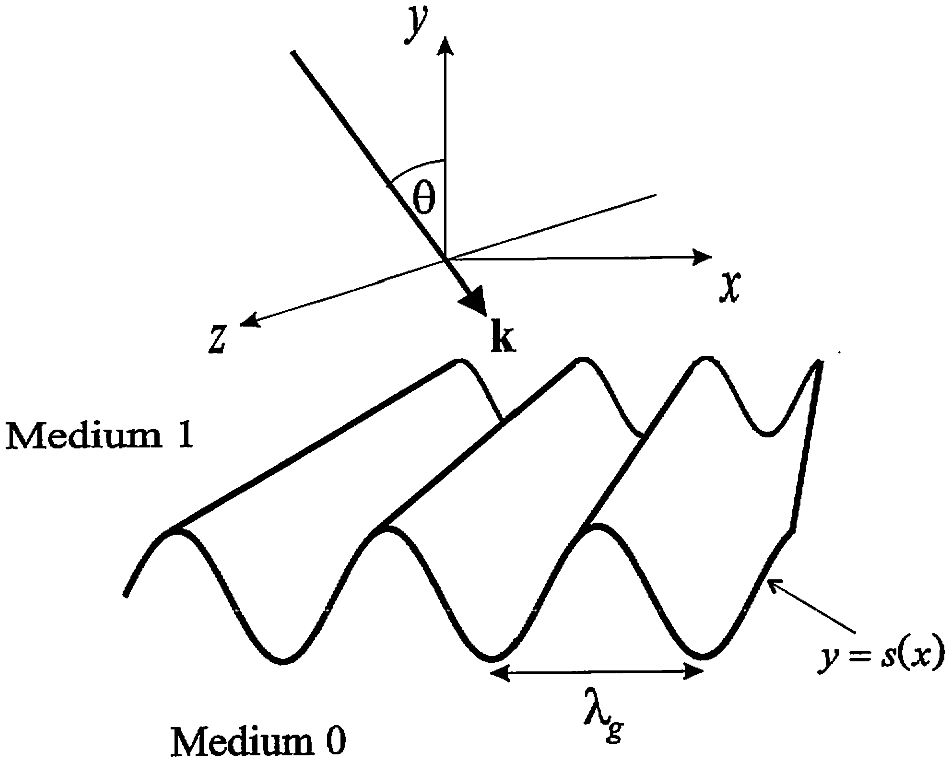

**Figure 1.3:** The surface-relief grating

Such an interface whose profile is periodic in the $x$ direction will give rise to Bragg scattering in much the same way as the permittivity modulation of the phase grating does. For the remainder of this thesis I will concentrate on this second type of grating, giving theoretical calculations that will enable us to determine the optical response of structures with varying complexity.

### *1.1.2 The kinematics of a typical grating*

To give the reader a better understanding of what is to follow I will first give an example of a typical surface-relief grating and show it's optical response to various parameters connected with the incident radiation. The grating in figure 1.3 is a prototype for the simplest type of surface-relief grating - two semi-infinite media separated by a sinusoidal boundary. Suppose we choose medium 1 to be vacuum, medium 0 to be a metal, such as silver, and the grating period $\lambda_g$ to be 800*nm*. Now consider what happens if we illuminate this structure with a plane monochromatic wave of wavelength $\lambda = 632.8nm$, corresponding to a wavevector of $k_0 = \frac{2\pi}{\lambda}$, propagating at an angle $\theta$ to the $y$ axis, in the $xy$ plane. We can distinguish two fundamental cases of polarisation: Transverse Magnetic (TM) or $p$ - polarised light where the magnetic field vector lies perpendicular to the saggital plane (this is the plane containing the Bragg vector $\boldsymbol{K}$ and the $y$ axis), and Transverse Electric (TE) or $s$ - polarised light where the electric field vector is perpendicular to the saggital plane. Here I choose TM or $p$ - polarisation.

What happens as we rotate the incident wavevector and sweep through angle $\theta$, and hence incident $x$ - wavevector $k_x^i = k_0 \sin\theta$, is shown in figures 1.4-6. Figures 1.4a-c, and 1.5a-c show the number of propagating orders and their directions of propagation, while figures 1.4d, 1.5d, and 1.6 show graphs plotting $R_{pp}$: the proportion of incident energy carried in a given propagating reflected order (referred to as the efficiency), as a function of the incident wavevector parallel to the surface. The subscripts pp denote that in order, we are dealing with a $p$ - polarised incident beam, and looking at the efficiency of a $p$ - polarised propagating diffracted order.

I start at $\theta = 90^\circ$, corresponding to $k_x^i = k_0$, (figures 1.4a,d) and find that $m$ = -2,-1,0 correspond to propagating beams each one carrying a proportion of the energy carried by the incident wave. In this case the grating is metallic so we can expect that a large proportion of that incident intensity will be reflected in the propagating orders of which the zeroth order typically carries the most energy - see figure 1.4d. As angle $\theta$ is increased so the -2, -1, and zeroth order wavevectors in figure 1.4a rotate anticlockwise about the origin until at $k_x^i = \frac{1}{2}.(2K) = 0.791k_0$ we reach the situation where the -2 order wavevector points back along the direction of the incident beam. This situation, when any of the diffracted beams point back along the incident wavevector is referred to as Littrow incidence. It is interesting to note that the efficiency of any particular order is symmetrical about it's own Littrow wavevector - referring to figure 1.4d we can see this to be true of the -2 order.

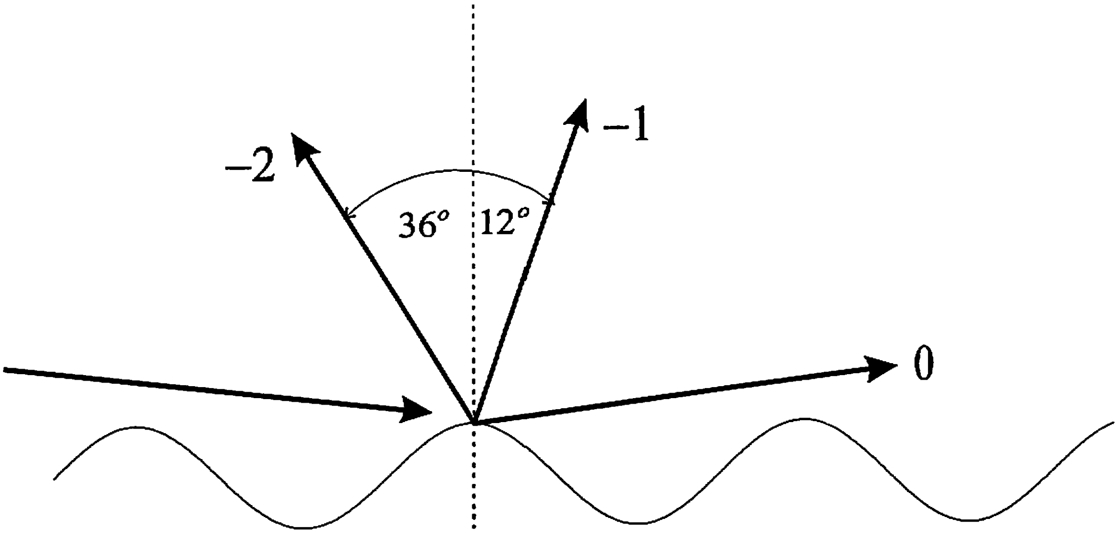

**Figure 1.4a:** Propagating beams at grazing incidence

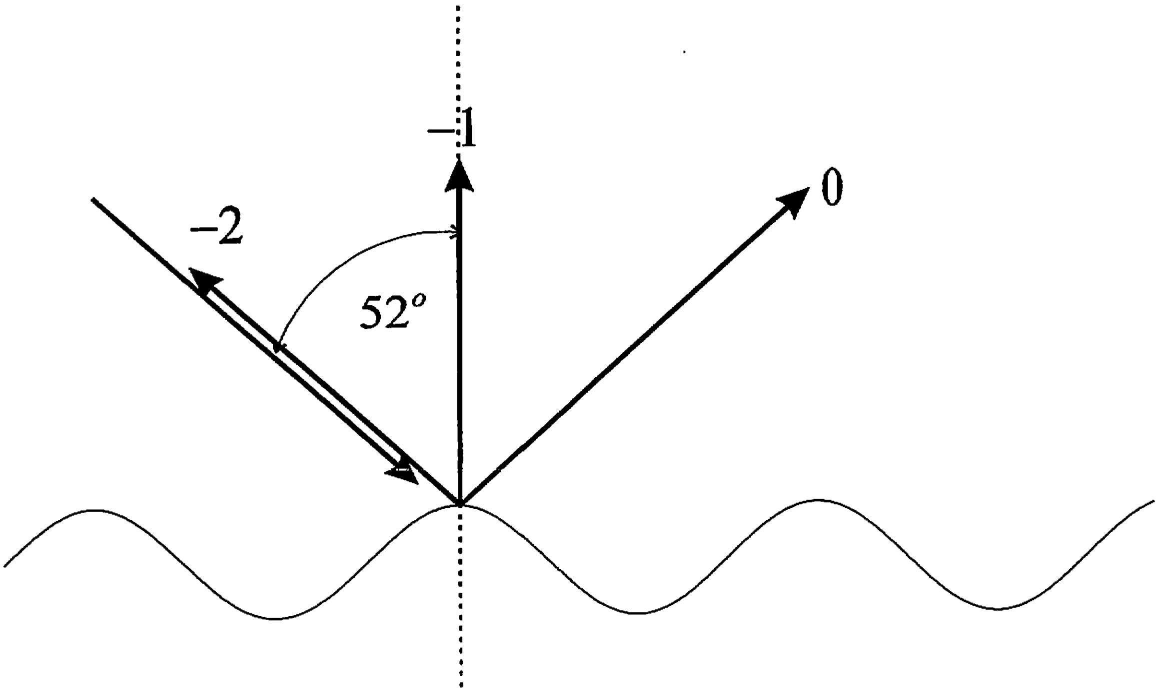

**Figure 1.4b:** Propagating beams at the -2 order Littrow incidence

The -2, -1, and zeroth orders remain the only propagating beams until we reach $k_x^i = 0.582k_0$ where the $m$ = -2 order grazes the negative $x$ - axis. Beyond this angle it becomes evanescent and ceases to propagate. When this happens the intensity previously carried by the three orders m = -2, -1, 0 now has to be distributed among only the m = -1 and 0 orders so we see a sudden increase in the energy carried by these remaining beams - see figure 1.4d. Such increases are called critical edges in line with planar optics.

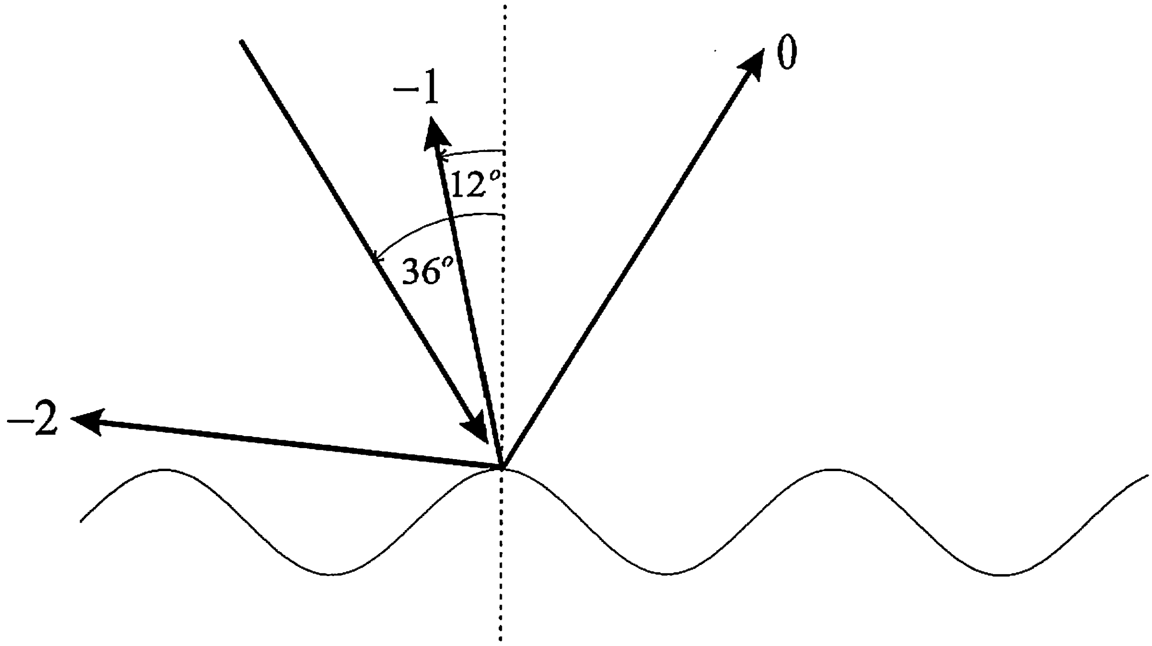

**Figure 1.4c:** The -2 order critical edge

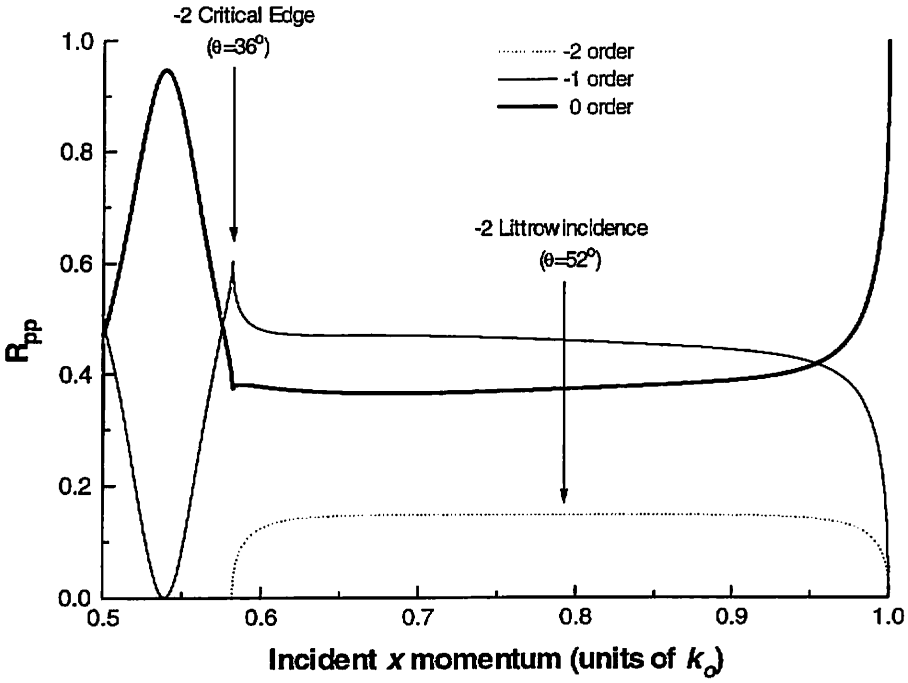

**Figure 1.4d:** Efficiencies of the -2, -1, and zeroth orders in the vicinity of the -2 critical edge as a function of the incident *x* wavevector. The range of incident momenta corresponds to figures 1.4a-c.

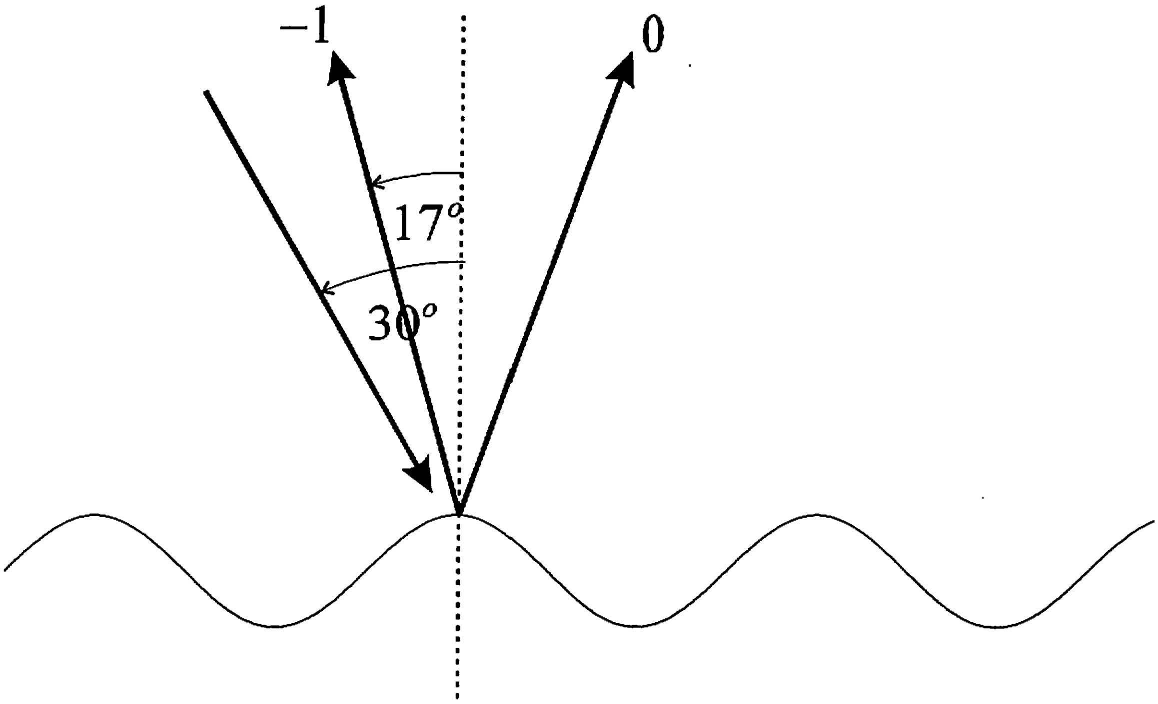

**Figure 1.5a:** Propagating beams just beyond the -2 critical edge

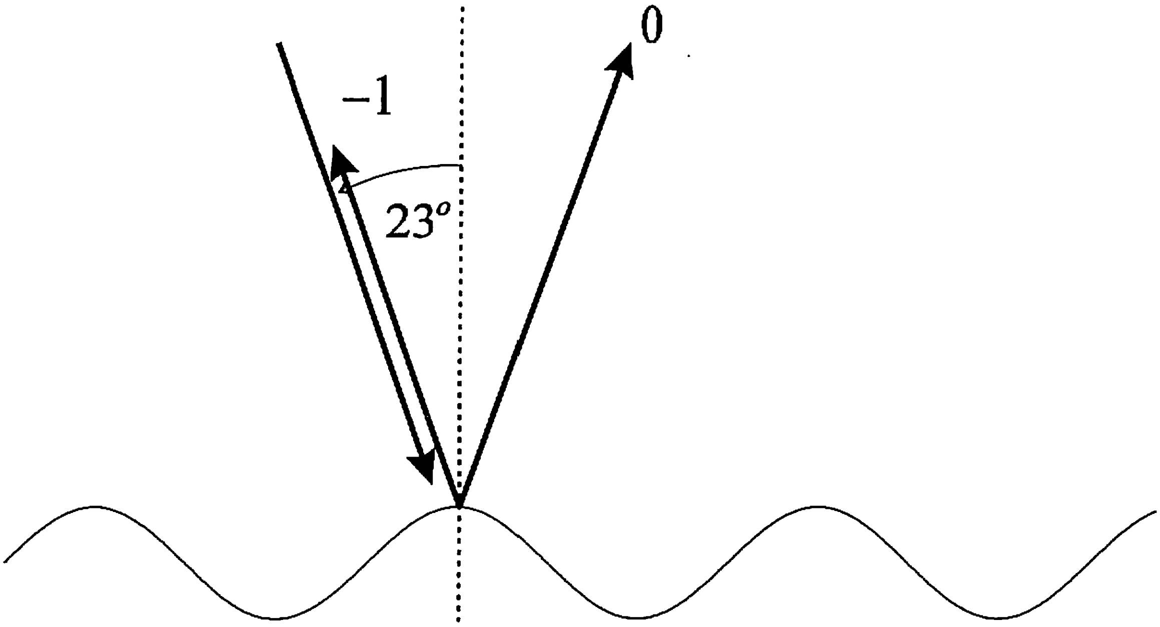

**Figure 1.5b:** The -1 order Littrow incidence

Rotating the incident wavevector further towards the normal we first reach Littrow incidence for the -1 order, - again the order's efficiency is symmetric about this wavevector. Then at $k_x^i = 0.209k_0$ we encounter a second critical edge where the m = +1 order starts to propagate. In this case the accompanying redistribution of energy causes a decrease in the efficiency of the previously propagating m = -1 and 0 orders which can be seen in figure 1.5d.

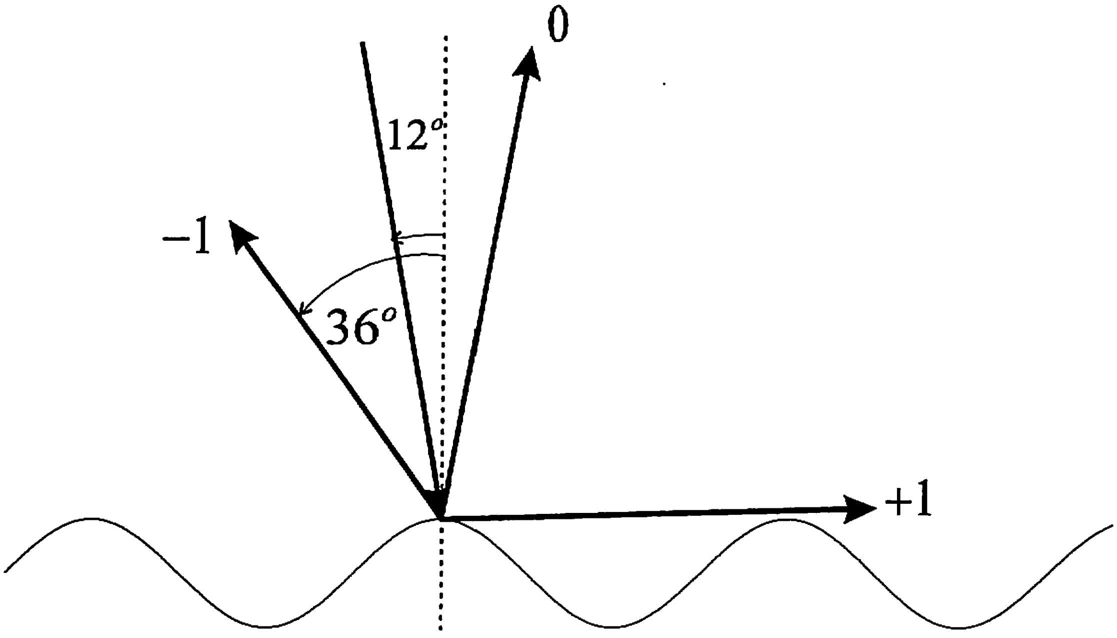

**Figure 1.5c:** Emergence of the +1 beam

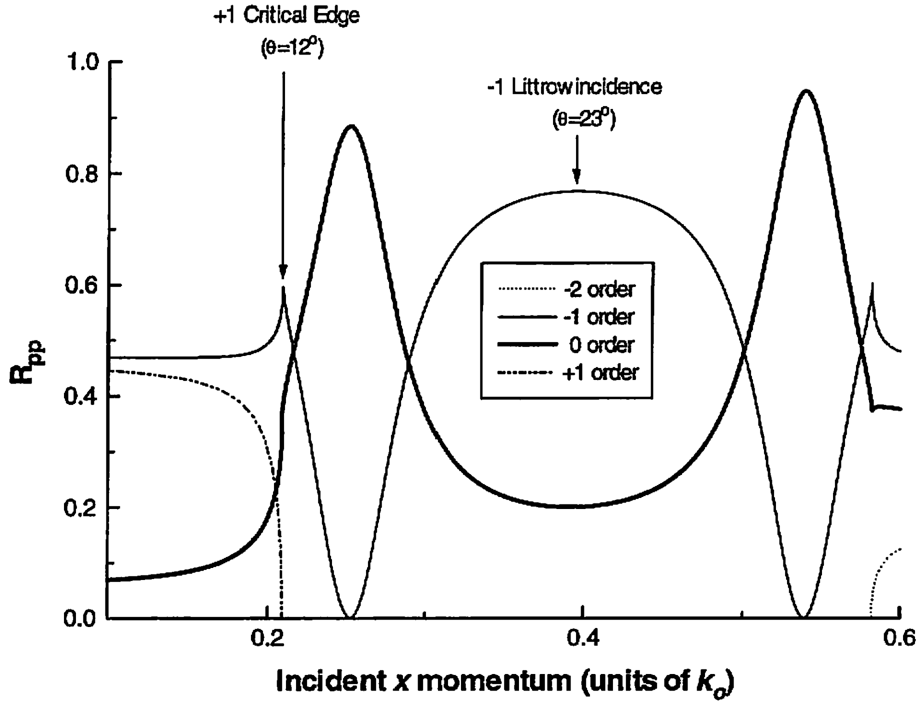

**Figure 1.5d:** Efficiencies of the -1, 0, and +1 orders in the vicinity of the +1 critical edge as a function of the incident $x$ wavevector. The range of incident momenta corresponds to figures 1.5a-c.

This situation with the three orders -1, 0, and +1 all propagating continues as the incident wavevector is rotated through the grating normal, at which point the specular beam is in Littrow incidence (it's efficiency can be seen to be symmetric about $k_x^i = 0$), until finally the -1 order grazes the grating surface at $k_x^i = -0.209$. This situation corresponds to the reflection of figure 1.5c in the $y$ - axis (dotted line) and from this point on the behaviour of all propagating beams for any negative angle of incidence is just the reflection of the positive angle case in the $y$ - axis.

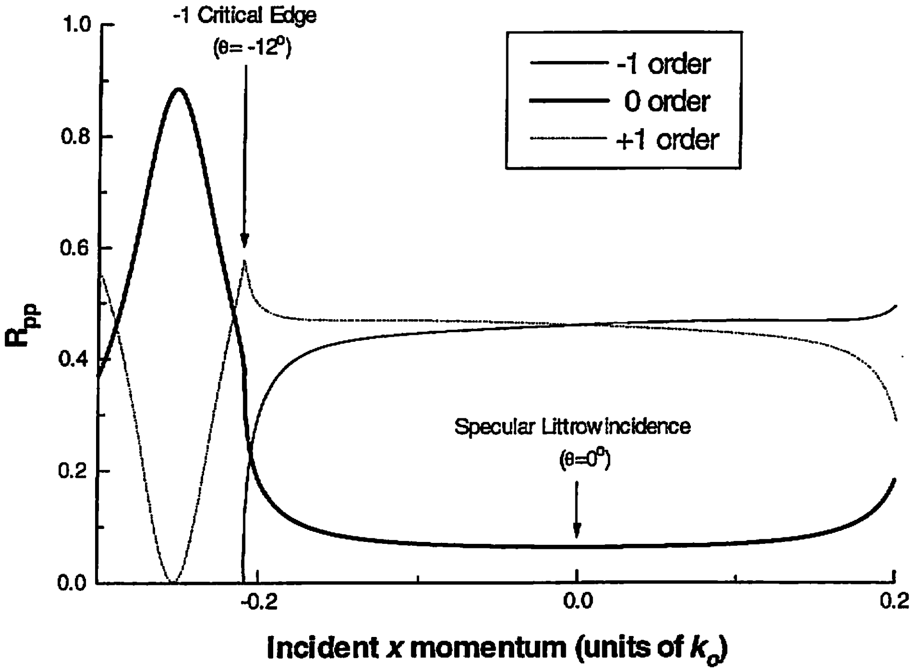

**Figure 1.6:** Efficiencies of the -1, 0, and +1 orders in the vicinity of the -1 critical edge as a function of the incident $x$ wavevector.

## *1.2 Theoretical preliminaries*

### *1.2.1 Presentation of the problem*

A prototype for the simplest type of diffraction grating has already been given in figure 1.3. Here I will start by giving a slightly more detailed description of the system to be modelled: For what is to follow I will assume a time dependence of $\exp(-i\omega t)$. In the rectangular co-ordinate system *Oxyz* we can identify two semi - infinite media separated by an interface *S* of profile $y=s(x)$, periodic in $x$ with period $\lambda_g$ giving a basis scattering vector **K**, of magnitude $K=\frac{2\pi}{\lambda_g}$, in the direction of the positive $x$ - axis. The unit normal vector to the surface $s(x)$ will be denoted by $\hat{\mathbf{n}}$, while the maximum and minimum values of $s(x)$ are labelled $y_{\max}$ and $y_{\min}$ respectively. The uppermost region 1 is a non - absorbing dielectric of relative permittivity $\varepsilon_r^1$, which for the most part will be taken to be vacuum so that $\varepsilon_r^1 = 1$. Medium 0 which has relative permittivity $\varepsilon_r^0$ may be a dielectric or metal, with or without absorption.

The system as a whole is illuminated through medium 1 with a monochromatic plane wave of wavevector **k** where $k=|\mathbf{k}|=\frac{2\pi}{\lambda}$, $\lambda$ being the wavelength, lying in the *Oxy* plane and making an angle of incidence $\theta$ with the $y$ - axis. Defining the complex vector amplitudes of the electric and magnetic fields associated with this wave to be $\mathbf{E}^i_{amp}$ and $\mathbf{H}^i_{amp}$ respectively we can write the incident electric and magnetic fields as

$$\mathbf{E}^i(x,y)=\mathbf{E}^i_{amp}\exp i(\alpha_0 x-\beta_0 y) \qquad \mathbf{H}^i(x,y)=\mathbf{H}^i_{amp}\exp i(\alpha_0 x-\beta_0 y) \qquad (1.1)$$

where $\alpha_0$ and $\beta_0$ are the two components of the incident wavevector **k**:

$$\alpha_0 = k\sin\theta \qquad \beta_0 = k\cos\theta \qquad (1.2)$$

Note that there is no $z$ dependence associated with these fields since all the incident momentum is contained within the $xy$ plane.

The problem is then to find the total vector fields $\mathbf{E}(x, y)$ and $\mathbf{H}(x, y)$ at any point in space.

### *1.2.2 Decoupling of the two fundamental polarisations*

Assuming a time dependence of $\exp(-i\omega t)$, I can write the diffracted fields in region 1 - defined by $\mathbf{E}^{\mathrm{d}} = \mathbf{E} - \mathbf{E}^{\mathrm{i}}$ and $\mathbf{H}^{\mathrm{d}} = \mathbf{H} - \mathbf{H}^{\mathrm{i}}$ using the time independent Maxwell equations:

$$Curl\mathbf{E}^{\mathrm{d}} = i\omega\mu_0\mathbf{H}^{\mathrm{d}} \tag{1.3}$$

$$Curl\mathbf{H}^{\mathrm{d}} = -i\omega\varepsilon_0\mathbf{E}^{\mathrm{d}} \tag{1.4}$$

$$Div\mathbf{E}^{\mathrm{d}} = 0 \tag{1.5}$$

$$Div\mathbf{H}^{\mathrm{d}} = 0 \tag{1.6}$$

The reader should appreciate that both polarisation and free charges have been absorbed into the permittivity so the free charge density $\rho_e$, may be set to zero. This also implies that there are effectively no currents and we may set $\mathbf{J} = 0$ in the *Curl***H** equation. These facts become particularly important in the analysis of *chapter* 2 where I will exploit the continuity of tangential **H** - a condition which is compromised by the appearance of surface currents. Note that the two divergence equations are consequences of the Curl equations associated with the propagation of plane waves. Consequently we do not need to consider them in our analysis.

Introducing the components of the diffracted fields and noting that $i\omega\mu_0 = ik_0Z_0$, $-i\omega\varepsilon_0 = -i\frac{k_0}{Z_0}$, where $Z_0 = \left(\frac{\mu_0}{\varepsilon_0}\right)^{1/2}$, we have

$$\frac{\partial E_z^d}{\partial y} = i\mu_r k_0 Z_0 H_x^d \tag{1.7}$$

$$\frac{\partial E_z^d}{\partial x} = -i\mu_r k_0 Z_0 H_y^d \tag{1.8}$$

$$\frac{\partial E_y^d}{\partial x} - \frac{\partial E_x^d}{\partial y} = i\mu_r k_0 Z_0 H_z^d \tag{1.9}$$

$$\frac{\partial H_z^d}{\partial y} = -i\varepsilon_r \frac{k_0}{Z_0} E_x^d \tag{1.10}$$

$$\frac{\partial H_z^d}{\partial x} = i\varepsilon_r \frac{k_0}{Z_0} E_y^d \tag{1.11}$$

$$\frac{\partial H_y^d}{\partial x} - \frac{\partial H_x^d}{\partial y} = -i\varepsilon_r \frac{k_0}{Z_0} E_z^d \tag{1.12}$$

The important point to note is that these six equations can be split into two distinct groups: one containing the field components $E_x^d$, $E_y^d$, $H_z^d$, the other containing $H_x^d$, $H_y^d$, $E_z^d$. From this we can deduce that provided the boundary conditions do not necessitate mixing these two groups, the general problem can be decoupled into two elementary polarisations: TM (transverse magnetic) or $p$ - polarised light with field components $E_x^d$, $E_y^d$, $H_z^d$, and TE (transverse electric) or $s$ - polarised light with field components $H_x^d$, $H_y^d$, $E_z^d$. Generally I will work with one or the other of these two fundamental states of polarisation.

### *1.2.3 The mathematical boundary problem*

In order to simplify the ensuing analysis in this chapter I will from now on assume that medium 0 is perfectly conducting and can thus contain no electric fields. While this may lead to a loss of generality it does not hinder the reader's understanding of the underlying theoretical formalisms which I will describe throughout the remainder of this chapter.

For either of the two fundamental cases of polarisation it proves convenient to work in terms of the tangential field component whose vector always points in the same direction for the in - plane calculations we will consider here. Thus for the TE problem we will look at the field component $E_z$ while for the TM case we will consider $H_z$.

In the TE problem $\mathbf{E} = (0,0,E_z)$ and equations (1.7-9) show that $E_z^d$ satisfies the Helmholtz equation

$$\nabla^2 E_z^d + k^2 E_z^d = 0 \qquad \text{in region 1} \tag{1.13}$$

while $E_z^d = 0$ in region 0. Similarly in the TM problem equations (1.10-12) show that $H_z^d$ satisfies

$$\begin{aligned} &\nabla^2 H_z^d + k^2 H_z^d = 0 && \text{in region 1} \\ &H_z^d = 0 && \text{in region 0} \end{aligned} \tag{1.14}$$

Regardless of the polarisation we can identify two boundary conditions on the grating surface, namely the continuity of the tangential components of **E** and the normal components of **H**:

$$\hat{\mathbf{n}} \wedge (\mathbf{E}^i + \mathbf{E}^d) = 0, \tag{1.15}$$

$$\hat{\mathbf{n}} . (\mathbf{H}^i + \mathbf{H}^d) = 0 \tag{1.16}$$

For plane wave solutions we have $\mathbf{E} \wedge \mathbf{H} = \mathbf{k}$ which contrives to make these two boundary conditions equivalent. Thus it suffices to consider only the first, which gives two conditions:

$$\begin{aligned} &E_z^d = -E_z^i \\ &n_x E_y^d - n_y E_x^d = -\left(n_x E_y^i - n_y E_x^i\right) \end{aligned} \quad \text{or} \quad \begin{aligned} &E_z^d + E_z^i = 0 \\ &n_x E_y^d + n_x E_y^i - \left(n_y E_x^d + n_y E_x^i\right) = 0 \end{aligned} \tag{1.17}$$

For the TE case (1.17) gives us the Dirichlet boundary condition

$$E_z^d = -E_z^i \qquad \text{on } S \tag{1.18}$$

while for the TM case (1.10,11,17) give us the Neumann boundary condition

$$\frac{dH_z^d}{dn} = -\frac{dH_z^i}{dn} \qquad \text{on } S \tag{1.19}$$

The pairs (1.13,18) and (1.14,19) alone are not sufficient to determine the transverse components of the fields - we must impose an outgoing wave condition on the diffracted field, namely that it must propagate upward and remain finite as $y \to \infty$.

Gathering all this information together we can state the mathematical boundary value problem. First I define the field component $F$ such that $F = H_z^d$ for TM polarisation, and $F = E_z^d$ for TE polarisation. Then we have the following conditions

$$\begin{aligned} &\nabla^2 F + k^2 F = 0 && \text{in region 1,} \\ &F = 0 && \text{in region 0,} \end{aligned} \tag{1.20}$$

the following boundary conditions on the grating surface

$$F = -F^i = -\exp i(\alpha_0 x - \beta_0 s(x)) \qquad \text{for TE polarisation,} \tag{1.21}$$

$$\frac{dF}{dn} = -\frac{dF^i}{dn} = i(\beta_0 n_y - \alpha_0 n_x)\exp i(\alpha_0 x - \beta_0 s(x)) \quad \text{for TM polarisation,} \tag{1.22}$$

and an outgoing wave condition on the diffracted field, namely that it must propagate upward and remain finite as $y \to \infty$. Note that for convenience I have normalised the incident field amplitude to unity.

### *1.2.4 The pseudo - periodicity of the field*

I will show that $F^p(x,y) = F(x,y)\exp(-i\alpha_0 x)$ is a periodic function with the same periodicity as the grating profile. For this to be true $F^p(x+d,y) = F^p(x,y)$ which reduces to the condition $F(x+d,y)\exp(-i\alpha_0 d) = F(x,y)$. Due to the uniqueness of the solution, (which although intuitively obvious has yet to be proved mathematically) this equality will be satisfied if $F(x+d,y)\exp(-i\alpha_0 d)$ obeys equations (1.13,14,18,19). This can be seen by virtue of the fact that $F(x,y)$ obeys these same equations.

## *1.3 The Rayleigh method*

Historically, the Rayleigh method [Rayleigh, 1907] was the first theory designed to model the optical response of diffraction gratings. It is also without doubt the simplest formalism and makes an ideal starting point when looking at modern grating theories.

### *1.3.1 Formalism*

Section 1.2.4 showed how $F^p(x,y)=F(x,y)\exp(-i\alpha_0 x)$ is a periodic function, sharing the same periodicity as the grating profile. It can thus be expanded in a Fourier series

$$F^p(x,y)=\sum_n F_n(y)\exp inKx \tag{1.23}$$

Thus the total field is given by

$$F(x,y)=\sum_n F_n(y)\exp i\alpha_n x \tag{1.24}$$

with $\alpha_n=\alpha_0+nK$, leaving us to determine the $F_n(y)$. Introducing the above expansion into (1.20), multiplying by $\exp(-i\alpha_n x')$ and integrating over $x'$ gives

$$\sum_n\left[\frac{d^2}{dy^2}+\left(k^2-\alpha_n^2\right)\right]F_n(y)=0 \qquad \text{in region 1} \tag{1.25}$$

If $y>y_{\max}$, where $y_{\max}$ is the maximum value of $y$ on the grating surface $s(x)$, the above equation is valid for any value of $x$. Since the right hand side of (1.25) may be regarded as the Fourier expansion of the null function, each term of the left hand Fourier series must be zero:

$$\left[\frac{\partial^2}{\partial y^2}+\left(k^2-\alpha_n^2\right)\right]F_n(y)=0 \qquad y>y_{\max} \tag{1.26}$$

The above equation has solution

$$F_n(y)=A_n\exp(-i\beta_n y)+B_n\exp i\beta_n y \qquad y>y_{\max} \tag{1.27}$$

where

$$\begin{aligned} \beta_n &= \left(k^2 - \alpha_n^2\right)^{1/2} \quad |\alpha_n| \leq k \\ \beta_n &= i\left(\alpha_n^2 - k^2\right)^{1/2} \quad |\alpha_n| > k \end{aligned} \tag{1.28}$$

If $n \in U$: $|\alpha_n| < k$ then $\beta_n$ is a real number, otherwise it is purely imaginary. Bearing in mind the outgoing wave condition of section 1.2.3 we find that the $A_n$ vanish since for $n \notin U$, $\exp(-i\beta_n y) \to \infty$ as $y \to \infty$, and for $n \in U$, $\exp(-i\beta_n y)$ represents an incoming plane wave propagating downwards. Thus we arrive at the 'Rayleigh expansion', first used by Lord Rayleigh in 1907:

$$F(x,y) = \sum_n B_n \exp i(\alpha_n x + \beta_n y) \qquad y > y_{\max} \tag{1.29}$$

Rayleigh made the assumption that this expansion was a valid representation of the diffracted field $F$ not only for $y > y_{\max}$ but throughout medium 1 including the region within the grating grooves. I will postpone any discussion on the validity of the Rayleigh expansion until section 1.3.3 as I will first look at the most common methods of determining the $B_n$ numerically.

### *1.3.2 Numerical methods*

The equation (1.29) has been shown to satisfy both the Helmholtz equation and the outgoing wave condition stated in section 1.2.3. It must also satisfy a boundary condition on the grating surface given by equations (1.21,22) so that for TE polarisation we obtain

$$\sum_n B_n \exp i(\alpha_n x + \beta_n s(x)) + \exp i(\alpha_0 x - \beta_0 s(x)) = 0 \tag{1.30}$$

The unknowns we seek are the $B_n$ which are effectively the coefficients of the expansion of $-\exp i(\alpha_0 x - \beta_0 s(x))$ into a set of functions $\exp i(\alpha_n x + \beta_n s(x))$.

The most common numerical method for obtaining the $B_n$ is the Fourier series method. To perform any numerical analysis on (1.30) we must first truncate the series expansion, limiting $n$ to the range $-N \leq n \leq N$, giving $2N+1$ terms. By using orthogonality with $\exp i\alpha_m x$ it is possible to single out individual series terms and obtain a linear system of $2N+1$ equations.

$$\sum_n B_n \frac{1}{\lambda_g} \int_0^{\lambda_g} \exp(-i\alpha_m x).\exp i(\alpha_n x + \beta_n s(x))\, dx = -\frac{1}{\lambda_g} \int_0^{\lambda_g} \exp(-i\alpha_m x).\exp i(\alpha_0 x - \beta_0 s(x))\, dx \tag{1.31}$$

In some cases the integrals may be calculated analytically but typically numerical integration is required, after which the system of $2N+1$ equations may be solved numerically to obtain the $B_n$.

### *1.3.3 Validity*

The fact that equation (1.29) is only valid for $y > y_{\max}$ should lead us to question the validity of the above analysis. In fact it can be shown that if the Rayleigh expansion converges at any point within the grating grooves, $s(x) < y < y_{\max}$, then it does indeed represent the diffracted field at that point [Maystre, 1984]. The validity of the Rayleigh series thus reduces to a study of it's convergence properties within the groove region. If we were to perform the appropriate analysis we would find that there exists a critical value of $y = y_c$ within the groove region such that the Rayleigh series converges for $y > y_c$ and diverges for $y < y_c$. So the Rayleigh expansion is a valid representation of the diffracted field throughout medium 1 if $y_{\min} > y_c$ limiting the expansions validity to those gratings shallow enough to accommodate this condition. Calculations by Petit and Cadilhac [1966] show that for sinusoidal gratings $y_c$ takes values such that the aspect ratio $\frac{y_{\max} - y_{\min}}{\lambda_g} < 0.1425$.

## *1.4 The differential method*

We have seen how the determination of the electromagnetic fields diffracted by a grating reduces to the solution of partial differential equations together with the appropriate boundary conditions. I will now look a ways of solving these equations directly - the so called differential methods which fall into three broad classes: first there are the direct differential methods where Maxwell's equations are projected onto Cartesian co-ordinates giving a system of coupled partial differential equations [Moaveni, Kalhor, and Afrashteh, 1975]; next there are methods which project the propagation equations onto a suitable set of functions giving a set of ordinary differential equations [Petit, 1966]; and finally there are those methods that utilise conformal mapping to map the grating profile onto the complex plane [Nevière, Cerutti-Maori, and Cadilhac, 1971; Nevière, Cadilhac, and Petit, 1973].

The first method is the simplest but requires long computation times and is limited by numerical instabilities for high aspect ratios. The third method can be highly efficient under certain circumstances but is too complicated to present here. Instead I will go some way to describe the second method which is both simple to formulate and solve numerically.

In region 1 of figure 1.3 the transverse field component $F$ satisfies a Helmholtz equation:

$$\nabla^2 F(x,y) + k^2(x,y)F(x,y) = 0 \tag{1.32}$$

The field which is a pseudo - periodic function of $x$ may be expanded in Bloch waves as per equation (1.23). Additionally we may expand the periodic function $k^2$ in a Fourier series:

$$k^2(x,y) = \sum_n \left[k^2(y)\right]_n \exp inKx \tag{1.33}$$

Using orthogonality with $\exp i\alpha_m x$ it is possible to single out individual series terms leading to a set of coupled ordinary differential equations:

$$\frac{d^2 F_n(y)}{dy^2} = \alpha_n^2 F_n(y) - \sum_m \left[k^2(y)\right]_{n-m} F_m(y) \tag{1.34}$$

For a given value of $y$ the $\left(k^2\right)_n$ coefficients are calculated and (1.34) is integrated numerically.

### *1.5 The integral method*

Traditionally the integral method [Petit and Cadilhac, 1964] has been the formalism used whenever accuracy is of paramount importance. Although complex both mathematically and in numerical implementation the method is capable of modelling deep and complex grating structures rigorously in regions where other methods fail or encounter numerical difficulty.

The method is based on the intuitive idea that the incident field sets up a current density $j_S(x)$ on the grating surface which in turn generates the diffracted field. The problem thus reduces to the determination of $j_S(x)$ [D. Maystre, 1984].

Consider the 'generalised diffracted field' $F^d(x,y)$ which I will define as the difference between the total field and the incident field *at any point in space.* In particular this means that in medium 0 (figs 1.3,6) where the total field is zero

$$F^d(x,y) = -F^i(x,y) = -\exp i(\alpha_0 x - \beta_0 y) \tag{1.35}$$

where $F^i(x,y)$ represents the (non-physical) extension of the incident field into medium 0. This definition in no way invalidates the analysis provided it is used consistently throughout, and we remember that $F^d(x,y)$ does not represent the actual diffracted field in medium 0.

In media 0 and 1 $F^d(x,y)$ satisfies a Helmholtz equation

$$\nabla^2 F^d(x,y) + k^2 F^d(x,y) = 0 \tag{1.36}$$

and the outgoing wave condition that $F^d(x,y)$ must propagate upward and remain finite as $y \to \infty$. The first step in finding an expression for $F^d(x,y)$ is to define the Green's function $G(x,y)$ for the grating problem.

On the simplest level Green's functions are used to solve inhomogeneous problems of the type $L_{op}\Psi(x) = \rho(x)$ where $L_{op}$ is a differential operator in $x$. By constructing the appropriate Green's function which solves $L_{op}G(x-x') = \delta(x-x')$ we may obtain $\Psi(x)$ by integration of the Green's function multiplied by an appropriate weight function which in this case is the inhomogeneous term $\rho(x)$.

$$\Psi(x) = \int_{-\infty}^{\infty} G(x-x')\rho(x')dx' \tag{1.37}$$

To see this it is only necessary to operate on both sides of this equation with $L_{op}$ giving $L_{op}\Psi(x) = \rho(x)$.

For 2D problems the best approach is somewhat different centring around the second Green's identity which is written below for the two arbitrary functions $\Psi(\mathbf{r})$ and $\Phi(\mathbf{r})$.

$$\int_S [\Psi\nabla^2\Phi - \Phi\nabla^2\Psi]\, dS = \oint_C \left[\Psi\frac{d\Phi}{dn} - \Phi\frac{d\Psi}{dn}\right] ds \tag{1.38}$$

where $dS$ denotes an element of a surface $S$ bounded by the contour C, $n$ is the modulus of the outward normal vector to the contour C, and $ds$ is an element of the contour C.

To solve the Helmholtz equation (1.36) we use a Green's function solving the equation

$$(\nabla^2 + k^2)G(\mathbf{r}-\mathbf{r}') = \delta(\mathbf{r}-\mathbf{r}') \tag{1.39}$$

Then by appealing to (1.38) with $\Psi = F^d(\mathbf{r}')$ and $\Phi = G(\mathbf{r}-\mathbf{r}')$, all integration being carried out over the primed variables, the LHS of reduces to $F^d(\mathbf{r})$ so that

$$F^d(\mathbf{r}) = \oint_C \left[F^d(\mathbf{r}')\frac{dG(\mathbf{r}-\mathbf{r}')}{dn} - G(\mathbf{r}-\mathbf{r}')\frac{dF^d(\mathbf{r}')}{dn}\right] ds' \tag{1.40}$$

Note that the unprimed variable $\mathbf{r}$ is used to denote the position at which we want to know the field, while the primed variable $\mathbf{r}'$ is used as an integrand parameter. The contour C over which the integration takes place is usually some physical boundary so that under Dirichlet boundary conditions ($F^d = 0$ on C), made possible by our definition of $F^d$ in medium 0, the first integral vanishes, while under Neumann boundary conditions ($\frac{dF^d}{dn} = 0$ on C) the second vanishes. The problem may then be solved with a knowledge of $\frac{dF^d(\mathbf{r}')}{dn}$ in the Dirichlet problem, or $F^d(\mathbf{r}')$ in the Neumann case, and of course $G(\mathbf{r}-\mathbf{r}')$ which is obtained by solving (1.39).

Looking now at the grating problem in particular it is apparent that we should take part of the contour C to be the grating. Pseudo - periodicity would then suggest that we need only integrate over one period. In light of this figure 1.7 shows an appropriate contour C: the path ABCD.

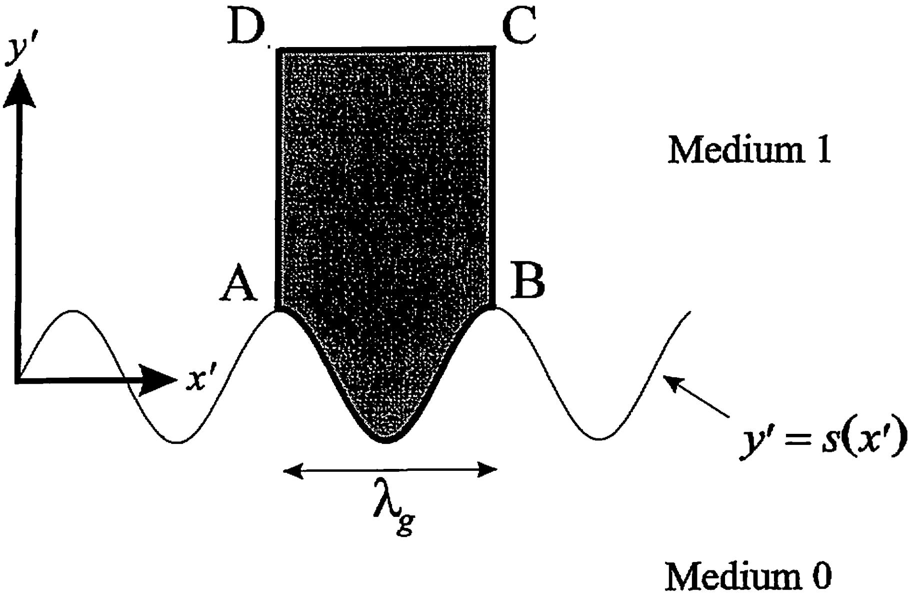

**Figure 1.7:** The area of the $x'y'$ plane (shaded) and it's boundary ABCD, used in the integral equations.

Since the integrands are periodic in $x$ the contributions from BC and DA cancel. That the contribution from CD is zero is not at all obvious until one considers that, under co-ordinates $x', y'$, $F^d(x', y')$ contains only outgoing waves, while $G(x - x', y - y')$ contains only incoming waves. Since the integration is carried out over one period at constant $y$, orthogonality with the set $\exp i\alpha_m x$ dictates that the two contributions cancel each other [D. Maystre 1984]. Thus (1.40) reduces to

$$\begin{aligned} F^d(x,y) = &\int_0^{\lambda_g} \left( \frac{dF^d(x', s(x'))}{dn} G(x - x', y - s(x')) \right) \left(1 + s(x')^2\right)^{1/2} dx' \\ &- \int_0^{\lambda_g} \frac{dG(x - x', y - s(x'))}{dn} F^d(x', s(x')) \left(1 + s(x')^2\right)^{1/2} dx' \end{aligned} \quad (1.41)$$

This equation embodies the *Fundamental Theorem of the Integral Method*: any pseudo - periodic function $F^d(x,y)$, continuous except on S, the grating surface, satisfying a Helmholtz equation in region 1 and being zero in region 0 may be expressed at any point in space in terms of the jumps that $F^d(x,y)$ and $\frac{dF^d(x,y)}{dn}$ make on crossing S.

Given this approach it is necessary that the defining equation for our Green's function, which in the absence of pseudo - periodicity was given by (1.39), now needs to be modified so that $G$ satisfies the expression

$$(\nabla^2 + k^2)G(\bar{x},\bar{y}) = \sum_n A_n \delta\left(\bar{x} - n\lambda_g\right)\delta\left(\bar{y}\right) \tag{1.42}$$

where I have introduced the notation $\bar{x} = x - x'$, $\bar{y} = y - y'$, and $A_n$ are a set of constants.

In grating theory the pseudo - periodicity of the problem is such that we are led to look for solutions of the form $G(x + \lambda_g, y) = G(x,y)\exp i\alpha_0\lambda_g$ whence

$$(\nabla^2 + k^2)G(\bar{x},\bar{y}) = \sum_n A_n \delta\left(\bar{x} - n\lambda_g + m\lambda_g\right)\delta(\bar{y})\exp\left(-i\alpha_0 m\lambda_g\right) \tag{1.43}$$

That the right hand members of (1.42) and (1.43) must be equal necessitates that $A_n = \exp i\alpha_0 n\lambda_g$ which leads us to define our Green's function as

$$(\nabla^2 + k^2)G(\bar{x},\bar{y}) = \left[\sum_n \delta\left(\bar{x} - n\lambda_g\right)\exp i\alpha_0 n\lambda_g\right]\delta\left(\bar{y}\right) \qquad \text{in all space} \tag{1.44}$$

as well as the outgoing wave condition that $G(\bar{x},\bar{y})$ must propagate upward and remain finite as $y \rightarrow \infty$.

Since $G(\bar{x},\bar{y})$ is necessarily pseudo - periodic in $x$ it may be expanded in a Fourier series over momenta $\alpha_n$:

$$G(\bar{x},\bar{y}) = \sum_n G_n(\bar{y})\exp i\alpha_n\bar{x} \tag{1.45}$$

Introducing this expansion into (1.43) and isolating individual series terms via orthogonality with $\exp i\alpha_m \bar{x}$ we arrive at the following equation

$$\frac{d^2 G_n(\bar{y})}{dy^2} + \beta_n^2 G_n(\bar{y}) = \frac{\delta(\bar{y})}{\lambda_g} \tag{1.46}$$

Since the effect of the RHS is zero for $\bar{y} \neq 0$ we have

$$G_n(\bar{y}) = A \exp i\beta_n \bar{y} + B \exp(-i\beta_n \bar{y}) \qquad \bar{y} > 0 \tag{1.47}$$

$$G_n(\bar{y}) = A' \exp i\beta_n \bar{y} + B' \exp(-i\beta_n \bar{y}) \qquad \bar{y} < 0 \tag{1.48}$$

Substituting these relations back into (1.45) we find the full $x$, $y$ dependence:

$$G(\bar{x}, \bar{y}) = \sum_n \left[ A \exp i(\alpha_n \bar{x} + \beta_n \bar{y}) + B \exp i(\alpha_n \bar{x} - \beta_n \bar{y}) \right] \qquad \bar{y} > 0 \tag{1.49}$$

$$G(\bar{x}, \bar{y}) = \sum_n \left[ A' \exp i(\alpha_n \bar{x} + \beta_n \bar{y}) + B' \exp i(\alpha_n \bar{x} - \beta_n \bar{y}) \right] \qquad \bar{y} < 0 \tag{1.50}$$

So that $G(\bar{x}, \bar{y})$ takes the form of a sum of plane waves. Using the outgoing wave condition that the diffracted field must propagate upward and remain finite as $y \rightarrow \infty$, and (1.44) we find that $B = A' = 0$. Additionally we have the discontinuity condition from (1.47) which tells us that

$$\left.\frac{dG_n}{dy}\right|_{\bar{y}+} - \left.\frac{dG_n}{dy}\right|_{\bar{y}-} = \frac{1}{\lambda_g} \tag{1.51}$$

where $\bar{y}+$ denotes an infinitesimal increment from $\bar{y} = 0$, while $\bar{y}-$ denotes an infinitesimal decrement from $\bar{y} = 0$. This condition shows that $A = B' = \dfrac{1}{2i\lambda_g \beta_n}$ whence we obtain our elementary solution of the Helmholtz equation:

$$G(\bar{x},\bar{y})=\frac{1}{2i\lambda_g}\sum_n\frac{1}{\beta_n}\exp i\left(\alpha_n\bar{x}+\beta_n|\bar{y}|\right) \tag{1.52}$$

To illustrate the final solution I will consider the TE case described by equations (1.20,21) which shows that the transverse field satisfies the Dirichlet boundary condition $F^d(x',s(x'))=0$ on S so that the second integral in (1.41) vanishes. Writing the Green's function explicitly we are left with

$$F^d(x,y)=$$
$$\int_0^{\lambda_g}\left(\frac{dF^d(x',s(x'))}{dn}\frac{1}{2i\lambda_g}\sum_n\frac{1}{\beta_n}\exp i\left(\alpha_n(x-x')+\beta_n(y-s(x'))\right)\right)\left(1+s(x')^2\right)^{1/2}dx' \tag{1.53}$$

in medium 1, for $y>y_{\max}$. Rearranging, this can be written in the form

$$F^d(x,y)=\sum_n R_n\exp i\left(\alpha_n x+\beta_n y\right) \tag{1.54}$$

where

$$R_n=\int_0^{\lambda_g}\left(\frac{dF^d(x',s(x'))}{dn}\frac{1}{2i\lambda_g}\frac{1}{\beta_n}\exp i\left(-\alpha_n x'-\beta_n s(x')\right)\right)\left(1+s(x')^2\right)^{1/2}dx' \tag{1.55}$$

This expression can be evaluated by noting that $F^d=-F^i$ on S so that

$$\frac{dF^d(x',s(x'))}{dn}=-\frac{dF^i(x',s(x'))}{dn}=-i\left(s'(x')\alpha_0+\beta_0\right)\exp i\left(\alpha_0x'-\beta_0 s(x')\right) \tag{1.56}$$

The TM problem proceeds in a similar manner starting from the observation that in this state of polarisation the first, rather than second, integral in (1.53) vanishes.

### *1.6 Summary*

In this chapter I have outlined the fundamentals of grating theory, covering the most basic concepts through to the complexity of integral methods. Where the differential and integral methods are concerned I have only illustrated the basic ideas and most simple methods of solution. Since their conception both methods have been steadily refined and generalised to other grating geometries to the point where almost any system can be modelled rigorously. However it is still the case that certain formalisms naturally lend themselves to the study of particular grating geometries: In the case of sinusoidal-like surfaces, differential methods which must Fourier analyse the grating profile provide a natural choice.

The motivation behind this thesis stems from a desire to model such sinusoidal surfaces. The necessary formalism and it's generalisation to other geometries is described in the remaining chapters of this thesis.

# 2. The Differential Method of Chandezon

## *2.1 Introduction*

The aim of this chapter is to provide the reader with a sound understanding of both the problem to be solved and the method of solution as first used by J.Chandezon, M.T.Dupuis, G.Cornet, and D.Maystre in 1982. It is the formalism which underlies the whole of this thesis, for as will become apparent the topics discussed in later chapters are essentially generalisations of the simple case first addressed by Chandezon *et al.*

The problem then is to determine the optical response of a grating such as that shown in figure 2.1. We consider a system consisting of two semi-infinite media, labelled 0 and 1, separated by an interface $y = s(x)$ where $s(x)$ is periodic in $x$ with period $\lambda_g$ giving a basis scattering vector of magnitude $K=2\pi/\lambda_g$ in the direction of the $x$ axis. Both media are required to be electrically and magnetically isotropic. In addition it is assumed that the relative permeabilities of both media are unity. Medium 0 is defined to be the substrate with complex relative permittivity $\varepsilon^0$ and may be metallic or dielectric. The grating is illuminated through medium 1 (which is consequently required to be non-absorbing), by a homogeneous plane wave with angle of incidence $\theta$ and wave vector $k=(\varepsilon^1)^{1/2}k_0$ $(k_0=\omega/c)$ situated in the $Oxy$ plane.

Although the development can allow for general polarisation of incoming light, for our purposes this will be limited to the case of transverse magnetic ( TM, or *p*- polarised with the H - field perpendicular to the plane of incidence ), or transverse electric ( TE, or *s*- polarised with the E - field perpendicular to the plane of incidence ).

As discussed in *chapter 1* this will give rise to a number of propagating diffracted beams in reflection (and also in transmission if medium 0 is a non-absorbing dielectric). Chandezon's key paper sought to calculate the proportion of incident light contained within these propagating diffracted beams.

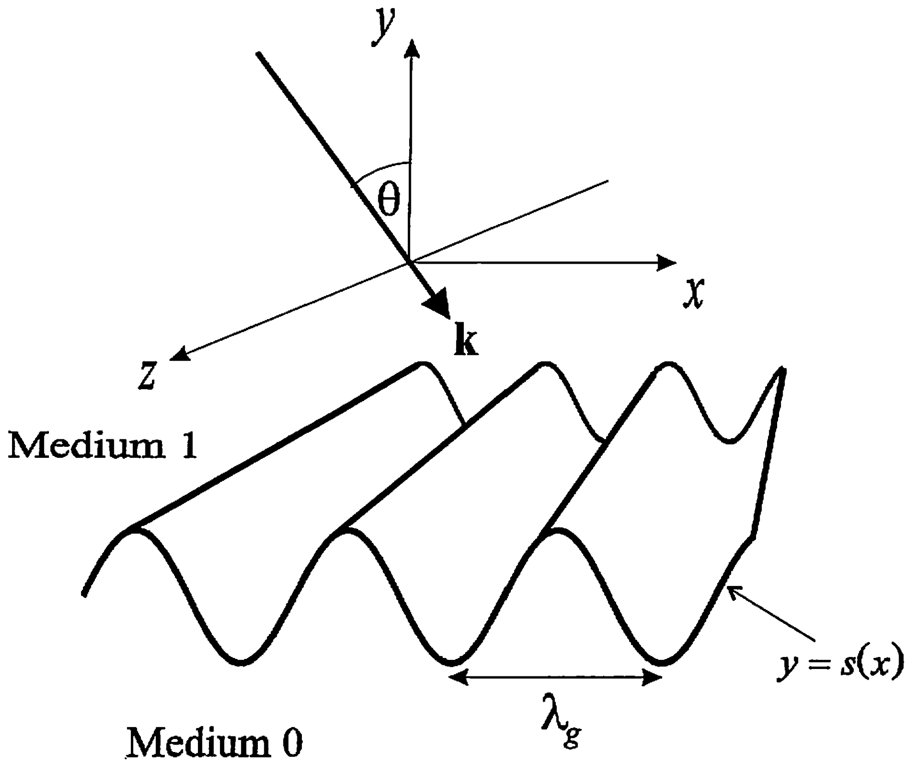

**Figure 2.1:** The system under consideration

### *2.2 The single frequency Maxwell equations*

We start from Maxwell's equations for media containing no sources or currents

$$Curl\mathbf{E} = -\frac{\partial \mathbf{B}}{\partial t} \qquad Curl\mathbf{H} = \frac{\partial \mathbf{D}}{\partial \mathbf{t}} \qquad Div\mathbf{E} = 0 \qquad Div\mathbf{B} = 0 \tag{2.1}$$

The two divergence equations contain redundant information concerning the propagation of plane waves, and we shall only require the two curl equations.

In what is to follow we only consider systems illuminated by monochromatic light. All fields will then oscillate at the same frequency so that we may assume a time dependence $\exp(-i\omega t)$. The two curl equations then become

$$Curl\mathbf{E} = i\mathbf{H} \qquad \text{and} \qquad Curl\mathbf{H} = -i\varepsilon_r\,\mathbf{E} \tag{2.2}$$

Where I have adopted a system of units in which the free space incident wavenumber, $|k_0| = \frac{2\pi}{\lambda} = \frac{\omega}{c}$ and impedance, $Z_0 = \left(\frac{\mu_0}{\varepsilon_0}\right)^{1/2}$ are both equated to unity. This will ensure that in certain matrices to be defined later all terms have comparable magnitude. This proves essential to the stability of the numerical methods employed.

### *2.3 Co-ordinate system*

In most electromagnetic problems the first question we should ask ourselves is which set of co-ordinates would best suit our needs. Often a suitable choice will simplify the ensuing analysis and perhaps shed light on otherwise unapparent symmetries. Here we have a choice of two sets of co-ordinates. The first is just the familiar Cartesian system, labelled $x,y,z$ in figure 2.1, which enables us to write Maxwell's equations in simple form but result in fairly complicated expressions for the boundary conditions. The second, and that used by Chandezon, is the non-orthogonal curvilinear co-ordinate transformation

$$v = x \qquad u = y - s(x) \qquad w = z \tag{2.3}$$

Thus $u$ is a variable which is related to the shape of the interface, where it takes the constant value $u=0$, and we have effectively mapped the grating interface onto a parallel plane. Expressed in this system of co-ordinates Maxwell's equations are more complicated but the boundary conditions are much simplified. This is because we can now work directly with vector components that are always tangential to the grating surface.

To put these ideas mathematically, first consider the unit vector $\mathbf{r} = v\mathbf{i} + (u + s(v))\mathbf{j} + w\mathbf{k}$ whose differential is

$$\delta\mathbf{r} = \frac{\partial \mathbf{r}}{\partial v}\delta v + \frac{\partial \mathbf{r}}{\partial u}\delta u + \frac{\partial \mathbf{r}}{\partial w}\delta w = (\mathbf{i} + s'\mathbf{j})\delta v + \mathbf{j}\delta u + \mathbf{k}\delta w \equiv \sum_i \mathbf{e}_i \delta q_i \tag{2.4}$$

where $\delta q_i \equiv (\delta v, \delta u, \delta w)$ are the three co-ordinate differentials and

$$\mathbf{e}_1 = \mathbf{i} + s'\mathbf{j} \qquad \mathbf{e}_2 = \mathbf{j} \qquad \mathbf{e}_3 = \mathbf{k} \tag{2.5}$$

are basis vectors from which all contravariant components can be defined by $\mathbf{A} = \mathbf{e}_i \mathbf{A}^i$, summation convention applying.

As we are working in a non-orthogonal system of co-ordinates there exists a second, complimentary set of basis vectors satisfying the orthogonality condition $\mathbf{e}_i . \mathbf{e}^j = \delta_i^j$. From this condition we can find the vectors

$$\mathbf{e}^1 = \mathbf{i} \qquad \mathbf{e}^2 = \mathbf{j} - s'\mathbf{i} \qquad \mathbf{e}^3 = \mathbf{k} \tag{2.6}$$

from which all covariant components can be defined by $\mathbf{A} = \mathbf{e}^i A_j$. Note that the set $\mathbf{e}_1$, $\mathbf{e}^2$, $\mathbf{e}_3$ form a locally Cartesian system which aligns itself with the grating surface with $\mathbf{e}_1$ and $\mathbf{e}^2$ parallel and perpendicular to the surface, respectively. The corresponding set $\mathbf{e}^1$, $\mathbf{e}_2$, $\mathbf{e}^3$ are just the Cartesian basis vectors **i**, **j**, and **k**.

Since the triads $\mathbf{e}_i$ and $\mathbf{e}^i$ are not orthogonal $A^i \neq A_i$ : $i$=1,2. There are of course only three independent components and

$$\begin{aligned} A^1 &= CA_1 - DA^2 \\ A_2 &= DA_1 + CA^2 \\ A^3 &= A_3 \end{aligned} \tag{2.7}$$

where

$$C = \frac{1}{1+s'^2} \qquad D = s'C \qquad s' = \frac{ds}{dx} \tag{2.8}$$

### *2.4 Maxwell's equations in the new co-ordinate system*

Our aim is to write the two Maxwell curl equations $Curl\mathbf{E} = i\mathbf{H}$ and $Curl\mathbf{H} = -i\varepsilon_r \mathbf{E}$ in terms of the mixed field components $E_1$, $E^2$, $H_3$ for *p*-polarised light and $H_1$, $H^2$, $E^3$, for *s*-polarised light since these correspond to 'components' that are locally parallel and normal to the surface. They are defined by $E_1 = \mathbf{e}_1.\mathbf{E}$, $E^2 = \mathbf{e}^2.\mathbf{E}$, and $E_3 = \mathbf{e}_3.\mathbf{E}$, with similar relationships for the components of **H**. It should be noted that only the vectors $\mathbf{e}_3 = \mathbf{e}^3 = \mathbf{k}$ are normalised. Consequently, although it is convenient to formulate the equations in terms of $E_1$, $E^2$, $E_3$, and their magnetic counterparts, the actual field components of **E** in the directions defined by $\mathbf{e}_1$ and $\mathbf{e}^2$, are given by $E_1\left(1+s'^2\right)^{-\frac{1}{2}}$ and $E^2\left(1+s'^2\right)^{-\frac{1}{2}}$. Similar relations hold for the field components of **H**.

We start by noting that since $\nabla = \mathbf{e}^i \dfrac{\partial}{\partial q^i}$, $\mathbf{e}^i \wedge \mathbf{e}^j = \varepsilon_{ijk}\mathbf{e}_k$, and $\dfrac{\partial}{\partial v}\left(\mathbf{e}^2\right) = -s''\mathbf{e}^1$

$$Curl\mathbf{A} = \begin{vmatrix} \mathbf{e}_1 & \mathbf{e}_2 & \mathbf{e}_3 \\ \dfrac{\partial}{\partial v} & \dfrac{\partial}{\partial u} & \dfrac{\partial}{\partial w} \\ A_1 & A_2 & A_3 \end{vmatrix} \tag{2.9}$$

Even though the $\mathbf{e}_i$ are not orthogonal $\mathbf{e}^1.Curl\mathbf{A} = \dfrac{\partial A_3}{\partial u} - \dfrac{\partial A_2}{\partial w}$ etc. Thus taking the dot product of the two Maxwell equations with $\mathbf{e}^i$ : $i$=1,2,3 we arrive at six coupled equations

$$\left(\frac{\partial \mathrm{E}_3}{\partial \mathrm{u}} - \frac{\partial}{\partial w}\left(DE_1 + CE^2\right)\right) = iH^1 = i\left(CH_1 - DH^2\right) \tag{2.10}$$

$$\left(\frac{\partial E_1}{\partial \mathrm{w}} - \frac{\partial E_3}{\partial v}\right) = iH^2 \tag{2.11}$$

$$\left(\frac{\partial}{\partial v}\left(DE_1 + CE^2\right) - \frac{\partial E_1}{\partial \mathrm{u}}\right) = iH_3 \tag{2.12}$$

$$\left(\frac{\partial H_3}{\partial u} - \frac{\partial}{\partial w}\left(DH_1 + CH^2\right)\right) = -i\varepsilon_r E^1 = -i\varepsilon_r\left(CE_1 - DE^2\right) \tag{2.13}$$

$$\left(\frac{\partial H_1}{\partial \mathrm{w}} - \frac{\partial H_3}{\partial v}\right) = -i\varepsilon_r E^2 \tag{2.14}$$

$$\left(\frac{\partial}{\partial v}\left(DH_1 + CH^2\right) - \frac{\partial H_1}{\partial u}\right) = -i\varepsilon_r E_3 \tag{2.15}$$

Here unwanted components of the form $A^1$, $A_2$ and $A^3$ have been eliminated using (2.7).

The fact that we are constraining the incident beam to the saggital (Oxy) plane means that for a given polarisation there are only three non zero field vector components and the six equations (2.8-2.13) decouple leaving three equations.

For *p*-polarisation with **E**=($E_x$, $E_y$, 0) and **H**=(0, 0, $H_z$) these are

$$\left(\frac{\partial}{\partial v}\left(DE_1 + CE^2\right) - \frac{\partial E_1}{\partial u}\right) = iH_3 \tag{2.16}$$

$$\frac{\partial H_3}{\partial u} = -i\varepsilon_r\left(CE_1 - DE^2\right) \tag{2.17}$$

$$\frac{\partial H_3}{\partial v} = i\varepsilon_r E^2 \tag{2.18}$$

For *s*-polarisation, **E**=($E_x$, $E_y$, 0) and **H**=(0, 0, $H_z$), and we have

$$\frac{\partial E_3}{\partial u} = i\left(CH_1 - DH^2\right) \tag{2.19}$$

$$\frac{\partial E_3}{\partial v} = -iH^2 \tag{2.20}$$

$$\left(\frac{\partial}{\partial v}\left(DH_1 + CH^2\right) - \frac{\partial H_1}{\partial u}\right) = -i\varepsilon_r E_3 \tag{2.21}$$

Since it is the tangential components of E and H that are conserved across any material interface it is these that we want to retain. The normal components $E^2$ and $H^2$ can be eliminated to give two coupled equations for each polarisation. By using the notation $F=H_3$, $G=-\varepsilon E_1$ for *p*-polarisation and $F=E_3$, $G=H_1$ for *s*-polarisation we may write both sets of equations, that is (2.16-2.18) and (2.19-2.21) as

$$\frac{\partial F}{\partial u} = D\frac{\partial F}{\partial v} + iCG \tag{2.22}$$

$$\frac{\partial G}{\partial u} = \frac{\partial}{\partial v}\left(iC\frac{\partial F}{\partial v} + DG\right) + i\varepsilon F \tag{2.23}$$

### *2.5 Expansion of the fields in Bloch waves*

As mentioned in *Chapter 1* the periodic nature of the grating enables incident photons of transverse momentum $k_x$ to pick up multiples of the grating vector ***K***, and we have the familiar Bragg condition

$$k_x' = k_x + mK \tag{2.24}$$

where $k_x'$ denotes the photon's final $x$ - momentum. To put this on a more mathematical foundation I first consider the field to have derived its $x$ - momentum from two sources: the incident fields $x$ - momentum $\alpha_0 = (\varepsilon^1)^{1/2}\sin\theta$, and from the periodicity of the grating whereby the field can pick up or lose integer multiples of the Bragg momentum vector ***K***. With this in mind I write the field as (see p.13)

$$F(v,u) = F^p(v,u)\exp i\alpha_0 v \tag{2.25}$$

where $F^p$ reflects the periodicity of the grating and can be expanded in Fourier series

$$F^p(v,u) = \sum_n F_n(u)\exp inKv \tag{2.26}$$

so that finally we have the Bloch wave pseudo-periodic condition

$$F(v,u) = \sum_n F_n(u)\exp i\alpha_n v \tag{2.27}$$

where

$$\alpha_n = (\varepsilon')^{\frac{1}{2}} \sin\theta + nK \tag{2.28}$$

In addition we note that in equations (2.22) and (2.23) the grating profile only enters the problem through the pair of periodic functions $C$ and $D$ as defined in equation (2.15). These are expanded as Fourier series in the periodicity of the grating giving

$$C(v) = \sum_p C_p \exp ipKv \quad \text{and} \quad D(v) = \sum_p D_p \exp ipKv \tag{2.29}$$

We have already found a series expression for the fields in Eq. (2.27) whereby

$$F(v,u) = \sum_n F_n(u) \exp i\alpha_n v \quad \text{and} \quad G(v,u) = \sum_n G_n(u) \exp i\alpha_n v \tag{2.30}$$

Introducing these expansions for the profile of the grating surface, and for the fields into equations (2.22) and (2.23) individual coefficients of the fields F and G may be singled out by using orthogonality with $\exp i\alpha_m K$. This leads to a system of infinite coupled differential equations.

$$-i\frac{\partial F_n}{\partial u} = \sum_m \{\alpha_m D_{n-m} F_m + C_{n-m} G_m\} \tag{2.31}$$

$$-i\frac{\partial G_n}{\partial u} = \sum_m \{(-\alpha_n \alpha_m C_{n-m} + \varepsilon_r \delta_{nm}) F_m + \alpha_n D_{n-m} G_m\} \tag{2.32}$$

where $\delta_{nm}$ denotes the Kronecker delta function. In practice any calculation will limit the expansion of the field components ($F$ and $G$) to a range of $\pm N$ (typically values of $N$=5 up to $N$=10 are sufficient to ensure adequate convergence) in equations (2.31) and (2.32) giving 2(2$N$+1) terms.

We then write a new generalised field vector $\xi$ containing the expanded field components.

$$\xi(u)^T = (F_{-N}, \ldots, F_N, G_{-N}, \ldots, G_N) \qquad \text{for TE polarisation} \tag{2.33}$$

$$\xi(u)^T = \left( F_{-N}, \ldots, F_N, {}^{G_{-N}}\!/_{\varepsilon_r}, \ldots, {}^{G_N}\!/_{\varepsilon_r} \right) \quad \text{for TM polarisation} \tag{2.34}$$

where the permittivity $\varepsilon_r$ is that of the layer in question. With these restrictions equations (2.31) and (2.32) can be written as an eigenvalue equation.

$$-i\frac{\partial \xi(u)}{\partial u} = \mathbf{T}\xi(u) \tag{2.35}$$

where **T** is a 2(2$N$+1) square matrix constructed from four 2$N$+1 square submatrices reflecting the strength of scattering between the various orders. For TE polarised light this matrix can be written as

$$\mathbf{T} = \begin{bmatrix} \alpha_m D_{n-m} & C_{n-m} \\ -\alpha_n \alpha_m C_{n-m} + \varepsilon_r \delta_{nm} & \alpha_n D_{n-m} \end{bmatrix} \tag{2.36}$$

While For TM polarised light it takes the form

$$\mathbf{T} = \begin{bmatrix} \alpha_m D_{n-m} & \varepsilon_r C_{n-m} \\ \dfrac{-\alpha_n \alpha_m C_{n-m}}{\varepsilon_r} + \delta_{nm} & \alpha_n D_{n-m} \end{bmatrix} \tag{2.37}$$

so that for TM polarised light equation (2.37) can be written in full as

$$-i\frac{\partial}{\partial u}\begin{pmatrix} F_{-N} \\ \cdot \\ F_N \\ - \\ G_{-N}/\varepsilon_r \\ \cdot \\ G_N/\varepsilon_r \end{pmatrix} = \begin{bmatrix} \alpha_m D_{n-m} & \varepsilon_r C_{n-m} \\ & \\ \dfrac{-\alpha_n \alpha_m C_{n-m}}{\varepsilon_r} + \delta_{nm} & \alpha_n D_{n-m} \end{bmatrix} \begin{pmatrix} F_{-N} \\ \cdot \\ F_N \\ - \\ G_{-N}/\varepsilon_r \\ \cdot \\ G_{-N}/\varepsilon_r \end{pmatrix} \qquad (2.38)$$

The matrix **T** is constant in each medium and so the truncated equations have eigensolutions of the form $\mathbf{V}^q \exp ir_q u$. The field vector ξ(u) may then be expanded as a linear combination of these

$$\xi(u) = \sum_{q=1}^{2N+1} b_q \mathbf{V}_q \exp ir_q u \qquad (2.39)$$

where $r_q$ are the eigenvalues of the matrix **T**, $\mathbf{V}_q$ the eigenvectors, and $b_q$ the amplitude associated with the $q^{\text{th}}$ eigenmode. Note that for a given eigenmode the corresponding eigenvector gives the relative field strengths while the eigenvalue gives us the spatial dependence. Finally using the above we may state the form of $\xi(u)$ in the $j^{\text{th}}$ medium.

$$\xi^j(u) = \mathbf{M}^j \phi^j(u) \mathbf{b}^j \qquad (2.40)$$

where $\mathbf{M}^j$ is a matrix whose columns are the eigenvectors of $\mathbf{T}^j$, $\phi^j$ is a square matrix with elements $\phi^j_{qp} = \delta_{qp} \exp ir^j_q u$ , and $\mathbf{b}^j$ is a vector of amplitude coefficients which need to be determined in order to define the field in each medium. Although the co-ordinate transformation used in each medium is the same, the matrix **M** varies from medium to medium because of the dependence of **T** upon $\varepsilon_r$, hence the eigensolutions depend upon the changing values of $\varepsilon_r$.

In any one medium $\xi$ contains an equal number of upward and downward propagating waves some of which are real and some of which are evanescent. The $u$ dependence of these waves is characterised by the eigenvalues $r_q$ since $\xi(u) \sim \exp ir_q u$. To put this in perspective table 2.1 shows a set of eigenvalues calculated for a typical grating profile.

| Type | Real part | Imaginary part |
|---|---|---|
| Bragg | -0.9567230201886436 | -3.6552118651983229E-16 |
| | -0.8660254037121197 | -9.8800169280092556E-16 |
| | 0.9567230202363647 | 2.4482325160801449E-15 |
| | 0.8660254036300796 | -1.3249493331105796E-15 |
| Evanescent | -7.0289674577672518E-11 | 2.505048370007350 |
| | -7.0287640692818362E-11 | -2.505048370007346 |
| | 1.6464996022195497E-10 | -1.568443280496440 |
| | 1.6465020828101449E-10 | 1.568443280496439 |
| | -1.6253307171190806E-10 | 1.827930568618574 |
| | -1.6254340510979531E-10 | -1.827930568618577 |
| | 8.8728577120402290E-11 | -0.4131876987660740 |
| | 8.8728497381840832E-11 | 0.4131876987660735 |
| | -1.0585680853740256E-10 | 0.8165053228582656 |
| | -1.0585680853845024E-10 | -0.8165053228582653 |
| Truncation | -0.8548866924132034 | 2.920870533166090 |
| | 0.8548866936083748 | 2.920870533927917 |
| | -0.5312678563844827 | 2.211998264949311 |
| | 0.5312678556152906 | 2.211998264395520 |
| | 0.8548866936083560 | -2.920870533927908 |
| | -0.8548866924131892 | -2.920870533166081 |
| | 0.5312678556152994 | -2.211998264395531 |
| | -0.5312678563844968 | -2.211998264949309 |

**Table 2.1:** A typical set of eigenvalues

There are three distinct groups within the whole set. First note the subset of real waves with $\mathrm{Im}(r_q)=0$ - propagating upwards if $\mathrm{Re}(r_q)>0$ and downwards if $\mathrm{Re}(r_q)<0$. Secondly there are evanescent waves bound to the dielectric interfaces which are planes of constant u. For these waves $\mathrm{Re}(r_q)=0$ so that the field does not propagate in the u direction but falls off exponentially according to $\exp\left(-\mathrm{Im}\left(r_q\right)u\right)$ - upward decaying waves have $\mathrm{Im}(r_q)<0$ while those decaying downward have $\mathrm{Im}(r_q)>0$. Finally there are so called truncation terms having both real and imaginary parts of the order of unity. These do not correspond directly to physical waves but are an artefact of the numerical calculation which must consider a truncated set of equations rather than the infinite set which exist in reality.

By using the eigenvalues in this way the diffracted orders within $\xi$ are sorted as follows

$$\xi = \left[\begin{array}{ccccccc} & \cdot & & | & & \cdot & \\ & \cdot & & | & & \cdot & \\ & \cdot & & | & & \cdot & \\ \mathbf{REAL+} & \cdot & \mathbf{EVAN+} & | & \mathbf{REAL-} & \cdot & \mathbf{EVAN-} \\ & \cdot & & | & & \cdot & \\ & \cdot & & | & & \cdot & \\ & \cdot & & | & & \cdot & \end{array}\right] \left[\begin{array}{ccccc} \cdot & & & & \\ & \phi_{qq} & & & \\ & & \cdot & & \\ \cdot & & \cdot & / & \\ & & & \cdot & \\ & & & & \cdot \\ & & & & \cdot \end{array}\right] \left[\begin{array}{c} \mathbf{b}_+ \\ - \\ \mathbf{b}_- \end{array}\right]$$

where + denotes upward propagation and - denotes downward propagation. (For reasons that will be described later the real waves are further sorted into ascending Bragg order)

### *2.6 Internal boundary conditions*

The internal boundary conditions at the interface require that the tangential components of **E** and **H** are continuous, which is equivalent to the matching condition $\xi^{j-1}(u=0)=\xi^{j}(u=0)$ at the interface.

### *2.7 Method of solution*

We must now consider the overall scheme used to solve the problem, in which we will impose outgoing wave conditions on the far field. Figure 2.2 shows schematically the effect of radiation incident on the sample:

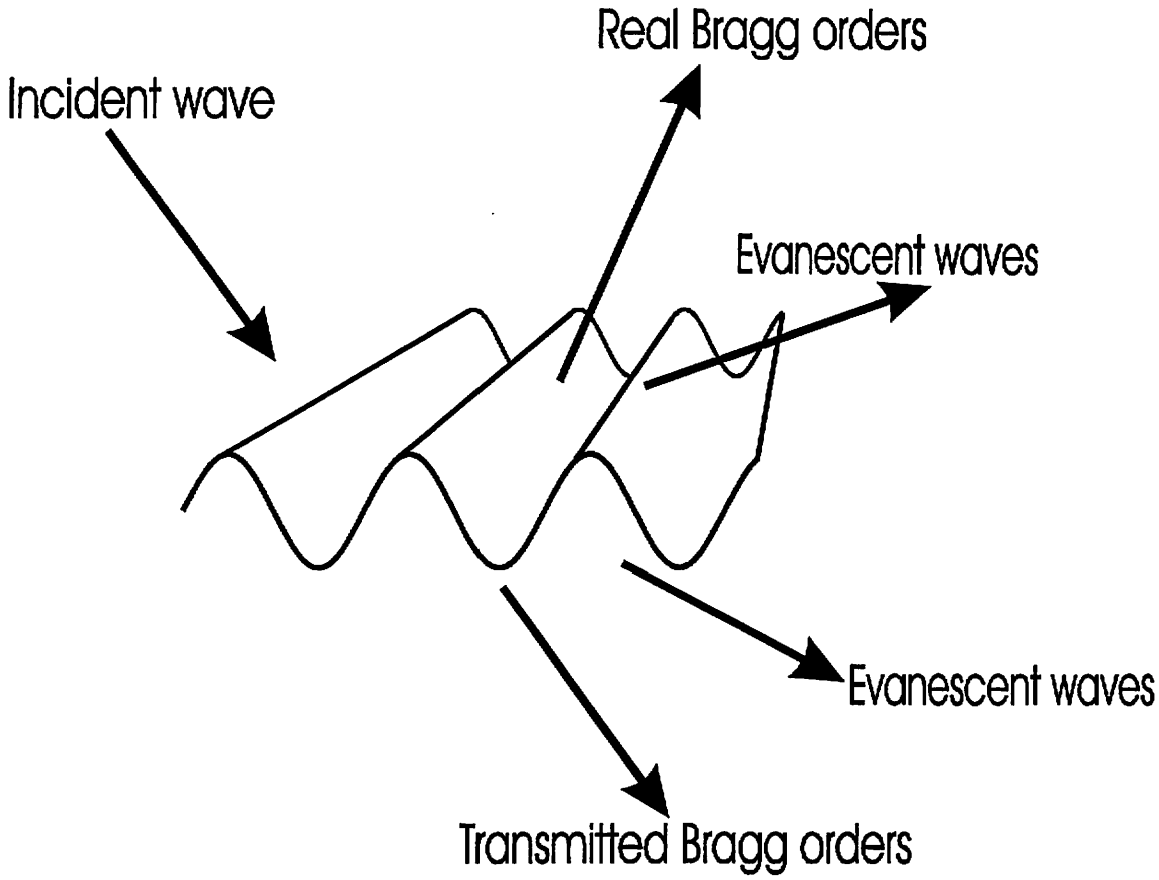

**Figure 2.2:** The various electromagnetic waves caused by the incident radiation

The disturbance on the uppermost interface is due to the incident plane wave, reflected Bragg modes, which are also plane waves, and evanescent fields which are surface waves bound to the grating interface, and decay with increasing $y$ into medium 1.

The disturbance just below the lowest interface is due to transmitted Bragg modes and evanescent fields which decay with decreasing y into medium 0.

Using boundary conditions described in *section 2.6* to match the two enables the complex amplitudes of the reflected and transmitted Bragg modes to be determined, and hence the reflectivities $R_n$ and transmissivities $T_n$.

The incident field is written as a plane wave of unit amplitude which 'primes' the system. We now impose the outgoing wave condition in medium 1 that all propagating diffracted waves must travel upwards, that is the direction of increasing y, and all evanescent modes must decay in the same direction. This is done by explicitly writing the propagating diffracted waves as upward going plane waves, and writing the evanescent waves in eigenmode form such that only modes decaying with increasing y have non-zero amplitudes ( $\mathbf{b}_-^1 = 0$ ). A similar scheme is used in medium 0.

### *2.8 Asymptotic field expansions*

We shall from now on restrict the discussion to TM polarised incident light to tie in with later anisotropic work.

### *2.8.1 Incident field*

The incident beam is defined to be a plane wave with transverse $H_z$ field of amplitude unity so that we may write

$$F^i = \exp ik(x\sin\theta - y\cos\theta) = \exp i(\alpha_0 x - \beta_0 y) \qquad (2.41)$$

where $\beta^0 = (\varepsilon^1 - \alpha_0^2)^{1/2}$. We now require the form of these fields in the transformed co-ordinates, that is in terms of $v$, $u$, and $w$ so that

$$F^i = \exp i\alpha_0 v.\exp(-i\beta_0 u).\exp(-i\beta_0 s(v)) \qquad (2.42)$$

By Fourier expanding in the $v$ variable this may be written in a form consistent with eq. (2.40)

$$F^i = \sum_m L_m(\beta_0)\exp i(\alpha_m v - \beta_0 u) \tag{2.43}$$

where

$$L_m(t) = \frac{1}{\lambda_g}\int_0^{\lambda_g} \exp -i(s(v)t + mKv)dv \tag{2.44}$$

so that the field's $v$ dependence is expressed as a sum over plane waves of momenta $\alpha_m$. The corresponding expression for $G$ is found after substitution into eq. (2.23). To achieve this I first derive two useful expressions from eq. (2.42)

$$\frac{\partial F^i}{\partial u} = -i\beta_0 F^i \tag{2.45}$$

and

$$\frac{\partial F^i}{\partial v} = i(\alpha_0 - \beta_0 s')F^i \tag{2.46}$$

which can be substituted into a re-arranged eq. (2.22):

$$iG^i = \frac{1}{C}\left(\frac{\partial F^i}{\partial u} - D\frac{\partial F^i}{\partial v}\right) = (1+s'^2)\frac{\partial F^i}{\partial u} - s'\frac{\partial F^i}{\partial v} \tag{2.47}$$

to give

$$G^i = -(\beta_0 + \alpha_0 s')F^i \tag{2.48}$$

writing $\alpha_0 s' F^i = \left(\frac{\alpha_0}{\beta_0}\right)\beta_0 s' F^i$ the $s'$ dependence can be removed since equations (2.43,46) give

$$i\beta_0 s' F^i = i\alpha_0 F^i - \frac{\partial F^i}{\partial v} = \sum_m i(\alpha_0 - \alpha_m) L_m(\beta_0) \exp i(\alpha_m v - \beta_0 u) \tag{2.49}$$

When substituted back into eq. (2.48) this gives the required form of $G^i$

$$G^i = -\sum_m \left(\beta_0 - \left(\frac{\alpha_0}{\beta_0}\right) mK\right) L_m(\beta_0) \exp i(\alpha_m v - \beta_0 u) \tag{2.50}$$

which like $F^i$ is now written as a sum over plane waves of momenta $\alpha_m$.

### *2.8.2 Propagating diffracted field*

For a single frequency component $\mathbf{E}(\mathbf{r},t) = \mathbf{E}(\mathbf{r})\exp(-i\omega t)$ the time - independent Maxwell equations are

$$Curl\mathbf{E} = i\omega\mathbf{B} \tag{2.51}$$

$$Curl\mathbf{H} = \mathbf{j} - i\omega\mathbf{D} \tag{2.52}$$

$$div\mathbf{D} = \rho \tag{2.53}$$

$$div\mathbf{B} = 0 \tag{2.54}$$

If in some region R there is neither free charge nor free current ( $\rho=0$, $\mathbf{j}=0$ ) and if $\varepsilon$ is constant throughout R then taking the curl of Eq. (2.51)

$$CurlCurl\mathbf{E} = i\omega\mu_0 Curl\mathbf{H} \tag{2.55}$$

$$-\nabla^2\mathbf{E} + grad(div\mathbf{E}) = i\omega\mu_0 Curl\mathbf{H} \tag{2.56}$$

But from Eq. (2.53) divE is zero and from Eq. (2.52) CurlH can be expressed in terms of E so that finally E is seen to satisfy the Helmholtz equation

$$\nabla^2\mathbf{E} + k^2\mathbf{E} = 0 \tag{2.57}$$

where

$$k^2 = \varepsilon_r\varepsilon_0\mu_0\omega^2 \tag{2.58}$$

Likewise starting from Eqs (2.51,52,54) it can be shown that H satisfies a similar equation

$$\nabla^2\mathbf{H} + k^2\mathbf{H} = 0 \tag{2.59}$$

If $y>\max[s(x)]$ then **F** satisfies the Helmholtz equation $\nabla^2\mathbf{F} + k^2\mathbf{F} = 0$ and substituting eq. (2.27) we have

$$\sum_n \left[ \frac{d^2F_n}{dy^2} + \left(k^2 - \alpha_n^2\right)F_n \right] \exp i\alpha_n x = 0 \tag{2.60}$$

The left hand side of the equation may be regarded as the Fourier expansion of the null function which implies that for any value of the integer $n$

$$\frac{d^2F_n}{dy^2} + \left(k^2 - \alpha_n^2\right)F_n = 0 \tag{2.61}$$

with general solution

$$F_n(y) = A_n \exp(-i\beta_n y) + B_n \exp i\beta_n y \tag{2.62}$$

where

$$\beta_n = \left(k^2 - \alpha_n^2\right)^{1/2} \tag{2.63}$$

However the outgoing wave condition on the diffracted field in the upper halfspace implies that $A_n$=0 as this second term would represent an incoming wave for real $\beta_n$ and would not be bounded for imaginary $\beta_n$. Finally from eqs. (2.27,2.52), above the grooves when $y$>max[$s(x)$] the diffracted field can be represented asymptotically by a plane wave expansion over the various Bragg orders called the Rayleigh expansion.

$$F^d = \sum_n R_n \exp i(\alpha_n x + \beta_n y) \tag{2.64}$$

(where I have replaced $B_n$ with $R_n$ for reflection), reflecting the ability of the diffracted field to pick up integer multiples of the Bragg momentum vector $K$. For our purposes we only require propagating waves to be described in this way and so we limit the summation so that $n \in U$: $|\alpha_n| < \varepsilon_r^{1/2}$, and $\beta_n$ is real. If eq. (2.64) is written in terms of the co-ordinates $v$,$u$, and $w$,

$$F^d = \sum_{n\in U} R_n \exp i\alpha_n v . \exp i\beta_n u . \exp i\beta_n s(v), \tag{2.65}$$

and expanded as a Fourier series over plane waves of momenta $\alpha_m$ as per the Bloch field expansion

$$\begin{aligned} &\text{then} \quad F^d = \sum_m F_m^d \exp i\alpha_m v \\ &\text{where} \quad F_m^d = \frac{1}{\lambda_g} \int_0^{\lambda_g} \sum_{n\in U} R_n \exp i(n-m)Kv . \exp i\beta_n s(v) dv . \exp i\beta_n u \end{aligned} \tag{2.66}$$

Hence

$$F^d = \sum_m \frac{1}{\lambda_g} \int_0^{\lambda_g} \sum_{n \in U} R_n \exp i(n-m)Kv . \exp i\beta_n s(v) dv . \exp i\alpha_m v . \exp i\beta_n u \tag{2.67}$$

giving the required expansion for the diffracted field

$$F^d = \sum_n R_n \sum_m L_{m-n}(-\beta_n) \exp i(\alpha_m v + \beta_n u) \tag{2.68}$$

with each diffracted order expanded as a sum over plane waves of momenta $\alpha_m$. In a similar manner to that described for the incident field, $G^d$ can be obtained via substitution into eq. (2.22)

$$G^d = \sum_n R_n \sum_m \left( \beta_n - (m-n)K\left( \frac{\alpha_n}{\beta_n} \right) \right) L_{m-n}(-\beta_n) \exp i(\alpha_m v + \beta_n u) \tag{2.69}$$

## *2.9 Final Equations*

### *2.9.1 Reflection calculations*

The boundary calculation in *section 2.6* related field components derived solely from the eigenvalue expansion (2.40). Now in the top medium alone we wish to express the field components in a different way: the evanescent field is still expanded as a sum of eigenmodes but the incident and real diffracted field is now replaced by plane wave expansions represented in co-ordinates *u,v,w*. If we are to combine these two formalisms we must be sure that in both cases the field components within $\xi$ are stacked in the same order. To ensure this the eigenvalue generated field vectors were arranged with the real field components sorted in ascending Bragg order. We may then order the transformed Rayleigh expansion in the same way.

Equations (2.43) and (2.50) describe the incident field in the transformed co-ordinates and these now need to be written in the same form as the $\xi$ field vector. Comparing these equations with the Bloch field expansions $F=\sum_m F_m \exp i\alpha_m v$ and $G=\sum_m G_m \exp i\alpha_m v$ and noting that $\xi^T = \left(F_m, {G_m}/{\varepsilon_r}\right)$ we can write

$$\xi^i = \mathbf{L}\exp(-\mathrm{i}\,\beta_0 u) \equiv \begin{bmatrix}\mathbf{L}' \\ \mathbf{L}''/\varepsilon_r^1\end{bmatrix}\exp(-i\beta_0 u) \tag{2.70}$$

where $\mathbf{L}'$ and $\mathbf{L}''$ are column vectors containing

$$L_m(\beta_0) \quad \text{and} \quad \frac{1}{\varepsilon_r^1}\left[\beta_0 - \frac{\alpha_n}{\beta_n} mK\right] L_m(\beta_0) \tag{2.71}$$

respectively.

The diffracted field is represented in the transformed space by equations (2.68) and (2.69). Again comparison with the Bloch field expansions shows that

$$\xi^d = \mathbf{M}'\phi'(u)\mathbf{R} \equiv \begin{bmatrix}\mathbf{M}'' \\ \mathbf{M}'''/\varepsilon_r^1\end{bmatrix}\phi'(u)\mathbf{R} \tag{2.72}$$

where $\mathbf{M}''$ and $\mathbf{M}'''$ are two $P$ by $2N$+1 matrices containing

$$L_{m-n}(-\beta_n) \quad \text{and} \quad \frac{1}{\varepsilon_r^1}\left[\beta_n - (m-n)\frac{\alpha_n}{\beta_n} K\right] L_{m-n}(-\beta_n) \tag{2.73}$$

respectively, and $\phi'(u)$ is a diagonal matrix of size $P$ with elements $\exp(i\beta_n u).\delta_{nm}$.

So in the top medium we leave the evanescent fields as an expansion over the eigenmodes of the system but re-express the incident and real diffracted fields in terms of plane wave expansions. The outgoing wave condition in this medium requires the diffracted field to propagate upward and remain finite as $y \to \infty$. For the real diffracted orders this has been taken care of in our choice of equation (2.64) to represent these fields. For the evanescent waves the condition is met by setting

$$\mathbf{b}^1_- = \mathbf{0} \tag{2.74}$$

The field in the top medium is then given by

$$\mathbf{M}^1\phi^1(u)\begin{pmatrix}\mathbf{b}^1_+\\ \mathbf{0}\end{pmatrix} + \begin{pmatrix}\mathbf{L}'\\ \mathbf{L}''/\varepsilon^1_r\end{pmatrix}\exp(-i\beta_0 u) + \begin{pmatrix}\mathbf{M}''\\ \mathbf{M}'''/\varepsilon^1_r\end{pmatrix}\phi'(u)\mathbf{R}_n \tag{2.75}$$

where the first term now contains only those elements corresponding to the upward evanescent field.

We now combine the evanescent and real diffracted terms, on the uppermost interface. Here, $u$=0 so that the two terms in $\phi$ equate to unity and

$$\mathbf{M}^1\phi^1(u)\begin{pmatrix}\mathbf{b}^1_+\\ \mathbf{0}\end{pmatrix} + \begin{pmatrix}\mathbf{M}''\\ \mathbf{M}'''/\varepsilon^1_r\end{pmatrix}\phi'(u)\mathbf{R}_n \tag{2.76}$$

becomes

$$\left(\begin{array}{cc|c} \mathbf{0} & \mathbf{M}^1_{11} & \mathbf{M}^1_{12} \\ \hline \mathbf{0} & \mathbf{M}^1_{21} & \mathbf{M}^1_{22} \end{array}\right)\left(\begin{array}{c} \mathbf{0} \\ \mathbf{b}^1_+ \\ \hline \mathbf{0} \\ \mathbf{0} \end{array}\right) + \left(\begin{array}{c} \mathbf{M}'' \\ \hline \mathbf{M}'''/\varepsilon^1_r \end{array}\right)\left(\begin{array}{c} \mathbf{R}_n \\ \mathbf{0} \\ \hline \mathbf{0} \\ \mathbf{0} \end{array}\right)$$

$$= \left(\begin{array}{cc|c} \mathbf{M}'' & \mathbf{M}^1_{11} & \mathbf{M}^1_{12} \\ \hline \mathbf{M}'''/\varepsilon^1_r & \mathbf{M}^1_{21} & \mathbf{M}^1_{22} \end{array}\right)\left(\begin{array}{c} \mathbf{R}_n \\ \mathbf{b}^1_+ \\ \hline \mathbf{0} \\ \mathbf{0} \end{array}\right) \equiv \hat{\mathbf{M}}^1\begin{pmatrix}\hat{\mathbf{R}}\\ \mathbf{0}\end{pmatrix} \tag{2.77}$$

where we have defined a new matrix $\hat{\mathbf{M}}^1$ and the vector $\hat{\mathbf{R}} = \begin{pmatrix} \mathbf{R}_n \\ \mathbf{b}_+^1 \end{pmatrix}$ contains the coefficients of the real and evanescent diffracted fields in the uppermost medium.

So we now have two equivalent representations of the field in the top medium and we equate these on the uppermost interface

$$\begin{pmatrix} \mathbf{M}_{11}^1 & \mathbf{M}_{12}^1 \\ \mathbf{M}_{21}^1 & \mathbf{M}_{22}^1 \end{pmatrix} \begin{pmatrix} \mathbf{b}_+^1 \\ \mathbf{b}_-^1 \end{pmatrix} = \begin{pmatrix} \hat{\mathbf{M}}_{11}^1 & \hat{\mathbf{M}}_{12}^1 \\ \hat{\mathbf{M}}_{21}^1 & \hat{\mathbf{M}}_{22}^1 \end{pmatrix} \begin{pmatrix} \hat{\mathbf{R}} \\ \mathbf{0} \end{pmatrix} + \begin{pmatrix} \mathbf{L}' \\ \mathbf{L}'' / \varepsilon_r^1 \end{pmatrix} \tag{2.78}$$

Boundary conditions described in *section 2.6* tell us that

$$\begin{pmatrix} \mathbf{M}_{11}^1 & \mathbf{M}_{12}^1 \\ \mathbf{M}_{21}^1 & \mathbf{M}_{22}^1 \end{pmatrix} \begin{pmatrix} \mathbf{b}_+^1 \\ \mathbf{b}_-^1 \end{pmatrix} = \begin{pmatrix} \mathbf{M}_{11}^0 & \mathbf{M}_{12}^0 \\ \mathbf{M}_{21}^0 & \mathbf{M}_{22}^0 \end{pmatrix} \begin{pmatrix} \mathbf{b}_+^0 = 0 \\ \mathbf{b}_-^0 \end{pmatrix} \tag{2.79}$$

So that we arrive at two equations

$$\mathbf{M}_{12}^0 \mathbf{b}_-^0 = \hat{\mathbf{M}}_{11}^1 \hat{\mathbf{R}} + \mathbf{L}' \tag{2.80}$$

$$\mathbf{M}_{22}^0 \mathbf{b}_-^0 = \hat{\mathbf{M}}_{21}^1 \hat{\mathbf{R}} + \mathbf{L}'' / \varepsilon_r^1 \tag{2.81}$$

Solving then gives

$$\mathbf{b}_-^0 = \left(\mathbf{M}_{22}^0\right)^{-1} \left( \hat{\mathbf{M}}_{21}^1 \hat{\mathbf{R}} + \mathbf{L}'' / \varepsilon_r^1 \right) \tag{2.82}$$

$$\hat{\mathbf{R}} = \left(\hat{\mathbf{M}}_{11}^1 - \mathbf{A}\hat{\mathbf{M}}_{21}^1\right) \left( \mathbf{A}\mathbf{L}'' / \varepsilon_r^1 + \mathbf{L}' \right) \qquad \mathbf{A} = \mathbf{M}_{12}^0 \left(\mathbf{M}_{22}^0\right)^{-1} \tag{2.83}$$

with the $n^{\text{th}}$ order reflection efficiency given by

$$e_n^r = (\mathbf{R}_n)^* \mathbf{R}_n \frac{\cos\theta_n^r}{\cos\theta} \tag{2.84}$$

where $n$ specifies that row corresponding to the $n^{\text{th}}$ propagating order and $\cos\theta_n^r = \frac{\beta_n}{(\varepsilon^1)^{1/2}}$ is the angle that order makes with the $y$-axis.

### *2.9.2 Transmission calculations*

In a method completely analogous to that for reflection, in the bottom medium we separate the real diffracted beams from the evanescent fields so as to obtain a second description of the field with real waves represented by the plane wave expansion appropriate to the lower medium. Outgoing wave conditions in this medium imply no upward propagating waves in the form of equation (2.64) appropriate to medium 0 giving the plane wave expansion for transmitted orders

$$F^t = \sum_n T_n \exp i(\alpha_n x - \beta_n^0 y) \tag{2.85}$$

along with a similar expression for $G^t$. For both fields the summation is taken over the subset of real waves $n \in U^0$, where $U^0$ is the set of integers such that $|\alpha_n| < (\varepsilon^0)^{1/2}$.

The $v$, $u$ space representation of these fields proceeds in exactly the same manner as for those reflected giving

$$F^t = \sum_{n\in U^0} T_n \sum_m L_{m-n}(\beta_n^0) \exp i(\alpha_m v - \beta_n^0 u) \tag{2.86}$$

and

$$G^t = \sum_{n\in U^0} T_n \sum_m \left(\beta_n^0 - (m-n)\frac{\alpha_n}{\beta_n^0}K\right) L_{m-n}(\beta_n^0) \exp i(\alpha_m v - \beta_n^0 u) \tag{2.87}$$

$$\text{where } L_m(t) = \frac{1}{\lambda_g}\int_0^{\lambda_g} \exp -i(s(v)t + mKv)dx \tag{2.88}$$

We write these in the same form as the $\xi$ field vector by comparison with the Bloch field expansions $F = \sum_m F_m \exp i\alpha_m v$ and $G = \sum_m G_m \exp i\alpha_m v$. Remembering that $\xi^T = \left(F_m, {}^{G_m}\!/_{\varepsilon_r}\right)$ we can write

$$\xi' = \mathbf{M}'^0 \phi'^0(u)\mathbf{T}_n \equiv \begin{bmatrix} \mathbf{M}''^0 \\ \mathbf{M}''^0 / \varepsilon_r^0 \end{bmatrix} \phi'^0(u)\mathbf{T}_n \tag{2.89}$$

where $\mathbf{M}''^0$ and $\mathbf{M}'''^0$ are $P_0$ by $2N$+1 matrices containing

$$L_{m-n}\left(\beta_n^0\right) \text{ and } \frac{1}{\varepsilon_\mathrm{r}^0}\left[\beta_n^0 - (m-n)\frac{\alpha_n}{\beta_n^0}K\right] L_{m-n}\left(\beta_n^0\right) \tag{2.90}$$

respectively, and $\phi'^0(u)$ is a diagonal matrix with elements $\exp i\beta_n^0 u.\delta_{nm}$.

So as for reflection we leave the evanescent fields as an expansion over the eigenmodes of the system but re-express the real transmitted field in terms of the plane wave expansions (2.88) and (2.89). The outgoing wave condition in the bottom medium requires the total field to propagate downward and remain finite as $y \to -\infty$. For the real transmitted field this has been taken care of in the appropriate plane wave expansion (2.46). For the evanescent waves the condition is met by setting

$$\mathbf{b}_+^0 = \mathbf{0} \tag{2.91}$$

We now combine the eigenmode generated evanescent terms with the plane wave representation of the real fields. As the phase of fields in the bottom medium is defined to be zero on the interface we can write the two terms in question as

$$\mathbf{M}^0 \begin{pmatrix} \mathbf{0} \\ \mathbf{b}_-^0 \end{pmatrix} + \begin{pmatrix} \mathbf{M}''^0 \\ \mathbf{M}'''^0 / \varepsilon_r^0 \end{pmatrix} \mathbf{T}_n \equiv$$

$$\left(\begin{array}{c|cc} \mathbf{M}^0_{11} & \mathbf{0} & \mathbf{M}^0_{12} \\ \hline \mathbf{M}^0_{21} & \mathbf{0} & \mathbf{M}^0_{22} \end{array}\right)\begin{pmatrix}\mathbf{0}\\ \mathbf{0}\\ -\\ \mathbf{0}\\ \mathbf{b}^0_-\end{pmatrix} + \left(\begin{array}{c} {}^0\mathbf{M}'' \\ \hline {}^0\mathbf{M}'''\big/\varepsilon_r^0 \end{array}\right)\begin{pmatrix}\mathbf{0}\\ \mathbf{0}\\ -\\ \mathbf{T}_n\\ \mathbf{0}\end{pmatrix} \tag{2.92}$$

which we now combine in one matrix

$$\left(\begin{array}{c|cc} \mathbf{M}^0_{11} & \mathbf{M}''^0 & \mathbf{M}^0_{12} \\ \hline \mathbf{M}^0_{21} & \mathbf{M}'''^0\big/\varepsilon_r^0 & \mathbf{M}^0_{22} \end{array}\right)\begin{pmatrix}\mathbf{0}\\ \mathbf{0}\\ -\\ \mathbf{T}_n\\ \mathbf{b}^0_-\end{pmatrix} \equiv \hat{\mathbf{M}}^0\begin{pmatrix}\mathbf{0}\\ \hat{\mathbf{T}}\end{pmatrix} \tag{2.93}$$

where as in the top medium $\hat{\mathbf{M}}^0$ is a new matrix representing the evanescent field by an eigenmode expansion and the real field by the *v*, *u* space Rayleigh expansion. The vector $\hat{\mathbf{T}} = \begin{pmatrix}\mathbf{T}_n\\ \mathbf{b}^0_-\end{pmatrix}$ contains the coefficients of the real and evanescent transmitted fields.

As in medium 1 we now have two equivalent representations of the field in the bottom medium and we equate these on the interface

$$\begin{pmatrix}\mathbf{M}^0_{11} & \mathbf{M}^0_{12}\\ \mathbf{M}^0_{21} & \mathbf{M}^0_{22}\end{pmatrix}\begin{pmatrix}\mathbf{0}\\ \mathbf{b}^0_-\end{pmatrix} = \begin{pmatrix}\hat{\mathbf{M}}^0_{11} & \hat{\mathbf{M}}^0_{12}\\ \hat{\mathbf{M}}^0_{21} & \hat{\mathbf{M}}^0_{22}\end{pmatrix}\begin{pmatrix}\mathbf{0}\\ \hat{\mathbf{T}}\end{pmatrix} \tag{2.94}$$

and using the $\mathbf{b}_-^0$ vector calculated during reflection calculations we finally arrive at an expression for the transmitted field amplitudes

$$\begin{pmatrix}\mathbf{0}\\ \hat{\mathbf{T}}\end{pmatrix} = \begin{pmatrix}\hat{\mathbf{M}}^0_{11} & \hat{\mathbf{M}}^0_{12}\\ \hat{\mathbf{M}}^0_{21} & \hat{\mathbf{M}}^0_{22}\end{pmatrix}^{-1}\begin{pmatrix}\mathbf{M}^0_{11} & \mathbf{M}^0_{12}\\ \mathbf{M}^0_{21} & \mathbf{M}^0_{22}\end{pmatrix}\begin{pmatrix}\mathbf{0}\\ \mathbf{b}^0_-\end{pmatrix} = \begin{pmatrix}\mathbf{I} & \mathbf{0}\\ \mathbf{0} & \mathbf{Q}\end{pmatrix}\begin{pmatrix}\mathbf{0}\\ \mathbf{b}^0_-\end{pmatrix} \tag{2.95}$$

from which

$$\hat{\mathbf{T}} = \mathbf{Q}\mathbf{b}_{-}^{0} \qquad (2.96)$$

The $n^{\text{th}}$ order transmission efficiency is then given by

$$e_n^t = (T_n)^*(T_n)\frac{\cos\theta_n^t}{\cos\theta} \qquad (2.97)$$

where $n$ specifies that row corresponding to the $n^{\text{th}}$ propagating order which makes an angle $\cos\theta_n^t = \frac{\beta_n^0}{(\varepsilon_r^0)^{1/2}}$ with the $y$ axis.

## *2.10 Testing the computer code*

Details of how the formalism was implemented as a computer code may be found in appendix A. Here I will only point out a number of fundamental tests that any grating model must pass before further investigation can take place.

The first and most obvious test is to make the grating flat and check that the code agrees with planar optics.

A second more subtle test is the energy balance criterion. Given an incident field, the proportion of energy carried in the $n^{\text{th}}$ reflected order is given by equation (2.84), while the corresponding expression for the transmitted orders must take into account the different medium in which they are propagating and is given by (2.97). The energy balance criterion tells us that the energy carried in all the diffracted orders must equate to the energy carried in the incident beam. Mathematically $\sum_{n\in U} e_n^r + \sum_{n\in U^0} e_n^t = 1$ provides us with a self consistent test of the theory, given that there is no absorption in the system.

The last condition we can test is the reciprocity theorem [Maystre, 1984].

## *2.11 Numerical examples*

The power of the Chandezon technique lies in its simplicity: The simplest theories are naturally the easiest to code and often the least computationally intensive. These features are essential if a robust, workable computer code is required.

Despite this we can model deep gratings rigorously with Chandezon's technique. Naturally the formalism lends itself to certain grating configurations whose response can be calculated with relative ease - these are in fact the subset of gratings whose profile is sinusoidal.

To model a square grating for example we would find ourselves dealing with a number of quite significant higher order harmonics in the necessary Fourier expansion of the grating profile producing significant scattering to higher orders. The size of the truncation parameter $M$ must be such that that all essential information is included in the set of equations we retain - the result being that we need to keep more equations to cover the range of appreciable scattered orders. This in turn takes more time computationally.

Traditionally integral and modal methods have been used for such systems, although the convergence of the solution often depends on delicate tweaking of the numerical techniques used. The advantage of the Chandezon method is that different systems can be modelled without adjustment of the numerical techniques used, although the size of the truncation parameter $M$ may need to vary. Here I will show calculations for gratings with different shapes and aspect ratios, noting the value of $M$ necessary for convergence and the corresponding calculation times per point on a Silicon Graphics Indy workstation running at 134*Mhz*.

### *2.11.1 The sinusoidal grating*

First I will consider a reasonably deep silver grating of pitch 1000*nm* and depth 50*nm* illuminated with TM or $p$ - polarised light of wavelength 632.8*nm*. Such a grating is difficult to make in practice due to it's undistorted sinusoidal profile and I use it here purely as a test case - an example of a real grating will be given next. The exact parameters of the system are given in table 2.2. Figure 2.3 shows the resulting zeroth order $R_{pp}$ reflectivity, where the subscripts denote settings on the input and output polarisers respectively. Table 2.3 gives a few of the calculated efficiencies.

| Incident light | Grating profile | Permittivities |
|---|---|---|
| $\lambda$=632.8*nm* | $\lambda_g$=1000*nm* | $\varepsilon^1$=(1.0,0) |
| TM polarisation | Fundamental only of 50.0*nm* | $\varepsilon^0$=(-17.5,0.7) |

***Table 2.2:*** Parameters of the system modelled in figure 2.3

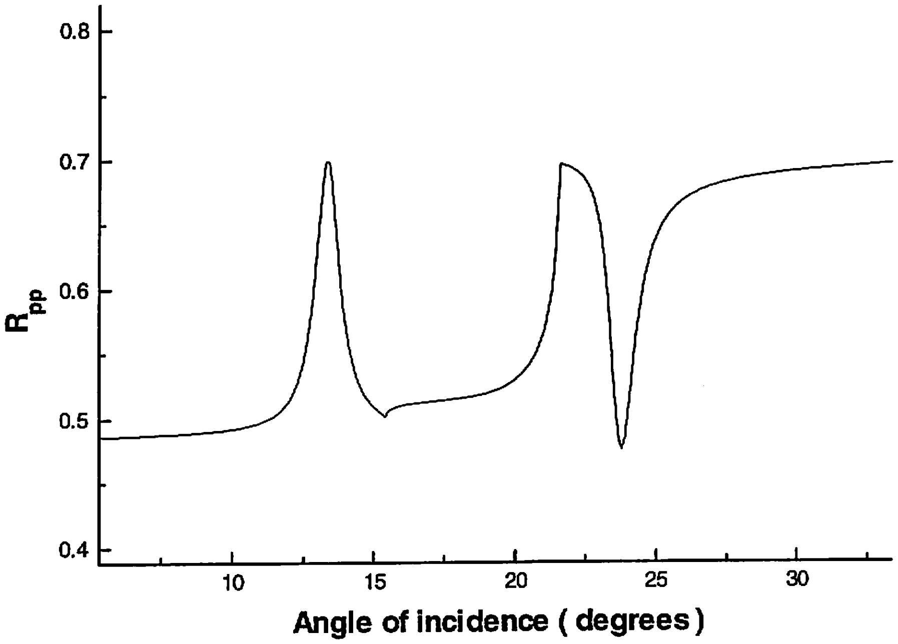

**Figure 2.3:** Zeroth order reflectivity trace for a shallow sinusoidal silver grating

We can identify two strong features in the reflectivity trace both of which are associated with the surface plasmon resonance. The minimum centred on ~ 24° is the first order resonance while the peak at ~ 13° is the second order resonance. By this I mean that the momentum necessary to couple to the plasmon has been achieved via one and two Bragg scattering events respectively.

For this calculation $M$=5 was sufficient to ensure convergence of the solution to 6 decimal places over the whole range of incident momenta (from this point on when I refer to convergence I am referring to convergence to 6 d.p.). This corresponds to a computation time of 0.3*s* per point.

| Angle of Incidence ( degrees) | Zeroth order efficiency $R_{pp}$ |
|---|---|
| 10 | 0.4923159 |
| 15 | 0.5092233 |
| 20 | 0.5303237 |
| 25 | 0.6396551 |
| 30 | 0.6913143 |

**Table 2.3:** A selection of the calculated efficiencies

I have already mentioned two factors affecting the size of the truncation parameter *M*: one of these was the aspect ratio of the grating, the other was the presence of appreciable higher order Fourier harmonics in the grating profile. Both can result in relatively strong coupling to higher scattered orders so we must ensure that the range of equations we retain after truncation includes these orders. The final factor affecting our choice of *M* is the relative size of the incident wavelength and the grating pitch - a large grating pitch in comparison to the wavelength of incident light gives rise to a large number of propagating orders. As a minimum our truncated system of equations must cover the set of propagating diffracted orders so here we have another constraint on the size of *M*.

To give an example I will now consider a slightly deeper, longer pitch grating which has a number of higher Fourier harmonics in its profile ( although nowhere near as many as for the square grating of *section 2.10.2* ). I will represent all such surfaces by a sum of sine waves $y = a_0 \sin(Kx) + a_1 \sin(2Kx + \chi_1) + a_2 \sin(3Kx + \chi_2) + \ldots$ where the $a_i$ and $\chi_i$ are amplitudes and phase factors respectively. The first term is referred to as the fundamental. Thereafter we speak of the first, second and third harmonics and so on.

The parameters describing this more complicated system are given in table 2.4 while figure 2.4 shows the resulting zeroth order reflectivity curve. Finally a selection of the calculated efficiencies are provided in table 2.5.

| Incident light $\lambda=632.8nm$ | Grating profile $\lambda_g=930nm$ | | Permittivities |
|---|---|---|---|
| | Amplitude | Phase | |
| TM polarisation | $64.9821nm$ | $0^0$ | $\varepsilon^1=(2.122,0)$ |
| | $13.7528nm$ | $90^{\circ}$ | $\varepsilon^0=(-18.0,0.6)$ |
| | $-6.0054nm$ | $0^{\circ}$ | |
| | $-2.7128nm$ | $90^{\circ}$ | |

**Table 2.4:** Parameters of the system modelled in figure 2.4

For this system we have a more complicated reflectivity response due to the higher harmonics in the grating profile providing stronger coupling to higher diffracted orders. Again there is strong coupling to the first order surface plasmon resonance with a pronounced minimum at ~ $40^{\circ}$ along with several other peaks corresponding to higher order coupling into the resonance.

Here it was necessary to use $M=16$ in order to ensure convergence of the solution to 6 d.p. over the whole range of incident momenta. This corresponds to a computation time of approximately 5*s* per point.

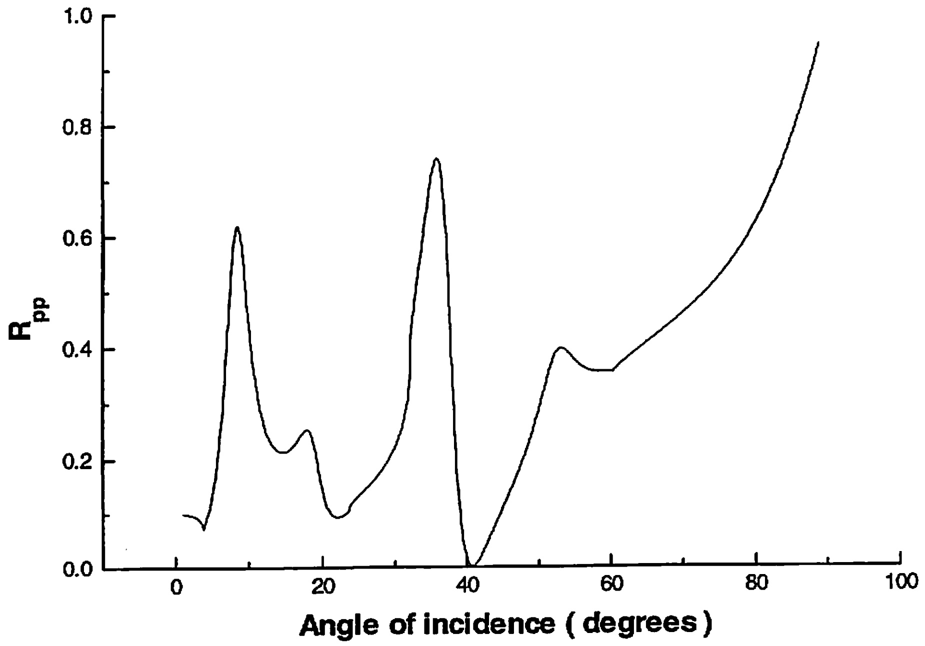

**Figure 2.4:** Zeroth order reflectivity trace for a distorted sinusoidal silver grating

| Angle of incidence (degrees) | $R_{pp}$ efficiencies for order | | | | |
|---|---|---|---|---|---|
| | -3 | -2 | -1 | zeroth | +1 |
| 20 | - | 0.0410056 | 0.3465162 | 0.1450929 | 0.4158503 |
| 40 | 0.2366756 | 0.3866453 | 0.2355621 | 0.0181451 | - |
| 60 | 0.0321183 | 0.1990150 | 0.3765563 | 0.3559276 | - |
| 80 | 0.0358831 | 0.1008208 | 0.1957197 | 0.6231396 | - |

**Table 2.5:** A selection of the calculated efficiencies

### *2.11.2 The square grating*

For completeness I will now calculate the optical response of a square grating with its associated higher Fourier harmonics. Rather than use a square step profile directly I will Fourier analyze the square shape and retain as many harmonics as gives a reasonable approximation to a square wave. As it turns out this number is 7 and as the plot in figure 2.5 shows, the resulting profile is indeed square - like.

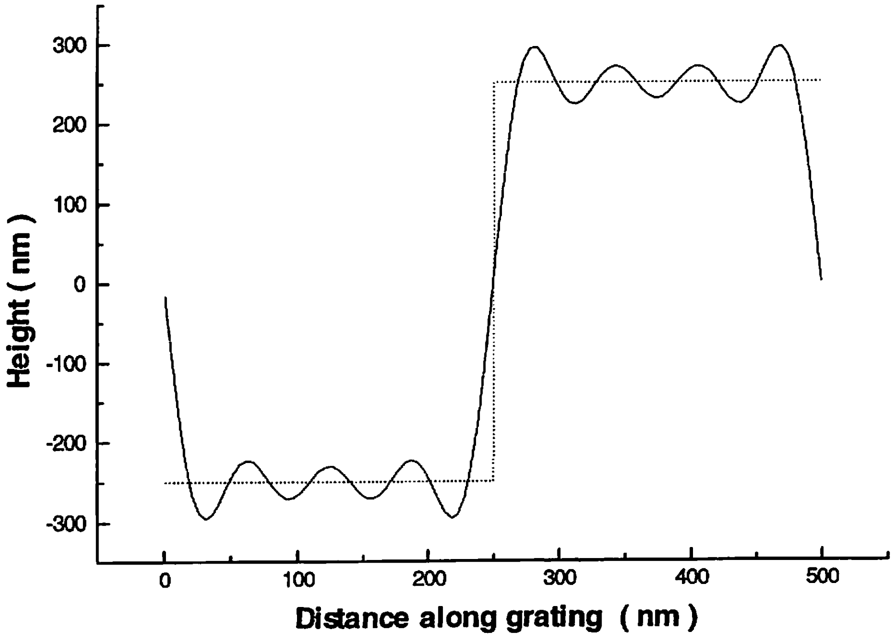

**Figure 2.5:** Approximation to a squarewave using 7 Fourier harmonics

Table 2.6 shows the exact parameters we will use to model the square grating system. For a more complete coverage of possible systems I will make this grating a palladium one rather than the silver based systems covered in the previous section.

| Incident light | Grating profile $\lambda_g=500nm$ | | Permittivities |
|---|---|---|---|
| $\lambda=632.8nm$ | Amplitude | Phase | |
| Both polarisations in turn | $-318.0nm$ | $0^0$ | $\varepsilon^1=(1.0,0)$ |
| | $0.0nm$ | $90^o$ | $\varepsilon^0=(-15.0,20.0)$ |
| | $-106.0nm$ | $0^o$ | |
| | $0.0nm$ | $90^o$ | |
| | $-63.6nm$ | $0^o$ | |
| | $0.0nm$ | $90^o$ | |
| | $-45.4nm$ | $0^o$ | |

**Table 2.6:** Parameters for the square grating

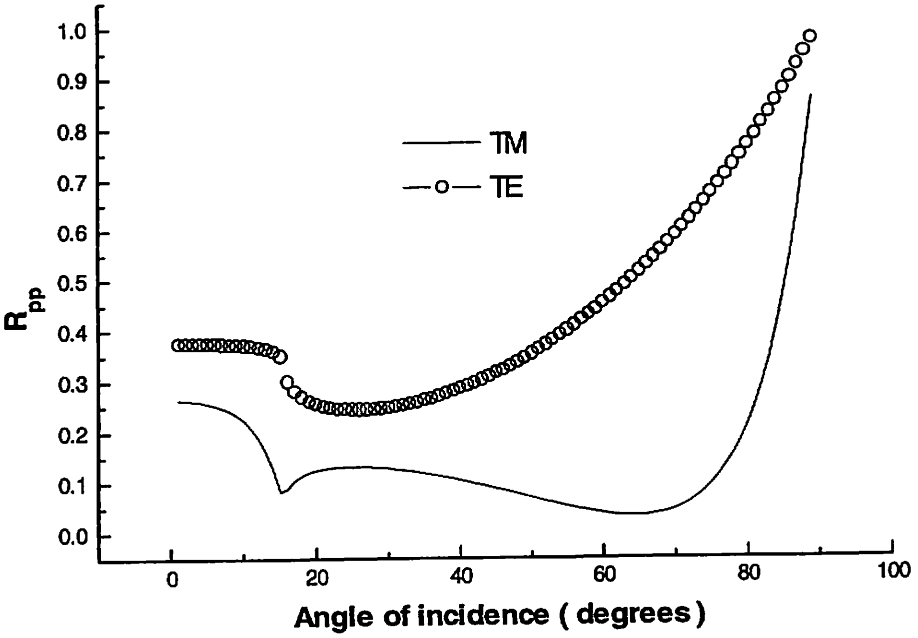

**Figure 2.6:** Zeroth order reflectivity traces for a square palladium grating

Due to the extreme depth of the grating and the large number of significant higher harmonics in it's profile $M$=30 was required before a convergent solution could be obtained across the range of incident momenta looked at. Computation time was 49s per point.

| Angle of incidence | TM efficiencies | | TE efficiencies | |
|---|---|---|---|---|
| ( degrees ) | -1 | zeroth | -1 | zeroth |
| 20 | 0.1482196 | 0.1245495 | 0.1625119 | 0.2561800 |
| 40 | 0.1437154 | 0.1050076 | 0.2342418 | 0.2857161 |
| 60 | 0.1487655 | 0.0382647 | 0.1945049 | 0.4535711 |
| 80 | 0.1211530 | 0.2138300 | 0.0854807 | 0.7668918 |

**Table 2.7:** A selection of the calculated efficiencies

### *2.12 Convergence: Chandezon vs. Rayleigh*

Concerning the convergence of the numerical solution with increasing truncation parameter $M$ there are two questions we can ask: Firstly, does the solution converge? and second, does it converge to the right answer? Obviously there is no point in singing the praises of a formalism with excellent convergence properties if it doesn't give a sensible answer, and herein lies the fundamental difference between the two methods: The Rayleigh method represents the whole field as a Rayleigh expansion (2.64) which as discussed in *section* 1.3 is generally an invalid representation of the diffracted field for a certain range of $y$ co-ordinates $y < y_c$ intersecting the grating profile, so in this sense it is by no means certain that the method will give the right answer at all. However it does turn out that the Rayleigh expansion is capable of modeling quite deep gratings under some circumstances and provided it is used within its zone of validity, remains a very useful tool for modeling shallow gratings.

To compare the convergence of the two methods we need to look at how the diffracted field is represented in each case: The Rayleigh expansion is

$$R(x,y) = \sum_n B_n \Phi_n(x,y) \qquad \text{where} \quad \Phi_n(x,y) = \exp i(\alpha_n x + \beta_n y) \tag{2.98}$$

while in the Chandezon method we have

$$\xi(v,u)=\sum_{n}\sum_{q} f_{nq}\Gamma_{nq}(v,u) \quad \text{where } \Gamma_{nq}(v,u)=\exp i(\alpha_n v + r_q u) \tag{2.99}$$

For the series to converge we must be able to choose a positive integer $n_c$ such that every $\Phi_n$ , $\Gamma_{nq}$ with $|n|>n_c$ makes no significant difference to the existing sum at a given position $x$, $y$.

Taking the Rayleigh expansion within its domain of validity, and assuming that the $B_n \to 0$ as $n \to \infty$, we find that the convergence of the series is dependent (although not wholly dependent) on the set of functions $\Phi_n(x,y)$ as $n \to \infty$. Provided we choose a high enough value for $|n|$ all the $\beta_n$ are complex and $\Phi_n(x,y) \to \exp inKx.\exp(-nKy)$. So the convergence of $\Phi_n(x,y)$ as $n \to \infty$ is governed by the non-oscillatory terms $\exp(-nKy)$, where the $nK$ play the role of decay constants. These decay constants increase with $n$ so the contribution of these terms to the field at a given value of $y$ decreases with $n$ and eventually the series converges.

However as one moves over the grating $\Phi_n(x,y)$ will vary in magnitude by $\exp(-nKd)$ where $d$ is the depth of the grating. Consequently the convergence properties of the series varies markedly across the grating and this is the essential problem with the use of the Rayleigh expansion.

Turning to the Chandezon expansion it is important to first realise that the set of functions $\Gamma_{nq}(v,u)$ are determined by the grating surface since the coefficients $f_{nq}$ are just the elements of the eigenvectors associated with the solution of Maxwell's equations in the transformed space; secondly on the surface $u$=0 and no exponential terms are present to affect the convergence behavior.

We can apply exactly the same reasoning to the Chandezon expansion (2.68) as was used to investigate the convergence of the Rayleigh expansion.

Table 2.7 provides a direct comparison between the two sets of eigenvalues, showing them to be remarkably similar. Looking at the table it is clear that as $M \to \infty$ there are $P$ values of $r_q$ that must tend towards the $P$ values of $\beta_n$ corresponding to $n \in U$. In fact it is true to say that as $M \to \infty$ there are a finite number $4M'+2$ of $r_q$ that tend toward the $\beta_n$ $(-M'<n<M')$. So it would seem advantageous to use the analytical solution

for the eigenvalues and eigenvectors of the matrix **T** with $M = \infty$ . Somewhat surprisingly it can be shown that this approach is equivalent to the Rayleigh expansion method which as I have discussed generally leads to numerical failure. The success of the Chandezon technique lies in the truncation of **T** and subsequent numerical calculation of it's eigenvalues and eigenvectors. Referring to table 2.7 we can see that for $n$ = 1-3 the Rayleigh $\beta_n$ and Chandezon $r_q$ both follow the same trend: zero real part and imaginary part increasing with $n$. However for values of $n > 3$ the behavior of the Chandezon eigenvalues changes dramatically with $r_q$ forming distinct pairs having both real and imaginary parts of the order of unity. Generally it is clear that those eigenvalues corresponding to values of $n$ around the truncation limit are significantly different from their Rayleigh counterparts .

| n | Re($\beta_n$) | Im($\beta_n$) | Re($r_q$) | Im($r_q$) |
|---|---|---|---|---|
| -6 | 0 | 3.141479 | +0.177991 | 2.580086 |
| -5 | 0 | 2.469189 | 0 | 2.176565 |
| -4 | 0 | 1.767986 | 0 | 1.807714 |
| -3 | 0 | 0.977508 | 0 | 0.977459 |
| -2 | 0.643317 | 0 | 0.643317 | 0 |
| -1 | 0.991143 | 0 | 0.991143 | 0 |
| 0 | 0.866025 | 0 | 0.866025 | 0 |
| 1 | 0 | 0.532199 | 0 | 0.532199 |
| 2 | 0 | 1.455109 | 0 | 1.455114 |
| 3 | 0 | 2.179982 | 0 | 2.129697 |
| 4 | 0 | 2.861498 | -0.177991 | 2.580086 |
| 5 | 0 | 3.524897 | -0.3970652 | 3.484660 |
| 6 | 0 | 4.178714 | +0.3970652 | 3.484660 |

**Table 2.8:** Comparison between Rayleigh and Chandezon method eigenvalues

That this leads to improved numerical convergence of the Chandezon technique over Rayleigh methods is obvious if we remember that it is the speed at which the higher order imaginary eigenvalues decrease that governs the overall convergence of the series. For instance if, at some point away from the boundary, we look at the field contribution arising from the $n$ = 3 terms then it is apparent that the Rayleigh term with it's larger decay constant makes a smaller contribution than the corresponding Chandezon term. Consequently we need less Chandezon terms to describe a given field. Note that the Chandezon eigenvalues are associated with the co-ordinate $u$ not $y$ and that this helps rather than hinders the argument given above.

The most enlightening way of looking at the difference between the two methods is to consider how evanescent fields are represented on a grating surface. Figure 2.7 illustrates the problem: The crucial difference is that the Chandezon technique describes fields in terms of a set of functions defined on the interface, so that a given eigenmode has spatial dependence characterized by the $u$ variable which is related to the shape of the grating profile on which it takes the value $u = 0$. No matter where we move along the surface, a given eigenmode will always retain the same field strength.

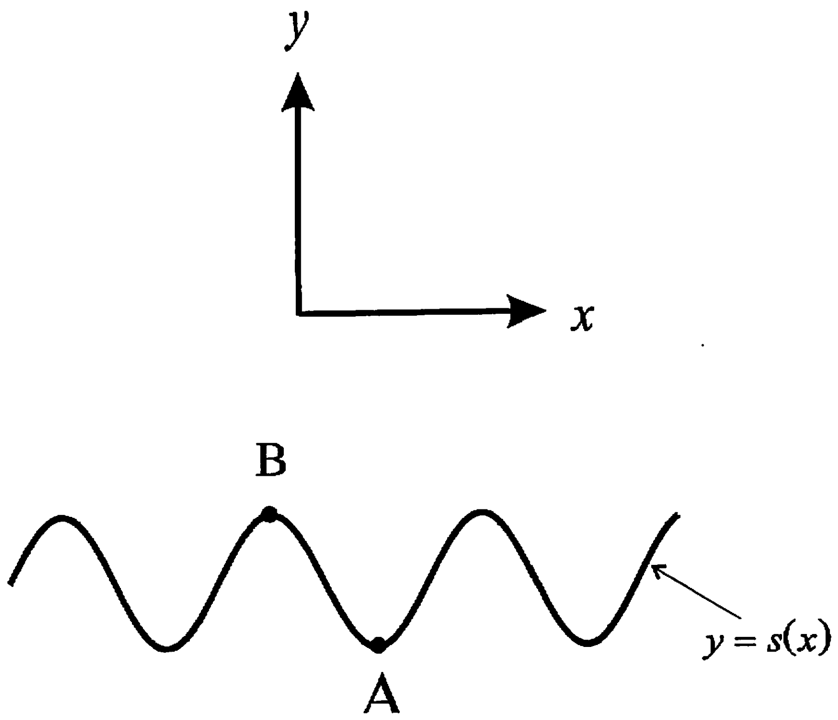

**Figure 2.7:** Comparison of Rayleigh methods and the Chandezon technique

This is not true of the Rayleigh eigenmodes which are a set of functions defined in Cartesian co-ordinates - thus their spatial dependence dictates that a given eigenmode can give rise to very different field strengths at points A and B corresponding to the minimum and maximum values of $y$ on the grating surface. If the fields at these two points are sufficiently different then, matching fields across the interface we may find that the contribution from point A is insignificant compared to that at point B. The resulting loss of significant digits may then lead to numerical failure.

### *2.13 Summary*

In this chapter I have laid the theoretical foundations of the Chandezon technique and given some examples of its use. Given that the method has been shown to be a powerful tool for modeling the simple systems considered so far it is only natural to apply the same formalism to more complicated structures. The remaining chapters of this thesis deal with generalizing Chandezon's method to include conical scattering, multicoated gratings made with liquid crystals, and bi-gratings.

# 3. Field calculations

While the analysis of *chapter 2* sought to determine the reflectivities and transmissivities of propagating orders, no attempt was made to investigate the electric and magnetic field strengths for a given system as a function of position. Previously Popov, Tsonev, and Maystre [1989 and 1994] have used the Chandezon technique for such an investigation, showing how a knowledge of the spatial distribution of field vectors near metallic gratings can give valuable insight into the physical processes behind a number of diffraction phenomenon.

In this chapter I will derive expressions for the field amplitudes as a function of position and make an introductory investigation of the electromagnetic fields and Poynting vectors near metallic gratings.

## *3.1. The surface plasmon resonance*

When light is incident on a dielectric or metallic substrate, be it a grating or planar surface, the amount of radiation absorbed is determined by the dielectric response function of the substrate material.

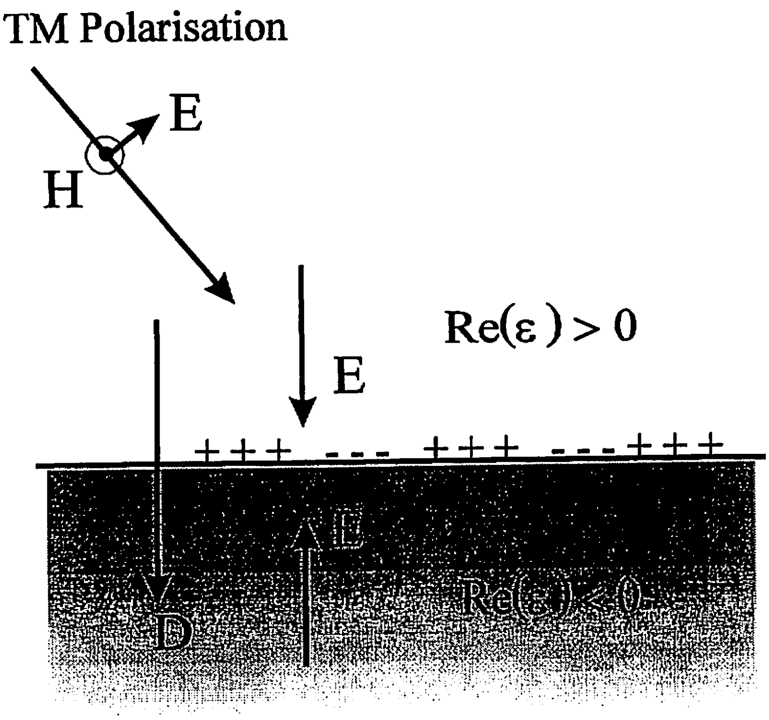

**Figure 3.1:** The surface plasmon polariton

For metallic substances there exists a resonance in this response function with an associated surface wave called the surface plasmon polariton [Raether, 1988]. Figure 3.1 shows how such a surface wave is supported: Across any material interface lines of normal electric displacement $\mathbf{D} = \varepsilon\mathbf{E}$ are continuous so that if $\varepsilon$ changes sign from one medium to the other the direction of **E** must reverse on the interface. Since lines of electric field always end on free charges this results in a layer of trapped charge on the dielectric/metal interface. It is this layer of charge which may be stimulated to oscillate and propagate as a surface wave.

### *3.2. Theory*

From now on I will consider medium1 to be a dielectric and medium 0 to be metallic, giving the necessary sign change in the real part of the permittivities to support a plasmon resonance, and ensuring that medium 0 supports no propagating orders.

With this in mind I will first calculate the field distributions in this medium. Referring to *chapter 2* equation (2.40) tells us that

$$\begin{pmatrix} F_{-N}(u) \\ \cdot \\ F_{N}(u) \\ - \\ G_{-N}(u)\big/\varepsilon_r \\ \cdot \\ G_{N}(u)\big/\varepsilon_r \end{pmatrix} = \mathbf{M}^0\phi^0\mathbf{b}^0 \tag{3.1}$$

so that for TM polarised light

$$\begin{pmatrix} H_{z(-N)}(u) \\ \cdot \\ H_{z(N)}(u) \\ - \\ -E_{1(-N)}(u) \\ \cdot \\ -E_{1(N)}(u) \end{pmatrix} = \mathbf{M}^0\phi^0\mathbf{b}^0 \tag{3.2}$$

from which we can determine the full $v$, $u$ and hence $x$, $y$ dependence via the following summation:

$$\begin{aligned} H_z(x,y) &= \sum_m H_{z(m)}(u)\exp i\alpha_m v = \sum_m H_{z(m)}(y-s(x))\exp i\alpha_m x \\ E_1(x,y) &= \sum_m E_{1(m)}(u)\exp i\alpha_m v = \sum_m E_{1(m)}(y-s(x))\exp i\alpha_m x \end{aligned} \tag{3.3}$$

where, following the conventions and definitions of *chapter* 2, the summation runs over $-M < m < M$, and $s(x)$ describes the grating surface.

Outgoing wave conditions force $\mathbf{b}_+^0 = 0$ so that equation (3.2) may be simplified

$$\begin{pmatrix} H_{z(-N)}(u) \\ \cdot \\ H_{z(N)}(u) \\ - \\ -E_{1(-N)}(u) \\ \cdot \\ -E_{1(N)}(u) \end{pmatrix} = \begin{pmatrix} \mathbf{M}_{11}^0 & \mathbf{M}_{12}^0 \\ \mathbf{M}_{21}^0 & \mathbf{M}_{22}^0 \end{pmatrix} \begin{pmatrix} \phi_1 & 0 \\ 0 & \phi_2 \end{pmatrix} \begin{pmatrix} 0 \\ \mathbf{b}_-^0 \end{pmatrix} = \begin{pmatrix} \mathbf{M}_{12}^0 \phi_2 \mathbf{b}_-^0 \\ \mathbf{M}_{22}^0 \phi_2 \mathbf{b}_-^0 \end{pmatrix} \tag{3.4}$$

and we can write equation (3.3) explicitly as

$$\begin{aligned} H_z(x,y) &= \sum_m H_{z(m)}(u)\exp i\alpha_m v = \sum_q \sum_m \left(\mathbf{M}_{12}^0\right)_{mq} \left(\mathbf{b}_-^0\right)_q \exp i\left(\alpha_m x + r_q^0 (y - s(x))\right) \\ E_1(x,y) &= \sum_m E_{1(m)}(u)\exp i\alpha_m v = \sum_q \sum_m \left(\mathbf{M}_{22}^0\right)_{mq} \left(\mathbf{b}_-^0\right)_q \exp i\left(\alpha_m x + r_q^0 (y - s(x))\right) \end{aligned} \tag{3.5}$$

where the superscript on $r_q^0$ denotes the $q^{\text{th}}$ eigenvalue from medium 0.

Rather than $E_1$, which is the component of the E field lying in the plane of incidence that is tangential to the grating, we require the Cartesian components $E_x$ and $E_y$. For TM polarised light $\mathbf{H} = (0,0,H_z)$ and *Curl*$\mathbf{H} = -i\varepsilon_r \mathbf{E}$ simplifies to

$$\begin{vmatrix} \mathbf{i} & \mathbf{j} & \mathbf{k} \\ \dfrac{\partial}{\partial x} & \dfrac{\partial}{\partial y} & \dfrac{\partial}{\partial z} \\ 0 & 0 & H_z \end{vmatrix} = -i\varepsilon_r \mathbf{E} \tag{3.6}$$

Evaluating the determinant we find that

$$E_x = \frac{i}{\varepsilon_r}\frac{\partial H_z}{\partial y} \qquad E_y = -\frac{i}{\varepsilon_r}\frac{\partial H_z}{\partial x} \tag{3.7}$$

Since all fields have the dependence $\exp i(\alpha_m v \pm \beta_m u)$ we can evaluate the quantities $\frac{\partial H_z}{\partial x}$ and $\frac{\partial H_z}{\partial y}$ with a knowledge of the co-ordinate transformation (2.3). From $\delta F = \frac{\partial F}{\partial v}\delta v + \frac{\partial F}{\partial u}\delta u$ we can derive the relations

$$\frac{\partial F}{\partial x} = \frac{\partial F}{\partial v} - s'\frac{\partial F}{\partial u} \qquad \frac{\partial F}{\partial y} = \frac{\partial F}{\partial u} \tag{3.8}$$

where $s'$ denotes differentiation of the surface profile with respect to $v$ or equivalently $x$. Using these expressions we find that

$$E_x = \frac{i}{\varepsilon_r}\frac{\partial H_z}{\partial u} \qquad E_y = -\frac{i}{\varepsilon_r}\frac{\partial H_z}{\partial v} + s'E_x \tag{3.9}$$

In medium 0 all field components are expressed as an eigenmode expansion. Equation (3.5) can be written entirely in terms of $v$ and $u$ to gives the transverse field in terms of these co-ordinates: $H_z(v,u) = \sum_q \sum_m \left(\mathbf{M}^0_{12}\right)_{mq}\left(\mathbf{b}^0_-\right)_q \exp i\left(\alpha_m v + r^0_q u\right)$. The in - plane fields are then given by

$$\begin{aligned}
E_x(x,y) &= -\frac{1}{\varepsilon^0_r}\sum_q \sum_m \left(\mathbf{M}^0_{12}\right)_{mq}\left(\mathbf{b}^0_-\right)_q r^0_q \exp i\left(\alpha_m x - r^0_q\left(y - s(x)\right)\right) \\
E_y(x,y) &= \frac{1}{\varepsilon^0_r}\sum_q \sum_m \left(\mathbf{M}^0_{12}\right)_{mq}\left(\mathbf{b}^0_-\right)_q \left(\alpha_m - s'(x) r^0_q\right) \exp i\left(\alpha_m x - r^0_q\left(y - s(x)\right)\right) \\
&= \frac{1}{\varepsilon^0_r}\sum_q \sum_m \left(\mathbf{M}^0_{12}\right)_{mq}\left(\mathbf{b}^0_-\right)_q \alpha_m \exp i\left(\alpha_m x - r^0_q\left(y - s(x)\right)\right) - s'(x)E_x(x,y)
\end{aligned} \tag{3.10}$$

In medium 1 I use a different representation in which the field is split into three parts: the incident field, the propagating reflected field, and the evanescent reflected field. Starting first with the incident field

$$\begin{pmatrix} H_{z(-N)}(u) \\ \cdot \\ H_{z(N)}(u) \\ - \\ -E_{1(-N)}(u) \\ \cdot \\ -E_{1(N)}(u) \end{pmatrix} = \begin{pmatrix} \mathbf{L}' \\ \mathbf{L}''/\varepsilon_r \end{pmatrix} \exp(-i\beta_0 u) \tag{3.11}$$

The propagating and evanescent fields are combined in one representation so that

$$\begin{pmatrix} H_{z(-N)}(u) \\ \cdot \\ H_{z(N)}(u) \\ - \\ -E_{1(-N)}(u) \\ \cdot \\ -E_{1(N)}(u) \end{pmatrix} = \begin{pmatrix} \hat{\mathbf{M}}^1_{11} & \hat{\mathbf{M}}^1_{12} \\ \hat{\mathbf{M}}^1_{21} & \hat{\mathbf{M}}^1_{22} \end{pmatrix} \begin{pmatrix} \phi_1' & \mathbf{0} \\ \mathbf{0} & \phi_2' \end{pmatrix} \begin{pmatrix} \hat{\mathbf{R}} \\ \mathbf{0} \end{pmatrix} = \begin{pmatrix} \hat{\mathbf{M}}^1_{12}\phi_1\hat{\mathbf{R}} \\ \hat{\mathbf{M}}^1_{21}\phi_1\hat{\mathbf{R}} \end{pmatrix} \tag{3.12}$$

From which equation (3.3) gives the complete $x$, $y$ dependence of the field vector components $H_z$ and $E_1$.

Using equations (3.9) to obtain the in - plane field amplitudes it is possible to derive expressions for the incident, propagating diffracted, and evanescent diffracted fields in medium 1:

Incident field

$$\begin{aligned} H_z(x,y) &= \sum_m L_m(\beta_0)\exp i(\alpha_m x - \beta_0(y - s(x))) \\ E_x(x,y) &= \frac{1}{\varepsilon_r^1}\sum_m L_m(\beta_0)\beta_m \exp i(\alpha_m x - \beta_0(y - s(x))) \\ E_y(x,y) &= \frac{1}{\varepsilon_r^1}\sum_m L_m(\beta_0)\alpha_m \exp i(\alpha_m x - \beta_0(y - s(x))) + s'(x)E_x(x,y) \end{aligned} \tag{3.13}$$

Propagating diffracted field (summation in $q$ runs over propagating eigenmodes only)

$$\begin{aligned}
H_z(x,y) &= \sum_q \sum_m (\hat{\mathbf{M}}_{11})_{qm} (\hat{\mathbf{R}})_q \exp i\left(\alpha_m x + \beta_q (y - s(x))\right) \\
E_x(x,y) &= \frac{1}{\varepsilon_r^1} \sum_q \sum_m (\hat{\mathbf{M}}_{11})_{qm} (\hat{\mathbf{R}})_q (-\beta_q) \exp i\left(\alpha_m x + \beta_q (y - s(x))\right) \\
E_y(x,y) &= \frac{1}{\varepsilon_r^1} \sum_q \sum_m (\hat{\mathbf{M}}_{11})_{qm} (\hat{\mathbf{R}})_q \alpha_m \exp i\left(\alpha_m x + \beta_q (y - s(x))\right) + s'(x) E_x(x,y)
\end{aligned} \tag{3.14}$$

Evanescent diffracted field (summation in $q$ runs over non-propagating eigenmodes only)

$$\begin{aligned}
H_z(x,y) &= \sum_q \sum_m (\hat{\mathbf{M}}_{11})_{qm} (\hat{\mathbf{R}})_q \exp i\left(\alpha_m x + r_q^1 (y - s(x))\right) \\
E_x(x,y) &= \frac{1}{\varepsilon_r^1} \sum_q \sum_m (\hat{\mathbf{M}}_{11})_{qm} (\hat{\mathbf{R}})_q (-r_q^1) \exp i\left(\alpha_m x + r_q^1 (y - s(x))\right) \\
E_y(x,y) &= \frac{1}{\varepsilon_r^1} \sum_q \sum_m (\hat{\mathbf{M}}_{11})_{qm} (\hat{\mathbf{R}})_q \alpha_m \exp i\left(\alpha_m x + r_q^1 (y - s(x))\right) + s'(x) E_x(x,y)
\end{aligned} \tag{3.15}$$

We can derive a similar set of equations for the TE case where $\mathbf{E} = (0,0,E_z)$ and the second Maxwell Curl equation: $Curl\mathbf{E} = i\mathbf{H}$ simplifies to:

$$\begin{vmatrix} \mathbf{i} & \mathbf{j} & \mathbf{k} \\ \frac{\partial}{\partial x} & \frac{\partial}{\partial y} & \frac{\partial}{\partial z} \\ 0 & 0 & E_z \end{vmatrix} = i\mathbf{H} \tag{3.16}$$

As before we evaluate the determinant to find

$$H_x = -i\frac{\partial E_z}{\partial y} \qquad H_y = i\frac{\partial E_z}{\partial x} \tag{3.17}$$

and consequently from (3.8)

$$H_x = -i\frac{\partial E_z}{\partial u} \qquad H_y = i\frac{\partial E_z}{\partial v} + s'H_x \tag{3.18}$$

The fields in media 0 are then given by

$$\begin{aligned}
E_z(x,y) &= \sum_q \sum_m \left(\mathbf{M}_{12}^0\right)_{qm} \left(\mathbf{b}_-^0\right)_q \exp i\left(\alpha_m x + r_q^0\left(y - s(x)\right)\right) \\
H_x(x,y) &= \sum_q \sum_m \left(\mathbf{M}_{12}^0\right)_{qm} \left(\mathbf{b}_-^0\right)_q r_q^1 \exp i\left(\alpha_m x + r_q^0\left(y - s(x)\right)\right) \\
H_y(x,y) &= \sum_q \sum_m \left(\mathbf{M}_{12}^0\right)_{qm} \left(\mathbf{b}_-^0\right)_q \left(-\alpha_m\right) \exp i\left(\alpha_m x + r_q^0\left(y - s(x)\right)\right) + s'(x) H_x(x,y)
\end{aligned} \tag{3.19}$$

while the three representations of the field in medium 1 are:

Incident field

$$\begin{aligned}
E_z(x,y) &= \sum_q \sum_m (\mathbf{L}')_m \exp i\left(\alpha_m x + \beta_0\left(y - s(x)\right)\right) \\
H_x(x,y) &= \sum_q \sum_m (\mathbf{L}')_m \left(-\beta_0\right) \exp i\left(\alpha_m x + \beta_0\left(y - s(x)\right)\right) \\
H_y(x,y) &= \sum_q \sum_m (\mathbf{L}')_m \left(-\alpha_m\right) \exp i\left(\alpha_m x + \beta_0\left(y - s(x)\right)\right) + s'(x) H_x(x,y)
\end{aligned} \tag{3.20}$$

Propagating diffracted field (summation in $q$ runs over propagating eigenmodes only)

$$\begin{aligned}
E_z(x,y) &= \sum_q \sum_m \left(\hat{\mathbf{M}}_{11}\right)_{qm} \left(\hat{\mathbf{R}}\right)_q \exp i\left(\alpha_m x + \beta_q\left(y - s(x)\right)\right) \\
H_x(x,y) &= \sum_q \sum_m \left(\hat{\mathbf{M}}_{11}\right)_{qm} \left(\hat{\mathbf{R}}\right)_q \beta_q \exp i\left(\alpha_m x + \beta_q\left(y - s(x)\right)\right) \\
H_y(x,y) &= \sum_q \sum_m \left(\hat{\mathbf{M}}_{11}\right)_{qm} \left(\hat{\mathbf{R}}\right)_q \left(-\alpha_m\right) \exp i\left(\alpha_m x + \beta_q\left(y - s(x)\right)\right) + s'(x) H_x(x,y)
\end{aligned} \tag{3.21}$$

Evanescent diffracted field (summation in $q$ runs over non-propagating eigenmodes only)

$$\begin{aligned}
E_z(x,y) &= \sum_q \sum_m \left(\hat{\mathbf{M}}_{11}\right)_{qm} \left(\hat{\mathbf{R}}\right)_q \exp i\left(\alpha_m x + r_q^1\left(y - s(x)\right)\right) \\
H_x(x,y) &= \sum_q \sum_m \left(\hat{\mathbf{M}}_{11}\right)_{qm} \left(\hat{\mathbf{R}}\right)_q r_q^1 \exp i\left(\alpha_m x + r_q^1\left(y - s(x)\right)\right) \\
H_y(x,y) &= \sum_q \sum_m \left(\hat{\mathbf{M}}_{11}\right)_{qm} \left(\hat{\mathbf{R}}\right)_q \left(-\alpha_m\right) \exp i\left(\alpha_m x + r_q^1\left(y - s(x)\right)\right) + s'(x) H_x(x,y)
\end{aligned} \tag{3.22}$$

### *3.3 Testing the code*

Unlike the analysis presented in chapter 2 there are no tabulated calculations in the literature for comparison with. Instead I must ensure that the calculated field amplitudes obey a number of basic rules in planar systems, and compare them qualitatively with published contour plots [Popov, Tsonev, and Maystre, 1989 and 1994] for metallic gratings. As an example of the first type of condition, consider the case of a planar interface bounding two semi - infinite media, one a metal the other vacuum. If a plane monochromatic light beam is incident on this interface from the vacuum then a number of simple criterion apply to the field amplitudes generated as a result. First, in the metal all field amplitudes must decay exponentially away from the metal / vacuum interface with a characteristic decay length, which may be calculated and compared with accepted values. Second, above the metal, the incident and reflected beams interfere to produce bands of high and low intensity, the position and strength of which can be calculated by simple analysis.

Comparing field plots with those already published is a less accurate but nonetheless useful test of the code. In particular the inconsistency of rival commercial vector plotting routines places limits on how far this kind of comparison can be taken. Despite this there is good qualitative agreement between those plots shown in the literature and similar ones calculated with my code.

As an aid to future testing I have tabulated field amplitudes calculated for the grating described in chapter 2: table 2.4, which is repeated here for clarity as table 3.1.

| Incident light $\lambda$=632.9*nm* | Grating profile $\lambda_g$=930*nm* | | Permittivities |
|---|---|---|---|
| | Amplitude | Phase | |
| | 64.9821*nm* | $0^0$ | $\varepsilon^1$=(2.122,0) |
| | 13.7528*nm* | 90° | $\varepsilon^0$=(-18.0,0.6) |
| | -6.0054*nm* | 0° | |
| | -2.7128*nm* | 90° | |

**Table 3.1:** Parameters of the system modelled in tables 3.2 and 3.3

In chapter 2 I adopted a system of units in which the free space incident wavenumber, $|k_0| = \frac{2\pi}{\lambda} = \frac{\omega}{c}$, and impedance, $Z_0 = \left(\frac{\mu_0}{\varepsilon_0}\right)^{\frac{1}{2}}$ are both equated to unity. The field amplitudes tabulated below are thus written in these units, scaled so that the transverse incident field ($E_z$ or $H_z$ depending on the incident polarisation) is normalised to unity.

| Incident Angle | Position (*nm*) | | Field amplitudes | | |
|---|---|---|---|---|---|
| | $x$ | $y$ | $E_x$ | $E_y$ | $H_z$ |
| 20° | 100 | -200 | 0.00003 | 0.00001 | 0.0014 |
| | 100 | 0 | 0.10237 | 0.05942 | 0.46477 |
| | 100 | 200 | 0.57306 | 0.77723 | 1.80622 |
| | 100 | 400 | 0.71589 | 0.80083 | 1.11827 |
| 40° | 100 | -200 | 0.0001 | 0.0001 | 0.00004 |
| | 100 | 0 | 0.07376 | 0.03489 | 0.26787 |
| | 100 | 200 | 0.31668 | 1.19839 | 1.94589 |
| | 100 | 400 | 0.70938 | 0.37715 | 1.27521 |
| 60° | 100 | -200 | 0.00002 | 0.00001 | 0.00007 |
| | 100 | 0 | 0.05044 | 0.01958 | 0.21798 |
| | 100 | 200 | 0.77475 | 0.69606 | 1.14401 |
| | 100 | 400 | 0.61307 | 0.84030 | 1.37561 |
| 80° | 100 | -200 | 0.00001 | 0.00000 | 0.00003 |
| | 100 | 0 | 0.03351 | 0.01470 | 0.14295 |
| | 100 | 200 | 0.37836 | 0.18206 | 0.26144 |
| | 100 | 400 | 0.05722 | 0.63917 | 1.21535 |

**Table 3.2:** Field amplitudes calculated for the grating described in table 3.1 under TM polarisation

| Incident Angle | Position (*nm*) |  | Field amplitudes |  |  |
|---|---|---|---|---|---|
|  | $x$ | $y$ | $E_x$ | $E_y$ | $H_z$ |
| 20° | 100 | -200 | 0.00000 | 0.00002 | 0.00004 |
|  | 100 | 0 | 3.84732 | 0.94960 | 0.11455 |
|  | 100 | 200 | 2.11548 | 1.06540 | 0.84461 |
|  | 100 | 400 | 2.16633 | 0.52586 | 0.67581 |
| 40° | 100 | -200 | 0.00000 | 0.00004 | 0.00004 |
|  | 100 | 0 | 0.48580 | 0.12741 | 0.12724 |
|  | 100 | 200 | 1.93568 | 1.02893 | 1.61627 |
|  | 100 | 400 | 0.58333 | 1.69380 | 2.32971 |
| 60° | 100 | -200 | 0.00000 | 0.00003 | 0.00002 |
|  | 100 | 0 | 0.19828 | 0.08074 | 0.08753 |
|  | 100 | 200 | 0.42762 | 2.42968 | 2.22411 |
|  | 100 | 400 | 1.40249 | 0.32940 | 0.22559 |
| 80° | 100 | -200 | 0.00000 | 0.00001 | 0.00001 |
|  | 100 | 0 | 0.02115 | 0.04098 | 0.03101 |
|  | 100 | 200 | 0.41574 | 1.46498 | 1.12511 |
|  | 100 | 400 | 0.30486 | 2.28497 | 1.49993 |

**Table 3.3:** Field amplitudes calculated for the grating described in table 3.1 under TE polarisation

### *3.4 Numerical examples*

In what is to follow I will calculate field distributions above a number of metallic gratings, starting first with the simplest systems and then moving on to some cases of particular interest involving deep gratings.

### *3.4.1 A few simple examples*

To illustrate the distribution of field intensities we might observe in a given system I will start by looking at the simplest possible situations and gradually introduce more complexity into the system.

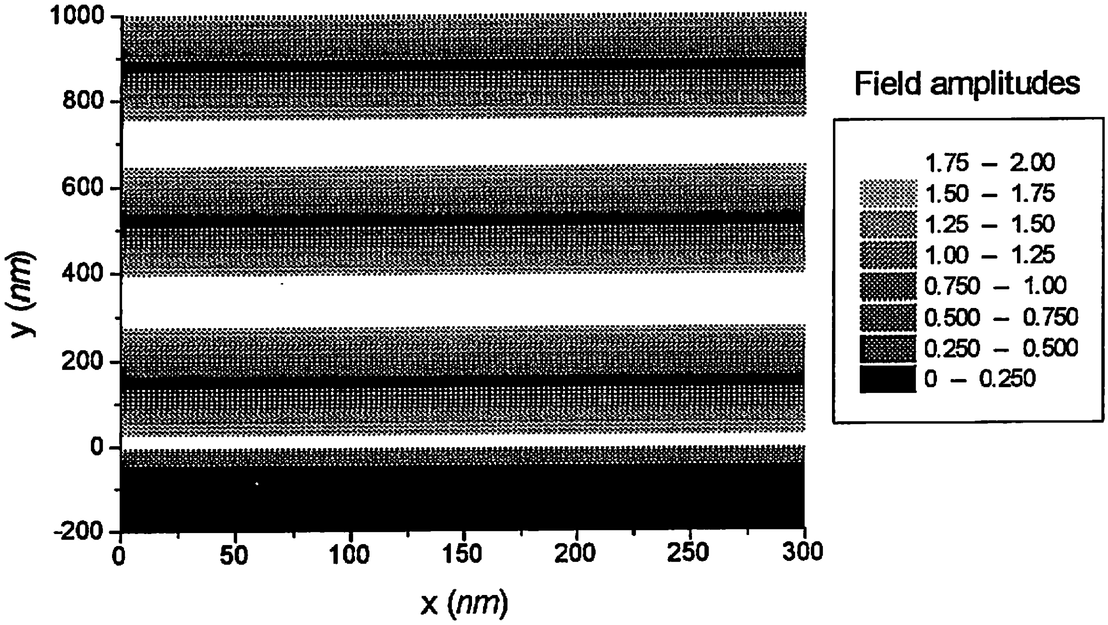

**Figure 3.2:** Magnetic field strength amplitudes in the vicinity of a planar silver/vacuum interface.

Initially then I will calculate the field distribution above a planar interface separating a semi - infinite layer of silver $(\varepsilon_r = -17.5 + 0.7i)$ and vacuum from which the system is illuminated with TM polarised light of wavelength $632.8nm$ propagating at an angle of $30^\circ$ to the surface normal. Figure 3.2 shows the distribution of H field amplitudes in such a system: below the interface $(y < 0)$ we can clearly see the rapid evanescent decay into the semi - infinite silver layer, while in the uppermost vacuum the incident and specular beams interfere to produce bands of high and low intensity parallel to the silver surface.

Since the incident H field amplitude has been normalised to unity these bands range in intensity from 0 to just under 2 - as expected given that nearly all the incident energy emerges in the specular beam at this angle of incidence. The $y$ spacing of the maxima can be predicted from simple kinematics to be $\lambda / 2\cos\theta$ which is equal to $365nm$ in this case.

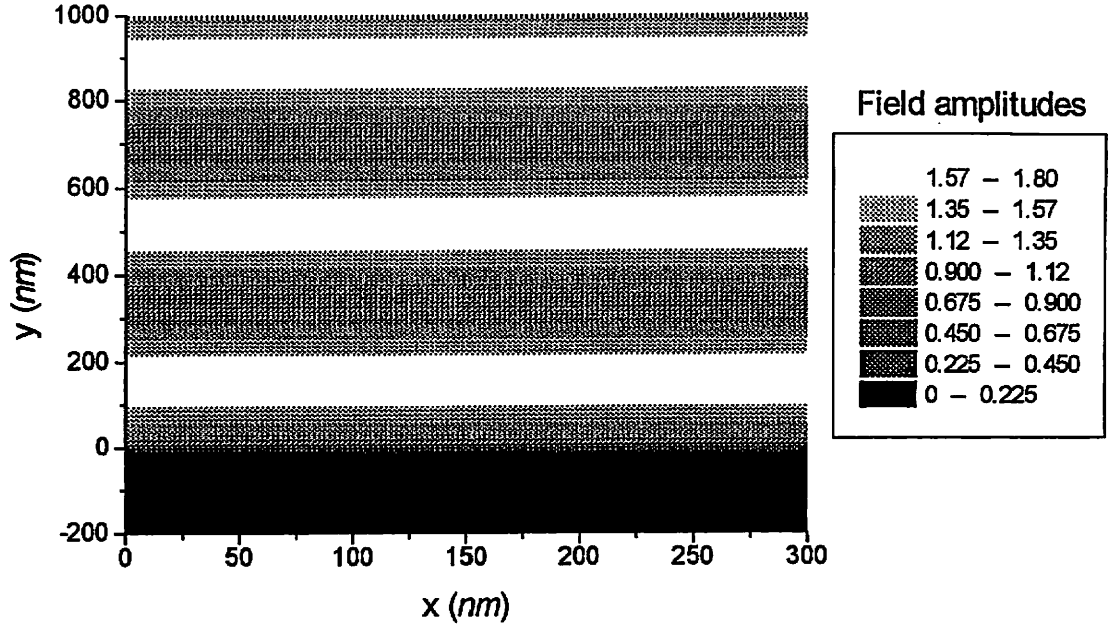

**Figure 3.3:** Electric field amplitudes in the vicinity of a planar silver/vacuum interface.

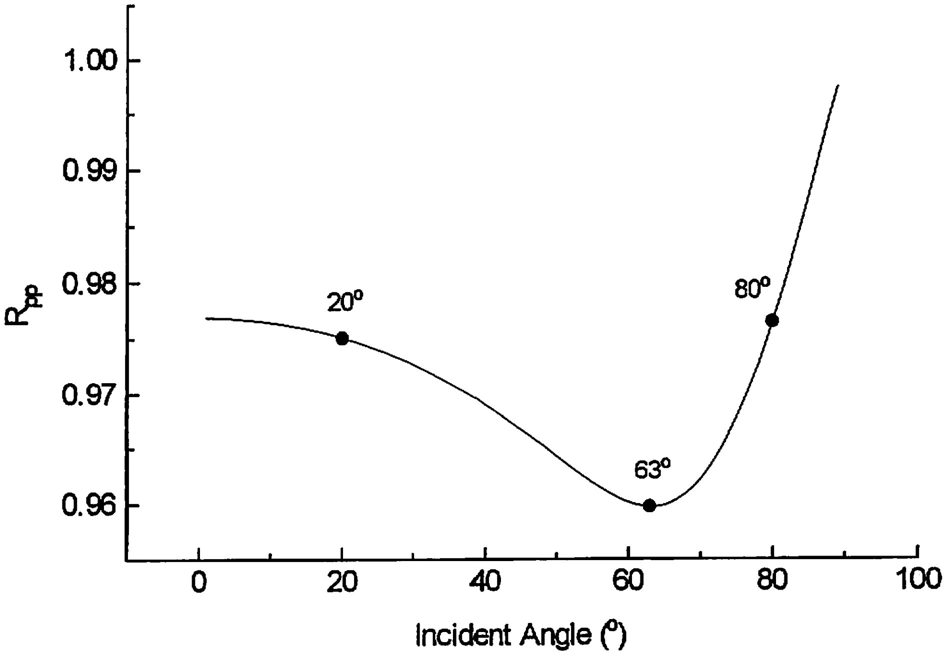

**Figure 3.4:** Plot of $R_{pp}$ vs. Angle of incidence for a shallow zero order silver grating showing angles at which field profiles have been calculated.

The electric field amplitudes follow a similar pattern with the top medium interference bands shifted in phase by $\pi^c$ with respect to corresponding the magnetic field bands. This equates to a shift in $y$ of $\lambda_g/4\cos\theta$ which again can be derived from simple kinematics.

Suppose I now corrugate the silver/vacuum interface with a sine wave of pitch 300*nm* and amplitude 30*nm*. The short pitch compared with the illumination wavelength of 632.8*nm* ensures that only the specular beam propagates across the entire range of incident angles, while the small amplitude/pitch ratio gives relatively weak diffraction effects. It is instructive to first look at the reflectivity curve of the specular beam and them examine the field distributions for various incident angles along this curve. Figure 3.4 shows a plot of $R_{pp}$ vs. angle of incidence for the system described above. Clearly visible is the Brewster minimum at 63°.

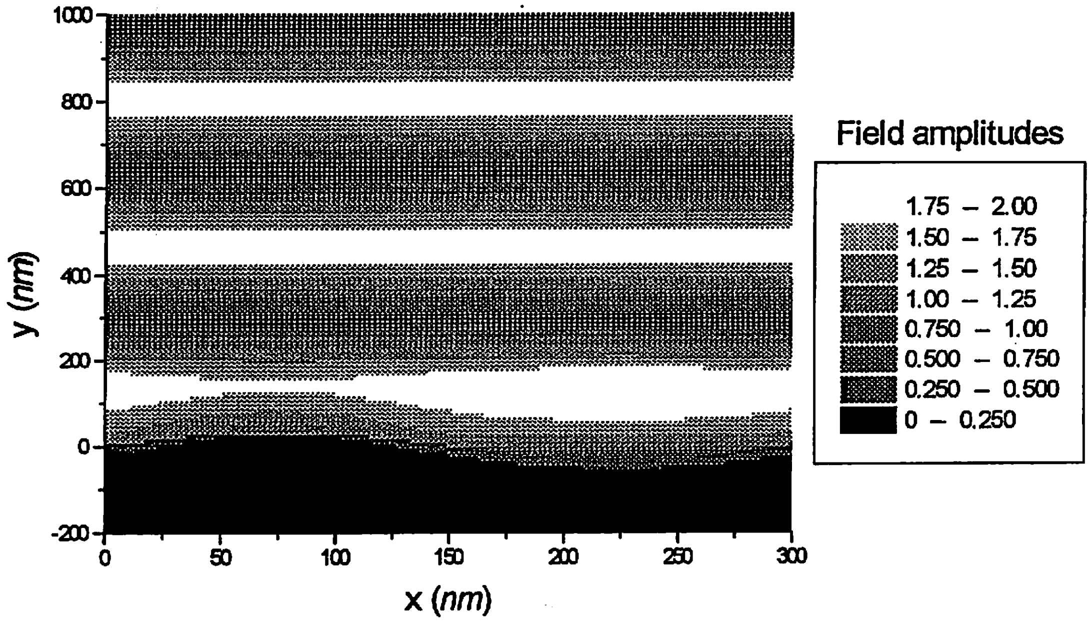

**Figure 3.5:** E field amplitudes for a 20° angle of incidence

I have chosen the three points marked on the graph to look at field distributions. The first at angle of incidence 20° is a control away from influence of the Brewster minimum. Figure 3.5 shows the E field distribution at this point which for large values of $y$ looks very similar to the planar case presented in figure 3.3. This is of course just what we would expect as the far field consists of two interfering plane waves whether we are looking at a planar surface or a zero order grating. Closer to the grating surface, the near field contains additional evanescent surface waves with a visible decay length comparable to the grating pitch in this case. Their most noticeable effect is to bend the lines of equal E field amplitude to follow the grating surface - a direct manifestation of the continuity of tangential E. Moving on to figure 3.6 we find the E field amplitude distribution at the Brewster angle which in this case is 63°. The oscillatory nature of the far field amplitudes is no longer visible in this range because the interfering beams are both propagating closer to the grating normal with the effect that the $y$ co-ordinate periodicity distance of the far field interference maxima is now $\lambda / \cos\theta = 1400nm$.

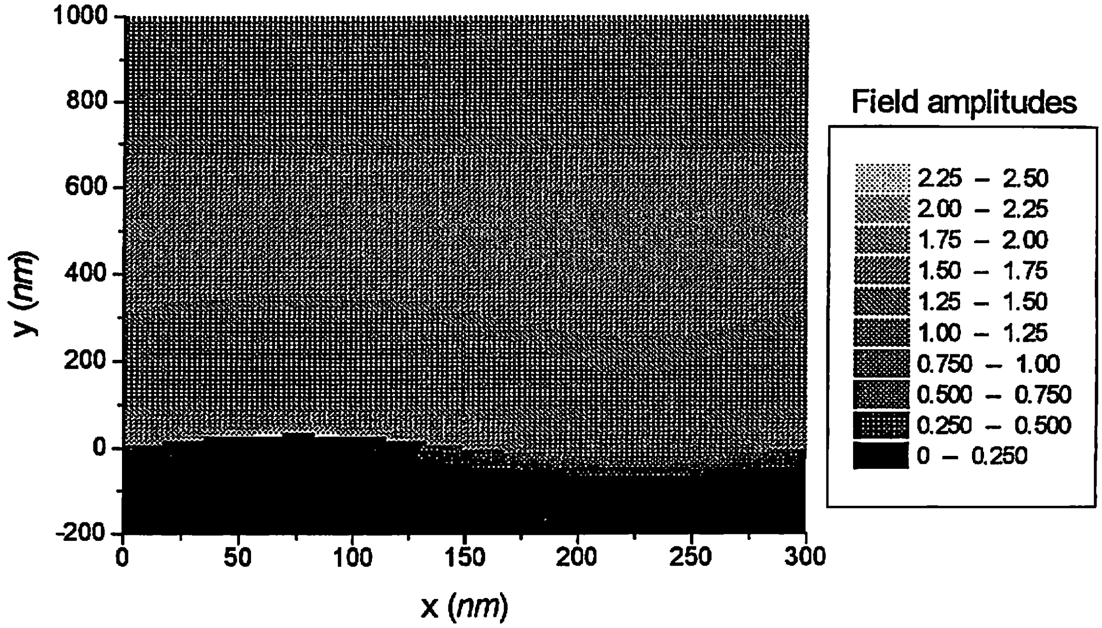

**Figure 3.6:** E field amplitudes for a 63° angle of incidence corresponding to the Brewster minimum.

More interesting is the behaviour of the near field which exhibits enhancement for a few tens of nanometers above the grating surface peaks. To accompany this increase there is a lowering of the average field amplitude just above the grating troughs. Such modulation of the field amplitudes is certainly connected with the occurrence of a non - radiative plasmon at the Brewster angle.

At higher angles still we move away from the Brewster minimum until at an 80° angle of incidence we find a distribution of E field amplitudes similar to that observed at 20°.

### *3.4.2 Deep gratings and field loops*

As a grating gets deeper so the strength of scattering associated with that grating increases. This could result in strong coupling to a non - specular propagating order, leading to comparatively large efficiencies in that order. More interesting however is the effect on the higher diffracted orders making up the evanescent near field - something that, at present, is not directly accessible through experimentation. It turns out that for deep gratings this near field exhibits interesting structure, and can provide considerable insight into that behaviour of the far field.

In particular the phenomena of blazing, anti-blazing and the tendency for deep gratings to behave like much shallower ones can all be explained in terms of the near field structure. Here I will only look at the latter of the three.

It has long been known that the optical response of a grating can vary periodically as a function of it's depth. As the depth of a grating is increased it's optical response changes accordingly. Increase the depth further and the optical response will slowly but surely tend back to that of the shallow grating, and so on seemingly ad infinitum.

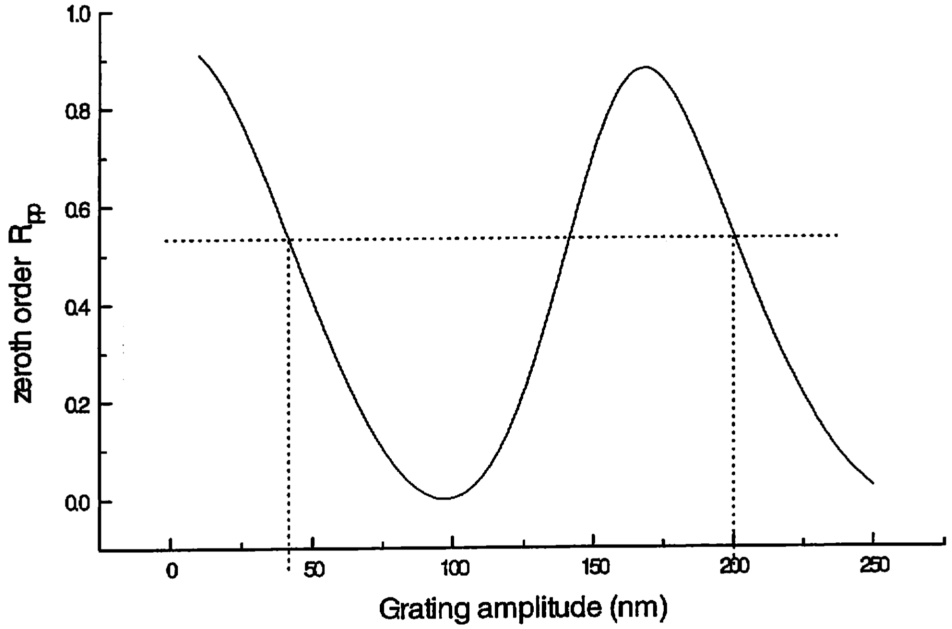

**Figure 3.7:** Graph of zeroth order $R_{pp}$ vs. Grating amplitude for a bare aluminium grating illuminated in the -1 Littrow configuration.

Figure 3.7 illustrates this phenomenon for a bare aluminium grating $(\varepsilon_r = -56.1, 10.5)$ of pitch 500*nm* illuminated with light of wavelength 632.8*nm* such that the incident wavevector is lying in the plane of incidence in the -1 Littrow configuration. The graph shows how the zeroth order $R_{pp}$ efficiency varies periodically with the grating amplitude. The dotted straight lines show that grating amplitudes of 40 and 200*nm* give rise to similar efficiencies and it is instructive to look at the field distributions for these two cases. With hindsight I will look at the energy flow $\frac{1}{2}\mathrm{Re}\left(\mathbf{E}\wedge\mathbf{H}^*\right)$, rather than **E** or **H** field amplitudes. The two figures 3.8,9 give a good indication of how the periodicity evidenced in figure 3.7 comes about. Efficiencies are calculated from the asymptotic energy flow so it is no surprise that away from the metal surface both gratings appear very similar in this respect. The reason for this similarity in energy flow can be seen in figure 3.9 where the perturbing effect of the deeper grating gives rise to closed loops within the grooves. These in turn modify the energy flow above the grating so that it takes on the character of the shallower grating.

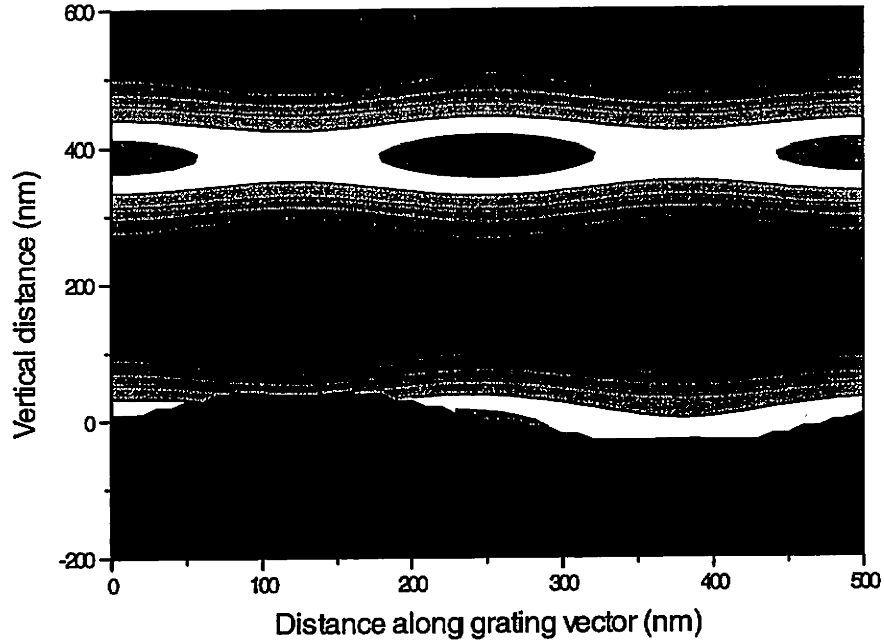

**Figure 3.8:** Poynting vector amplitudes for a 40*nm* amplitude aluminium grating illuminated under -1 Littrow incidence.

By filling the grooves these closed loops prevent the flow lines immediately above the grating from entering the groove region. Instead they can only flow into that part of the groove unoccupied by closed loops. It is as though the grooves have been filled with an effective dielectric thus shallowing the overall profile of the grating.

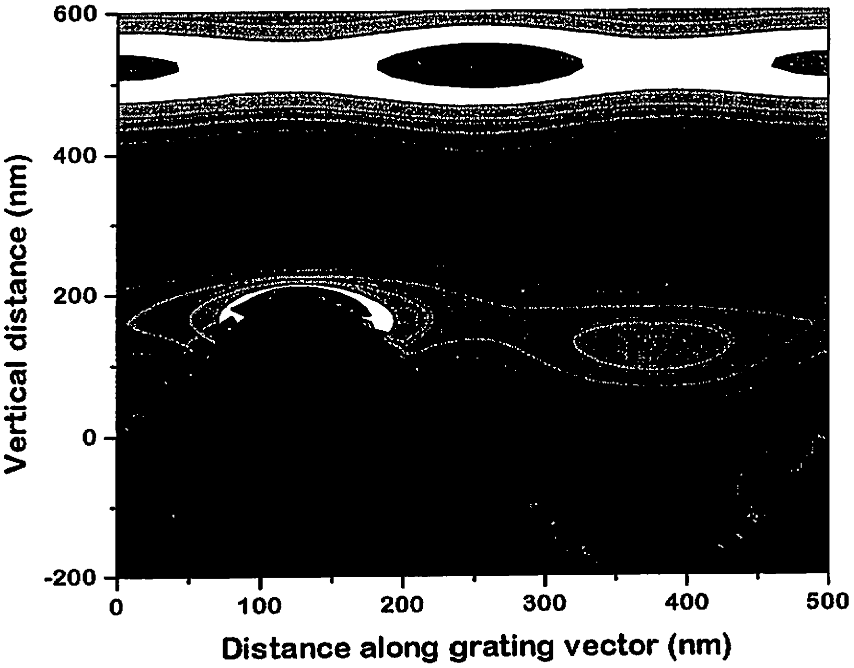

**Figure 3.9:** Poynting vector amplitudes for a 200*nm* amplitude aluminium grating illuminated under -1 Littrow incidence.

### *3.5 Conclusion*

Although I have barely touched the surface of the subject, it is clear that an analysis of the field profiles above a grating surface can provide valuable insight into the physical processes responsible for it's optical response. The surface plasmon polariton is one response feature that could certainly benefit from such investigation, as given the important role it plays it shaping the optical response of metallic gratings, little is known about the dynamics of it's propagation.

# 4. Generalisation to the conical mount

I shall now adapt the analysis of *Chapter* 2 so that we may consider the case where the plane of incidence does not contain the grating vector. This generalisation of the Chandezon technique was first performed by Popov and Mashev [1986], and then again separately by Elston, Bryan-Brown, and Sambles [1991].

Much of what has already been discussed in *chapter 2* will be repeated here, both for clarity and so that this chapter stands alone as a complete analysis of conical scattering.

## *4.1 Presentation of the problem*

The system under consideration is presented diagramatically in figure 4.1. Two semi-infinite media, labelled 0 and 1, are separated by an interface $y = s(x)$ where $s(x)$ is periodic in $x$ with period $\lambda_g$ giving a basis scattering vector of magnitude $K=2\pi/\lambda_g$ in the direction of the $x$ axis.

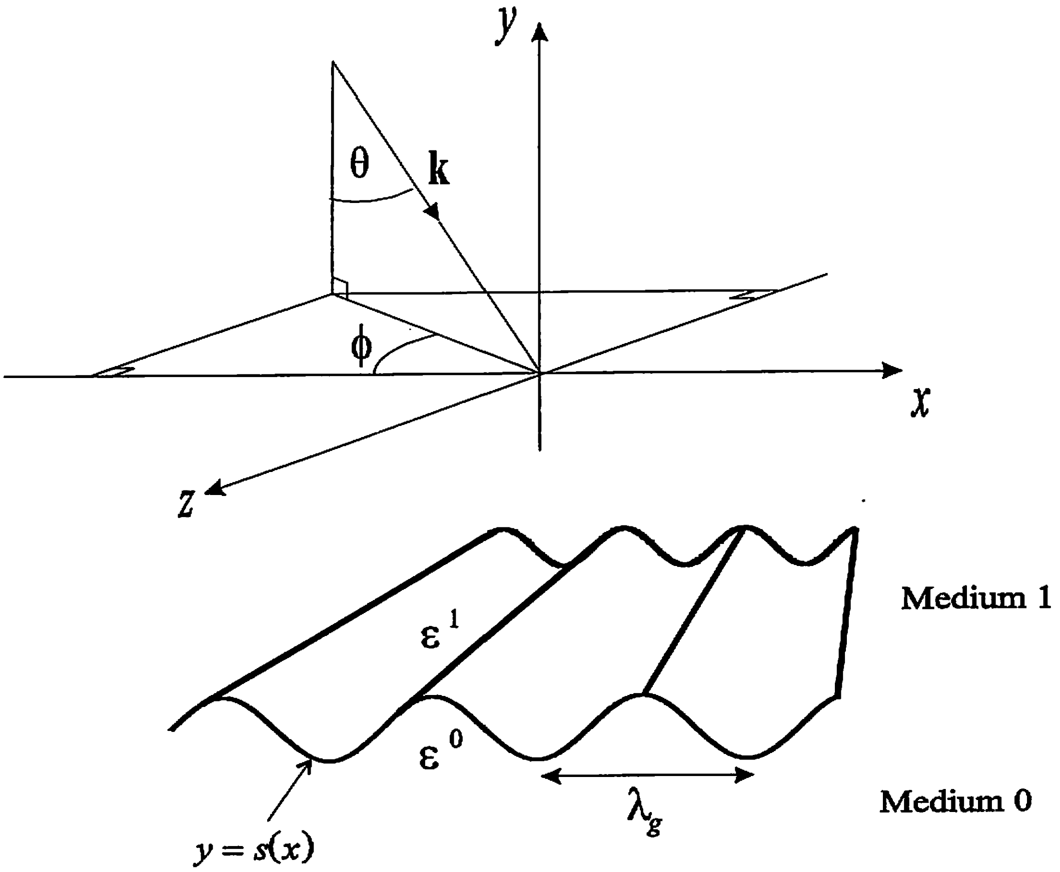

**Figure 4.1:** The system under consideration

Both media are required to be electrically and magnetically isotropic. Unlike the analysis of *chapter* 2 it is no longer assumed that the relative permeabilities of both media are unity, and they are allowed to take arbitrary values. Medium 0 is defined to be the substrate with complex relative permittivity $\varepsilon_r^0$ and complex relative permeability $\mu_r^0$. It may be metallic or dielectric. The grating is illuminated through medium 1 (which is consequently required to be non-absorbing having complex relative permittivity $\varepsilon_r^1$ and complex relative permeability $\mu_r^1$), by a homogeneous plane wave of wave vector $\mathbf{k}=\left(\varepsilon_r^1\mu_r^1\right)^{1/2}\mathbf{k}_0$ $(k_0=\omega/c)$ oriented at angle $\theta$ to the $y$ axis and azimithal angle $\phi$ in the $x$-$z$ plane. Although the development can allow for general polarisation of incoming light, for our purposes this will be limited to the case of incident transverse magnetic ( TM, or p- polarised with the **H** - field perpendicular to the plane of incidence ) or transverse electric ( TE, or s- polarised with the **E** - field perpendicular to the plane of incidence ).

## *4.2 The co-ordinate frame*

I will apply exactly the same co-ordinate transformation as that used in the non-conical case of *chapter 2*, the only difference being that I must now consider all three co-ordinate axes. As before then, I use a non-orthogonal curvilinear co-ordinate transformation to simplify the boundary conditions at the interfaces. The field in each medium will be expressed in terms of $v$, $u$ and $w$ where

$$v=x \qquad u=y-s(x) \qquad w=z \tag{4.1}$$

Thus $u$ is a variable which is related to the shape of the grating profile, where it takes the constant value $u=0$, and we have effectively mapped the grating interface onto a plane. Expressed in this system of co-ordinates Maxwell's equations are more complicated but the boundary conditions are much simplified. This is because we can now work directly with vector components that are always tangential to the grating surface.

Our non-orthogonal co-ordinate system gives rise to a set of basis vectors identical to those arising from the non-conical case. Here, however we must also include the two basis vectors in the $z$ direction. It turns out that both are just equal to **k** so that we have

$$\mathbf{e}_1 = \mathbf{i} + s'\mathbf{j} \qquad \mathbf{e}_2 = \mathbf{j} \qquad \mathbf{e}_3 = \mathbf{k} \tag{4.2}$$

with $s' = \dfrac{ds}{dx}$, from which all contravariant components can be defined by $\mathbf{A} = \mathbf{e}_i A^i$. Their dual vectors

$$\mathbf{e}^1 = \mathbf{i} \qquad \mathbf{e}^2 = \mathbf{j} - s'\mathbf{i} \qquad \mathbf{e}^3 = \mathbf{k} \tag{4.3}$$

provide a corresponding definition of the covariant components $\mathbf{A} = \mathbf{e}^i A_i$. By equating the two vector representations the following relations between the covariant and contravariant components can be found:

$$\begin{aligned} A^1 &= CA_1 - DA^2 \\ A_2 &= DA_1 + CA^2 \\ A^3 &= A_3 \end{aligned} \tag{4.4}$$

where the following definitions have been made

$$C = \frac{1}{1+s'^2} \qquad D = s'C \tag{4.5}$$

From here onwards I will adopt a system of units in which all lengths are written in units of the inverse of the free space incident wavenumber, $|k_0| = \frac{2\pi}{\lambda}$ and 'magnetic fields' denoted by H are $Z_0$ times real magnetic fields where $Z_0 = \left(\frac{\mu_0}{\varepsilon_0}\right)^{1/2}$ is the free space impedance. This will ensure that in certain matrices to be defined later all terms have comparable magnitude. This proves essential to the stability of the numerical methods employed.

### *4.3 Maxwell's equations*

Our aim is to write the two Maxwell curl equations $Curl\mathbf{E} = i\mu_r\mathbf{H}$ and $Curl\mathbf{H} = -i\varepsilon_r\mathbf{E}$ in terms of the mixed field components $E_1$, $E^2$, $H_3$ for *p*-polarised light and $H_1$, $H^2$, $E^3$, for *s*-polarised light since these correspond to 'components' that are locally parallel and normal to the surface. They are defined by $E_1 = \mathbf{e}_1.\mathbf{E}$, $E^2 = \mathbf{e}^2.\mathbf{E}$, and $E_3 = \mathbf{e}_3.\mathbf{E}$, with similar relationships for the components of **H**. It should be noted that only the vectors $\mathbf{e}_3 = \mathbf{e}^3 = \mathbf{k}$ are normalised. Consequently, although it is convenient to formulate the equations in terms of $E_1$, $E^2$, $E_3$, and their magnetic counterparts, the actual field components of **E** in the directions defined by $\mathbf{e}_1$ and $\mathbf{e}^2$, are given by $E_1\left(1+s'^2\right)^{-1/2}$ and $E^2\left(1+s'^2\right)^{-1/2}$. Similar relations hold for the field components of **H**.

We start by noting that since $\nabla = \mathbf{e}^i \dfrac{\partial}{\partial q^i}$, $\mathbf{e}^i \wedge \mathbf{e}^j = \varepsilon_{ijk}\mathbf{e}_k$, and $\dfrac{\partial}{\partial v}\left(\mathbf{e}^2\right) = -s''\mathbf{e}^1$

$$Curl\mathbf{A} = \begin{vmatrix} \mathbf{e}_1 & \mathbf{e}_2 & \mathbf{e}_3 \\ \dfrac{\partial}{\partial v} & \dfrac{\partial}{\partial u} & \dfrac{\partial}{\partial w} \\ A_1 & A_2 & A_3 \end{vmatrix} \tag{4.6}$$

The $\mathbf{e}_i$ are orthogonal to their dual vectors $\mathbf{e}^i$ and so $\mathbf{e}^1.Curl\mathbf{A} = \dfrac{\partial A_3}{\partial u} - \dfrac{\partial A_2}{\partial w}$ etc. Thus taking the dot product of the two Maxwell equations with $\mathbf{e}^i$ : $i$=1,2,3 we arrive at six coupled equations:

$$\left(\frac{\partial \mathrm{E}_3}{\partial \mathrm{u}} - \frac{\partial}{\partial w}\left(DE_1 + CE^2\right)\right) = i\mu_r\left(CH_1 - DH^2\right) \tag{4.7}$$

$$\left(\frac{\partial E_1}{\partial \mathrm{w}} - \frac{\partial E_3}{\partial v}\right) = i\mu_r H^2 \tag{4.8}$$

$$\left(\frac{\partial}{\partial v}\left(DE_1 + CE^2\right) - \frac{\partial E_1}{\partial \mathrm{u}}\right) = i\mu_r H_3 \tag{4.9}$$

$$\left(\frac{\partial H_3}{\partial u} - \frac{\partial}{\partial w}\left(DH_1 + CH^2\right)\right) = -i\varepsilon_r\left(CE_1 - DE^2\right) \tag{4.10}$$

$$\left(\frac{\partial H_1}{\partial \mathrm{w}} - \frac{\partial H_3}{\partial v}\right) = -i\varepsilon_r E^2 \tag{4.11}$$

$$\left(\frac{\partial}{\partial v}\left(DH_1 + CH^2\right) - \frac{\partial H_1}{\partial u}\right) = -i\varepsilon_r E_3 \tag{4.12}$$

Here unwanted components of the form $A^1$ , $A_2$ and $A^3$ have been eliminated using (4.4). Previously in *chapter* 2 I described the non-conical case where the TM-like and TE-like fields de-couple so that for a given polarisation the six equations (4.7-12) reduce down to three. However, in the case of conical scattering there is no such de-coupling of the fields and we must consider all six equations at once. As before I eliminate the normal fields $E^2$ and $H^2$ so that only those tangential to the surface $y = s(x)$ remain in my equations. I retain these tangential fields because it is they that are continuous across the grating interface. Also since momentum is conserved in the $z$ / $w$ direction we can make the substitution $\frac{\partial}{\partial w} \leftrightarrow i\gamma$ . Previously we had six coupled equations in six unknowns. Eliminating $E^2$ and $H^2$ leaves us with four coupled equations in four unknowns:

$$\frac{\partial E_1}{\partial u} = \frac{\partial}{\partial v}\left[DE_1 - \frac{\gamma C}{\varepsilon_r} H_1 - i\frac{C}{\varepsilon_r}\frac{\partial H_3}{\partial v}\right] - i\mu_r H_3 \tag{4.13}$$

$$\frac{\partial E_3}{\partial u} = D\frac{\partial E_3}{\partial v} + iC\left(\mu_r - \frac{\gamma^2}{\varepsilon_r}\right)H_1 + \frac{\gamma C}{\varepsilon_r}\frac{\partial H_3}{\partial v} \tag{4.14}$$

$$\frac{\partial H_1}{\partial u} = \frac{\partial}{\partial v}\left[DH_1 + \frac{\gamma C}{\mu_r} E_1 + i\frac{C}{\mu_r}\frac{\partial E_3}{\partial v}\right] + i\varepsilon_r E_3 \tag{4.15}$$

$$\frac{\partial H_3}{\partial u} = D\frac{\partial H_3}{\partial v} + iC\left(\frac{\gamma^2}{\mu_r} - \varepsilon_r\right)E_1 - \frac{\gamma C}{\mu_r}\frac{\partial E_3}{\partial v} \tag{4.16}$$

### *4.4 Expansion of the fields in Bloch waves*

I can now exploit the periodic nature of the system and expand the field components in terms of Bloch waves:

$$\Psi(v,u)=\sum_m \Psi_m(u)\exp i\alpha_m v \tag{4.17}$$

$$\text{where } \alpha_m=\left(\mu_r^1\varepsilon_r^1\right)^{1/2}\sin\theta\,\cos\phi+mK \tag{4.18}$$

reflecting the fact that the incident beam makes an angle $\phi$ with the $x$-$y$ plane. $\Psi$ represents any one of the four field components $E_1$, $E_3$, $H_1$ and $H_3$. Similarly the functions C and D defined in equation (4.5) are expanded in Fourier series:

$$C(v)=\sum_p C_p\exp ipKv \qquad D(v)=\sum_p D_p\exp ipKv \tag{4.19}$$

Introducing these expansions into equations (4.13-16) individual Fourier components of the fields may be singled out by using orthogonality with $\exp i\alpha_m v$ leading to an infinite system of coupled differential equations:

$$-i\frac{\partial E_{1(m)}}{\partial u}=\sum_n\left\{\alpha_m D_{m-n}E_{1(n)}-\frac{\gamma}{\varepsilon_r}\alpha_m C_{m-n}H_{1(n)}+\left(\frac{\alpha_m\alpha_n}{\varepsilon_r}C_{m-n}-\mu_r\delta_{mn}\right)H_{3(n)}\right\} \tag{4.20}$$

$$-i\frac{\partial E_{3(m)}}{\partial u}=\sum_n\left\{\alpha_n D_{m-n}E_{3(n)}+C_{m-n}\left(\mu_r-\frac{\gamma^2}{\varepsilon_r}\right)H_{1(n)}+\frac{\gamma}{\varepsilon_r}\alpha_n C_{m-n}H_{3(n)}\right\} \tag{4.21}$$

$$-i\frac{\partial H_{1(m)}}{\partial u}=\sum_n\left\{\frac{\gamma}{\mu_r}\alpha_m C_{m-n}E_{1(n)}+\left(\varepsilon_r\delta_{mn}-\frac{\alpha_m\alpha_n}{\mu_r}C_{m-n}\right)E_{3(n)}+\alpha_m D_{m-n}H_{1(n)}\right\} \tag{4.22}$$

$$-i\frac{\partial H_{3(m)}}{\partial u}=\sum_n\left\{\left(\frac{\gamma^2}{\mu_r}-\varepsilon_r\right)C_{m-n}E_{1(n)}-\frac{\gamma}{\mu_r}\alpha_n C_{m-n}E_{3(n)}+\alpha_n D_{m-n}H_{3(n)}\right\} \tag{4.23}$$

In preparation for the necessary numerical calculation we truncate these expansions, limiting them to the range $-M\le m,n\le M$ and write the four coupled equations as a single eigenvalue equation:

$$-i\frac{\partial}{\partial u}\begin{pmatrix} E_{1(m)} \\ E_{3(m)} \\ H_{1(m)} \\ H_{3(m)} \end{pmatrix} = \begin{pmatrix} t_{11} & t_{12} & t_{13} & t_{14} \\ t_{21} & t_{22} & t_{23} & t_{24} \\ t_{31} & t_{32} & t_{33} & t_{34} \\ t_{41} & t_{42} & t_{43} & t_{44} \end{pmatrix} \begin{pmatrix} E_{1(m)} \\ E_{3(m)} \\ H_{1(m)} \\ H_{3(m)} \end{pmatrix} \tag{4.24}$$

$$t_{11} : \alpha_m D_{m-n}$$
$$t_{12} : 0$$
$$t_{21} : 0$$
$$t_{22} : \alpha_n D_{m-n}$$

$$t_{13} : -\frac{\gamma}{\varepsilon_r}\alpha_m C_{m-n}$$
$$t_{14} : \frac{\alpha_m \alpha_n}{\varepsilon_r} C_{m-n} - \mu_r \delta_{mn}$$
$$t_{23} : \left(\mu_r - \frac{\gamma^2}{\varepsilon_r}\right) C_{m-n}$$
$$t_{24} : \frac{\gamma}{\varepsilon_r}\alpha_n C_{m-n}$$

$$t_{31} : \frac{\gamma}{\varepsilon_r}\alpha_m C_{m-n}$$
$$t_{32} : \varepsilon_r \delta_{mn} - \frac{\alpha_m \alpha_n}{\mu_r} C_{m-n}$$
$$t_{41} : \left(\frac{\gamma^2}{\mu_r} - \varepsilon_r\right) C_{m-n}$$
$$t_{42} : -\frac{\gamma}{\varepsilon_r}\alpha_n C_{m-n}$$

$$t_{33} : \alpha_m D_{m-n}$$
$$t_{34} : 0$$
$$t_{43} : 0$$
$$t_{44} : \alpha_n D_{m-n}$$

We can write this in the more readable form

$$-i\frac{\partial \xi(u)}{\partial u} = \mathbf{T}\xi(u) \tag{4.25}$$

in which $\xi(u) = \left(E_{1(m)}, E_{3(m)}, H_{1(m)}, H_{3(m)}\right)^{\mathrm{T}}$ and **T** is a 4(2$M$+1) square matrix constructed from sixteen 2$M$+1 square submatrices reflecting the strength of scattering between the various orders. This matrix is constant in each medium and so the field vector $\xi(u)$ can be expanded as a sum of its eigenfunctions:

$$\xi(u) = \sum_{q=1}^{8M+4} b_q \mathbf{V}_q \exp i r_q u \tag{4.26}$$

where $r_q$ are the eigenvalues of the matrix $\mathbf{T}$, $\mathbf{V}_q$ its eigenvectors and $b_q$ the amplitude associated with the $q^{\text{th}}$ eigenmode. Finally using the above we may state the form of $\xi(\mathrm{u})$ in the $j^{\text{th}}$ medium where $j = 0$ or 1:

$$\xi^j(u) = \mathbf{M}^j \phi^j(u)\mathbf{b}^j \tag{4.27}$$

where $\mathbf{M}^j$ is a matrix whose columns are the eigenvectors of $\mathbf{T}^j$, $\phi^j$ is a square matrix with elements $\phi^j_{qp} = \delta_{qp} \exp ir^j_q u$ , and $\mathbf{b}^j$ is a vector of amplitude coefficients which need to be evaluated in order to find the field in each medium.

### *4.5 Boundary conditions on the interface*

As in *chapter 2* I have formulated a field vector $\xi(u) = \left(E_{1(m)}, E_{3(m)}, H_{1(m)}, H_{3(m)}\right)^{\mathrm{T}}$ in which all field components are tangential to the grating surface and thus continuous across it. Defining the phase of the fields in both media to be zero on the interface, we have the condition $\xi^1(u) = \xi^0(u)$.

### *4.6 Asymptotic field expansions*

Having developed the Maxwell equations I now require the form of the incoming and scattered fields in the transformed frame, that is in terms of the co-ordinates *v*, *u*, and *w*. The incoming field which propagates as a single plane wave has spatial dependence

$$\Psi(v,u,w) = \Psi^i \exp i(\alpha_0 x - \beta_0 y + \gamma z) = \Psi^i \exp i(\alpha_0 v - \beta_0 (u + s(v)) + \gamma w) \tag{4.28}$$

where $\Psi^i$ represents any one of the four incident field components $E^i_1$, $E^i_3$, $H^i_1$, and $H^i_3$. Developing a Fourier series over momenta $\alpha_m$ this may be written in a form consistent with equation (4.27):

$$\Psi(v,u,w) = \sum_m (\Psi^i)_m L_m(\beta_0) \exp i(\alpha_m v - \beta_0 u + \gamma w) \tag{4.29}$$

where $L_m(t) = \frac{1}{\lambda_g}\int_0^{\lambda_g} \exp - (s(v)t + mKv)dv$ as in *chapter 2.*

I will choose to write the "in-plane" field components $E_1^i$ and $H_1^i$ in terms of the two transverse components $E_3^i$ and $H_3^i$. Thus I set

$$E_3^i(v,u,w) = \sum_m \left(E_3^i\right)_m L_m(\beta_0)\exp i(\alpha_m v - \beta_0 u + \gamma w) \tag{4.30}$$

and

$$H_3^i(v,u,w) = \sum_m \left(H_3^i\right)_m L_m(\beta_0)\exp i(\alpha_m v - \beta_0 u + \gamma w) \tag{4.31}$$

The corresponding expression for the $E_1^i$ field component can be obtained using a rearranged equation (4.16):

$$\left(E_1^i\right)_m = \frac{-i}{\left(\varepsilon_r - \frac{\gamma^2}{\mu_r}\right)}\left((1+s'^2)\frac{\partial\left(H_3^i\right)_m}{\partial u} - s'\frac{\partial\left(H_3^i\right)_m}{\partial v} + \frac{\gamma}{\mu_r}\frac{\partial\left(E_3^i\right)_m}{\partial v}\right) \tag{4.32}$$

Referring to equation (4.28) we can evaluate the required differentials giving

$$\left(E_1^i\right)_m = \frac{1}{\left(\varepsilon_r - \frac{\gamma^2}{\mu_r}\right)}\left(-\beta_0\left(H_3^i\right)_m - s'\alpha_0\left(H_3^i\right)_m + \frac{\gamma}{\mu_r}(\alpha_0 - s'\beta_0)\left(E_3^i\right)_m\right) \tag{4.33}$$

Here we want to eliminate all terms in $s'$ so that any spatial dependence in the $v$ variable is represented purely in terms of Bloch waves. The following identity proves useful in this context:

$$\beta_0 s'\sum_m L_m(\beta_0)\exp i(\alpha_0 v - \beta_0 u + \gamma w) \equiv -\sum_m (mK)L_m(\beta_0)\exp i(\alpha_0 v - \beta_0 u + \gamma w) \tag{4.34}$$

Substituting this identity into equation (4.33) leaves us with a suitable expression for $\left(E_1^i\right)_m$:

$$\left(E_1^i\right)_m = \frac{1}{\left(\varepsilon_r - \frac{\gamma^2}{\mu_r}\right)}\left(\left(-\beta_0 + \frac{\alpha_0}{\beta_0} mK\right)\left(H_3^i\right)_m + \frac{\gamma\alpha_m}{\mu_r}\left(E_3^i\right)_m\right) \tag{4.35}$$

Following the same procedure with equation (4.14) I can derive a corresponding expression for $H_1^i$:

$$\left(H_1^i\right)_m = \frac{1}{\left(\mu_r - \frac{\gamma^2}{\varepsilon_r}\right)}\left(\left(-\beta_0 + \frac{\alpha_0}{\beta_0} mK\right)\left(H_3^i\right)_m + \frac{\gamma\alpha_m}{\varepsilon_r}\left(E_3^i\right)_m\right) \tag{4.36}$$

We can apply exactly the same analysis to the propagating diffracted field in medium 1, which is a sum of plane waves. Asymptotically this field can be represented by a partial Rayleigh expansion over the propagating orders only:

$$\Psi(v,u,w) = \sum_{n\in U} \Psi_n^i \exp i\left(\alpha_n x - \beta_n y + \gamma z\right) = \sum_{n\in U} \Psi_n^i \exp i\left(\alpha_n v - \beta_n (u + s(v)) + \gamma w\right) \tag{4.37}$$

where $U$ is the set of integers such that $\left|\alpha_n^2 + \gamma^2\right| < \left(\mu_r^1 \varepsilon_r^1\right)$. Following the analysis through it is possible to derive four equations analogous to (4.30,31,35,36).

Generally we can say that for a Bragg plane wave with momentum component $\alpha_s$ in the direction of the grating vector, the four associated field components have the common expansion form

$$\Psi^s(u,v,w) = \sum_m \Psi_m^s(u) \exp i\left(\alpha_m v + \beta_s u + \gamma w\right) \tag{4.38}$$

with

$$\left(E_3\right)_m^s = E_3^s L_{m-s}(-\beta_s) \tag{4.39}$$

$$\left(H_3\right)_m^s = H_3^s L_{m-s}(-\beta_s) \tag{4.40}$$

$$\left(E_1\right)_m^s = \frac{1}{f_1}\left(\left(\beta_s - \frac{\alpha_s}{\beta_s}(m-s)K\right)H_3^s + \gamma\alpha_m E_3^s\right)L_{m-s}(-\beta_s) \tag{4.41}$$

$$\left(H_1\right)_m^s = \frac{1}{f_2}\left(\left(\beta_s - \frac{\alpha_s}{\beta_s}(m-s)K\right)E_3^s - \frac{\gamma}{\varepsilon}\alpha_m H_3^s\right)L_{m-s}(-\beta_s) \tag{4.42}$$

$f_1 = \varepsilon_r - \frac{\gamma^2}{\mu_r}$, $f_2 = \mu_r - \frac{\gamma^2}{\varepsilon_r}$ and $\beta_s$ takes the values

$$\begin{array}{lll}
\text{Incident field:} & \beta_s = -\left(\mu_r^1\varepsilon_r^1 - \alpha_s^2 - \gamma^2\right)^{1/2} & s = 0 \\
\text{Reflected field} & \beta_s = +\left(\mu_r^1\varepsilon_r^1 - \alpha_s^2 - \gamma^2\right)^{1/2} & s = \pm 0,1,2,\ldots. \\
\text{Transmitted field} & \beta_s = -\left(\mu_r^0\varepsilon_r^0 - \alpha_s^2 - \gamma^2\right)^{1/2} & s = \pm 0,1,2,\ldots.
\end{array} \tag{4.43}$$

The incident wave expansions provide us with a vector describing the incident field in the transformed co-ordinates. By normalising the incident H field we may set values for $E_3^s$ and $H_3^s$ ( s=0 ) which 'prime' the system.

The remaining summations describing the real reflected and transmitted fields run over the subset of real diffracted waves $n \in P \Leftrightarrow \left|\alpha_n^2 + \gamma^2\right| < \mu_r\varepsilon_r$ where the values of $\varepsilon_r$ and $\mu_r$ must be taken appropriate to the medium in which the wave is propagating. The field coefficients $E_3^s$ and $H_3^s$ are the unknowns we ultimately seek from which the TM-like and TE-like reflectivities for a given order s can be determined. Note that the $L_{m-s}$ integrals describe a transformation from the curvilinear space (*v*, *u*, *w*) into Cartesian co-ordinates for incident and reflected waves in medium 1 and for transmitted waves in medium 0.

### *4.7 Method of solution*

The mechanics of the final solution have been discussed previously for the in-plane case and apply equally to our twisted geometry with the understanding all matrices are now doubled in size. We write the reflected wave amplitudes as

$$\hat{\mathbf{R}} = \left(\hat{\mathbf{M}}_{11}^1 - \mathbf{A}\hat{\mathbf{M}}_{21}^1\right)\left(\mathbf{A}\mathbf{L}'' + \mathbf{L}'\right) \qquad \mathbf{A} = \mathbf{M}_{12}^0\left(\mathbf{M}_{22}^0\right)^{-1} \tag{4.44}$$

in which $\hat{\mathbf{M}}^1$ is the same as $\mathbf{M}^1$ with those columns representing the eigenvectors of the real upward propagating modes replaced by the appropriate forms of (4.39-4.42). Similarly $\mathbf{L}=\begin{pmatrix}\mathbf{L}'\\ \mathbf{L}''\end{pmatrix}$ is a column vector containing the incident wave forms of those expansions. A related calculation gives the transmitted wave amplitudes

$$\begin{pmatrix}\mathbf{0}\\ \hat{\mathbf{T}}\end{pmatrix}=\begin{pmatrix}\hat{\mathbf{M}}^0_{11} & \hat{\mathbf{M}}^0_{12}\\ \hat{\mathbf{M}}^0_{21} & \hat{\mathbf{M}}^0_{22}\end{pmatrix}^{-1}\begin{pmatrix}\mathbf{M}^0_{11} & \mathbf{M}^0_{12}\\ \mathbf{M}^0_{21} & \mathbf{M}^0_{22}\end{pmatrix}\begin{pmatrix}\mathbf{0}\\ \mathbf{b}^0_-\end{pmatrix}=\begin{pmatrix}\mathbf{I} & \mathbf{0}\\ \mathbf{0} & \mathbf{Q}\end{pmatrix}\begin{pmatrix}\mathbf{0}\\ \mathbf{b}^0_-\end{pmatrix} \tag{4.45}$$

with

$$\mathbf{b}^0_-=\left(\mathbf{M}^0_{22}\right)^{-1}\left(\hat{\mathbf{M}}^1_{21}\hat{\mathbf{R}}+\mathbf{L}''\right) \tag{4.46}$$

from which we can derive

$$\hat{\mathbf{T}}=\mathbf{Q}\mathbf{b}^0_- \tag{4.47}$$

Note that $\hat{\mathbf{M}}^0$ is the exit medium equivalent of $\hat{\mathbf{M}}^{Q+1}$.

### *4.8 Testing the code*

As in chapter 2 there are two types of test I can perform: mathematical and numerical. Mathematically the four coupled equations (4.13-16) must reduce to their non - conical counterparts (2.22,23) in the limit of $\gamma = 0$. The reader can verify that this is indeed the case.

From a numerical point of view I performed the same tests on the code as described in chapter 2, namely checking that the code was consistent with the energy balance and reciprocity theorems for a variety of input parameters. To back up the mathematical check described above I set the azimuthal angle to zero and compared with the original in - plane code as applied to the parameters shown in table 2.4. As with the non conical calculation of *chapter* 2 a value of $M$=16 was sufficient to achieve convergence to 6 decimal places over the whole range of incident momenta. Table 4.1 shows the efficiencies calculated in this way - the reader may verify that they are in exact agreement with those calculated in table 2.5.

| Angle of incidence ( degrees ) | $R_{pp}$ efficiencies for order | | | | |
|---|---|---|---|---|---|
| | -3 | -2 | -1 | zeroth | +1 |
| 20 | - | 0.0410056 | 0.3465162 | 0.1450929 | 0.4158503 |
| 40 | 0.2366756 | 0.3866453 | 0.2355621 | 0.0181451 | - |
| 60 | 0.0321183 | 0.1990150 | 0.3765563 | 0.3559276 | - |
| 80 | 0.0358831 | 0.1008208 | 0.1957197 | 0.6231396 | - |

**Table 4.1:** Calculated efficiencies with $\phi=0^\circ$ for comparison with the previous, non-conical code

### *4.9 Numerical examples*

The extension of the Chandezon technique to conical scattering does not alter the mechanics of the numerical solution, save for the doubling in size of all matrices. As a result the conclusions about convergence and validity arrived at towards the end of *chapter* 2 still hold true here. I will give one sample calculation as a test case and then show comparisons between theory and experimental data.

### *4.9.1 The distorted sinusoidal grating*

Taking the same grating used in table 4.1, I will now give examples of calculated theoretical reflectivities for the conical mount with azimuthal angle $\phi = 20^\circ$. Figure 4.2 shows the resulting $R_{pp}$ plot while table 4.2 shows a selection of the calculated efficiencies.

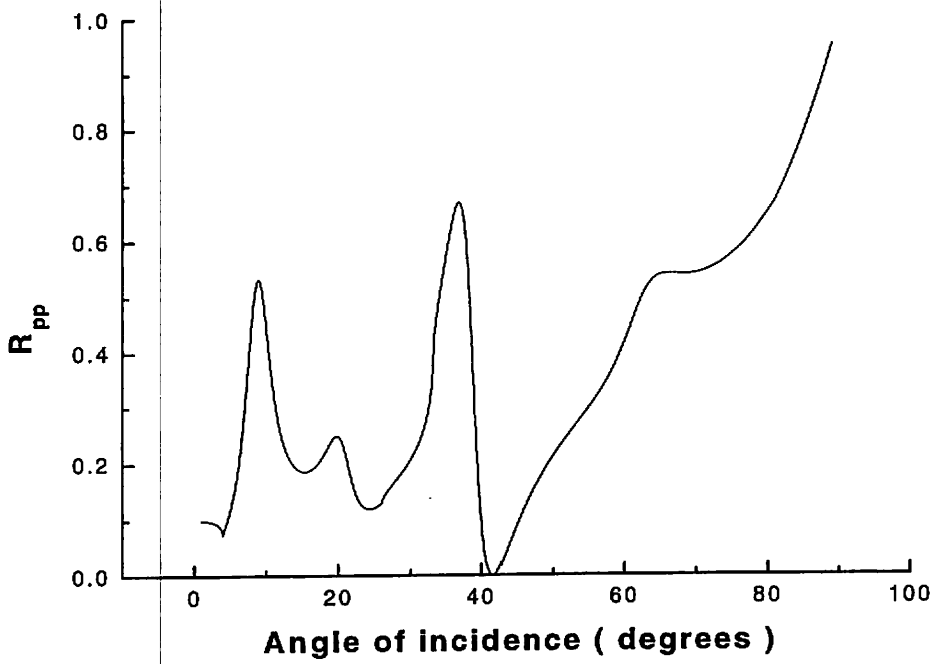

**Figure 4.2:** $R_{pp}$ plot for the system described in table 2.6 with azimuthal angle $\phi = 20^{\circ}$

| Polar angle ( degrees ) | $R_{pp}$ efficiencies for order | | |
|---|---|---|---|
| | -1 | zeroth | +1 |
| 20 | 0.1457921 | 0.2487083 | 0.2723300 |
| 40 | 0.1315993 | 0.1023605 | - |
| 60 | 0.2133007 | 0.4191634 | - |
| 80 | 0.2081143 | 0.6518692 | - |

**Table 4.2:** A selection of the calculated efficiencies

### *4.9.2 Comparison with experimental data*[1]

In this section I will show how the theory was used to characterise a paladium grating of aspect ratio 0.1. The parameters of the system are shown in table 4.3.

---

[1] All experimental work was carried out by R. A. Watts

| Incident light<br>$\lambda$=632.8*nm* | Grating profile<br>$\lambda_g$=1078.8*nm* | Permittivities |
|---|---|---|
| TM polarisation | 4 harmonics which are<br>49.37*nm* phase $0^0$<br>-8.30*nm* phase $90^\circ$<br>-2.48*nm* phase $0^\circ$ | $\varepsilon^1$=(1,0)<br>$\varepsilon^0$=(-10.74,1.28) |

**Table 4.3:** Parameters of the system modelled in figures 4.3

All the following graphs comparing experimental data with theory have been fitted using the same parameters, namely those in table 4.3 above.

Figure 4.3a shows the $R_{pp}$ fit for azimuthal angle $\phi = 0^\circ$ with the surface plasmon resonance clearly visible at a polar angle of approximately $28^\circ$.

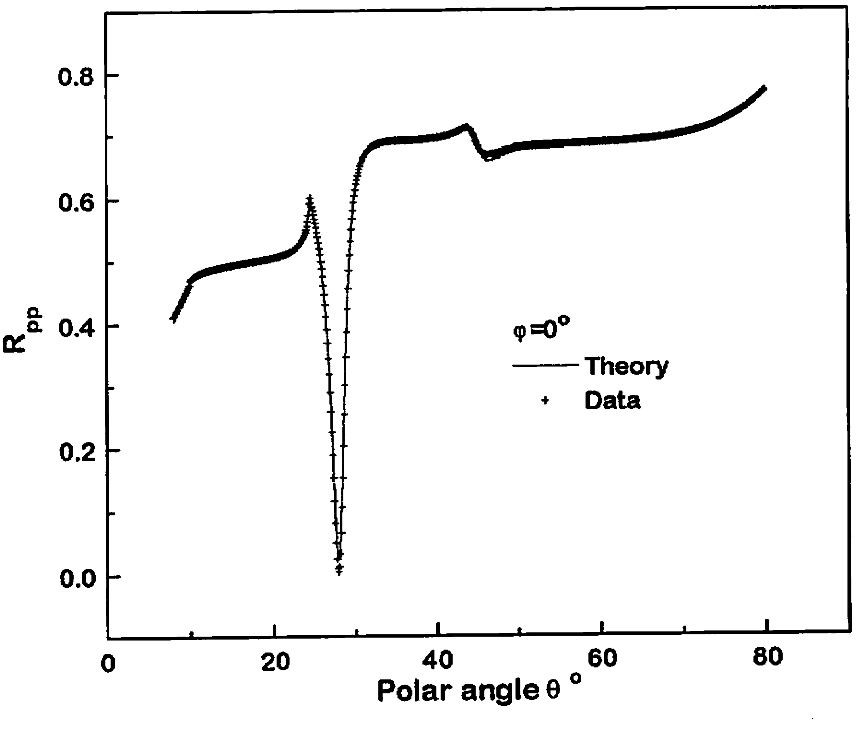

**Figure 4.3a:** Fit to $R_{pp}$ experimental data for $\phi = 0^\circ$.

To excite this plasmon requires a component of the electric field in the direction of the grating vector as is the case. We can achieve the same situation with $R_{ss}$ polarisation at azimuthal angle $\phi = 90^\circ$ - this is shown in figure 4.3b where again we can see the same plasmon resonance, now excited at $\theta = 60^\circ$.

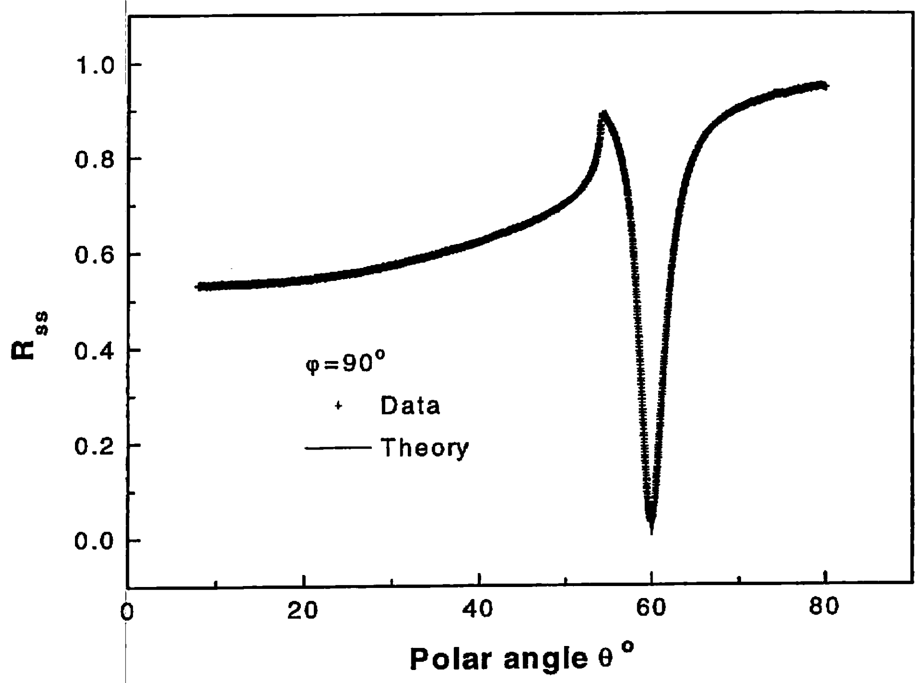

**Figure 4.3b:** Fit to the $R_{ss}$ data at azimuthal angle $\phi = 90^\circ$.

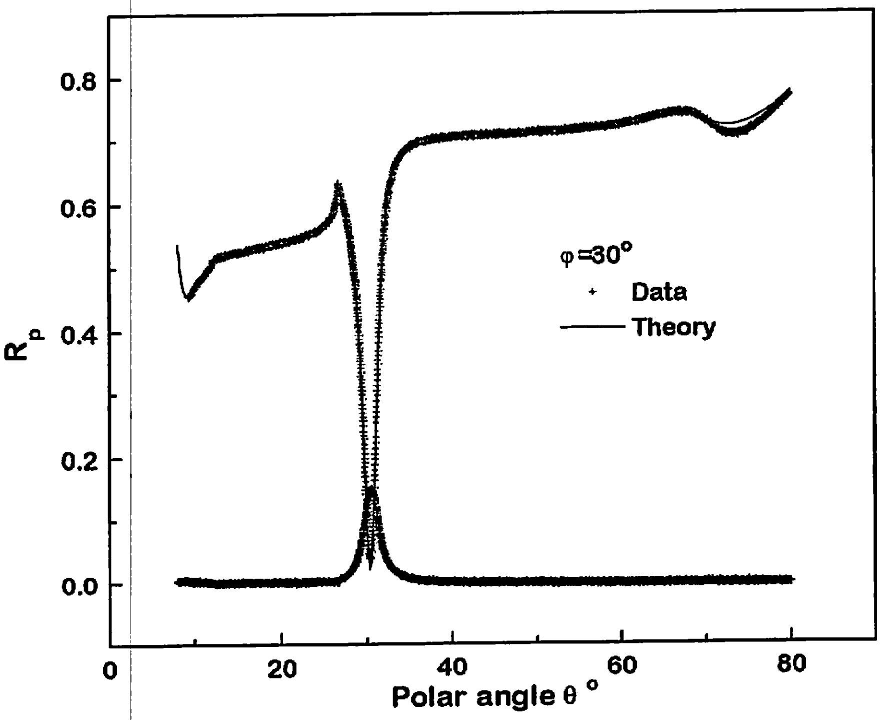

**Figure 4.3c:** Fits for $R_{pp}$ and $R_{ps}$ at azimuthal angle $\phi = 30^\circ$.

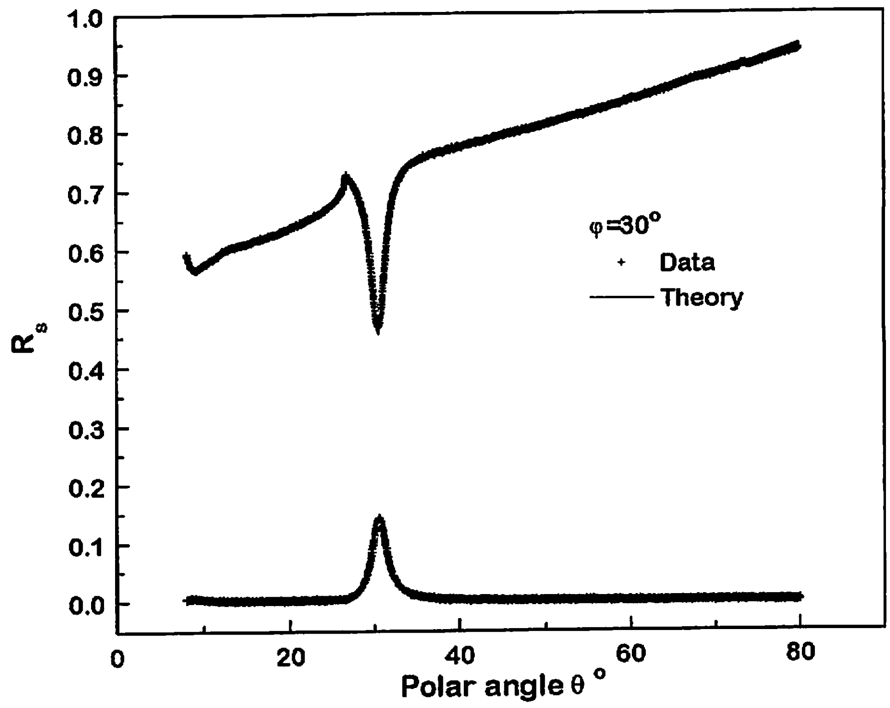

**Figure 4.3d:** Fits for $R_{ss}$ and $R_{sp}$ at azimuthal angle $\phi = 30^{\circ}$.

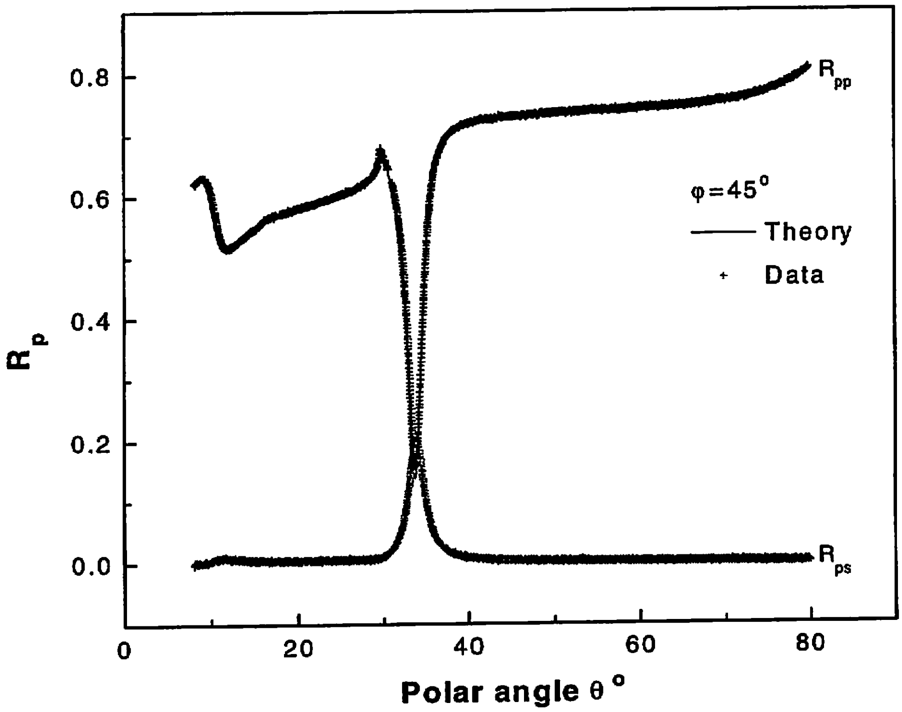

**Figure 4.3e:** Fits for $R_{ss}$ and $R_{sp}$ at azimuthal angle $\phi = 45^{\circ}$.

Moving on I now consider the case where $\phi = 30^{\circ}$. Figures 4.3c,d show fits to the $R_{pp}$, $R_{ps}$ and the $R_{ss}$, $R_{sp}$ data at this angle, illustrating the phenomenon of polarisation conversion, which in this case is strongest at an angle corresponding to the surface plasmon resonance. This of course is just what we expect as the conversion of one polarisation to another is due to a break in the symmetries associated with boundary conditions across the grating surface. The phenomenon is thus driven by surface currents of which the surface plasmon is the most prominent example.

Finally, in figure 4.3e I show the $R_{pp}$ and $R_{ss}$ experimental data for $\phi = 45^{\circ}$ along with the corresponding theoretical fits.

## *4.10 Conclusion*

The generalisation of Chandezon's formalism to the conical mount is a relatively straightforward procedure. Rotating the plane of incidence out of the $x$ - $y$ plane we find that both TM and TE polarisations give rise to four rather than two field components tangential to the grating surface. The result is four rather than two coupled equations and the resulting analysis is almost identical to that for the in - plane case with all matrices doubled in size.

The convergence properties of the conical case have been shown (empirically) to be identical to those of the in - plane case, the only difference being an increase in computation time due to the larger matrices involved. On the subject of computation times the reader should note that there exists an alternative approach [Li, 1995] whereby the conical eigenvalues and eigenvectors may be obtained from a single in - plane calculation with an associated reduction in run times.

# 5. Multicoated gratings

In *chapter* 2 I looked at the differential method of Chandezon as applied to bare gratings - that is gratings consisting of two semi-infinite media separated by a single interface. However, often the addition of a suitable dielectric overlayer can alter the optical response of a particular grating significantly. I now consider the necessary modifications required to Chandezon's formalism so that we may model these multicoated structures - work which was first carried out by Cotter *et. al.* [1995] for the non - conical case.

## *5.1 Strategy*

Our problem is to determine the optical response of the multicoated grating shown in figure 5.1. The dielectric or metallic substrate of relative permittivity $\varepsilon_r^0$ and relative permeability $\mu_r^0$ is coated by $Q$ dielectric or metallic overlayers with permittivities $\varepsilon_r^1$, ... , $\varepsilon_r^Q$, permeabilities $\mu_r^1$, ... , $\mu_r^Q$ and thicknesses $d^1$, ... , $d^Q$. All interfaces are constrained to be of the same profile $s(x)$ - periodic in $x$ with period $\lambda_g$ giving a Bragg scattering vector of magnitude $K = 2\pi/\lambda_g$ directed along the positive $x$ axis. The uppermost semi-infinite media, from which the structure is illuminated, is a non-absorbing dielectric of relative permittivity $\varepsilon_r^{Q+1}$ and relative permeability $\mu_r^{Q+1}$.

All the difficult analysis has already been done in *chapter* 2 where I described a plan for our method of solution:

- The disturbance on the uppermost interface is due to the incident plane wave, reflected Bragg modes, which are also plane waves, and evanescent fields which are surface waves bound to the grating interface, and decay with increasing $y$ into medium $Q$+1.

- The disturbance just below the lowest interface is due to transmitted Bragg modes and evanescent fields which decay with decreasing $y$ into medium 0.

Using boundary conditions described in *section 2.6* to match the two enables $R_n$ and $T_n$, the complex amplitudes of the $n^{th}$ reflected and transmitted Bragg modes to be determined, and hence the reflectivities and transmissivities.

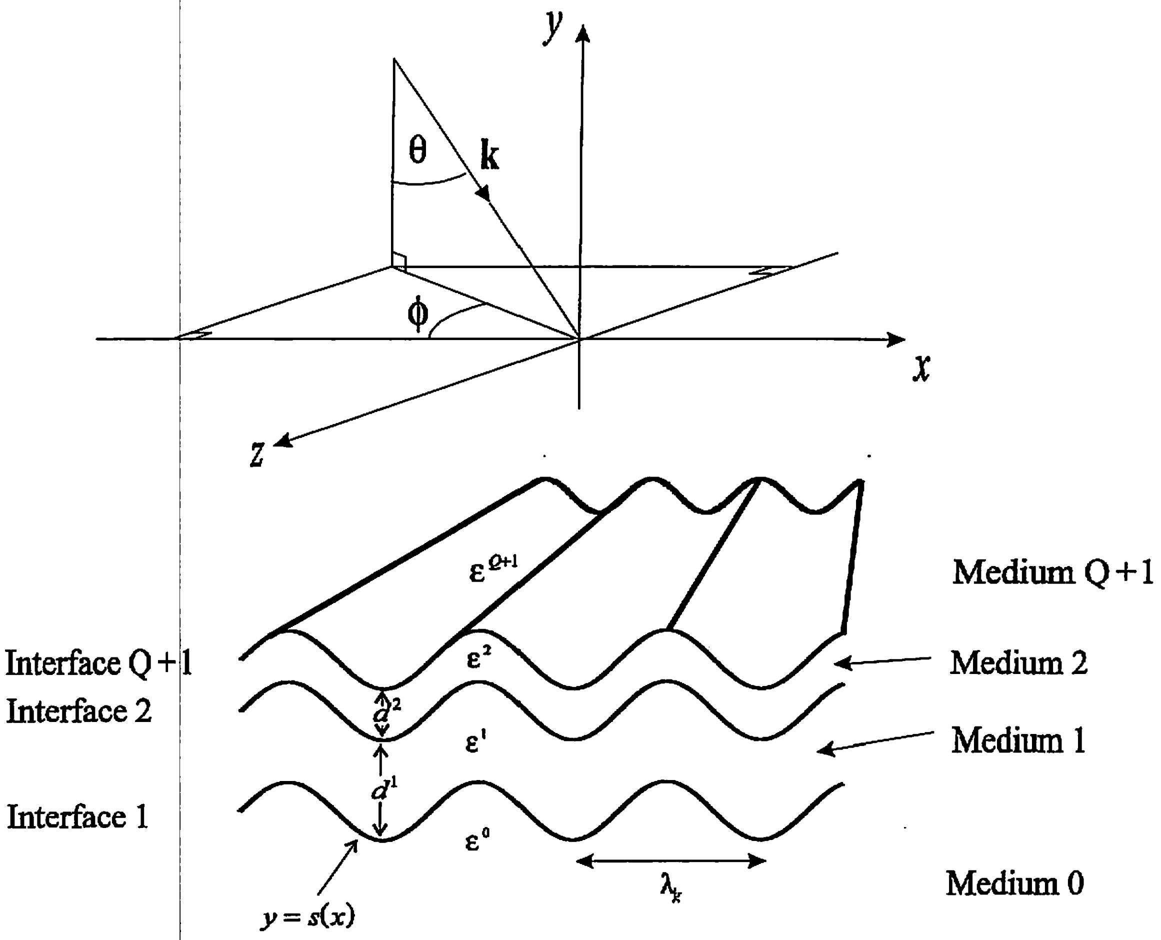

**Figure 5.1:** Diagrammatic representation of the multicoated grating

It is only this last step that we need modify - rather than match fields across a single interface we must now match through a series of overlayers with their corresponding material boundaries. Figure 5.2 shows a schematic representation of the fields present in the first dielectric overlayer. We have already mentioned that an equal number of upward and downward propagating waves exist in each medium and the reasons why we separate the two when representing the electromagnetic fields as a linear superposition of eigenmodes:

$$\xi = \begin{pmatrix} \mathbf{M}_{11} & \mathbf{M}_{12} \\ \mathbf{M}_{21} & \mathbf{M}_{22} \end{pmatrix} \begin{pmatrix} \phi_+ & \mathbf{0} \\ \mathbf{0} & \phi_- \end{pmatrix} \begin{pmatrix} \mathbf{b}_+ \\ \mathbf{b}_- \end{pmatrix} \tag{5.1}$$

where + denotes upward propagation and - denotes downward propagation. For the purpose of field matching all fields are defined to have zero phase on the lower bounding interface of the medium in which they exist. The exception to this rule is in the substrate or medium 0 where, in the absence of any lower boundary, the zero of phase is defined to be the 1st interface.

### *5.2 The Transfer matrix*

#### *5.2.1 Formulation*

With the aim of finding a relation between $b^0$ and $b^{Q+1}$ we match fields across this 1st interface $\xi^0(0) = \xi^1(0)$ and find that

$$M^0 b^0 = M^1 b^1 \tag{5.2}$$

The transfer matrix associated with propagating fields across interface 1 is defined by

$$b^0 = \mathbf{I}^1 \mathrm{b}^1 \qquad \Rightarrow \qquad \mathbf{I}^1 = [M^0]^{-1} M^1 \tag{5.3}$$

In this way the transfer matrix relates all fields on one side of an interface to all the fields on the other side of the interface - in this respect it is fundamentally different from the scattering matrix which I shall describe later.

In travelling to the 2nd interface the fields in region 1 experience a phase change $\phi(d^1)$ so that the continuity of fields across this interface: $\xi^1(d^1) = \xi^2(0)$, yields

$$M^1 \phi^1(d^1)\, b^1 = M^2 b^2 \tag{5.4}$$

The transfer matrix associated with interface 2 is then

$$\mathbf{I}^2 = [\phi^1(d^1)]^{-1}\, [M^1]^{-1} M^2 \tag{5.5}$$

In fact it is easy to see that the general form for the transfer matrix across interface $j$ is

$$\mathbf{I}^j = [\phi^{j-1}(d^{j-1})]^{-1}\, [M^{j-1}]^{-1} M^j \tag{5.6}$$

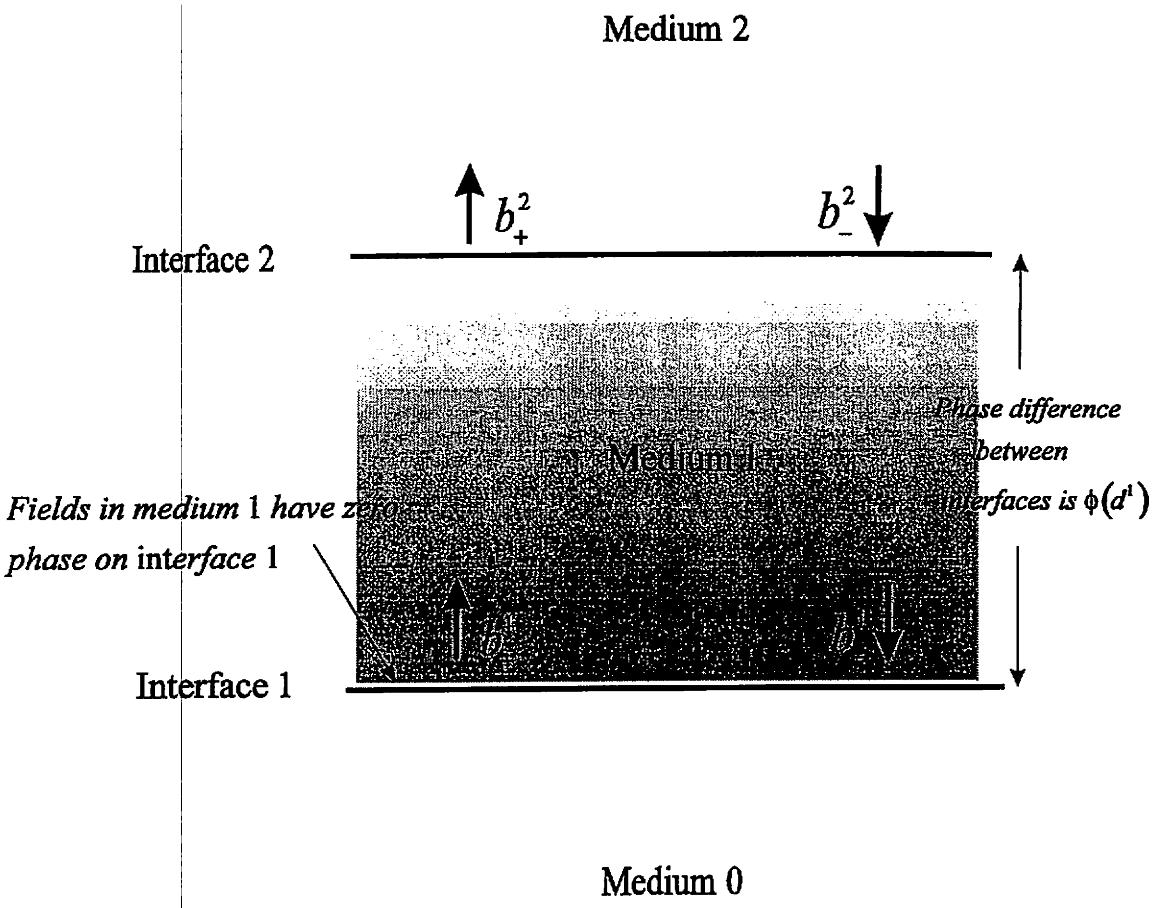

**Figure 5.2:** Schematic representation of the fields around medium 1

Using these expressions and iterating through to the uppermost interface a relation between the field vector in the top medium and that in the substrate is found.

$$\mathbf{M}^{Q+1}\mathbf{b}^{Q+1} = \left\{\mathbf{M}^{Q}\phi^{Q}\left(d^{Q}\right)\left[\mathbf{M}^{Q}\right]^{-1}\right\}\dots\dots\left\{\mathbf{M}^{1}\phi^{1}\left(d^{1}\right)\left[\mathbf{M}^{1}\right]^{-1}\right\}\mathbf{M}^{0}\mathbf{b}^{0} \tag{5.7}$$

or

$$\mathbf{M}^{Q+1}\mathbf{b}^{Q+1} = \mathbf{H}^{Q}\mathbf{H}^{Q-1}\dots\dots\mathbf{H}^{1}\mathbf{M}^{0}\mathbf{b}^{0} \tag{5.8}$$

where $\mathbf{H}^{j} = \left[\mathbf{I}^{j}\right]^{-1}$ is a matrix associated with propagation through the $j^{\text{th}}$ interface. We then complete the solution to the grating problem in the same manner as section 2.9: Outgoing wave conditions are imposed on the fields in media 0 and $Q$+1.

### *5.2.2 Reflection calculations*

If we want to calculate efficiencies for the propagating orders in the uppermost medium then, at the same time that we impose outgoing wave conditions, we express those orders as a sum of plane waves transformed into the curvilinear co-ordinates. Evanescent fields are still represented as a sum of eigenmodes. The left hand side of equation (5.8) is then replaced with this split representation of the fields.

$$\begin{pmatrix} \mathbf{M}_{11}^{Q+1} & \mathbf{M}_{12}^{Q+1} \\ \mathbf{M}_{21}^{Q+1} & \mathbf{M}_{22}^{Q+1} \end{pmatrix} \begin{pmatrix} \mathbf{b}_{+}^{1} \\ \mathbf{b}_{-}^{1} \end{pmatrix} = \begin{pmatrix} \hat{\mathbf{M}}_{11}^{Q+1} & \hat{\mathbf{M}}_{12}^{Q+1} \\ \hat{\mathbf{M}}_{21}^{Q+1} & \hat{\mathbf{M}}_{22}^{Q+1} \end{pmatrix} \begin{pmatrix} \hat{\mathbf{R}} \\ \mathbf{0} \end{pmatrix} + \begin{pmatrix} \mathbf{L}' \\ \mathbf{L}'' \end{pmatrix} \tag{5.9}$$

Note that for the in-plane case $\mathbf{L}''$ must be replaced with $\mathbf{L}''/\varepsilon_r^{Q+1}$ for all appearances of $\mathbf{L}''$ in this chapter due to the definition of $\xi$ as $\left(F_m, G_m/\varepsilon_r\right)^T$ in the symmetry case. $\hat{\mathbf{M}}$ and $\hat{\mathbf{R}}$ retain their definitions from section 2.9. Substituting (5.9) into (5.8) we have

$$\begin{pmatrix} \hat{\mathbf{M}}_{11}^{Q+1} & \hat{\mathbf{M}}_{12}^{Q+1} \\ \hat{\mathbf{M}}_{21}^{Q+1} & \hat{\mathbf{M}}_{22}^{Q+1} \end{pmatrix} \begin{pmatrix} \hat{\mathbf{R}} \\ \mathbf{0} \end{pmatrix} + \begin{pmatrix} \mathbf{L}' \\ \mathbf{L}'' \end{pmatrix} = \begin{pmatrix} \mathbf{H}_{11} & \mathbf{H}_{12} \\ \mathbf{H}_{21} & \mathbf{H}_{22} \end{pmatrix} \begin{pmatrix} \mathbf{0} \\ \mathbf{b}_{-}^{0} \end{pmatrix} \tag{5.10}$$

where $\mathbf{H}_{11}$, $\mathbf{H}_{12}$, $\mathbf{H}_{21}$, and $\mathbf{H}_{22}$ are the four submatrices of $\mathbf{H} = \mathbf{H}^{Q}\mathbf{H}^{Q-1}.......\mathbf{H}^{1}\mathbf{M}^{0}$. expanding equation (5.10) in terms of these submatrices we arrive at two equations identical to (2.80,81) but with $\mathbf{M}^0$ replaced by $\mathbf{H}$.

$$\mathbf{H}_{12}\mathbf{b}_{-}^{0} = \hat{\mathbf{M}}_{11}^{1}\hat{\mathbf{R}} + \mathbf{L}' \tag{5.11}$$

$$\mathbf{H}_{22}\mathbf{b}_{-}^{0} = \hat{\mathbf{M}}_{21}^{1}\hat{\mathbf{R}} + \mathbf{L}'' \tag{5.12}$$

Solving then gives

$$\mathbf{b}_{-}^{0} = \left(\mathbf{H}_{22}\right)^{-1}\left(\hat{\mathbf{M}}_{21}^{1}\hat{\mathbf{R}} + \mathbf{L}''\right) \tag{5.13}$$

$$\hat{\mathbf{R}} = \left(\hat{\mathbf{M}}_{11}^{1} - \mathbf{A}\hat{\mathbf{M}}_{21}^{1}\right)\left(\mathbf{A}\mathbf{L}'' + \mathbf{L}'\right) \qquad \mathbf{A} = \mathbf{H}_{12}\left(\mathbf{H}_{22}\right)^{-1} \tag{5.14}$$

Obviously these equations are very similar to those presented in *chapter* 2. In the same way if we want to calculate efficiencies for any propagating orders in medium 0 then we arrive at equations identical to (2.94-96) but with $\mathbf{M}^0$ replaced by **H**.

### *5.2.3 Limitations of the method*

The method of matching fields described above is essentially the same as that used by Chandezon *et al.* in their paper of 1982 and is generally unsuitable for overlayer thicknesses greater than the wavelength of light used, or for large numbers of overlayers ( > ~ 7 ). In this regime propagation of the solution is plagued by numerical instabilities arising from loss of significant digits in the transfer matrices.

Consider the single layer shown in figure 5.2 and in particular the contribution to the field at the upper interface made by a pair of evanescent waves. The first is bound to the upper interface and decays towards the lower interface, while the second is bound to the lower interface and decays towards the upper interface. The first wave then has a much greater contribution to the field at the upper interface than the second, which while propagating across the layer has decreased in magnitude. The result is that all information connected with the second, smaller wave is swamped by the larger contribution of the first wave. Note that it cannot be reasoned that the contribution offered by the second wave is then insignificant and of no importance to the final solution, for we may use our knowledge of the fields at the upper interface to calculate their value at the lower interface where the second wave now makes a larger contribution than the first. It is clear that we need a different approach in these situations.

## *5.3 The scattering matrix method*

### *5.3.1 Formalism*

We have seen how problems arise when upward and downward evanescent waves are evaluated at the same point in space. A natural approach would then be to separately consider the contributions arising from the upward and downward modes. This is exactly the approach taken in the scattering matrix formalism [Ko and Sambles, 1988], illustrated in figure 5.3:

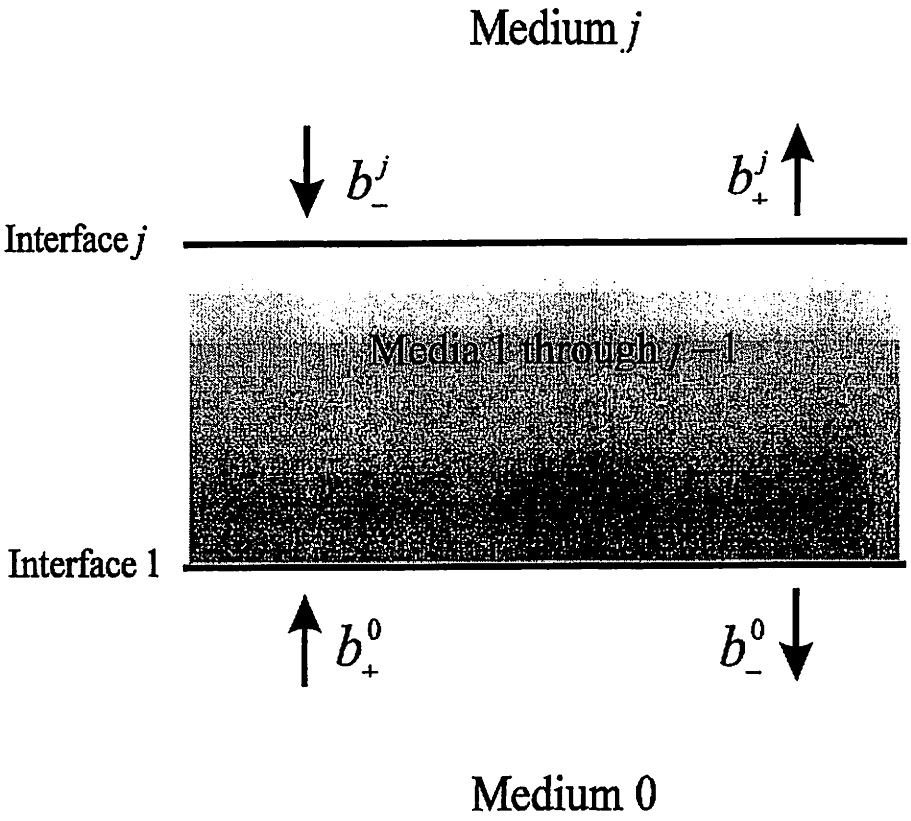

**Figure 5.3:** Matching fields across a material interface using a scattering matrix

I first define the scattering matrix relation between the field coefficients in the zeroth and $j^{th}$ layers:

$$\begin{pmatrix}\mathbf{b}_+^j\\ \mathbf{b}_-^0\end{pmatrix}=\mathbf{S}^j\begin{pmatrix}\mathbf{b}_+^0\\ \mathbf{b}_-^j\end{pmatrix} \tag{5.15}$$

In order to generate the scattering matrix S(0,$j$+1) for the subsystem up to the ($j$+1)$^{th}$ layer we refer to the transfer matrix equation for propagation through the $j^{th}$ interface. At this interface the electric and magnetic fields of the $j^{th}$ and the ($j$+1)$^{th}$ interfaces must match as described in section 2.6. This provides a set of equations coupling the coefficients $\mathbf{b}_+^j$,$\mathbf{b}_-^j$ and $\mathbf{b}_+^{j+1}$,$\mathbf{b}_-^{j+1}$ of the electromagnetic modes in the two adjacent layers:

$$\begin{pmatrix}\mathbf{b}_+^j\\ \mathbf{b}_-^j\end{pmatrix}=\begin{pmatrix}\mathbf{I}_{11}^{j+1} & \mathbf{I}_{12}^{j+1}\\ \mathbf{I}_{21}^{j+1} & \mathbf{I}_{22}^{j+1}\end{pmatrix}\begin{pmatrix}\mathbf{b}_+^{j+1}\\ \mathbf{b}_-^{j+1}\end{pmatrix} \tag{5.16}$$

which is the transfer matrix equation for propagation through the $(j+1)^{\text{th}}$ interface with $\mathbf{I}$ given by an expression similar to equation (5.6): $\mathbf{I}^{j+1} = [\phi^{j-1}(d^j)]^{-1}\,[M^j]^{-1}M^{j+1}$.

We take equation (5.15) which is the scattering matrix relation between the field coefficients in the zeroth and $j^{\text{th}}$ layers, and then use (5.6) to derive the corresponding relation between field coefficients in the zeroth and $(j+1)^{\text{th}}$ layers. Doing so we arrive at four simultaneous equations

$$\mathbf{b}_+^j = \mathbf{S}_{11}^j \mathbf{b}_+^0 + \mathbf{S}_{12}^j \mathbf{b}_-^j \tag{5.17}$$

$$\mathbf{b}_-^0 = \mathbf{S}_{21}^j \mathbf{b}_+^0 + \mathbf{S}_{22}^j \mathbf{b}_-^j \tag{5.18}$$

$$\mathbf{b}_+^j = \mathbf{I}_{11}^{j+1} \mathbf{b}_+^{j+1} + \mathbf{I}_{12}^{j+1} \mathbf{b}_-^{j+1} \tag{5.19}$$

$$\mathbf{b}_-^j = \mathbf{I}_{21}^{j+1} \mathbf{b}_+^{j+1} + \mathbf{I}_{22}^{j+1} \mathbf{b}_-^{j+1} \tag{5.20}$$

from which the coefficients associated with the $j^{\text{th}}$ interface can be eliminated to give

$$\begin{pmatrix} \mathbf{b}_+^{j+1} \\ \mathbf{b}_-^0 \end{pmatrix} = \begin{pmatrix} \mathbf{S}_{11}^{j+1} & \mathbf{S}_{12}^{j+1} \\ \mathbf{S}_{21}^{j+1} & \mathbf{S}_{22}^{j+1} \end{pmatrix} \begin{pmatrix} \mathbf{b}_+^0 \\ \mathbf{b}_-^{j+1} \end{pmatrix} \tag{5.21}$$

where

$$\mathbf{S}_{11}^{j+1} = \left(\mathbf{I}_{11}^{j+1} - \mathbf{S}_{12}^j \mathbf{I}_{21}^{j+1}\right)^{-1} \mathbf{S}_{11}^j \tag{5.22}$$

$$\mathbf{S}_{12}^{j+1} = \left(\mathbf{I}_{11}^{j+1} - \mathbf{S}_{12}^j \mathbf{I}_{21}^{j+1}\right)^{-1} \left(\mathbf{S}_{12}^j \mathbf{I}_{22}^{j+1} - \mathbf{I}_{12}^{j+1}\right) \tag{5.23}$$

$$\mathbf{S}_{21}^{j+1} = \mathbf{S}_{22}^j \mathbf{I}_{21}^{j+1} \mathbf{S}_{11}^{j+1} + \mathbf{S}_{21}^j \tag{5.24}$$

$$\mathbf{S}_{22}^{j+1} = \mathbf{S}_{22}^j \mathbf{I}_{21}^{j+1} \mathbf{S}_{12}^{j+1} + \mathbf{S}_{22}^j \mathbf{I}_{22}^{j+1} \tag{5.25}$$

To implement the full solution we must apply outgoing wave conditions on the fields in the outermost media. In medium 0 this means we can keep only those terms $\mathbf{b}_-^0$ that correspond to downward propagating waves and those evanescent waves whose amplitude decreases as $u \to \infty$. Hence in equation (5.21) we set $\mathbf{b}_+^0=0$ and obtain the relations

$$\mathbf{b}_+^{j+1} = \mathbf{S}_{12}^{j+1}\mathbf{b}_-^{j+1} \quad \text{and} \quad \mathbf{b}_-^0 = \mathbf{S}_{22}^{j+1}\mathbf{b}_-^{j+1} \tag{5.26}$$

### *5.3.2 Reflection calculations*

As with the transfer matrix method, if we want to calculate efficiencies for the propagating orders in the uppermost medium then, at the same time, we express those orders as a sum of plane waves transformed into the curvilinear co-ordinates. Evanescent fields are still represented as a sum of eigenmodes, and we have the split representation of equation (5.9) which is repeated here for clarity.

$$\begin{pmatrix} \mathbf{M}_{11}^{Q+1} & \mathbf{M}_{12}^{Q+1} \\ \mathbf{M}_{21}^{Q+1} & \mathbf{M}_{22}^{Q+1} \end{pmatrix} \begin{pmatrix} \mathbf{b}_+^{Q+1} \\ \mathbf{b}_-^{Q+1} \end{pmatrix} = \begin{pmatrix} \hat{\mathbf{M}}_{11}^{Q+1} & \hat{\mathbf{M}}_{12}^{Q+1} \\ \hat{\mathbf{M}}_{21}^{Q+1} & \hat{\mathbf{M}}_{22}^{Q+1} \end{pmatrix} \begin{pmatrix} \hat{\mathbf{R}} \\ \mathbf{0} \end{pmatrix} + \begin{pmatrix} \mathbf{L}' \\ \mathbf{L}'' \end{pmatrix} \tag{5.27}$$

Using the scattering matrix relations (5.26) to relate these fields and their outgoing wave conditions to those in medium 0 we have

$$\begin{pmatrix} \hat{\mathbf{M}}_{11}^{Q+1} & \hat{\mathbf{M}}_{12}^{Q+1} \\ \hat{\mathbf{M}}_{21}^{Q+1} & \hat{\mathbf{M}}_{22}^{Q+1} \end{pmatrix} \begin{pmatrix} \hat{\mathbf{R}} \\ \mathbf{0} \end{pmatrix} + \begin{pmatrix} \mathbf{L}' \\ \mathbf{L}'' \end{pmatrix} = \begin{pmatrix} \mathbf{M}_{11}^{Q+1} & \mathbf{M}_{12}^{Q+1} \\ \mathbf{M}_{21}^{Q+1} & \mathbf{M}_{22}^{Q+1} \end{pmatrix} \begin{pmatrix} \mathbf{S}_{12}^{Q+1}\left(\mathbf{S}_{22}^{Q+1}\right)^{-1}\mathbf{b}_-^0 \\ \left(\mathbf{S}_{22}^{Q+1}\right)^{-1}\mathbf{b}_-^0 \end{pmatrix} \tag{5.28}$$

Expanding in terms of sub-matrices we arrive at two equations

$$\hat{\mathbf{M}}_{11}^{Q+1}\hat{\mathbf{R}} + \mathbf{L}' = \mathbf{M}_{11}^{Q+1}\mathbf{S}_{12}^{Q+1}\left(\mathbf{S}_{22}^{Q+1}\right)^{-1}\mathbf{b}_-^0 + \mathbf{M}_{12}^{Q+1}\left(\mathbf{S}_{22}^{Q+1}\right)^{-1}\mathbf{b}_-^0 \tag{5.29}$$

$$\hat{\mathbf{M}}_{21}^{Q+1}\hat{\mathbf{R}} + \mathbf{L}'' = \mathbf{M}_{21}^{Q+1}\mathbf{S}_{12}^{Q+1}\left(\mathbf{S}_{22}^{Q+1}\right)^{-1}\mathbf{b}_-^0 + \mathbf{M}_{22}^{Q+1}\left(\mathbf{S}_{22}^{Q+1}\right)^{-1}\mathbf{b}_-^0 \tag{5.30}$$

Which we solve for $\hat{\mathbf{R}}$ and $\mathbf{b}_-^0$ to obtain

$$\begin{aligned} \hat{\mathbf{R}} = {} & \left[\hat{\mathbf{M}}_{11}^{Q+1} - \left(\mathbf{M}_{11}^{Q+1}\mathbf{S}_{12}^{Q+1} + \mathbf{M}_{12}^{Q+1}\right)\left(\mathbf{M}_{21}^{Q+1}\mathbf{S}_{12}^{Q+1} + \mathbf{M}_{22}^{Q+1}\right)^{-1}\hat{\mathbf{M}}_{21}^{Q+1}\right]^{-1} \cdot \\ & \cdot\left[\left(\mathbf{M}_{11}^{Q+1}\mathbf{S}_{12}^{Q+1} + \mathbf{M}_{12}^{Q+1}\right)\left(\mathbf{M}_{21}^{Q+1}\mathbf{S}_{12}^{Q+1} + \mathbf{M}_{22}^{Q+1}\right)^{-1}\mathbf{L}'' - \mathbf{L}'\right] \end{aligned} \tag{5.31}$$

$$\mathbf{b}_-^0 = \mathbf{S}_{22}^{Q+1}\left(\mathbf{M}_{11}^{Q+1}\mathbf{S}_{12}^{Q+1} + \mathbf{M}_{12}^{Q+1}\right)^{-1}\left(\hat{\mathbf{M}}_{11}^{Q+1}\hat{\mathbf{R}} + \mathbf{L}'\right) \tag{5.32}$$

The components of $\hat{\mathbf{R}}$ associated with the propagating Bragg orders are the corresponding reflection amplitudes.

### *5.3.3 Transmission calculations*

Similarly if we want to calculate efficiencies for the propagating orders in medium 0 then, at the same time as imposing outgoing wave conditions, we express those orders as a sum of plane waves transformed into the curvilinear co-ordinates field. Evanescent fields are still represented as a sum of eigenmodes, and we have the medium 0 equivalent of equation (5.27).

$$\begin{pmatrix} \mathbf{M}_{11}^0 & \mathbf{M}_{12}^0 \\ \mathbf{M}_{21}^0 & \mathbf{M}_{22}^0 \end{pmatrix}\begin{pmatrix} \mathbf{0} \\ \mathbf{b}_-^0 \end{pmatrix} = \begin{pmatrix} \hat{\mathbf{M}}_{11}^0 & \hat{\mathbf{M}}_{12}^0 \\ \hat{\mathbf{M}}_{21}^0 & \hat{\mathbf{M}}_{22}^0 \end{pmatrix}\begin{pmatrix} \mathbf{0} \\ \hat{\mathbf{T}} \end{pmatrix} \tag{5.33}$$

Again $\hat{\mathbf{M}}^0$ and $\hat{\mathbf{T}}$ retain their definitions from section 2.9.

Expanding in terms of sub-matrices we find an expression for the transmitted wave amplitudes

$$\hat{\mathbf{T}} = \left(\hat{\mathbf{M}}_{12}^0\right)^{-1}\mathbf{M}_{12}^0\mathbf{b}_-^0 \tag{5.34}$$

whereupon substitution of $\mathbf{b}_-^0$ from (5.32) determines $\hat{\mathbf{T}}$. The components of $\hat{\mathbf{T}}$ associated with the propagating Bragg orders are the corresponding transmission amplitudes.

### *5.4 Conclusion*

The problem of diffraction from a multilayered grating having identical interface profiles is what the Chandezon technique was designed for. The fact that each interface is identical means that the single co-ordinate transformation in $x$ given by equation (2.3) maps all of the boundaries onto a series of parallel planes. In this frame the boundary conditions on **E** and **H** are propagated through the system as though it were a planar stack. In essence we are able to define vectors in the transformed frame which are simultaneously tangential to all interfaces are must therefore be continuous in $y$.

In the next chapter I will show how the method of this chapter may be adapted to cope with multilayered systems having any number of different interface profiles - a modification with removes the easy-to-work-with properties of the transformation described in the above paragraph, but is none the less essential if we are to model real multilayered systems.

# 6. Multicoated gratings with interfaces of different profile

In this chapter I will consider the modifications of the analysis presented in *chapter 5* required to describe field matching across a multicoated grating having non-identical interface profiles sharing the same fundamental periodicity. The method which I will discuss departs from the rigorous nature of analysis presented so far in that it suffers convergence problems when adjacent interfaces differ substantially in profile. For the case of non - conical scattering this work has been looked at previously by Preist *et al.* [1995]. Here I will discuss their work and generalise it to allow for conical scattering.

## *6.1 Presentation of the problem*

The system under consideration is presented diagramatically in figure 6.1, where in line with *chapter* 2 I require that all permeabilities are equal to unity. The isotropic metallic or dielectric substrate with complex relative permittivity $\varepsilon_r^0$ is covered by $Q$ dielectric layers with mean thicknesses $d^j$, relative permittivities $\varepsilon_r^j$, and relative permeabilities $\mu_r^j$. Interfaces are allowed to vary in profile although they must all share the same periodicity. Choosing the origin of $y$ at the top ( $Q$+1 ) interface, the equation of the $j^{\text{th}}$ interface may be written as

$$y = D^j + s^j(x) \qquad \text{with } D^{Q+1} = 0,\ D^j = -\left(d^Q + d^{Q-1} + \ldots + d^j\right)\ ,\ \text{j=1,...,Q+1} \qquad (6.1)$$

where $s^j(x)$ is periodic in $x$ with period $\lambda_g$ giving a basis scattering vector of magnitude $K=2\pi/\lambda_g$ in the direction of the $x$ axis. The grating is illuminated through the top semi-infinite, non absorbing isotropic medium by a homogeneous plane wave with angle of incidence $\theta$ and wave vector $k=(\varepsilon^{Q+1})^{1/2}k_0$ $(k_0=\omega/c)$ situated in the $Oxy$ plane.

In each medium $j$, I will use following the co-ordinate transformation which maps the lower bounding interface of that layer onto a plane.

$$v = x \qquad u^j = y - s^j(x) \qquad w = z \qquad (6.2)$$

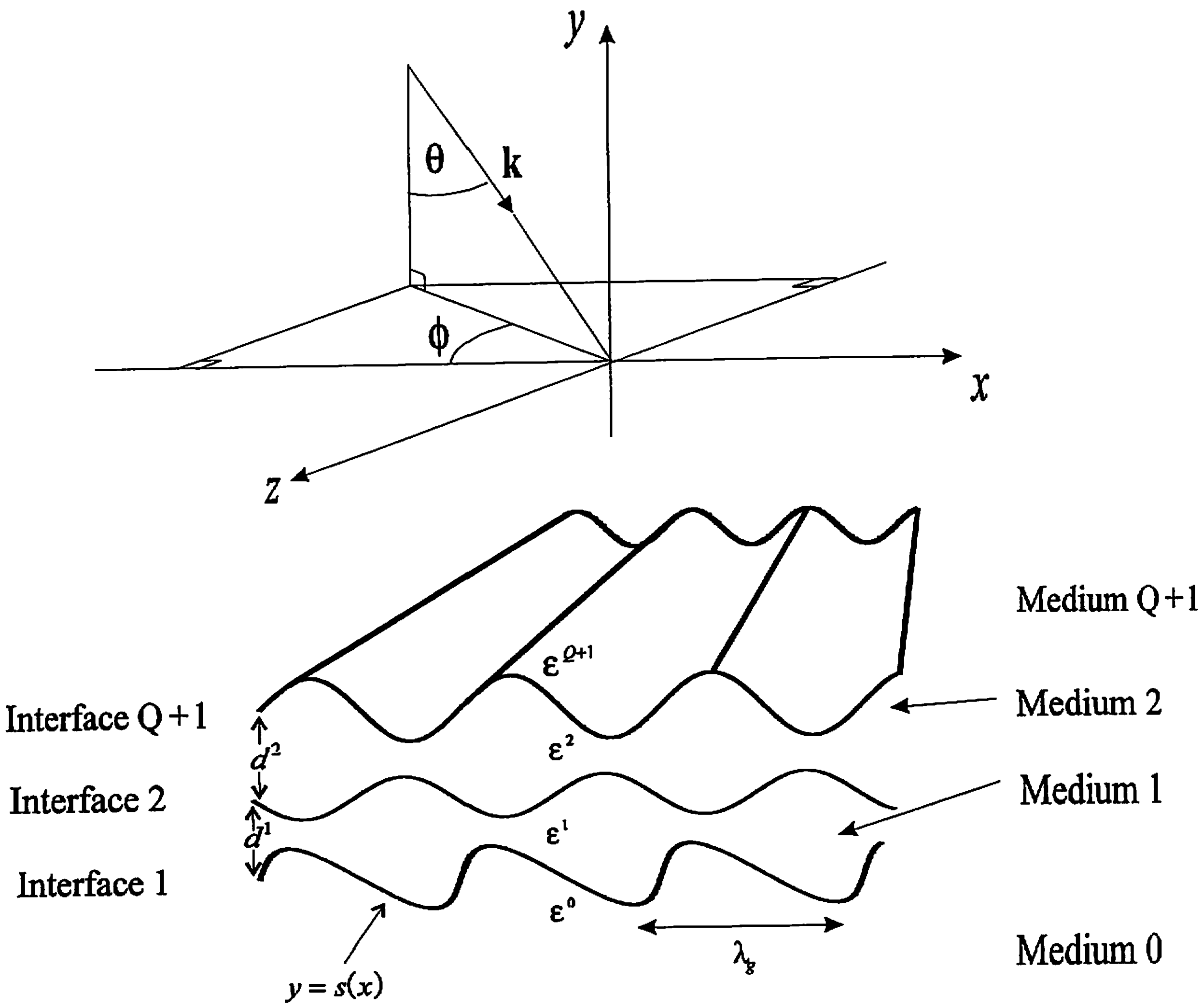

**Figure 6.1:** The system under consideration

### *6.2 Co-ordinate transformation*

The exception is the lowermost medium which does not have a lower bounding interface. The co-ordinate transformation in this layer is made with respect to the first interface and thus takes the form:

$$v = x \qquad u^0 = y - s^1(x) \qquad w = z \tag{6.3}$$

In the zeroth medium then, we are able to define field components that are tangential to the first interface for all *x*, while in all other layers we can define field components that are similarly tangential to the lower interface of the layer in which they are defined.

### *6.3 The symmetric case*

Here I am referring to the situation in which there is no $z$ dependence on the fields. Thus the plane of incidence must contain the grating vector.

Throughout the whole of this chapter we are concerned with matching **E** and **H** fields across material boundaries via the continuity of their tangential components. As I will only consider the two fundamental cases (TM or TE ) of polarisation, one of the two vectors **E** or **H** will be aligned along the $z$ axis which is tangential to all grating surfaces. In line with *chapter* 2 this component is called **F**. The remaining field vector will lie in the $xy$ plane at some arbitrary orientation to each of the grating surfaces. The Chandezon technique naturally lends itself to the study of multicoated gratings having interfaces of identical profile as it is then possible to map all these interfaces onto parallel planes using a single co-ordinate transformation. We may then work with a component of the $xy$ field vector which is simultaneously tangential to every interface (the **G** component of *chapter* 2) and the previous analysis of *chapter 5* will suffice.

When any of the grating surfaces differ in profile it is impossible to define a component of the $xy$ field vector which is simultaneously tangential to every interface. The strategy I will adopt is to use a separate co-ordinate transformation in each layer that maps the lower bounding interface of that layer onto a plane. The fields in any layer will then be represented by an eigenmode expansion defined with respect to the lower interface of that layer on which they will be defined to have zero phase. In this way I naturally select a component of the $xy$ field in a given layer that is tangential to the lower boundary of that layer but not necessarily tangential to the upper boundary. Consider the layer shown in figure 6.2 bounded by two non - identical interfaces: Following on from the notation used in *chapter* 2 I have defined ${}^{j}\mathbf{G}^{L}$ to be the in plane field vector in layer L, parallel to interface $j$. Similarly $\mathbf{G}_2^j$ is defined to be the in plane field vector in layer L, parallel to the $y$ axis. With these definitions in mind let us now look the problem of matching the in plane fields across interface $j+1$.

${}^{j+1}G^{j+1}$ is the in plane field component in layer $j+1$, parallel to the lower bounding interface ($j+1$) of that layer. Continuity of the tangential fields tells us that

$$ {}^{j+1}G^{j+1} = {}^{j+1}G^{j} \tag{6.4} $$

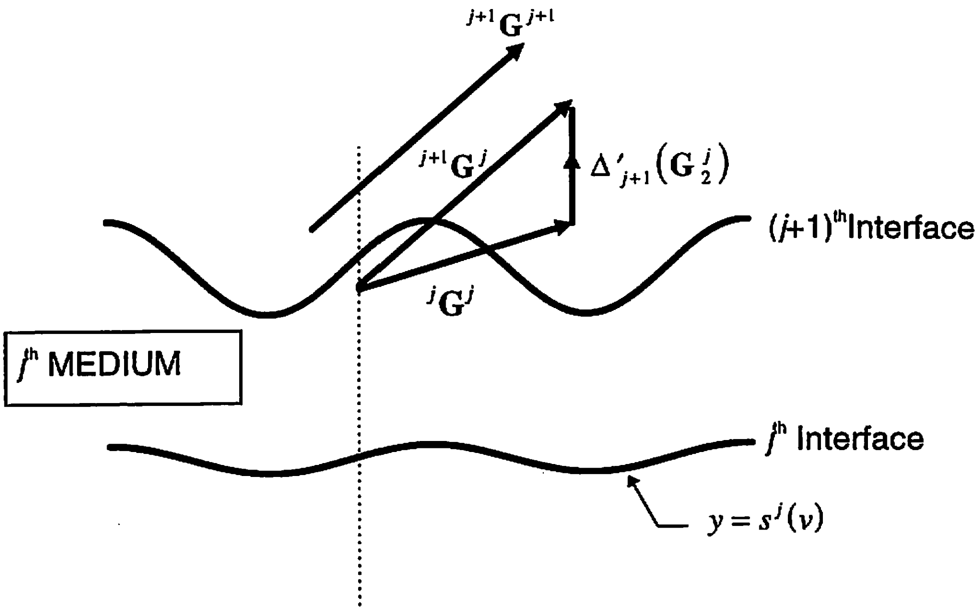

**Figure 6.2:** Definitions of the field component $G$ in neighbouring media. For a given value of $v$ along a particular interface only the $G$ component defined in the medium above that interface will be tangential to the groove profile and we must allow for this when matching fields.

Since all our eigenmode expansions in a given layer will be defined with respect to the lower bounding interface of that layer we replace the vector component ${}^{j+1}G^j$ on the RHS of equation (6.4) with an equivalent combination of vector components defined in the same way. That combination is

$$ {}^{j+1}G^j = {}^jG^j + \Delta'_j G_2^j \tag{6.5} $$

with $\Delta'_j = s'_{j+1} - s'_j$, so that equation (6.4) can be written as

$$ {}^{j+1}G^{j+1} = {}^jG^j + \Delta'_j G_2^j \tag{6.6} $$

where each field component is defined with respect to the lower bounding interface of the layer in which it exists. The Chandezon method is formulated in terms of the eigenmodes of the field components $F$ and $G$, but not $G_2$ so we are forced to redefine this quantity in terms of $F$ and $G$. Equations (2.18,20) of *chapter* 2 tell us that

$$G^2 = i\frac{\partial F}{\partial v} \tag{6.7}$$

from which (2.7) gives us $G_2$:

$$G_2 = DG + iC\frac{\partial F}{\partial v} \tag{6.8}$$

Remembering that $F$ is always tangential to all interfaces, and substituting (6.8) into (6.6) we have the appropriate boundary conditions for $F$ and $G$ across interface $j$+1:

$$\begin{aligned} &F^{j+1} = F^j \\ &{}^{j+1}G^{j+1} = {}^{j}G^j + \Delta'_j\left(D^jG^j + iC\frac{\partial F^j}{\partial v}\right) \end{aligned} \tag{6.9}$$

Let us consider the condition on $F$ first. While $F$ is the component of a vector which is simultaneously tangential to all interfaces, it is defined in a separate co-ordinate system in each layer. $F^{j+1}$ is defined with respect to the co-ordinate $u^{j+1}$ and is defined to have zero phase on interface $j$+1 where the condition $F^{j+1} = F^j$ is evaluated. $F^j$ on the other hand is defined with respect to the co-ordinate $u^j$ which takes the value $u^j = \Delta^j - \sum_{L=j+1}^{Q+1} d^L$ on interface $j$+1. Also, since $F^j$ is defined to have zero phase on interface $j$, it must have phase $\phi^j(d^j)$ on interface $j$+1.

In terms of eigenmode expansions the condition $F^{j+1} = F^j$ becomes

$$\sum_{mq} M(+)^{j+1}_{mq} b^{j+1}_q \exp i\alpha_m v = \sum_{mq} M(+)^{j}_{mq} \phi^j_q\left(\Delta_j + d^j\right) b^j_q \exp i\alpha_m v \tag{6.10}$$

where I have adopted the notation that any matrix followed by (+) indicates summation over the top 2$M$+1 rows only, and any matrix followed by a (-) indicates summation over the bottom 2$M$+1 rows only. Using orthogonality with $\exp i\alpha_n v$ equation (6.10) gives

$$\sum_{q} M(+)^{j+1}_{nq} b^{j+1}_q = \sum_{mq} M(+)^{j}_{mq} \phi^j_q\left(d^j\right) b^j_q L^j_{nmq} \tag{6.11}$$

where

$$L^j_{nmq} = \frac{1}{\lambda_g} \int_0^{\lambda_g} \exp\left(-i\left[(n-m)Kv - \Delta_j(v) r^j_q\right]\right) dv \tag{6.12}$$

Using the same reasoning the eigenmode representation of the condition ${}^{j+1}G^{j+1} = {}^jG^j + \Delta'_j \left( D^j G^j + iC \frac{\partial F^j}{\partial v} \right)$ is

$$\begin{aligned} \sum_{mq} M(-)^{j+1}_{mq} b^{j+1}_q \exp(i\alpha_m v) &= \sum_{mq} M(-)^j_{mq} \phi^j_q \left(\Delta_j + d^j\right) b^j_q \exp(i\alpha_m v) \\ &+ \sum_{pmq} \Delta'_j D^j_p \exp(ipKv).\, M(-)^j_{mq} \phi^j_q \left(\Delta_j + d^j\right) b^j_q \exp(i\alpha_m v) \\ &- \eta^j \sum_{pmq} \Delta'_j C^j_p \exp(ipKv).\, M(+)^j_{mq} \phi^j_q \left(\Delta_j + d^j\right) b^j_q \alpha_m \exp(i\alpha_m v) \end{aligned} \tag{6.13}$$

where $\eta^j = \frac{1}{\varepsilon^j_r}$ for TM polarisation, and $\eta^j = \frac{1}{\mu^j_r}$ for TE polarisation.

Previously when I used orthogonality with $\exp i\alpha_n v$ all $v$ dependence was held in exponential terms. It is useful to maintain this order and to this end I will use the identity

$$\Delta'_j \exp\left(ir^j_q \Delta_j\right) \exp(i\alpha_m v) = \frac{1}{r^j_q} \sum_s (s-m) K L^j_{smq} \exp(i\alpha_m v) \tag{6.14}$$

to remove the $\Delta'_j$ whence (6.13) may be written

$$\begin{aligned} \sum_{mq} M(-)^{j+1}_{mq} b^{j+1}_q \exp(i\alpha_m v) &= \sum_{mq} M(-)^j_{mq} \phi^j_q \left(\Delta_j + d^j\right) b^j_q \exp(i\alpha_m v) \\ &+ \sum_{spmq} D^j_p \exp(ipKv).\, M(-)^j_{mq} \phi^j_q (d^j) b^j_q \frac{1}{r^j_q} (s-m) K L^j_{smq} \exp(i\alpha_s v) \\ &- \eta^j \sum_{spmq} C^j_p \exp(ipKv).\, M(+)^j_{mq} \phi^j_q (d^j) b^j_q \frac{\alpha_m}{r^j_q} (s-m) K L^j_{smq} \exp(i\alpha_s v) \end{aligned} \tag{6.15}$$

Using orthogonality with $\exp i\alpha_n v$ I can isolate individual eigenmodes on the LHS of (6.15) to obtain

$$
\begin{aligned}
&\sum_{q} M(-)^{j+1}_{mq} b^{j+1}_{q} = \sum_{mq} M(-)^{j}_{mq} \phi^{j}_{q}\left(d^{j}\right) b^{j}_{q} L^{j}_{nmq} \\
&+\sum_{pmq} D^{j}_{p} M(-)^{j}_{mq} \phi^{j}_{q}\left(d^{j}\right) b^{j}_{q} \frac{1}{r^{j}_{q}} (n-p-m) K L^{j}_{smq} \qquad (6.16) \\
&-\eta^{j} \sum_{pmq} C^{j}_{p} . M(+)^{j}_{mq} \phi^{j}_{q}\left(d^{j}\right) b^{j}_{q} \frac{\alpha_{m}}{r^{j}_{q}} (n-p-m) K L^{j}_{smq}
\end{aligned}
$$

Gathering all this information together we may write the continuity of the tangential field components across interface $j$+1 as

$$
\mathbf{M}^{j+1}\mathbf{b}^{j+1} = \Omega^{j} \phi^{j}\left(d^{j}\right)\mathbf{b}^{j} \qquad (6.17)
$$

where

$$
\begin{aligned}
&\Omega(+)_{mq} = M(+)^{j}_{mq} L^{j}_{nmq} \\
&\Omega(-)^{j}_{nq} = \sum_{m} M(-)^{j}_{mq} L^{j}_{nmq} \qquad (6.18) \\
&+\sum_{pm} \left[ D^{j}_{p} M(-)^{j}_{mq} - \eta^{j} C^{j}_{p} M(+)^{j}_{mq} \alpha_{.m} \right]^{j}_{q} \frac{1}{r^{j}_{q}} (n-p-m) K L^{j}_{smq}
\end{aligned}
$$

The transfer matrix $I^{j+1}$,defined by $b^{j} = I^{j+1} b^{j+1}$ is then

$$
I^{j+1} = \left[\overset{j}{\phi}\left(d^{j}\right)\right]^{-1} \left[\Omega^{j}\right]^{-1} M^{j+1} \qquad (6.19)
$$

which may be used in the analysis of *chapter* 5 to define a scattering matrix, and obtain the solution to the grating problem as described in that chapter.

### *6.4 The general case*

Here I am placing no restriction on the orientation of the incident wavevector so that effects like conical scattering and polarisation conversion may be seen. What follows is then a generalisation of the work performed by Preist *et al.* [1995].

The analysis is much like that for the symmetric case except that in general there will now be two transverse field components and two in-plane field components. While the transverse field components are continuous across the interfaces, the in-plane components obey relation (6.6). Explicitly

$$ {}^{j+1}E_1^{j+1} = {}^{j}E_1^{j} + \Delta'_j E_2^j \tag{6.20} $$

$$ {}^{j+1}E_3^{j+1} = {}^{j}E_3^{j} \tag{6.21} $$

$$ {}^{j+1}H_1^{j+1} = {}^{j}H_1^{j} + \Delta'_j H_2^j \tag{6.22} $$

$$ {}^{j+1}H_3^{j+1} = {}^{j}H_3^{j} \tag{6.23} $$

Equations (4.9,13) of *chapter* 4 show us that

$$ E_2 = DE_1 - \frac{\gamma}{\varepsilon_r} CH_1 - \frac{i}{\varepsilon_r} C \frac{\partial H_3}{\partial v} \tag{6.24} $$

while (4.12,15) give the relation

$$ H_2 = DH_1 + \frac{\gamma}{\mu_r} CE_1 + \frac{i}{\mu_r} C \frac{\partial E_3}{\partial v} \tag{6.25} $$

Substituting these expressions into (6.20-23) and performing the same eigenmode analysis as for the symmetric case it is possible to derive the matching condition

$$ \mathbf{M}^{j+1}\mathbf{b}^{j+1} = \Omega^j \phi^j \left(d^j\right) \mathbf{b}^j \tag{6.26} $$

where

$$ \begin{aligned} \Omega(++)^j_{nq} &= \sum_m M(++)^j_{mq} L^j_{nmq} \\ &+ \sum_{pm} \left[ D^j_p M(++)^j_{mq} - \frac{\gamma}{\varepsilon^j_r} C^j_p M(-)^j_{mq} - \frac{1}{\varepsilon^j_r} C^j_p M(--)^j_{mq} \alpha_m \right]^j_q \frac{1}{r^j_q} (n-p-m) KL^j_{smq} \end{aligned} \tag{6.27} $$

$$ \Omega(+)_{mq} = M(+)^j_{mq} L^j_{nmq} \tag{6.28} $$

$$\Omega(-)^j_{nq} = \sum_m M(-)^j_{mq} L^j_{nmq}$$
$$+\sum_{pm}\left[ D^j_p M(-)^j_{mq} + \frac{\gamma}{\mu^j_r} C^j_p M(++)^j_{mq} + \frac{1}{\mu^j_r} C^j_p M(+)^j_{mq} \alpha_m \right]^j_q \frac{1}{r^j_q}(n-p-m) K L^j_{smq} \tag{6.29}$$

$$\Omega(--)_{mq} = M(--)^j_{mq} L^j_{nmq} \tag{6.30}$$

where due to the doubling in size of all matrices compared with the symmetric case I have revised my notation so that a matrix followed by (++) denotes summation over the first $2M+1$ rows only, (+) denotes summation over the second $2M+1$ rows only, (-) denotes summation over the third $2M+1$ rows only, and (--) denotes summation over the last $2M+1$ rows only.

Following this the transfer matrix can be constructed using (6.19) and from there the scattering matrix and hence solution to the problem using the analysis of *chapter* 5.

### *6.5 Numerical testing*

Before any numerical tests are carried out the expressions (6.27-30) should reduce to their symmetric counterparts (6.18) in the limit $\phi \to 0$ as is indeed the case. Additionally the matrix $\Omega^j$ defined by (6.27-30) must reduce to $M^j$ in the limit $s^{j+1} \to s^j$ and again this condition is true for those expressions.

With these requirements verified a numerical investigation can begin. A suitable starting point is to introduce a 'fake' interface within an overlayer and check that the reflectivity does not change. By a fake interface I mean one that separates two regions of identical material.

At the start of this chapter I mentioned that the method considered here suffered convergence problems when adjacent interfaces differed substantially in profile. The source of these instabilities arises in a similar manner to those that occur in the Rayleigh expansion whose validity has already been discussed in chapter 2. Consider an overlayer bounded by interfaces of different profile. Under the method presented here the eigenmodes are defined with respect to the lower interface on which they have constant phase, no matter where we move. Moving along the top interface those same eigenmodes will now change in phase so that an evanescent wave bound to the lower interface may take on appreciably different values at different positions on the top interface. It is this variation which ultimately leads to numerical breakdown and limits the use of the analysis presented in this chapter to gratings with interfaces that differ in amplitude by less than approximately 50% of their common pitch.

Granet *et al.* [1995] have contrasted a number of alternative calculational schemes to solve the problem of differing interfaces, all of which appear more numerically stable than that presented here, but at the expense of additional computation time. A sensible approach would be to use one of these only if the system to be modelled demands it.

However, the method was developed primarily to model real experimental cells and the parameters of these place them well within the limits of the theory. Evidence that the method developed does indeed model such systems successfully is postponed until chapter 8, since the experimental cells I will consider all contain liquid crystal material.

### *6.6 Conclusion*

The analysis presented in this chapter is essential if we are to characterise real multilayered systems. For example, working with liquid crystal overlayers it is often the case that a grating coupled cell is constructed from anisotropic material sandwiched between a grating substrate and flat glass slide. This particular geometry is modelled in *chapter* 8 where the difference between interface profiles is seen to have a marked effect on the optical response of the system, and is essential for a good fit to experimental data.

# 7. Uniaxial layers

Here I will generalise all aspects of the analysis presented so far (save field profiles) to allow for uniaxial overlayers. In the past much of the work in this area has been restrictive in the type of systems that can be modelled, constraining the incident wavevector and crystal director to certain orientations and typically looking at bare gratings only. The most significant work is due to Inchaussandague and Depine [1994], who presented a rigorous conformal mapping technique applied to a single periodic interface separating an isotropic dielectric, from which the system is illuminated with a plane monochromatic wave, and a uniaxial crystal. Both the incident wavevector and crystal director are allowed to take on arbitrary orientations.

The analysis presented here is capable of modelling similar systems, and more importantly those containing a number of uniaxial overlayers with potentially non - identical interfaces separating them. It is this kind of system which is found in most grating - coupled liquid crystal cells putting us in a position to compare theory with real experimental data.

## *7.1 Preliminaries*

I now turn to the problem of determining the optical properties of a general anisotropic layer [Born and Wolf, 1975]. I assume that the medium is homogeneous, non-conducting ($\sigma$=0), and magnetically isotropic, but allow dielectric anisotropy. In such a medium any electrical excitation will now depend on the direction of the applied electric field **E**, and **D** will no longer be collinear with **E**. The two vectors are related by the tensor equation

$$D_i = \varepsilon^{ij} E_j \qquad (7.1)$$

summation convention applying. Assuming that the electrical energy density retains its form in electrostatics we may write

$$\omega_e = \tfrac{1}{2}\mathbf{E}.\mathbf{D} = \tfrac{1}{2}E_i\varepsilon^{ij}E_j \qquad (7.2)$$

It may be shown by appealing to the differential conservation of energy that the dielectric tensor must be symmetric with $\varepsilon^{ij}=\varepsilon^{ji}$ reducing the number of independent components from nine to six. Equation (7.2) then reduces to

$$\varepsilon^{xx}E_x^2+\varepsilon^{yy}E_y^2+\varepsilon^{zz}E_z^2+2\left(\varepsilon^{xy}E_xE_y+\varepsilon^{yz}E_yE_z+\varepsilon^{zx}E_zE_x\right)=\omega_e=\text{constant}>0 \qquad (7.3)$$

If we consider $E_x$ , $E_y$ and $E_z$ as co-ordinate axes in E space, equation (7.3) then represents an ellipsoid and there exists a co-ordinate system such that the equation of this ellipsoid is

$$\varepsilon^{x'}E_{x'}^2+\varepsilon^{y'}E_{y'}^2+\varepsilon^{z'}E_{z'}^2=\text{constant} \qquad (7.4)$$

where $\varepsilon^{x'}$ , $\varepsilon^{y'}$ and $\varepsilon^{z'}$ are called the principle dielectric constants of the medium in question. The new co-ordinate axes $E_{x'}$ , $E_{y'}$ and $E_{z'}$ are called the principle dielectric axes. In this new system the tensor relation between **D** and **E** and the energy density take the simple forms

$$D_{x'}=\varepsilon^{x'}E_{x'} \qquad D_{y'}=\varepsilon^{y'}E_{y'} \qquad D_{z'}=\varepsilon^{z'}E_{z'} \qquad (7.5)$$

$$\omega_e={}^1\!/_2\left(\frac{D_{x'}^2}{\varepsilon^{x'}}+\frac{D_{y'}^2}{\varepsilon^{y'}}+\frac{D_{z'}^2}{\varepsilon^{z'}}\right) \qquad (7.6)$$

With reference to the above formulae it can be seen that **D** and **E** will have different directions unless **E** coincides in direction with one of the principle axes or all three principle dielectric constants are equal ( the latter case corresponding to an isotropic medium ). To take account of this we first consider a monochromatic plane wave of angular frequency $\omega$ propagating with phase velocity $v_p$ in the direction $\hat{\mathbf{k}}$. Any field vector is then proportional to

$$\exp i\omega\left[\frac{1}{v_p}\left(\hat{\mathbf{k}}.\mathrm{s}\right)-t\right] \qquad (7.7)$$

and Maxwell's curl equations

$$Curl\mathbf{H} = \frac{\partial \mathbf{D}}{\partial t} \qquad \text{and} \qquad Curl\mathbf{E} = -\frac{\partial \mathbf{B}}{\partial t} \tag{7.8}$$

reduce to the form

$$\frac{1}{v_p}\hat{\mathbf{k}}\wedge \mathbf{H} = -\mathbf{D} \qquad \text{and} \qquad \frac{1}{v_p}\hat{\mathbf{k}}\wedge \mathbf{E} = \mathbf{B} \tag{7.9}$$

Eliminating **H** and using a vector identity

$$\mathbf{D} = \frac{1}{v_p^2}\frac{1}{\mu}\left[\mathbf{E} - \hat{\mathbf{k}}\left(\hat{\mathbf{k}}.\mathbf{E}\right)\right] \tag{7.10}$$

Substituting from equation (7.5) for **D** into eq. (7.10) then gives

$$\varepsilon^{i} E_i = \frac{1}{v_p^2}\frac{1}{\mu}\left[E_i - \hat{k}_i\left(\hat{\mathbf{k}}.\mathbf{E}\right)\right] \qquad i=1,2,3 \tag{7.11}$$

or

$$E_i\hat{k}_i\left(\frac{1}{v_p^2} - \mu\varepsilon_i\right) = \frac{1}{v_p^2}\hat{k}_i^2\left(\hat{\mathbf{k}}.\mathbf{E}\right) \qquad i=1,2,3 \tag{7.12}$$

Adding these three equations and using the fact that $\hat{k}_{x'}^2 + \hat{k}_{y'}^2 + \hat{k}_{z'}^2 = 1$ we obtain Fresnel's equation of wave normals

$$\hat{k}_{x'}^2\left(v_p^2 - v_{y'}^2\right)\left(v_p^2 - v_{z'}^2\right) + \hat{k}_{y'}^2\left(v_p^2 - v_{z'}^2\right)\left(v_p^2 - v_{x'}^2\right) + \hat{k}_{z'}^2\left(v_p^2 - v_{x'}^2\right)\left(v_p^2 - v_{y'}^2\right) = 0 \tag{7.13}$$

where $\quad v_{x'} = \frac{c}{\sqrt{\mu\varepsilon^{x'}}} \qquad v_{y'} = \frac{c}{\sqrt{\mu\varepsilon^{y'}}} \qquad \mathrm{v}_{z'} = \frac{c}{\sqrt{\mu\varepsilon^{z'}}}$

are defined as the three principle velocities of propagation.

With the crystal director in the $x'$ direction, $v_{y'} = v_{z'}$. Writing $v_0$ in place of this common velocity and $v_e$ in place of $v_x$ (7.13) reduces to

$$\left(v_p^2 - v_o^2\right)\left[\hat{k}_{x'}^2\left(v_p^2 - v_o^2\right) + \left(\hat{k}_{y'}^2 + \hat{k}_{z'}^2\right)\left(v_p^2 - v_e^2\right)\right] = 0 \tag{7.14}$$

and we see that in general for a given direction of propagation there exist two possible phase velocities.

If the wave normal makes an angle $\theta$ with the $x'$ axis so that $\hat{k}_{x'}^2 = \cos^2\theta$ and $\hat{k}_{y'}^2 + \hat{k}_{z'}^2 = \sin^2\theta$ we obtain two solutions for the phase velocity

$$v_{p1}^2 = v_o^2 \tag{7.15}$$

and

$$v_{p2}^2 = v_o^2 \cos^2\theta + v_e^2 \sin^2\theta \tag{7.16}$$

Thus one of the waves that corresponds to any particular direction of propagation is an *ordinary* wave with velocity independent of that direction, the other an *extraordinary* wave with velocity depending on the direction of the wave normal and the optic axis.

The directions of vibration may be found with the aid of the ellipsoid of wave normals. If we take equation (7.6) , write $x', y', z'$ in place of $D_{y'} / c^{1/2}, D_{y'} / c^{1/2}, D_{z'} / c^{1/2}$ and consider these as Cartesian co-ordinates in space we have

$$\frac{x'^2}{\varepsilon_{x'}} + \frac{y'^2}{\varepsilon_{y'}} + \frac{z'^2}{\varepsilon_{z'}} = 1 \tag{7.17}$$

which is the equation of an ellipse the semi-axes of which are equal to the square roots of the principal dielectric constants. This is the *ellipsoid of wave normals.* Figure 7.1 shows this ellipse for a uniaxial crystal - in which two of the semi-axes are equal. The plane containing the wave normal **k** and the optic axis $x'$ is called the principal plane. It may be shown that the vector **D** of the ordinary wave vibrates at right angles to this plane whereas that of the extraordinary wave vibrates in the plane.

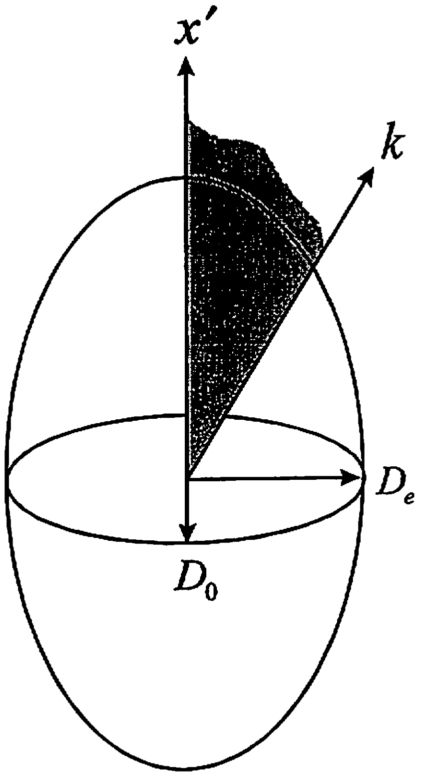

**Figure 7.1:** The ellipsoid of wave normals for a uniaxial crystal

Thus if we consider the case where light is incident, polarised so that its electric vector lies in the principal plane, only one wave will propagate within the crystal, that being the extraordinary mode.

## *7.2 The symmetric case*

### *7.2.1 Form of the permittivity tensor in the transformed space*

By this I am referring to the situation in which there is no $z$ dependence on the fields: Thus the plane of incidence must contain both the grating vector and the liquid crystal director - what follows is then an extension of the analysis presented in *Chapters* 2, 5 and 6.

Referring back to *chapter* 2, it was during the construction of equations (2.10-15) that I first assumed electrical (and magnetic) isotropy. In an electrically anisotropic medium we can only formulate these six equations in terms of **D** and **H** to start with, since there is no simple relation between **D** and **E**. Initially then we can write

$$\left(\frac{\partial E_3}{\partial u}-\frac{\partial}{\partial w}\left(DE_1+CE^2\right)\right)=iH^1 \tag{7.18}$$

$$\left(\frac{\partial E_1}{\partial w}-\frac{\partial E_3}{\partial v}\right)=iH^2 \tag{7.19}$$

$$\left(\frac{\partial}{\partial v}\left(DE_1+CE^2\right)-\frac{\partial E_1}{\partial u}\right)=iH^3 \tag{7.20}$$

$$\left(\frac{\partial H_3}{\partial u}-\frac{\partial}{\partial w}\left(DH_1+CH^2\right)\right)=-iD^1 \tag{7.21}$$

$$\left(\frac{\partial H_1}{\partial w}-\frac{\partial H_3}{\partial v}\right)=-iD^2 \tag{7.22}$$

$$\left(\frac{\partial}{\partial v}\left(DH_1+CH^2\right)-\frac{\partial H_1}{\partial u}\right)=-iD^3 \tag{7.23}$$

where I have omitted a layer index with the understanding that functions such as $C$ and $D$, and all vector components are defined with respect to the lower bounding interface of the layer in which they exist, except in medium 0 where they are defined on the first interface. I will adopt this convention from now on so that the following analysis is compatible with the ideas presented in chapter 6.

In the isotropic case it was only necessary to apply the relation $\mathbf{D}=\varepsilon\,\mathbf{E}$ in order to obtain a set of six equations in **E** and **H**. Now an anisotropic medium forces a tensorial relation between **D** and **E** and our first task is to find explicitly what form this takes.

Figure 7.2 shows the orientation of the optic axis within one of the uniaxial media. The director lies in the plane of incidence at an angle $\chi^j$ below the $x$ axis, so that within a particular medium the angle of orientation is constant, but it can vary from medium to medium. In what is to follow I will omit the layer index $j$ for clarity.

I define a new set of co-ordinates $x',y',z'$ whose axes coincide with the principle dielectric axes of the crystal layer, $x'$ being collinear with the optic axis. ( Note that it is not strictly necessary to consider the third co-ordinate $z'$, as it remains invariant under the following transformations, however it is included for completeness ). In this set of co-ordinates the electric displacement **D** and the electric field **E** are related by

$$D_{x'} = \varepsilon_\parallel E_{x'} \qquad D_{y'} = \varepsilon_\perp E_{y'} \quad \text{and} \quad D_{z'} = \varepsilon_\perp E_{z'} \tag{7.24}$$

where I have called the permittivity along the director $\varepsilon_\parallel$ and that perpendicular to it $\varepsilon_\perp$. Hence in $x', y', z'$ space the permittivity tensor has the simple form

$$\varepsilon_{ij} = \begin{pmatrix} \varepsilon_\parallel & 0 & 0 \\ 0 & \varepsilon_\perp & 0 \\ 0 & 0 & \varepsilon_\perp \end{pmatrix} \tag{7.25}$$

From this point on I will label tensors in $x', y', z'$ space with indices $i, j$, and those in $x$, $y$, $z$ space with indices $k$, $l$. I will not explicitly consider the form of the $v$, $u$, $w$ space permittivity tensor until we consider the general case presented in section 7.3, where it will take indices $m$, $n$.

We require the form of the tensor (7.25) in $v$, $u$, $w$ space which is arrived at by a rotation into $x$, $y$, $z$ space followed by the non-orthogonal transformation $u = y - s(x)$. The form of the tensor in $x$, $y$, $z$ space is obtained by a similarity transformation as follows:

Co-ordinates $x$, $y$, $z$ and $x', y', z'$ are related by

$$\begin{aligned} x &= x'\cos\chi + y'\sin\chi \\ y &= -x'\sin\chi + y'\cos\chi \\ z &= z' \end{aligned} \tag{7.26}$$

or

$$\begin{bmatrix} x \\ y \\ z \end{bmatrix} = \begin{pmatrix} \cos\chi & \sin\chi & 0 \\ -\sin\chi & \cos\chi & 0 \\ 0 & 0 & 1 \end{pmatrix} \begin{bmatrix} x' \\ y' \\ z' \end{bmatrix} = \mathbf{X} \begin{bmatrix} x' \\ y' \\ z' \end{bmatrix} \tag{7.27}$$

and the form of the permittivity tensor in $x$, $y$, $z$ space, obtained by a rotation in the $x$, $y$ plane, is given by the familiar matrix relation

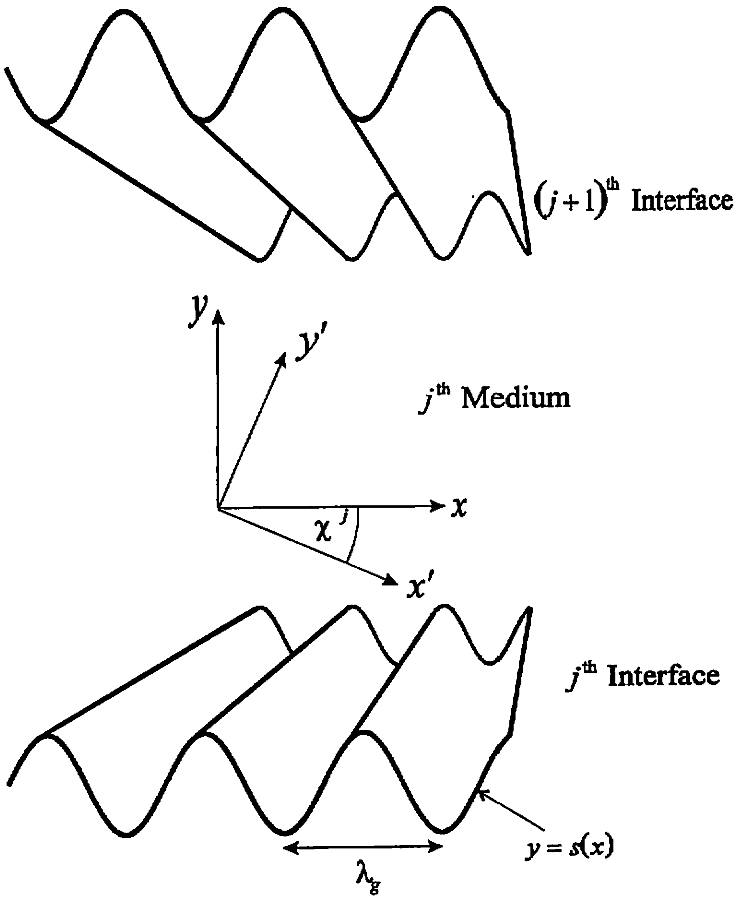

Figure 7.2: Orientation of the optic axis $x'$ within a uniaxial layer

$$\varepsilon_{kl} = \mathbf{X}\varepsilon_{ij}\mathbf{X}^T = \begin{pmatrix} \varepsilon_\parallel \cos^2\chi + \varepsilon_\perp \sin^2\chi & \sin\chi\cos\chi\left(\varepsilon_\perp - \varepsilon_\parallel\right) & 0 \\ \sin\chi\cos\chi\left(\varepsilon_\perp - \varepsilon_\parallel\right) & \varepsilon_\parallel \sin^2\chi + \varepsilon_\perp \cos^2\chi & 0 \\ 0 & 0 & \varepsilon_\perp \end{pmatrix}$$
$$\equiv \begin{pmatrix} \varepsilon_{11} & \varepsilon_{12} & 0 \\ \varepsilon_{21} & \varepsilon_{22} & 0 \\ 0 & 0 & \varepsilon_\perp \end{pmatrix} \qquad (7.28)$$

To obtain the permittivity tensor in $x$, $u$, $w$ space requires a non-orthogonal transformation for which the above method is no longer so clear cut. What we require is the components $D^n = \varepsilon^{nm}E_m$ in the transformed space. Rather than perform tensor analysis I will for simplicity use the following vector treatment.

For a small displacement in some arbitrary direction $\mathbf{r}$ as defined below we have the following relation

$$\delta\mathbf{r} = \frac{\partial \mathbf{r}}{\partial v}\delta v + \frac{\partial \mathbf{r}}{\partial u}\delta u + \frac{\partial \mathbf{r}}{\partial w} \tag{7.29}$$

with

$$\mathbf{r} = x\mathbf{i} + y\mathbf{j} + z\mathbf{k} = v\mathbf{i} + (u + s(v))\mathbf{j} + w\mathbf{k}$$
$$\Rightarrow \quad \frac{\partial \mathbf{r}}{\partial v} = \mathbf{i} + s'\mathbf{j}\,, \quad \frac{\partial \mathbf{r}}{\partial u} = \mathbf{j} \quad \text{and} \quad \frac{\partial \mathbf{r}}{\partial w} = \mathbf{k} \tag{7.30}$$

so that

$$\delta\mathbf{r} = (\mathbf{i} + s'\mathbf{j})\delta v + \mathbf{j}\delta u + \mathbf{k}\delta w \equiv \sum_i \mathbf{e}_i \delta q_i \tag{7.31}$$

giving one set of basis vectors in the transformed space, while their dual vectors, $\mathbf{e}^i$: $i$=1,2,3 can be obtained by inspection from the orthogonality relation $\mathbf{e}_i.\mathbf{e}^j = \delta_i{}^j$:

$$\begin{aligned} \mathbf{e}_1 &= \mathbf{i} + s'\mathbf{j} & \qquad \mathbf{e}^1 &= \mathbf{i} \\ \mathbf{e}_2 &= \mathbf{j} & \mathbf{e}^2 &= \mathbf{j} - s'\mathbf{i} \\ \mathbf{e}_3 &= \mathbf{k} & \mathbf{e}^3 &= \mathbf{k} \end{aligned} \tag{7.32}$$

In $x$, $y$, $z$ space both $\varepsilon$ and the basis vectors (**i**, **j**, **k**) are known giving

$$\begin{pmatrix} D_x \\ D_y \\ D_z \end{pmatrix} = \begin{pmatrix} \varepsilon_{11} & \varepsilon_{12} & 0 \\ \varepsilon_{21} & \varepsilon_{22} & 0 \\ 0 & 0 & \varepsilon_\perp \end{pmatrix} \begin{pmatrix} E_x \\ E_y \\ E_z \end{pmatrix} = \begin{pmatrix} \varepsilon_{11}E_x + \varepsilon_{12}E_y \\ \varepsilon_{21}E_x + \varepsilon_{22}E_y \\ \varepsilon_\perp E_z \end{pmatrix} \tag{7.33}$$

With reference to the vector analysis of *chapter* 2 any vector in $v$, $u$, $w$ space can be written in one of two ways: either in terms of the covariant basis vectors

$$\mathbf{E} = \mathbf{e}_1 E^1 + \mathbf{e}_2 E^2 + \mathbf{e}_3 E^3 = (\mathbf{i} + s'\mathbf{j})E^1 + \mathbf{j}E^2 + \mathbf{k}E^3 \tag{7.34}$$

or using the Cartesian basis vectors **i**, **j** and **k**

$$\mathbf{E} = E_x\mathbf{i} + E_y\mathbf{j} + E_z\mathbf{k} \tag{7.35}$$

Equating coefficients of the Cartesian vectors gives a relation between $E^1$, $E^2$, $E^3$ and $E_x$, $E_y$, $E_z$:

$$\begin{aligned} E_x &\equiv E^1 \\ E_y &\equiv s'E^1 + E^2 \\ E_z &\equiv E^3 \end{aligned} \tag{7.36}$$

substituting this into the $x$, $y$, $z$ expression for **D** equation (7.33) gives

$$\begin{pmatrix} D_x \\ D_y \\ D_z \end{pmatrix} = \begin{pmatrix} \varepsilon_{11}E^1 + \varepsilon_{12}\left(s'E^1 + E^2\right) \\ \varepsilon_{21}E^1 + \varepsilon_{22}\left(s'E^1 + E^2\right) \\ \varepsilon_{\perp}E^3 \end{pmatrix} \tag{7.37}$$

The components we need to evaluate are: $D^1$ - the component in the $x$ direction; and $D^2$ - the normal component to the grating surface. Using (7.32) we find that

$$D^1 = \mathbf{e}^1.\mathbf{D} = \left(\varepsilon_{11} + s'\varepsilon_{12}\right)E^1 + \varepsilon_{12}E^2 \tag{7.38}$$

$$D^2 = \mathbf{e}^2.\mathbf{D} = \left[\left(1 - s'^2\right)\varepsilon_{12} + s'\left(\varepsilon_{22} - \varepsilon_{11}\right)\right]E^1 + \left(\varepsilon_{22} - s'\varepsilon_{12}\right)E^2 \tag{7.39}$$

The third component $D^3$ - is that in the $z$ direction. The transformations I have used leave the $z$ co-ordinate unchanged and the electric field senses only $\varepsilon_{\perp}$ so as we expect:

$$D^3 = \mathbf{e}^3.\mathbf{D} = \varepsilon_{\perp}E^3 \tag{7.40}$$

### *7.2.2 Maxwells equations in the transformed space*

Substituting (7.38,40) into the six equations (7.18-23) we arrive at a set of equations in **E** and **H**.

$$\left(\frac{\partial \mathrm{E}_3}{\partial \mathrm{u}} - \frac{\partial}{\partial w}\left(DE_1 + CE^2\right)\right) = iH^1 = i\left(CH_1 - DH^2\right) \tag{7.41}$$

$$\left(\frac{\partial E_1}{\partial \mathrm{w}}-\frac{\partial E_3}{\partial v}\right)=iH^2 \tag{7.42}$$

$$\left(\frac{\partial}{\partial v}\left(DE_1+CE^2\right)-\frac{\partial E_1}{\partial \mathrm{u}}\right)=iH^3=iH_3 \tag{7.43}$$

$$\begin{aligned}\left(\frac{\partial H_3}{\partial u}-\frac{\partial}{\partial w}\left(DH_1+CH^2\right)\right)&=-i\left[\left(\varepsilon_{11}+s'\varepsilon_{12}\right)E^1+\varepsilon_{12}E^2\right]\\ &=-i\left[C\left(\varepsilon_{11}+s'\varepsilon_{12}\right)E_1+\left(C\varepsilon_{12}-D\varepsilon_{11}\right)E^2\right]\end{aligned} \tag{7.44}$$

$$\begin{aligned}\left(\frac{\partial H_1}{\partial \mathrm{w}}-\frac{\partial H_3}{\partial v}\right)&=-i\left\{\left[\left(1-s'^2\right)\varepsilon_{12}+s'\left(\varepsilon_{22}-\varepsilon_{11}\right)\right]E^1+\left(\varepsilon_{22}-s'\varepsilon_{12}\right)E^2\right\}\\ &=-i\left[\left(1-s'^2\right)\varepsilon_{12}+s'\left(\varepsilon_{22}-\varepsilon_{11}\right)\right]CE_1\\ &+i\left\{\left[\left(1-s'^2\right)\varepsilon_{12}+s'\left(\varepsilon_{22}-\varepsilon_{11}\right)\right]D+\left(\varepsilon_{22}-s'\varepsilon_{12}\right)\right\}E^2\end{aligned} \tag{7.45}$$

$$\left(\frac{\partial}{\partial v}\left(DH_1+CH^2\right)-\frac{\partial H_1}{\partial \mathrm{u}}\right)=-i\varepsilon_{\perp}E^3 \tag{7.46}$$

where it can be seen that unwanted components of the form $A^1$, $A_2$, and $A^3$ have been eliminated in favour of the remaining components which are tangential to the grating surface $y=s(x)$.

Note that in purely TM or $p$ - polarisation with **E**=($E_x$, $E_y$, 0) and **H**=(0, 0, $H_z$) the six equations (7.41-46) reduce to three coupled equations these being

$$\left(\frac{\partial}{\partial v}\left(DE_1+CE^2\right)-\frac{\partial E_1}{\partial \mathrm{u}}\right)=iH_3 \tag{7.47}$$

$$\frac{\partial H_3}{\partial u}=-i\left[C\left(\varepsilon_{11}+s'\varepsilon_{12}\right)E_1+\left(C\varepsilon_{12}-D\varepsilon_{11}\right)E^2\right] \tag{7.48}$$

$$\begin{aligned}\frac{\partial H_3}{\partial v}&=i\left[\left(1-s'^2\right)\varepsilon_{12}+s'\left(\varepsilon_{22}-\varepsilon_{11}\right)\right]CE_1\\ &-i\left\{\left[\left(1-s'^2\right)\varepsilon_{12}+s'\left(\varepsilon_{22}-\varepsilon_{11}\right)\right]D+\left(\varepsilon_{22}-s'\varepsilon_{12}\right)\right\}E^2\end{aligned} \tag{7.49}$$

By eliminating the unwanted components $E^2$ and $H^2$ we arrive at the uniaxial analogues of equations (2.22) and (2.23) for TM polarisation only:

$$\frac{\partial F}{\partial u} = X_1 \frac{\partial F}{\partial v} + iX_2 G \tag{7.50}$$

and

$$\frac{\partial G}{\partial u} = iF + \frac{\partial}{\partial v}\left(X_1 G - iX_3 \frac{\partial F}{\partial v}\right) \tag{7.51}$$

where $F = H_z$, $G = -E_1$, and

$$X_1 = \left(s'\varepsilon^{11} - \varepsilon^{12}\right)X_3$$

$$X_2 = \varepsilon_{\parallel}\varepsilon_{\perp}X_3 \tag{7.52}$$

$$X_3 = \frac{1}{-2s'\varepsilon^{12} + s'^2\varepsilon^{11} + \varepsilon^{22}}$$

Following through a similar analysis for TE or $s$ - polarisation we find an identical set of equations to the isotropic ones of chapter 2 with $\varepsilon$ replaced by $\varepsilon_{\perp}$. This is of course just what we would expect given that, for this polarisation, the electric field lies along one of the short dielectric axes no matter what angle of incidence we choose.

Following the analysis of section 2.5 equations (7.50,51) lead to the following eigenvalue equation.

$$-i\frac{\partial}{\partial u}\begin{pmatrix} F_{-N} \\ \cdot \\ F_N \\ - \\ G_{-N} \\ \cdot \\ G_N \end{pmatrix} = \begin{bmatrix} \alpha_m\left(X_1\right)_{n-m} & k_0\left(X_2\right)_{n-m} \\ & \\ \dfrac{-\alpha_n\alpha_m\left(X_1\right)_{n-m}}{k_0} + k_0\delta_{nm} & \alpha_n\left(X_3\right)_{n-m} \end{bmatrix} \begin{pmatrix} F_{-N} \\ \cdot \\ F_N \\ - \\ G_{-N} \\ \cdot \\ G_N \end{pmatrix} \tag{7.53}$$

whereby the eigenmodes of a given uniaxial layer can be calculated in the same way as the isotropic case.

### *7.2.3 Multicoated gratings with interfaces of different profile*

Referring to the analysis of *chapter* 6, equations (6.9) may be written explicitly for the case of TM incident polarisation which for the purposes of this section is the only polarisation to see the uniaxiality defined in section 7.2.1.

$$F_z^{j+1} = F_z^j$$

$$^{j+1}G_1^{j+1} = {}^jG_1^{j+1} + \Delta'_j G_2^j \tag{7.54}$$

The only difference from the isotropic case is that $G_2^j = -E_2^j$ is now given by

$$G_2^j = X_1^j G^j - iX_3^j \frac{\partial F^j}{\partial v} \tag{7.55}$$

Comparing this with it's isotropic counterpart in equation (6.8) and working through the same analysis presented for that condition we can write the continuity of the tangential field components across interface $j$+1 as

$$\mathbf{M}^{j+1}\mathbf{b}^{j+1} = \Omega^j \phi^j(d^j)\mathbf{b}^j \tag{7.56}$$

where

$$\Omega(+)_{mq} = M(+)_{mq}^j L_{nmq}^j$$

$$\Omega(-)_{nq}^j = \sum_m M(-)_{mq}^j L_{nmq}^j \tag{7.57}$$

$$+\sum_{pm}\left[\left(X_1^j\right)_p M(-)_{mq}^j + \left(X_3^j\right)_p M(+)_{mq}^j \alpha_m\right]_q^j \frac{1}{r_q^j}(n-p-m)KL_{(n-p)mq}^j$$

The transfer matrix $I^{j+1}$,defined by $b^j = I^{j+1}b^{j+1}$ is then

$$I^{j+1} = \left[\phi\left(d^{j}\right)\right]^{-1}\left[\Omega^{j}\right]^{-1} M^{j+1} \tag{7.58}$$

which may be used in the analysis of *chapter* 5 to define a scattering matrix. Since the two bounding media 0 and $Q$+1 must be isotropic, the remaining analysis concerning outgoing wave conditions and plane wave expansions in those media is identical to that presented for the isotropic case.

### *7.2.4 Basic tests on the code*

Initially I performed tests on the mathematical analysis - ultimately the uniaxial field equations (7.50,51) must reduce to their isotropic counterparts (2.22,23) when $\varepsilon_{\parallel} = \varepsilon_{\perp}$. When this equality holds we find from equation (7.28) that the *x*, *y* tensor has the form

$$\varepsilon_{kl} = \begin{pmatrix} \varepsilon & 0 & 0 \\ 0 & \varepsilon & 0 \\ 0 & 0 & \varepsilon \end{pmatrix} \qquad \lim \varepsilon_{\parallel} \to \varepsilon_{\perp} \tag{7.59}$$

and thus the anisotropic coefficients $X_1$, $X_2$, and $X_3$ reduce to

$$X_1 \to D \qquad X_2 \to \varepsilon C \qquad X_3 \to \frac{C}{\varepsilon} \tag{7.60}$$

whence equations (7.50,51) reduce to their isotropic counterparts (2.22,23). Similarly, in the same limit, the matching conditions (7.56,57) must reduce to their isotropic forms (6.17,18).

The next step was to test the energy balance criterion for a non - absorbing multilayered system made with uniaxial materials. Following this a test to verify the reciprocity theorem was performed. Having verified that the code satisfied these requirements, with grating amplitudes set to zero a comparison was made with an existing planar optics code for anisotropic materials.

### *7.2.5 Mode momenta within an anisotropic waveguide*

In this section I will outline some work performed to test all aspects of the non conical work presented so far. The most general system we can test is thus a multilayered grating made with uniaxial materials and having non identical interfaces. Since I am testing the non conical formalism the plane of incidence must contain both the grating vector and the uniaxial director.

As a suitable test, I will investigate the mode momenta within an anisotropic waveguide and compare grating coupling to modes as calculated in our theory with the simpler prism coupling derived from elementary planar theory [Azzam and Bashara, 1979].

Our prism coupled system consists of a $1\mu m$ planar waveguide containing E7 liquid crystal surrounded by vacuum, with the crystal layer aligned in the plane of incidence parallel to the interfaces. A high index prism coupler is placed a suitable distance above the anisotropic layer. The momenta of the 5 modes supported by this system at wavelength $632.8nm$ are calculated using the theory of Azzam and Bashara [1979].

These same modes can be coupled into via Bragg scattering from a grating and we can predict the transverse momenta $k_x$ of the incident light at which this happens using the mode momenta from Azzam and Bashara's theory. Since the light is incident in vacuum we have

$$k_x = k_{mode} - mK \tag{7.61}$$

from which

$$\sin\theta = \frac{k_{\text{mode}}}{k_0} - m\frac{\lambda}{\lambda_g} \tag{7.62}$$

where $\theta$ is the angle of incidence and $m$ denotes the Bragg order of the mode. This provides a cross check for the angles at which modes are excited in the grating - coupled waveguide, at least for small amplitude gratings, as large amplitudes significantly perturb the mode momenta.

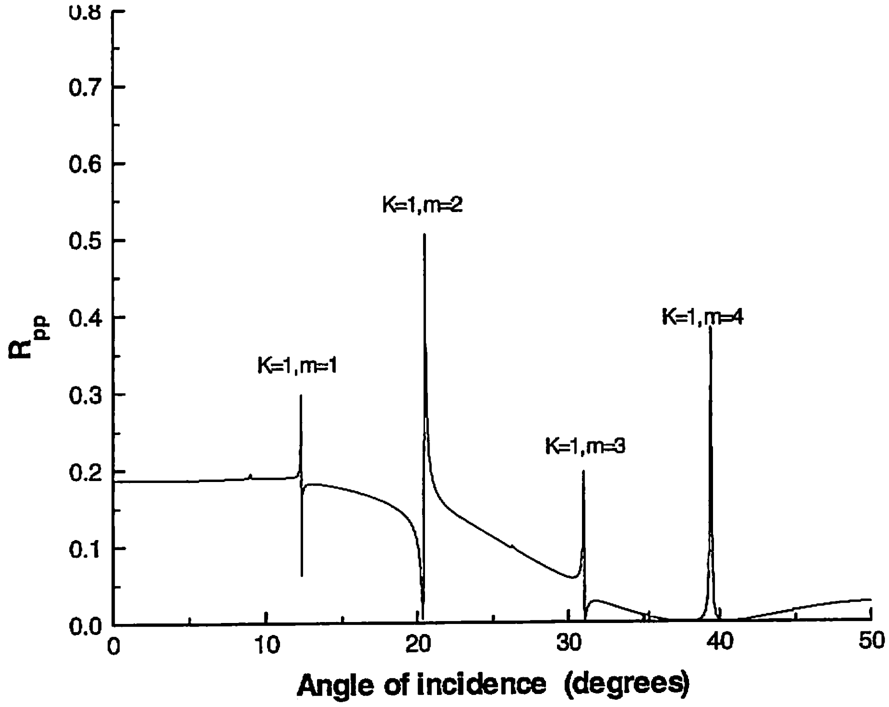

**Figure 7.3:** Optical response of an E7 liquid crystal waveguide (with optic axis aligned in the direction of grating periodicity) surrounded by vacuum and illuminated with light of wavelength 632.8*nm*. Both interfaces were sinusoidal with pitch 800*nm* and amplitude A=25*nm*.

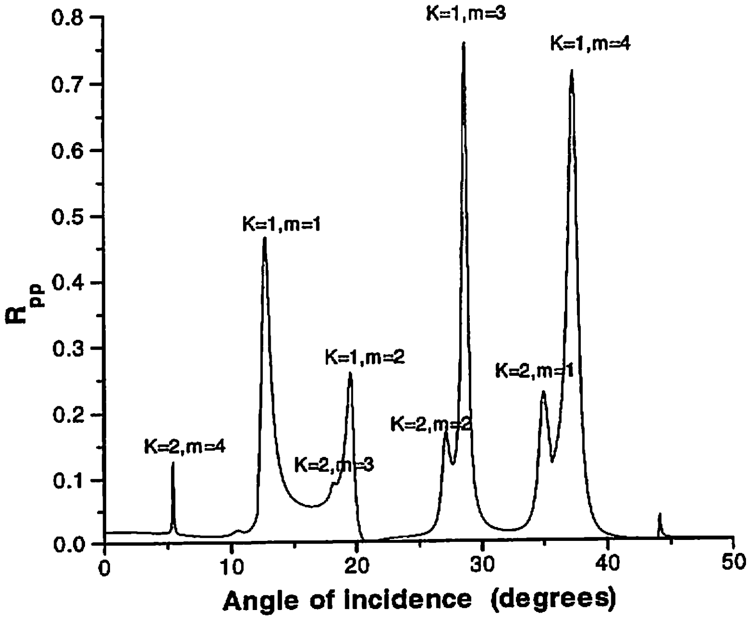

**Figure 7.4:** As figure 7.3 but with both interfaces having amplitude A=150*nm*.

I now superimpose a sinusoidal grating of pitch 800nm and amplitude 25*nm* on the 1$\mu m$ waveguide containing E7 liquid crystal aligned in the direction of the grating vector. This is surrounded by vacuum. Using the code this system was modelled with truncation parameter $M$=3, figure 7.3 showing the resulting zeroth order reflectivity curve. Angles of mode excitation were recorded and compared with those extrapolated from planar theory in Table 7.1. Differences are minimal and can be attributed to the small perturbing effect of the shallow grating used, although larger shifts are to be expected in systems employing deeper grooves. To illustrate this figure 7.4 shows the same system with a grating amplitude of 150*nm*. At this higher amplitude we see an increase in coupling via 2 Bragg scattering events reflecting the increased perturbation of the grating surface. In particular the 4th order mode (excited at approx. 5°) coupled to in this way shows considerable enhancement.

| Number of Bragg scatterings required for Coupling | Mode order | Predicted mode position per Azzam & Bashara (degrees) | Mode position per this paper (degrees) |
|---|---|---|---|
| 1 | 1 | 12.10 | 12.24 |
| | 2 | 20.49 | 20.51 |
| | 3 | 31.06 | 31.05 |
| | 4 | 39.50 | 39.48 |
| | 5 | 44.91 | 44.98 |
| 2 | 1 | 35.59 | 35.32 |
| | 2 | 27.17 | 27.23 |
| | 3 | 15.94 | 15.94 |
| | 4 | 8.92 | 8.98 |
| | 5 | 4.88 | 4.90 |

**Table 7.1:** Comparison of mode positions extrapolated from planar theory with those calculated from the grating theory of this chapter as applied to an E7 liquid crystal waveguide (with optic axis aligned in the direction of grating periodicity) surrounded by vacuum and illuminated with light of wavelength 632.8*nm*. Both interfaces were sinusoidal with pitch 800*nm* and amplitude 25*nm*.

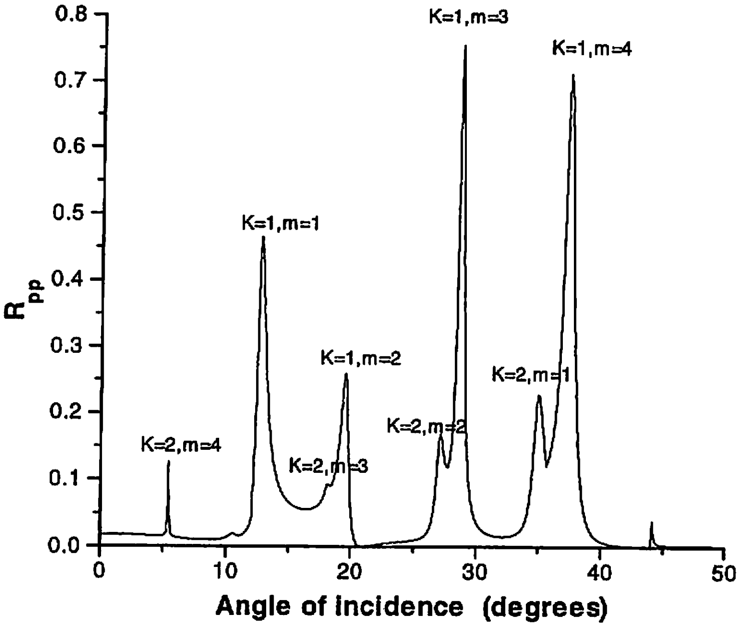

**Figure 7.5:** Reflectivity curve for an E7 liquid crystal waveguide (with optic axis aligned in the plane of incidence 20° down from the direction of grating periodicity) surrounded by vacuum and illuminated with light of wavelength 632.8*nm*. The grating interface is sinusoidal with pitch 800*nm* and amplitude 25*nm*.

| Number of Bragg scatterings required for Coupling | Mode order | Predicted mode position per Azzam & Bashara (degrees) | Mode position calculated here (degrees) |
|---|---|---|---|
| 1 | 1 | 12.77 | 13.04 |
|  | 2 | 24.71 | 24.65 |
|  | 3 | 37.37 | 37.29 |
|  | 4 | 45.89 | 45.89 |
| 2 | 1 | 34.75 | 34.42 |
|  | 2 | 21.90 | 21.99 |
|  | 3 | 10.60 | 10.68 |
|  | 4 | 4.19 | 4.19 |

**Table 7.2:** As per table 7.1 with the optic axis tilted 20° down from the $x$ - axis.

The system modelled above may be considered by some to be a special case with the optic axis aligned in the direction of grating periodicity. I can provide a more general system by tilting the optic axis 20° down from this orientation. The resulting reflectivity curve is shown in figure 7.5 for sinusoidal interfaces of amplitude 25*nm*. Using the same technique as before I can compare the mode positions obtained thereof with those extrapolated from planar theory. This is shown in table 7.2.

### *7.3 The general case*

The general case is that in which I place no restriction on the orientation of the incident wavevector and the liquid crystal director with respect to the grating.

#### *7.3.1 Form of the permittivity tensor in the transformed space*

Figure 7.6 shows the orientation of the dielectric axes within a uniaxial layer. The optic axis makes an angle $\Theta$ with the $y$ axis with azimuthal angle $\Phi$. As before we define a new set of co-ordinates $x', y', z'$ whose axes coincide with the principle dielectric axes of the crystal layer, but now $y'$ is collinear with the optic axis to facilitate any change from $\Theta$ and $\Phi$ to Euler angles. Note that unlike the symmetric case our $z'$ co-ordinate is no longer invariant under the following transformations.

In this primed set of co-ordinates the electric displacement $\mathbf{D}$ and the electric field $\mathbf{E}$ are related by

$$D_{x'} = \varepsilon_{\perp} E_{x'} \,, \quad D_{y'} = \varepsilon_{\parallel} E_{y'} \,, \quad \text{and} \qquad D_{z'} = \varepsilon_{\perp} E_{z'} \tag{7.63}$$

where we have called the permittivity along the director $\varepsilon_{\parallel}$ and that perpendicular to it $\varepsilon_{\perp}$. Hence in $x', y', z'$ space the permittivity tensor has the simple form

$$\varepsilon_{ij} = \begin{pmatrix} \varepsilon_{\perp} & 0 & 0 \\ 0 & \varepsilon_{\parallel} & 0 \\ 0 & 0 & \varepsilon_{\perp} \end{pmatrix} \tag{7.64}$$

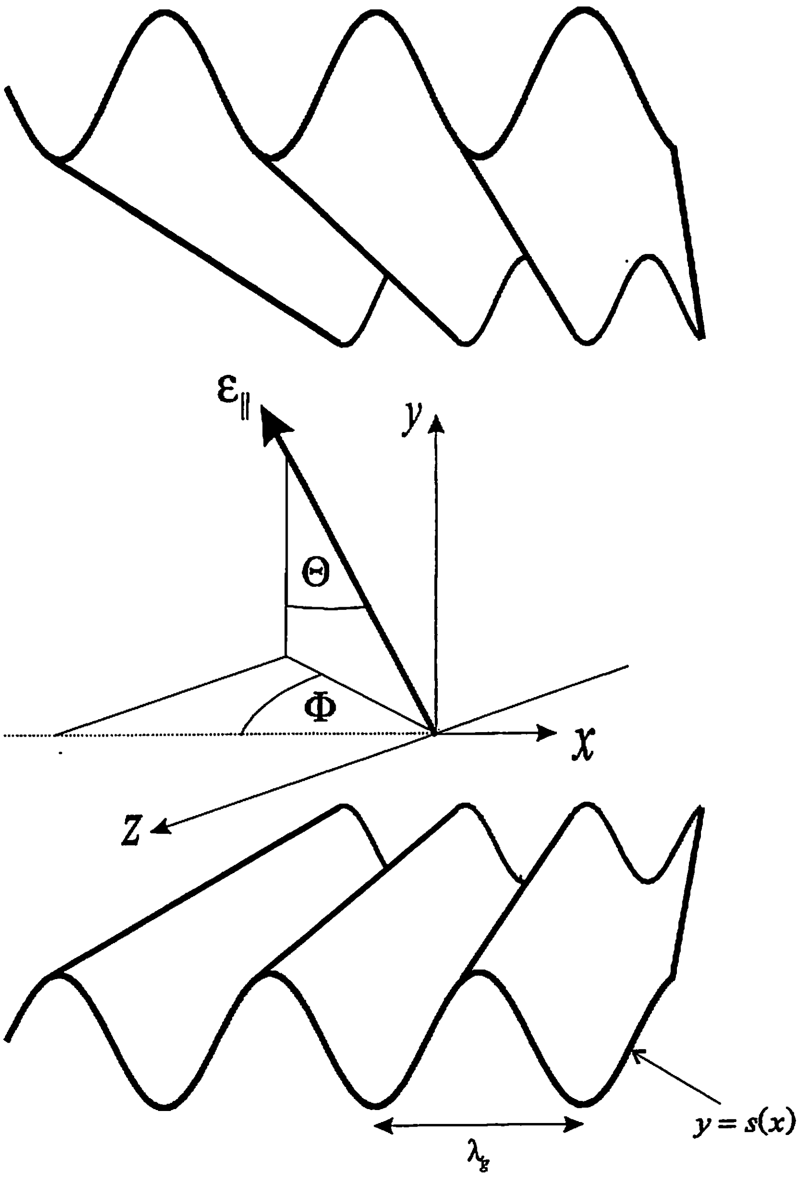

**Figure 7.6:** Orientation of the optic axis $y'$ within a uniaxial layer

We require the form of this tensor in $v$, $u$, $w$ space which is arrived at by a rotation into $x$, $y$, $z$ space followed by the non-orthogonal transformation $u = y - s(x)$. The form of the tensor in $x$, $y$, $z$ space is obtained by a similarity transformation as follows:

Co-ordinates $x$, $y$, $z$ and $x', y', z'$ are related by

$$\begin{aligned} x &= x'\cos\Theta\cos\Phi - y'\sin\Theta\cos\Phi - z'\sin\Phi \\ y &= x'\sin\Theta + y'\cos\Theta \\ z &= x'\cos\Theta\sin\Phi - y'\sin\Theta\sin\Phi + z'\cos\Phi \end{aligned} \tag{7.65}$$

or

$$\begin{bmatrix} x \\ y \\ z \end{bmatrix} = \begin{pmatrix} \cos\Theta\cos\Phi & -\sin\Theta\cos\Phi & -\sin\Phi \\ \sin\Theta & \cos\Theta & 0 \\ \cos\Theta\sin\Phi & -\sin\Theta\sin\Phi & \cos\Phi \end{pmatrix} \begin{bmatrix} x' \\ y' \\ z' \end{bmatrix} = \begin{pmatrix} & & \\ & \mathbf{X} & \\ & & \end{pmatrix} \begin{bmatrix} x' \\ y' \\ z' \end{bmatrix} \tag{7.66}$$

With knowledge of the tensor in $x', y', z'$ space we can obtain it's form in $x$, $y$, $z$ space by an appropriate tensor transformation. There are three classes of tensor: covariant, mixed and contravariant, with each defined according to the way it transforms from one co-ordinate system to another. However, in orthogonal co-ordinate systems all three variants are equivalent because only one set of basis vectors exists. All these ideas will appear familiar from *section 2.3*. Thus in Cartesian co-ordinates there are three basis vectors **i**, **j**, and **k** aligned along the three co-ordinate axes $x$, $y$, and $z$, while in co-ordinates $v$, $u$, $w$, associated with the Chandezon transformation there are two sets of three basis vectors $\mathbf{e}_1$, $\mathbf{e}_2$, $\mathbf{e}_3$, and $\mathbf{e}^1$, $\mathbf{e}^2$, $\mathbf{e}^3$. Thus we have two ways of representing a vector in co-ordinates $v$, $u$, $w$: $\mathbf{A} = \mathbf{e}_i \mathbf{A}^i$ or $\mathbf{A} = \mathbf{e}^i \mathbf{A}_j$.

For a given co-ordinate system, the covariant tensor relates the contravariant vector components of **D** and **E** so that

$$D^k = \varepsilon_{kl} E^l \tag{7.67}$$

(summation convention applying), and obeys the transformation rule

$$\varepsilon_{kl} = \frac{\partial x^i}{\partial x'^k} \frac{\partial x^j}{\partial x'^l} \varepsilon_{ij} \tag{7.68}$$

In this instance $x^i \equiv (x, y, z)$ and $x'^m \equiv (x', y', z')$ so that $\frac{\partial x^i}{\partial x'^k}$ and $\frac{\partial x^j}{\partial x'^l}$ refer to the elements of the matrix **X**.

The mixed tensor relates the covariant vector components of **D** to the contravariant vector components of **E**

$$D_k = \varepsilon^k{}_l E^l \tag{7.69}$$

Note how the mixed tensor is written with both subscript and superscript. It transforms according to

$$\varepsilon^{k}{}_{l}=\frac{\partial x'^{k}}{\partial x^{i}}\frac{\partial x^{j}}{\partial x'^{l}}\varepsilon'^{i}{}_{j} \tag{7.70}$$

Note that in this case $\frac{\partial x'^{k}}{\partial x^{i}}$ corresponds to the elements of $\mathbf{X}^{\mathrm{T}}$.

Finally there is the contravariant tensor relating the covariant components of **D** and **E**

$$D_{k}=\varepsilon^{kl}E_{l} \tag{7.71}$$

Written with superscripts it obeys the transformation rule

$$\varepsilon^{kl}=\frac{\partial x'^{k}}{\partial x^{i}}\frac{\partial x'^{l}}{\partial x^{j}}\varepsilon'^{ij} \tag{7.72}$$

However, in any Euclidean co-ordinate system (both $x$, $y$, $z$ and $x', y', z'$ are Euclidean) all three forms are equivalent. For convenience I will use the covariant notation. Equation (7.72) may be written as a matrix equation

$$\varepsilon_{kl}=\mathbf{X}\varepsilon'_{ij}\mathbf{X}^{T} \tag{7.73}$$

$$\text{giving } \varepsilon_{kl}=\varepsilon^{kl}=\varepsilon^{k}{}_{l}=\begin{pmatrix} a & b & c \\ b & d & e \\ c & e & f \end{pmatrix} \tag{7.74}$$

$$\begin{aligned}
a&=\varepsilon_{\parallel}\sin^{2}\Theta\cos^{2}\Phi+\varepsilon_{\perp}\left(\cos^{2}\Theta\cos^{2}\Phi+\sin^{2}\Phi\right)\\
b&=\left(\varepsilon_{\perp}-\varepsilon_{|}\right)\ \sin\Theta\cos\Theta\cos\Phi\\
c&=\left(\varepsilon_{\parallel}-\varepsilon_{\perp}\right)\ \sin^{2}\Theta\sin\Phi\cos\Phi\\
d&=\varepsilon_{|}\cos^{2}\Theta+\varepsilon_{\perp}\sin^{2}\Theta\\
e&=\left(\varepsilon_{\perp}-\varepsilon_{|}\right)\ \sin\Theta\cos\Theta\sin\Phi\\
f&=\varepsilon_{|}\sin^{2}\Theta\sin^{2}\Phi+\varepsilon_{\perp}\left(\cos^{2}\Theta\sin^{2}\Phi+\cos^{2}\Phi\right)
\end{aligned}$$

Having found the tensor in $x$, $y$, $z$ space we now determine its form in the $v$, $u$, $w$ co-ordinates. The covariant, mixed and contravariant forms are obtained from the usual transformation rules:

$$\varepsilon_{mn} = \frac{\partial x^k}{\partial q^m}\frac{\partial x^l}{\partial q^n}\varepsilon_{kl} \qquad \varepsilon^{m}{}_{n} = \frac{\partial q^m}{\partial x^k}\frac{\partial x^l}{\partial q^n}\varepsilon^{k}{}_{l} \qquad \varepsilon^{mn} = \frac{\partial q^m}{\partial x^k}\frac{\partial q^n}{\partial x^l}\varepsilon^{kl} \tag{7.75}$$

where $x^k \equiv (x, y, z)$ and $q^m \equiv (v, u, w)$. Note that I have retained the notation used for the symmetric case so that $k$ and $l$ have been used to label the $x$, $y$, $z$ tensor whose covariant, contravariant, and mixed variants all share the same form given by equation (7.74), while $m$ and $n$ are reserved for the $v$, $u$, $w$ tensors. The co-ordinate transformation matrices are given by

$$\frac{\partial x^i}{\partial q^k} = \begin{pmatrix} 1 & s' & 0 \\ 0 & 1 & 0 \\ 0 & 0 & 1 \end{pmatrix} \quad \text{and} \quad \frac{\partial q^k}{\partial x^i} = \begin{pmatrix} 1 & 0 & 0 \\ -s' & 1 & 0 \\ 0 & 0 & 1 \end{pmatrix} \tag{7.76}$$

Performing the operations (7.75) we obtain the three forms of the $v$, $u$, $w$ dielectric tensor

$$\varepsilon_{nm} = \left(\frac{\partial x^i}{\partial q^n}\right)\begin{pmatrix} a & b & c \\ b & d & e \\ c & e & f \end{pmatrix}\left(\frac{\partial x^i}{\partial q^m}\right)^T = \begin{pmatrix} a + 2s'b + s'^2 d & b + s'd & c + s'e \\ b + s'd & d & e \\ c + s'e & e & f \end{pmatrix} \tag{7.77}$$

$$\varepsilon^{n}{}_{m} = \left(\frac{\partial q^n}{\partial x^i}\right)\begin{pmatrix} a & b & c \\ b & d & e \\ c & e & f \end{pmatrix}\left(\frac{\partial x^i}{\partial q^m}\right)^T = \begin{pmatrix} a + s'b & b & c \\ \left(1 - s'^2\right)b + s'(d - a) & d - s'b & e - s'c \\ c + s'e & e & f \end{pmatrix} \tag{7.78}$$

$$\varepsilon^{nm} = \left(\frac{\partial q^n}{\partial x^i}\right)\begin{pmatrix} a & b & c \\ b & d & e \\ c & e & f \end{pmatrix}\left(\frac{\partial q^m}{\partial x^i}\right)^T = \begin{pmatrix} a & b - s'a & c \\ b - s'a & -2s'b + s'^2 a + d & e - s'c \\ c & e - s'c & f \end{pmatrix} \tag{7.79}$$

### *7.3.2 Maxwell's equations in the transformed space*

As in the isotropic case we start from the two Maxwell equations $Curl\mathbf{E} = i\mathbf{H}$ and $Curl\mathbf{H} = -i\mathbf{D}$, in which we need to express the vector components $D_1$ , $D^2$ and $D_3$ in terms of the corresponding vector components $E_1$ , $E^2$ and $E_3$. This is achieved through the relations $D_n = \sum_m \varepsilon_{nm} E^m$ , $D^n = \sum_m \varepsilon^{nm} E_m$ and $D^n = \sum_m \varepsilon^n{}_m E^m$ where the three ε tensors are the covariant, contravariant and mixed forms of the dielectric tensor in the co-ordinate system $v$, $u$, $w$. Taking the dot product of the two Maxwell equations with $\mathbf{e}^1$, $\mathbf{e}^2$, and $\mathbf{e}^3$ we arrive at six equations analogous to (7.41-46)

$$\left(\frac{\partial \mathrm{E}_3}{\partial \mathrm{u}} - \frac{\partial}{\partial w}\left(DE_1 + CE^2\right)\right) = iH^1 = i\left(CH_1 - DH^2\right) \tag{7.80}$$

$$\left(\frac{\partial E_1}{\partial \mathrm{w}} - \frac{\partial E_3}{\partial v}\right) = iH^2 \tag{7.81}$$

$$\left(\frac{\partial}{\partial v}\left(DE_1 + CE^2\right) - \frac{\partial E_1}{\partial \mathrm{u}}\right) = iH^3 = iH_3 \tag{7.82}$$

$$\begin{aligned}\left(\frac{\partial H_3}{\partial u} - \frac{\partial}{\partial w}\left(DH_1 + CH^2\right)\right) &= -i\left(\varepsilon^1{}_1 E^1 + \varepsilon^1{}_2 E^2 + \varepsilon^1{}_3 E^3\right)\\ &= -i\left(\varepsilon^1{}_1 E_1 + \left(\varepsilon^1{}_2 - \varepsilon^1{}_1 D\right)E^2 + \varepsilon^1{}_3 E_3\right)\end{aligned} \tag{7.83}$$

$$\begin{aligned}\left(\frac{\partial H_1}{\partial \mathrm{w}} - \frac{\partial H_3}{\partial v}\right) &= -i\left(\varepsilon^2{}_1 E^1 + \varepsilon^2{}_2 E^2 + \varepsilon^2{}_3 E^3\right)\\ &= -i\left(\varepsilon^2{}_1 E_1 + \left(\varepsilon^2{}_2 - \varepsilon^2{}_1 D\right)E^2 + \varepsilon^2{}_3 E_3\right)\end{aligned} \tag{7.84}$$

$$\begin{aligned}\left(\frac{\partial}{\partial v}\left(DH_1 + CH^2\right) - \frac{\partial H_1}{\partial \mathrm{u}}\right) &= -i\left(\varepsilon^3{}_1 E^1 + \varepsilon^3{}_2 E^2 + \varepsilon^3{}_3 E^3\right)\\ &= -i\left(\varepsilon^3{}_1 E_1 + \left(\varepsilon^3{}_2 - \varepsilon^3{}_1 D\right)E^2 + \varepsilon^3{}_3 E_3\right)\end{aligned} \tag{7.85}$$

As in the symmetric case unwanted components of the form $A^1$, $A_2$, $A^3$ have been eliminated using the relations

$$\begin{aligned} A^1 &= CA_1 - DA^2 \\ A_2 &= DA_1 + CA^2 \\ A^3 &= A_3 \end{aligned} \tag{7.86}$$

where

$$C = \frac{1}{1+s'^2} \qquad D = s'C \qquad s' = \frac{ds}{dx} \tag{7.87}$$

We now eliminate the normal fields $E^2$ and $H^2$ from the six equations (7.80-85) leaving four equations in the field components $E_1$ , $E_3$ , $H_1$ and $H_3$ which are always tangential to the interface profiles. In doing so we may utilise conservation of momentum in the direction of the grating grooves denoted by $\gamma = \left(\varepsilon_r^{Q+1}\right)^{1/2} \sin\theta \sin\phi$ and make the substitution $\frac{\partial}{\partial w} \leftrightarrow i\gamma$ .

$$\frac{\partial E_1}{\partial u} = \frac{\partial}{\partial v}\left[ X_1 E_1 + X_2 E_3 + \gamma X_3 H_1 + iX_3 \frac{\partial H_3}{\partial v} \right] - iH_3 \tag{7.88}$$

$$\frac{\partial E_3}{\partial u} = i\gamma X_4 E_1 + D\frac{\partial E_3}{\partial v} + i\gamma X_2 E_3 + iX_5 H_1 - \gamma X_3 \frac{\partial H_3}{\partial v} \tag{7.89}$$

$$\frac{\partial H_1}{\partial u} = \frac{\partial}{\partial v}[\gamma C E_1] + iX_6 E_1 + \frac{\partial}{\partial v}\left[ iC\frac{\partial E_3}{\partial v} \right] + iX_7 E_3 + \frac{\partial}{\partial v}[DH_1] + i\gamma X_2 H_1 - X_2 \frac{\partial H_3}{\partial v} \tag{7.90}$$

$$\frac{\partial H_3}{\partial u} = iX_8 E_1 - \gamma C\frac{\partial E_3}{\partial v} + iX_9 E_3 - i\gamma X_4 H_1 + X_1 \frac{\partial H_3}{\partial v} \tag{7.91}$$

with

$$X_1 = -\frac{\varepsilon^{12}}{\varepsilon^{22}} \qquad X_2 = -\frac{\varepsilon^2{}_3}{\varepsilon^{22}} \qquad X_3 = -\frac{1}{\varepsilon^{22}}$$

$$X_4 = -C\frac{\varepsilon^2{}_1}{\varepsilon^{22}} \qquad X_5 = C - \frac{\gamma^2}{\varepsilon^{22}} \qquad X_6 = C\left(\varepsilon_{31} - \frac{\varepsilon^2{}_1\varepsilon^2{}_3}{\varepsilon^{22}}\right)$$

$$X_7 = \varepsilon_{33} - \frac{\left(\varepsilon^{2}{}_{3}\right)^2}{\varepsilon^{22}} \qquad X_8 = C\left(\gamma^2 + C\left(\frac{\left(\varepsilon^{2}{}_{1}\right)^2}{\varepsilon^{22}} - \varepsilon_{11}\right)\right) \qquad X_9 = C\left(\frac{\varepsilon^{2}{}_{1}\varepsilon^{2}{}_{3}}{\varepsilon^{22}} - \varepsilon_{13}\right) \tag{7.92}$$

Expanding the field components in terms of Bloch waves and performing the analysis of section 4.4 we arrive at an eigenvalue equation

$$-i\frac{\partial}{\partial u}\begin{pmatrix} E_{1(m)} \\ E_{3(m)} \\ H_{1(m)} \\ H_{3(m)} \end{pmatrix} = \begin{pmatrix} t_{11} & t_{12} & t_{13} & t_{14} \\ t_{21} & t_{22} & t_{23} & t_{24} \\ t_{31} & t_{32} & t_{33} & t_{34} \\ t_{41} & t_{42} & t_{43} & t_{44} \end{pmatrix}\begin{pmatrix} E_{1(m)} \\ E_{3(m)} \\ H_{1(m)} \\ H_{3(m)} \end{pmatrix} \tag{7.93}$$

$t_{11}:\alpha_m\left(X_1\right)_{m-n}$

$t_{12}:\alpha_m\left(X_2\right)_{m-n}$

$t_{21}:\gamma\left(X_4\right)_{m-n}$

$t_{22}:\alpha_n D_{m-n} + \gamma\left(X_2\right)_{m-n}$

$t_{31}:\left(X_6\right)_{m-n} + \gamma\alpha_m C_{m-n}$

$t_{32}:\left(X_7\right)_{m-n} - \alpha_m\alpha_n C_{m-n}$

$t_{41}:\left(X_8\right)_{m-n}$

$t_{42}:\left(X_9\right)_{m-n} - \gamma\alpha_n C_{m-n}$

$t_{13}:\gamma\alpha_m\left(X_3\right)_{m-n}$

$t_{14}:-\alpha_m\alpha_n\left(X_3\right)_{m-n} - \delta_{mn}$

$t_{23}:\left(X_5\right)_{m-n}$

$t_{24}:-\gamma\alpha_n\left(X_3\right)_{m-n}$

$t_{33}:\alpha_m D_{m-n} + \gamma\left(X_2\right)_{m-n}$

$t_{34} = -t_{12}$

$t_{43} = -t_{21}$

$t_{44}:\alpha_n\left(X_1\right)_{m-n}$

### *7.3.3 Multicoated gratings with interfaces of different profile*

As with the symmetric case we can refer back to *chapter* 6 where the only difference is that in the conditions (6.20-23), the quantities $E_2^j$ and $H_2^j$ are now given by

$$E_2 = X_1E_1 + X_2E_3 + \gamma X_3H_1 + iX_3\frac{\partial H_3}{\partial v} \tag{7.94}$$

$$H_2 = DH_1 + \frac{\gamma}{\mu_r}CE_1 + \frac{i}{\mu_r}C\frac{\partial E_3}{\partial v} \tag{7.95}$$

Using these relations in (6.20,22) and following through the analysis it is straightforward to derive the matching condition

$$\mathbf{M}^{j+1}\mathbf{b}^{j+1} = \Omega^j \phi^j\left(d^j\right)\mathbf{b}^j \tag{7.96}$$

where

$$\begin{aligned}\Omega(++)^j_{nq} &= \sum_m M(++)^j_{mq}\, L^j_{nmq} \\ &+\sum_{pm}\begin{bmatrix}\left(X_1\right)^j_p M(++)^j_{mq} + \left(X_2\right)^j_p M(+)^j_{mq} \\ -\gamma\left(X_3\right)^j_p M(-)^j_{mq} - \left(X_3\right)^j_p M(--)^j_{mq}\alpha_m\end{bmatrix}^j_q \frac{1}{r^j_q}(n-p-m)KL^j_{smq}\end{aligned} \tag{7.97}$$

$$\Omega(+)_{mq} = M(+)^j_{mq}\, L^j_{nmq} \tag{7.98}$$

$$\begin{aligned}\Omega(-)^j_{nq} &= \sum_m M(-)^j_{mq}\, L^j_{nmq} \\ &+\sum_{pm}\left[D^j_p M(-)^j_{mq} + \frac{\gamma}{\mu^j_r} C^j_p M(++)^j_{mq} - \frac{1}{\mu^j_r} C^j_p M(+)^j_{mq}\alpha_m\right]^j_q \frac{1}{r^j_q}(n-p-m)KL^j_{smq}\end{aligned} \tag{7.99}$$

$$\Omega(--)_{mq} = M(--)^j_{mq}\, L^j_{nmq}$$

(7.100)

where, following *chapter* 6, I have revised my notation due to the doubling in size of all matrices compared with the symmetric case so that a matrix followed by (++) denotes summation over the first $2M+1$ rows only, (+) denotes summation over the second $2M+1$ rows only, (-) denotes summation over the third $2M+1$ rows only, and (--) denotes summation over the last $2M+1$ rows only.

Following this the transfer matrix can be constructed using (6.19) and from there the scattering matrix and hence solution to the problem using the analysis of *chapter* 5.

### *7.3.4 Testing the code*

As in the symmetric case I start by taking various limits of the equations (7.88-92). Putting $\gamma$=0 these equations reduce to the in - plane equations of *chapter 2* while in the outermost isotropic layers they take on the familiar forms (4.13-16). Similarly the matching conditions (7.97-100) must reduce to their isotropic counterparts (6.27-30) in the limit $\varepsilon_{\perp} \rightarrow \varepsilon_{\parallel}$.Computationally I again verified that the code obeyed the energy balance condition and the reciprocity theorem before setting all grating amplitudes to zero and comparing with a planar optics model for anisotropic materials.

### *7.4 Conclusion*

This chapter completes the analysis of diffraction from singly periodic structures leaving us able to model systems with the following features:

- Any orientation of the incident wavevector (conical diffraction).
- Any number of arbitrarily thick dielectric, metallic or uniaxial overlayers.
- For uniaxial layers the director can adopt any orientation.
- Interfaces may differ in profile although all must share the same fundamental periodicity.

Recently the method of Chandezon has been generalised further to allow for biaxial overlayers [Depine *et al.*, to be published], with identical interfaces. However the degree of biaxiality in most anisotropic materials is so small as to produce little optical effect in the situations discussed here.

The next chapter details the modelling and characterisation of two real grating - coupled liquid crystal cells, and uses of all aspects of the theory developed so far, providing a comprehensive test of the anisotropic analysis.

# 8. Modelling multicoated gratings made with uniaxial materials[1]

Here I will show how the theory developed so far has been used to model some real systems containing liquid crystals, providing a direct comparison between theory and experimental data.

## *8.1 Modelling a grating - coupled E7 liquid crystal cell in the conical mount*

The first piece of work I will describe was used to assess the potential of the theory to model a real system. As such it does not attempt to provide a complete characterisation of the experimental cell - that work is left to the second part of this chapter - section 8.2.

Figure 8.1 shows the system under consideration in which a five layer grating structure is illuminated with monochromatic (632.8*nm*) light at azimuthal angle 30°. The 1.48$\mu m$ thick E7 ($\varepsilon_{\parallel}$=3.025, $\varepsilon_{\perp}$=2.311) liquid crystal layer, aligned homogeneously using 60° evaporated SiOx so that the nematic director lies along the grating grooves, is confined between a silver-coated diffraction grating of pitch 554.02*nm*, groove depth 26*nm* and a flat glass top plate of refractive index 1.512.

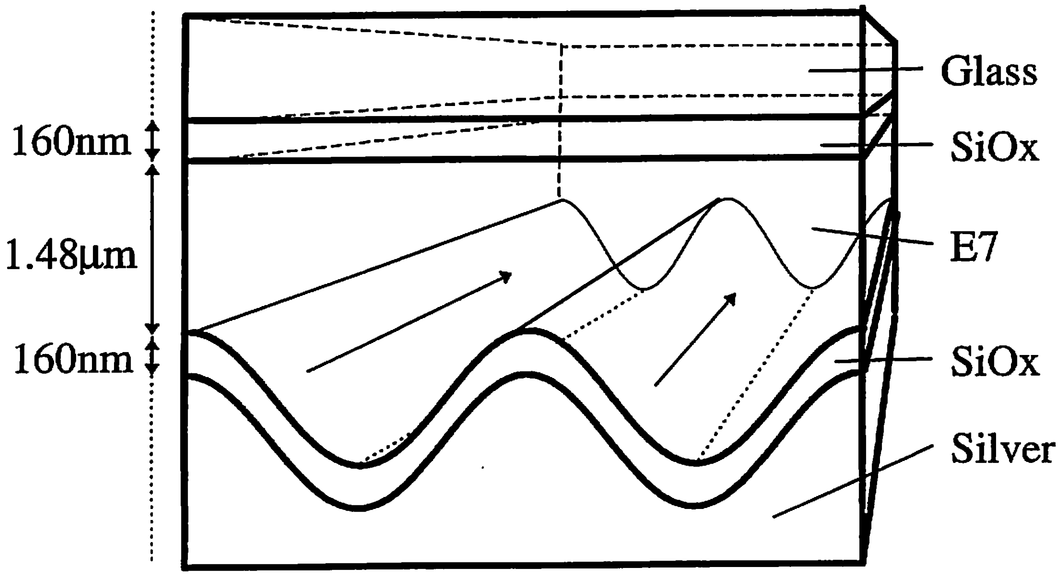

**Figure 8.1:** Cell configuration for comparison with experimental data.

---

[1] All experimental work in this chapter was performed by Dr. E. L. Wood

Figure 8.2 shows $R_{pp}$ experimental data overlaid with my theoretical calculation. Clearly visible are the first and second order surface plasmon polariton (SPP) resonances, excited at the silver / liquid crystal interface, at approximately $22^{\circ}$ and $31^{\circ}$ respectively along with the four TE guided modes excited within the liquid crystal layer. Agreement between these features and our calculation is compromised slightly because of a small $\left(< 5^{\circ}\right)$ twist within the liquid crystal layer, giving rise to a background $R_{ps}$ signal and small shifts in the mode positions. A comprehensive fit to experimental data was not attempted as all the primary features in the data are predicted correctly by the modelling and the incorporation of a small, yet unknown amount of twist, would not change this. The agreement of mode positions and depths with the model indicates a sound theoretical framework.

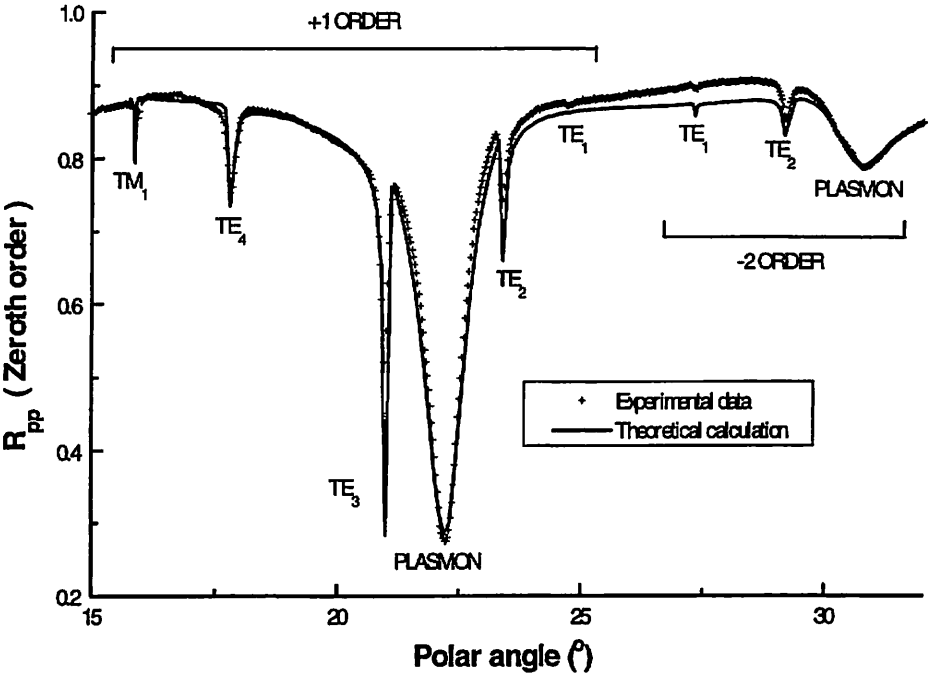

**Figure 8.2:** Experimental data from the grating shown in figure 8.1 is compared with our theoretical calculation when the grating is illuminated with $p$ - polarised monochromatic (632.8*nm*) light at azimuthal angle 30°.

Further to this we calculate the theoretical reflectivity response for the liquid crystal system across a wide range of polar and azimuthal angles. Figure 8.3 shows the $R_{pp}$

calculation: note that the polar angle range has been reversed with respect to figure 8.2 to obtain a more pleasing perspective. Clearly visible are the distinct coupling conditions of the +1 and -2 order resonances, the later showing a more pronounced dependence on azimuthal angle.

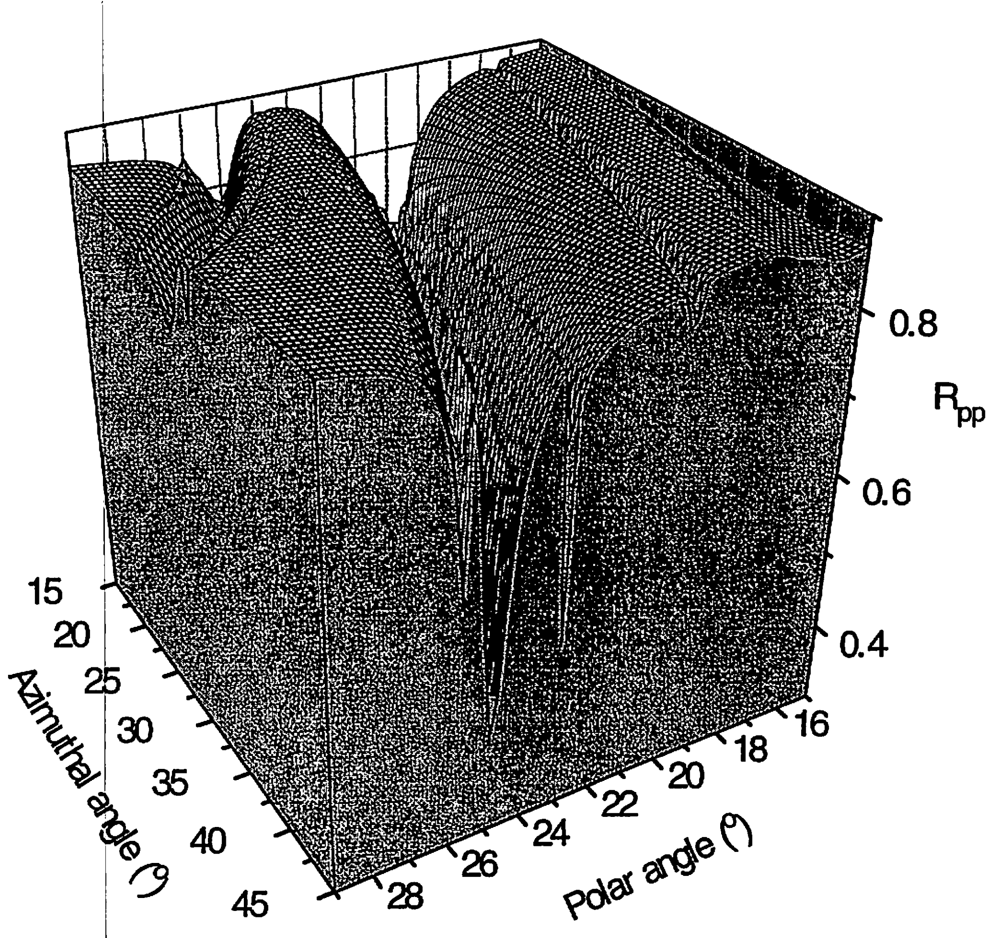

**Figure 8.3:** Theoretical calculation of $R_{pp}$ using the same parameters as in figure 8.2 but across a range of both polar and azimuthal angles: note that the polar angle range has been reversed with respect to figure 8.2 to obtain a more pleasing perspective. Variation in the position of the surface plasmon minima as a function of azimuthal angle can be seen clearly, and are compared with a *k*-space coupling diagram in figure 8.4.

Figure 8.4 shows a *k*-space representation of the modelled guided mode and SPP resonances, for the +1 order, compared with experimental data. The optic axis of my uniaxial layer is aligned along the *z* axis with the result that the modes propagating in the system are of two types. The TM-like ordinary modes have a momentum in the $x$ direction which is virtually independent of azimuthal angle $\phi$ and $\varepsilon_{\parallel}$. The other mode family are the TE-like extraordinary modes whose x momentum depends on $\varepsilon_{\parallel}$ , $\varepsilon_{\perp}$ and on $\phi$. As a result the ordinary modes describe circles in $k$ - space, while the extraordinary modes trace ellipses whose long axes are aligned in the direction of the optic axis. The SPP resonance is a surface mode with electric field oscillating predominately normal to the grating surface where it will sense primarily $\varepsilon_{\perp}$ with little or no dependence on angle $\phi$ and $\varepsilon_{\parallel}$. It will thus be largely ordinary in nature and nearly describes a circle in our $k$ - space map.

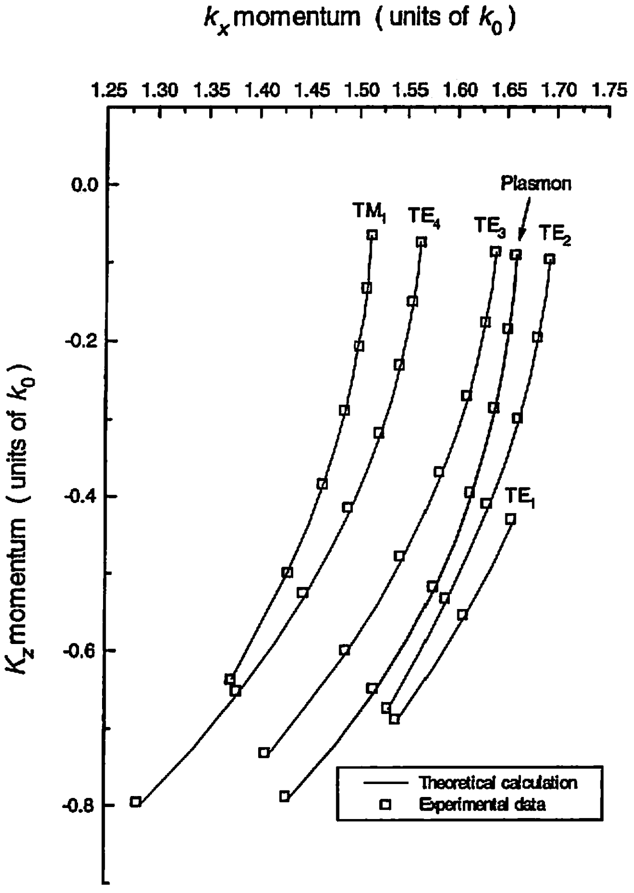

**Figure 8.4:** $k$-space representation of the +1 order guided modes and SPP resonance compared with experimental data. Agreement is best for the ordinary TM$_1$ mode and departs slightly for the extraordinary TE modes as their direction of propagation tends towards the optic axis. This behaviour can be attributed to a small $\left(< 5^{o}\right)$ twist within

the liquid crystal layer, and it can be concluded that the theory is providing a good description of the real system.

Everywhere agreement is good, being excellent for the ordinary TM$_1$ mode. The small differences between theory and data for the extraordinary TE modes tend to increase with azimuthal angle. As the momenta of these extraordinary modes is determined by the orientation of their direction of propagation with respect to the ellipsoid of wave normals, they are sensitive to any twist within the liquid crystal layer. So the behaviour we see is not entirely unexpected and we can conclude that the theory is providing a good description of the real system.

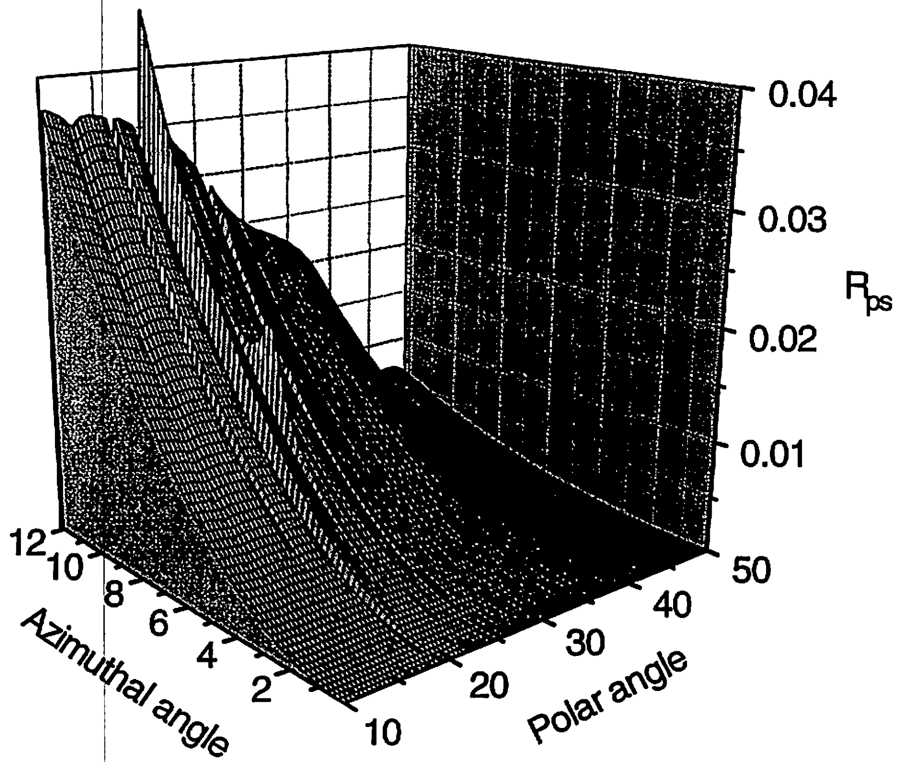

**Figure 8.5:** We show the results of a theoretical calculation using the same parameters as in figure 8.2 but for R$_{ps}$ across a range of both polar and azimuthal angles. As expected the overall intensity of *p* to *s* conversion increases as the incident wavevector twists away from the symmetry plane of the grating, and localised maxima are found at angles corresponding to the excitation of surface and guided modes.

Figure 8.5 shows the calculated *p* to *s* conversion for this structure which in this case arises from two distinct sources: Firstly, in the absence of any grating the liquid crystal layer gives rise to a slowly varying $R_{ps}$ signal due to the anisotropy of the liquid crystal itself. This polarisation conversion is a function of the relative orientations of the incident wavevector and the liquid crystal director, and accounts for the bulk of the signal. It is modulated further by the excitation of guided modes with the liquid crystal layer. Secondly, by providing a preferred direction, the grating gives rise to polarisation conversion, through the excitation of surface and guided modes, as the plane of incidence twists away from the grating vector. As the *p* to *s* conversion is mediated by surface currents we would expect the dominant grating caused conversion mechanism to be surface modes. This is indeed seen in our calculation with the largest contribution to p to s conversion corresponding to the excitation of SPP modes.

## *8.2 Characterisation of a grating coupled liquid crystal cell*

In this section I will show how the theory developed so far was used to characterise a grating coupled 5CB liquid crystal cell in detail.

### *8.2.1 Introduction*

The key features of the modelling theory were tested as far as possible by fabricating a liquid crystal cell bound on one side by a silver-coated diffraction grating and on the other by a flat silica substrate. The liquid crystal layer was aligned on both surfaces in the plane perpendicular to the grating grooves using obliquely evaporated silicon-oxide. The optical and alignment properties of liquid crystals are by now well documented [De Gennes and Prost, 1993], and the interested reader should consult the references for further information.

A nematic liquid crystal was chosen to give the necessary optical uniaxiality. The liquid crystal is expected to follow the shape of both the upper and lower aligning surfaces, giving a director profile that varies from sinusoidal, and therefore elastically distorted, on one surface, to flat and undistorted on the other. Under such circumstances, according to simple theory put forward by Berreman [1972], the liquid crystal will minimise its free energy by relaxing exponentially to the undistorted planar surface with a characteristic decay length. This in principle allows a test of the multilayer, multishape features of the theory.

In order to make a rigorous test of the theory, it is necessary to choose a geometry that yields experimental data that is both sensitive and specific to the cell parameters under investigation. Were this not the case, it might be possible to obtain an excellent comparison between theory and data that was nevertheless meaningless because of a multiplicity of degenerate solutions. For this reason, a geometry has been chosen which is specifically designed to allow the excitation of both guided modes (GM's) and surface plasmon polaritons (SPP's). The excitation of such resonant modes has been used extensively in planar geometries as an accurate and sensitive probe of liquid crystal director profiles [Yang and Sambles, 1991; Elston and Sambles, 1989 and 1991], and already isotropic waveguide materials have been accurately characterised using both prism and grating coupling to the modes [Bryan-Brown, Elston, and Sambles, 1991]. Unlike many other characterisation techniques, for example ellipsometry and polarising microscopy, excitation of GM's and SPP's gives the optical fields a spatial distribution through the cell that varies according to the mode momentum. This spatial specificity reduces many of the degeneracy problems which trouble the other techniques and constitutes the most rigorous experimental test of the theory possible.

### *8.2.2. Experimental details*

The cell shown diagrammatically in figure 8.6 was made from two silica substrates. On to the first, a diffraction grating with a nearly perfectly sinusoidal profile was written by holographic exposure of Shipley S1805 photoresist. This grating plate was then coated with optically thick silver. Both plates were then coated with 25.8*nm* of silicon oxide, obliquely evaporated at 60°. The plates were assembled with a cell gap of ~2.4$\mu m$ and filled in the isotropic phase with 5CB liquid crystal. Upon cooling into the nematic phase, the liquid crystal is aligned homogeneously by the silicon oxide with the director running approximately perpendicular to the grating groove direction. A laser beam of wavelength 632.8*nm* was made incident on the cell through the flat top plate with the cell orientated so that the grating vector lay in the plane of incidence. The optically thick silver acts as a mirror and enhances the coupling to diffracted orders because of the large refractive index mismatch that the silver/dielectric boundary introduces. As the angle of incidence of incoming *p* or *s*-polarised light is varied, there is a range of angles for which the internally diffracted light is incident on the top-plate with an angle $\geq$ the critical angle between the liquid crystal and the top plate. In this regime, when the incident momentum is matched correctly to that required for the excitation of a guided mode, light is strongly coupled into the liquid crystal waveguide resulting in a sharp feature in the angle dependent reflectivity.

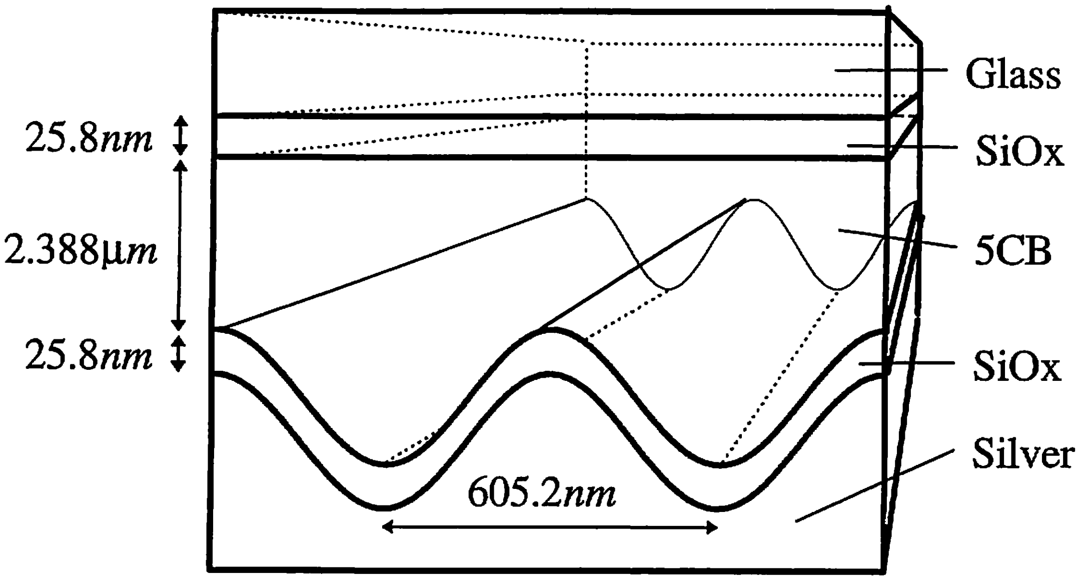

Figure 8.6: The cell to be characterised

Moreover, if the incident light is *p*-polarised the SPP may also be excited. Hence three datasets were recorded: $R_{pp}$, $R_{ss}$, and $R_{ps}$, where the subscripts denote the setting of the input and output polarises in that order. Typical data are shown by the crosses in figure 8.7. In each case the four strongly coupled modes between 16.5° and 20° are guided modes coupled to via a first order diffraction process, whilst the four modes between 22° and 25° are excited via a second order process. The feature at 27° on the $R_{pp}$ data is the SPP coupled to via first order diffraction. For both the $R_{ss}$ and $R_{pp}$ the broad minimum on the extreme left of the data is a leaky guided mode that arises because the light at the liquid crystal/glass interface is not beyond the critical angle at the flat top-plate. The $R_{ps}$ data is very significant. Its very presence tells us that the director does not lie exactly in the plane of incidence and alerts us to the fact that the director profile in the cell is non-trivial. In the $R_{ps}$ signal the resonant modes arise due to the fact that the liquid crystal is oriented at some angle to the grating vector and are coupled to via the grating. The broader, off-resonance low-level reflectivity arises purely from the birefringence of the liquid crystal layer and is largely independent of the grating.

A feature which is present on all the data but is particularly noticeable for the $R_{ss}$ data, is the beat oscillation centred about ~21°. This is due to the first diffracted order returning directly along the incident beam in the Littrow configuration. This causes interference within the flat glass top-plate and is more pronounced for the *s* than the *p* data because of the differing reflection coefficients at the glass/air interface for the two polarisations. This oscillation which is of no direct interest here is not modelled by the theory which treats the glass top-plate as semi-infinite.

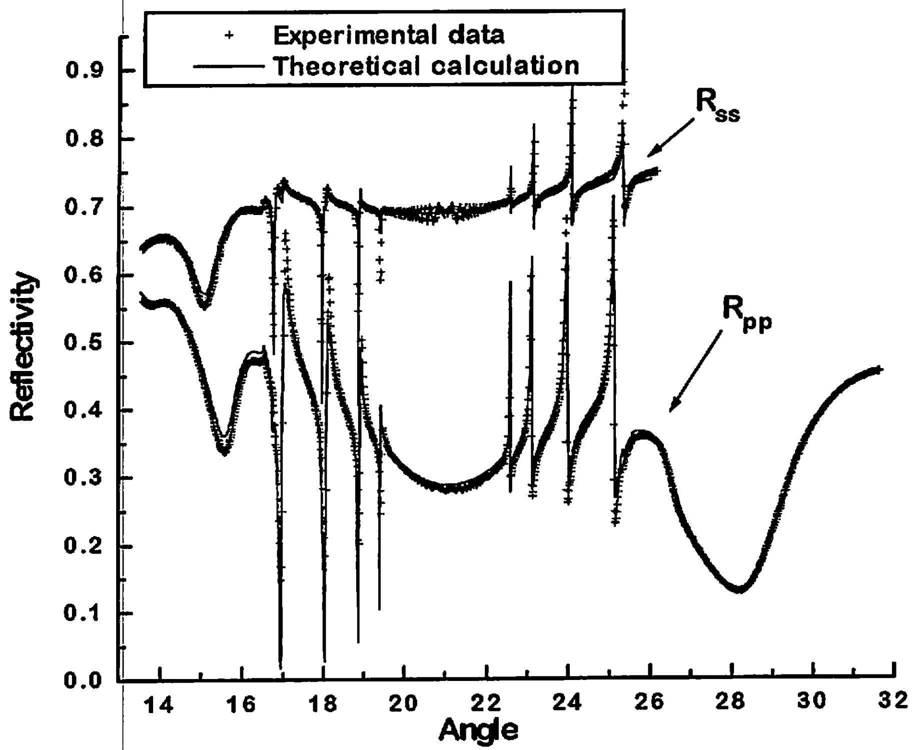

**Figure 8.7:** Fits to experimental data for zeroth-order $R_{pp}$ and $R_{ss}$ efficiencies.

The choice of the pitch and depth of the grating were both important for this work. The pitch (*605.2nm*) was chosen to give coupling to both first and second order modes, yielding as many features as possible for the theory to fit. Clearly, the deeper the grating, the more pronounced its effect on the optics, and the more effectively the theory is tested. In practice, however, as the grating becomes deeper it begins to contribute to the alignment of the liquid crystal layer working in opposition to the silicon-oxide alignment. The result is that above a certain threshold groove depth, the liquid crystal takes up a homeotropic configuration that is highly undesirable. In this work therefore a grating fundamental amplitude of 36.06*nm* is chosen to be as close as possible to this threshold to give the largest possible effect on the optics without perturbing the planar homogeneous alignment of the liquid crystal.

### *8.6.3 Comparison with theory*

In order to build up a non-degenerate fit to the data in the nematic phase a number of steps were taken. The silver-coated grating was characterised both before and after the deposition of silicon-oxide at a wavelength of 500*nm*. This silver coating allows excitation of both the first and second order surface plasmon polariton, and for reasons that are well documented [Wood *et. al.*, 1994], gives sensitivity to the first three coefficients in a Fourier expansion of the grating profile. In a second experiment the *pp* and *ss* reflectivities were measured for the liquid crystal in the isotropic phase. Fitting theory to these data allows further confirmation of the grating groove depth and gives values for the silver and silicon oxide parameters. The latter may be expected to change as the liquid crystal makes the transition to the nematic phase since silicon-oxide has a high porosity and hence its effective optical permittivity is dependent on that of the fluid that fills the voids in its structure. Having established a number of the cell parameters from these preliminary procedures, the anisotropic liquid crystal data was then modelled. Both the *pp* and *ss* data could be modelled approximately by assuming the director to be aligned perpendicular to the grating grooves. However this model yields zero reflectivity for the $R_{ps}$ data which turned out to have by far the most sensitive reflectivity response to the director profile. In Figure 8.8, the best fit to the $R_{ps}$ data (crosses) is denoted by the thick solid line and represents a linear variation in twist through the cell which is approximated by splitting the liquid crystal layer into seven smaller sections. The twist profile was determined using the total liquid crystal twist and the average twist angle as fitting parameters. The twist angle here is defined as the angle between the direction that the grating grooves run in and the liquid crystal director. The other two theoretical curves show the effect of varying these two parameters, to illustrate the lack of degeneracy here. It is clear from the figure that the average twist has a dramatic effect on the mode peak reflectivities, whilst the total twist mainly perturbs the off-resonance reflectivity. The exact cell parameters deduced from the fit to the *ps* data are shown in table 8.1.

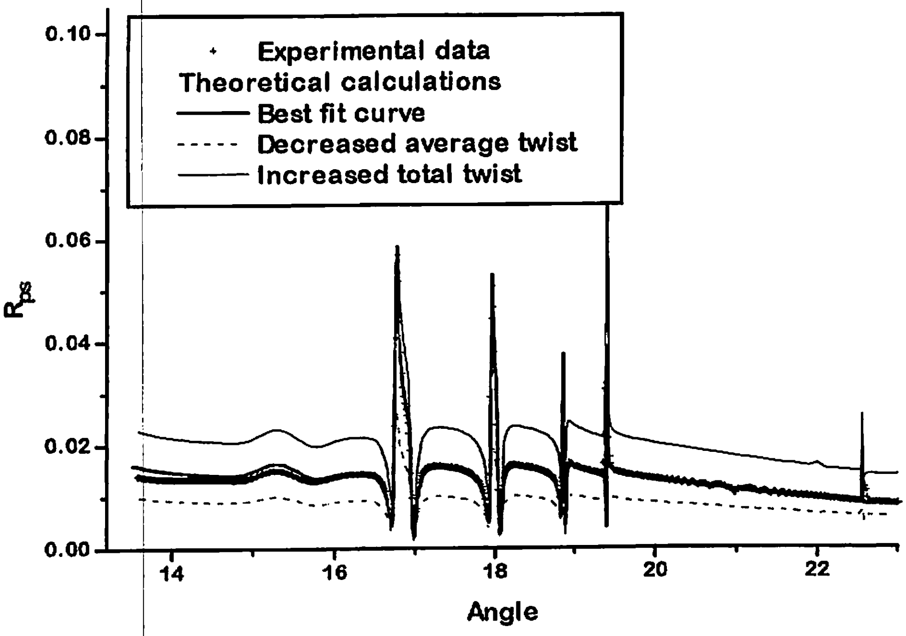

**Figure 8.8:** Effect of varying the director twist profile on the zeroth order $R_{ps}$ efficiency. This trace is particularly sensitive to any twist within the liquid crystal layer and we can use it to determine the spatial orientation of the liquid crystal director by fitting to experimental data. The graph shows three theoretical curves derived from different assumed twist profiles. In this case the best fit requires a linear twist through the cell with zero tilt throughout.

Although the *ps* reflectivity proved very sensitive to the director profile through the whole cell, it was relatively insensitive to the optics of the interaction between the liquid crystal and the grating which takes place within ~100*nm* of the silver-coated grating surface. The *pp* data were much more sensitive to this effect and hence these data were compared with theory in an attempt to unravel the interaction. In the first instance, it was assumed that the liquid crystal would follow exactly the profile of the grating at the silicon-oxide/liquid crystal interface while decaying in amplitude exponentially to the undistorted planar bulk of the liquid crystal. According to Berreman's theory [1972] (which makes a number of simplifying assumptions) the decay length of this exponential function is related only to the pitch of the grating and in this case is predicted to be 96*nm*. Starting with this model gave relatively poor fits to the data. Figure 8.9 shows the effect of varying the Berreman decay length in the model, when compared to the experimental data. The greater the decay length, the less convincing the fit.

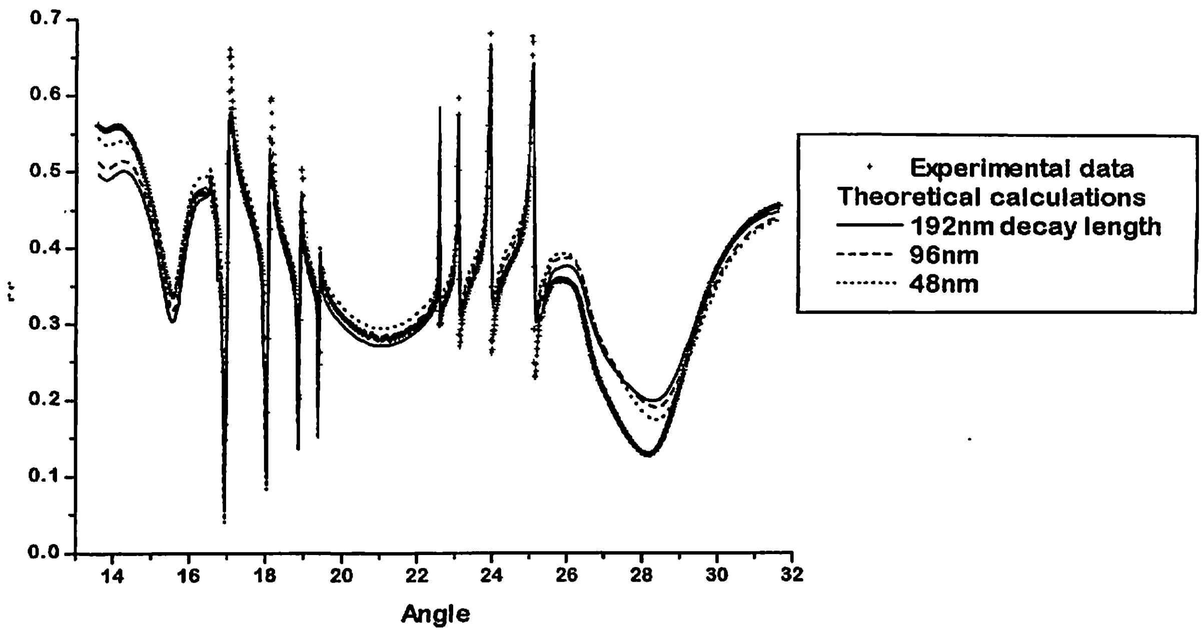

Figure 8.9: Effect of varying the degree of groove-following exhibited by the director on the zeroth order $R_{pp}$ efficiency: we show theoretical curves assuming different Berreman decay lengths from a profile that exactly follows the grating at the SiOx/liquid crystal interface. The greater the decay length, the less convincing the fit.

Surprisingly, the best fit to the data was obtained when the liquid crystal was modelled simply as a planar slab totally ignoring the effect of the grating. For such a model the theoretical fits to both the *pp* and the *ss* data are denoted by the solid lines in figure 8.7. This fitting immediately suggests that the silicon-oxide is not, as we had first conjectured, a surface that binds the liquid crystal with infinite polar anchoring energy; indeed this simplistic model implies a reduction of the polar anchoring energy to very nearly zero. Clearly, reality lies somewhere between the two. Close inspection of the fit to the *pp* data reveals some subtle differences from the theory that are obviously systematic. Moreover it is noteworthy that in order to obtain such a fit, the fundamental amplitude of the grating profile had to be reduced by 6.8% from the value used to obtain the isotropic liquid crystal fits.

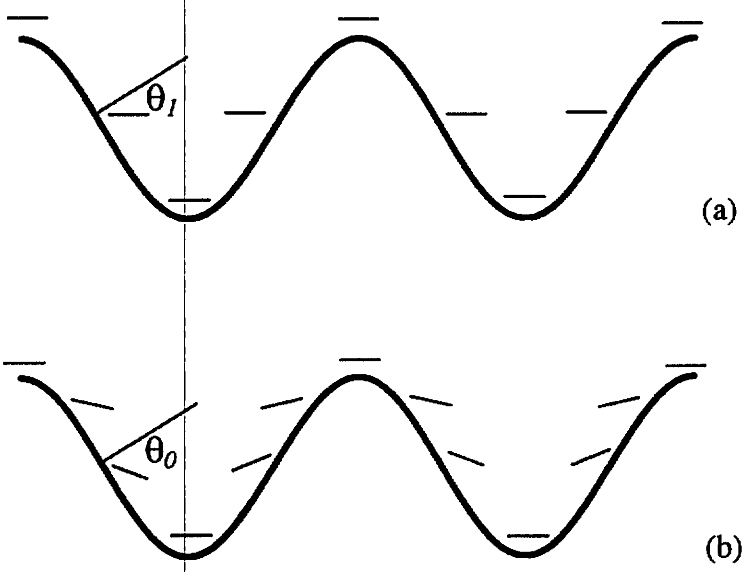

Figure 8.10: Two possible models of liquid crystal alignment with: (a) zero polar anchoring, and (b) finite polar anchoring. In both cases the index mismatch between the liquid crystal and silver layers is identical at the grating peaks and troughs. Away from these regions the two alignments make different angles with the silver interface causing a *p*-polarised light wave to 'see' a different effective index in each case.

Given that the silicon oxide anchors the liquid crystal with a finite polar anchoring energy, the director profile should adopt a more complex configuration just as shown in figure 8.10(b). In this case the liquid crystal lifts off the grating surface everywhere except at the peaks and troughs. It may be expected to have a lift-off angle that varies according to the differential of the grating groove profile and then to decay away exponentially into the bulk. As yet such a model has not been incorporated into the theory, but if one considers this model it becomes qualitatively clear why the simple zero polar anchoring energy model requires a reduction in the groove depth in order to approach a fit to the data. The coupling to grating scattered modes depends mainly on two factors. The first is the grating groove depth, and the second is the index mismatch between the corrugated surface and its surroundings. If we compare the two models of zero polar anchoring, and finite polar anchoring shown in figure 8.10(a) and (b) respectively, it is clear that at the grating peaks and troughs the index mismatch between the liquid crystal and the silver grating is identical. However, away from these regions, the angle made by the liquid crystal with respect to the silver layer is different, giving a slight modification to the effective index 'seen' by incident *p*-polarised light, hence altering the coupling strength. The largest effect is seen when the grating profile is at maximum slope. In the simple model we assume that the director is everywhere flat in the plane of the substrate hence at the position of maximum slope it makes an angle $\theta_l$ with the grating. In reality, because the polar anchoring energy is finite, the director follows the groove profile to a certain extent making an angle of $\theta_0$ with the grating at the equivalent position. Hence in the simple model to reduce $\theta_l$ towards $\theta_0$ one must reduce the groove profile accordingly. In this way one might imagine reaching a compromise between the coupling strength due to the grating groove depth and the coupling strength due to effective index mismatch in order to obtain a fit that is close but does not exactly overlie the data. The fit obtained using the simple model, therefore may be relied upon to reveal with considerable accuracy gross parameters like bulk twist profile in the liquid crystal layer. The nuances of the surface interaction, however, require a more detailed examination.

| Layer | Permittivity | Thickness | Grating amplitudes Fourier harmonics 0,1 & 2 (Pitch = 605.2*nm*) |
|---|---|---|---|
| Glass | $\varepsilon$=(2.1342,0) | - | - |
| Upper SiOx layer | $\varepsilon$=(2.745,0.058) | 25.8*nm* | - |
| 5CB liquid crystal | $\varepsilon_\perp$=(2.355,1.0e-5)<br>$\varepsilon_\parallel$=(2.968,1.0e-5)<br>Average twist 92.5°<br>Total twist 1.9° | 2.388$\mu$*m* | - |
| Lower SiOx layer | $\varepsilon$=(2.745,0.058) | 25.8*nm* | 36.1*nm*, 4.0*nm*, 1.0*nm* |
| Silver | $\varepsilon$=(-17.5,0.7) | - | 36.1*nm*, 4.0*nm*, 1.0*nm* |

**Table 8.1:** The cell parameters deduced from fitting to experimental data.

### *8.3 Conclusion*

Perhaps this chapter above all illustrates the power of the theory developed so far. Previously the optical response of multilayer gratings containing anisotropic layers was the domain of the experimentalist with no suitable theoretical model available to investigate such systems. Now with the power to investigate the response of such systems theoretically we are in a position to determine what set of physical parameters gives rise to a desired optical response. Obviously this sort of predictive ability has tremendous implications for device manufacture.

# *9. Bi - gratings*

In this chapter I develop the differential method of Chandezon to model doubly periodic surfaces.

## *9.1 Introduction*

In diffractive optics we often look to the possible applications of a particular diffractive element. In general the more complex the diffracting element, the more scope is afforded for modulation of the diffracted field, allowing us to tailor the input/output characteristics of our would-be device. The singly-periodic surface relief grating is one such diffractive element that has now found many applications, for example as beam selectors in high power optical devices and more recently to detect impurities via small changes in refractive index [Jory *et. al.,* 1995], observed through optical excitation of the surface plasmon resonance.

A more general structure is the doubly-periodic surface relief or bi-grating, whose properties have yet to be so widely exploited. With an increase in the number of physical parameters we can expect more complex behaviour in the diffracted field, and hopefully exploit this to our advantage. Interest in bi-gratings has generally centred around their ability to approximate rough surfaces and their potential as polarisation independent solar-selective absorbers [Derrick *et al.*, 1979], although other uses have been put forward [Kawatsuki and Uetsuki, 1990].

When we consider diffraction theories it is apparent that alongside singly-periodic gratings, the theory of doubly-periodic or bi-gratings has remained a relatively unexplored area over the past twenty years. Presumably this has been due to the scale of any numerical implementation, which in the past has been limited by the available computing power. With current resources such considerations are less important and we can proceed with the more ambitious numerical schemes required. In this chapter I will develop the differential method of Chandezon to model doubly periodic material interfaces.

The first papers devoted to the subject of bi-gratings presented techniques capable of describing only lossless structures and so were incapable of dealing with more realistic systems or those incorporating metals in which the surface plasmon resonance may play an important role. Following this early work came two papers [Maystre and Nevière, 1978; Vincent, 1978] describing the rigorous numerical integration of Maxwell's equations through a selvedge region, providing the first description of real (i.e. finitely conducting ) systems with deep gratings grooves.

Probably the most elegant formalism capable of modelling deep gratings was offered by Derrick *et al.* [1979 and 1984] who implemented a novel application of the differential method using a co-ordinate transformation similar to that of Chandezon although the stated problem was solved using an iterative technique.

Analyses based on the Rayleigh hypothesis have also been presented [Glass *et. al.*, 1983; Greffet *et. al.*, 1992] whose numerical implementation generally fails for gratings whose depth/pitch ratios are greater than ~ 0.14, although several authors have reported convergent results for much deeper gratings [Laks *et. al.*, 1981].

Of the methods listed above, the rigorous formalisms are perfectly capable of modelling reasonably deep gratings. However in my view most lack both the conceptual and numerical simplicity of Chandezon's theory which may be implemented with relative ease. It is for this very reason that I have developed the method.

The interested reader can find an alternative manuscript extending the Chandezon technique to doubly-periodic structures [Granet, 1995] which seems to have been developed in parallel with my own research. Principal differences lie in the ability of our formalism to model doubly - periodic surfaces with non - orthogonal periodicity directions as well as the treatment of the propagating diffracted field above the grating and the numerical implementation which is discussed towards the end of this chapter.

## *9.2 Presentation of the problem*

The system under consideration is presented diagramatically in figure 9.1. The isotropic metallic or dielectric substrate with complex relative permittivity $\varepsilon_r^0$ is covered by $Q$ isotropic layers with mean thicknesses $d^j$, relative permittivities $\varepsilon_r^j$, and relative permeabilities $\mu_r^j$. Unlike the systems considered in chapter 6 this analysis will require all interfaces to be of the same profile.

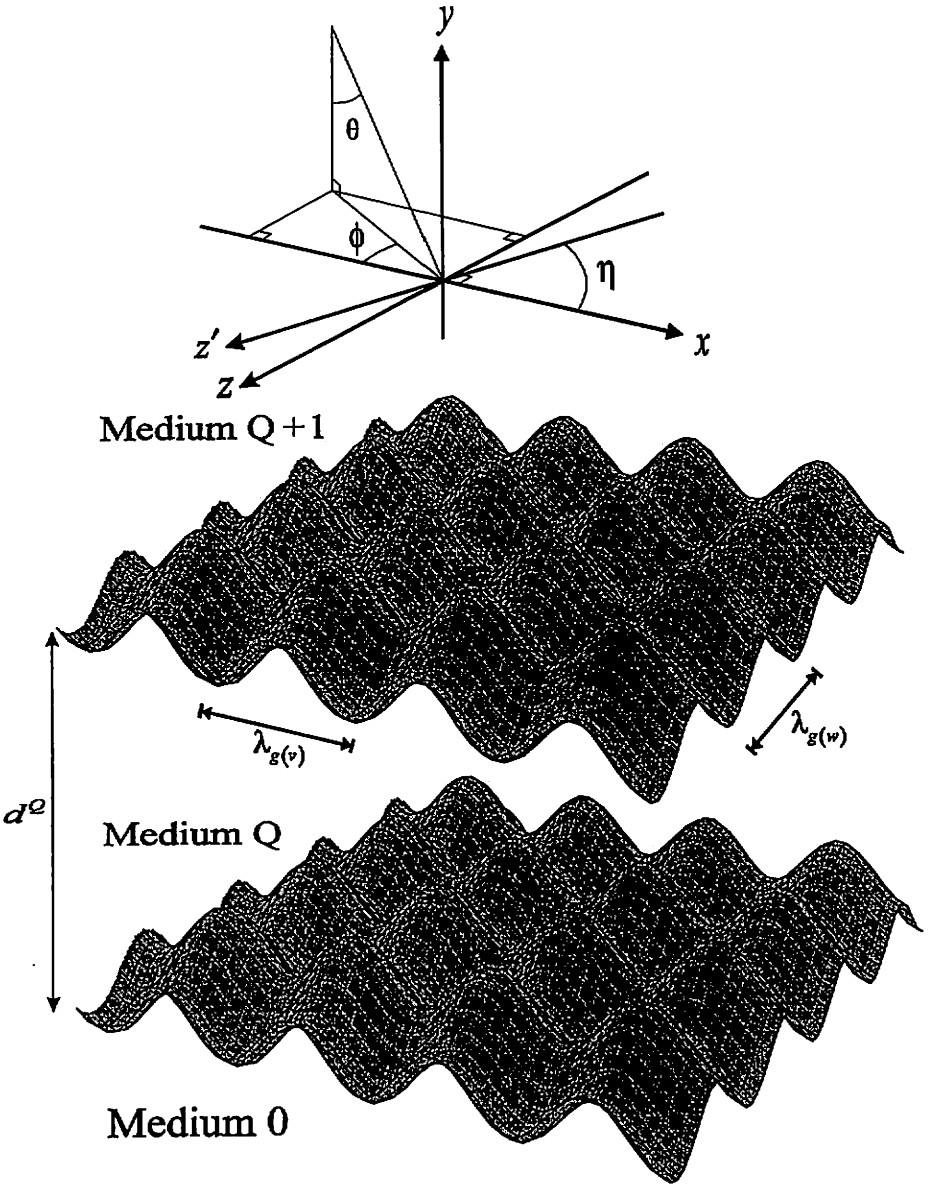

**Figure 9.1:** The system to be modelled

Choosing the origin of $y$ at the top ( $Q$+1 ) interface, the equation of the $j^{\text{th}}$ interface may be written as

$$y = D^j + s(x,z') \text{ with } D^{Q+1} = 0 \quad , \quad D^j = -\left(d^Q + d^{Q-1} + \ldots + d^j\right) \quad , \quad j=1,\ldots,Q+1 \qquad (9.1)$$

where $z' = x\cos\eta + z\sin\eta$; $s(x,z')$ is periodic in $x$ with period $\lambda_{g(v)}$, giving a basis scattering vector of magnitude $K_v = \frac{2\pi}{\lambda_{g(v)}}$ in the direction of the $x$ axis, and periodic in $z'$ with period $\lambda_{g(w)}$, giving a basis scattering vector of magnitude $K_w = \frac{2\pi}{\lambda_{g(w)}}$ in the direction of the $z'$ axis, these two scattering vectors are separated by angle $\eta$. The grating is illuminated through the top semi- infinite, non absorbing isotropic medium by a homogeneous plane wave with wave vector $k = \left(\varepsilon_r^{Q+1}\right)^{1/2} k_0$ $\left(k_0 = \omega/c\right)$ oriented at angle $\theta$ to the $y$ axis and having azimuthal angle $\phi$ in the $x$-$z$ plane.

### *9.3 The co-ordinate frame*

To simplify the boundary conditions at the interfaces, I use a non-orthogonal curvilinear co-ordinate transformation [Chandezon *et al.*, 1982] that maps all grating interfaces onto parallel planes. The field in any medium will be expressed in terms of co-ordinates $v$,$u$ and $w$ where

$$v = x \qquad u = y - s(x,z') \qquad w = z' = x\cos\eta + z\sin\eta \tag{9.2}$$

*For notational clarity I will omit the layer index j from now on, with the understanding that our reasoning applies layer by layer.*

Our non-orthogonal co-ordinate system gives rise to two sets of basis vectors

$$\begin{aligned} &\mathbf{e}_1 = \mathbf{i} + s_v\mathbf{j} - \cot\eta\mathbf{k} && \mathbf{e}^1 = \mathbf{i} \\ &\mathbf{e}_2 = \mathbf{j} && \mathbf{e}^2 = -(s_v + s_w\cos\eta)\mathbf{i} + \mathbf{j} - s_w\sin\eta\mathbf{k} \\ &\mathbf{e}_3 = s_w\mathbf{j} + \operatorname{cosec}\eta\mathbf{k} && \mathbf{e}^3 = \cos\eta\mathbf{i} + \sin\eta\mathbf{k} \end{aligned} \tag{9.3}$$

with $s_v = \frac{\partial s}{\partial v}$ , $s_w = \frac{\partial s}{\partial w}$, from which all contravariant components can be defined by $\mathbf{A} = \mathbf{e}_i A^i$ and all covariant components by $\mathbf{A} = \mathbf{e}^i A_i$.

The two basis sets satisfy the property that $\mathbf{e}^i.\mathbf{e}_j = \delta_{ij}$ and $\mathbf{e}^i \wedge \mathbf{e}^j = \varepsilon^{ijk}\mathbf{e}_k$, where $\varepsilon^{ijk}$ is the levi-civita symbol, whilst $\delta\mathbf{r} = \mathbf{e}_1\delta v + \mathbf{e}_2\delta u + \mathbf{e}_3\delta w$ and $\nabla = \mathbf{e}^1\frac{\partial}{\partial v} + \mathbf{e}^2\frac{\partial}{\partial u} + \mathbf{e}^3\frac{\partial}{\partial w}$.

*As in previous chapters I will, from now on, adopt a system of units in which the free space incident wavenumber,* $|k_0| = \frac{2\pi}{\lambda} = \frac{\omega}{c}$ *and impedance,* $Z_0 = \left(\frac{\mu_0}{\varepsilon_0}\right)^{1/2}$ *are both equated to unity. This will ensure that in certain matrices to be defined later all terms have comparable magnitude, which proves essential to the stability of the numerical methods employed here.*

My aim is to write the two time harmonic Maxwell curl equations $Curl\mathbf{E} = i\mu_r\mathbf{H}$ and $Curl\mathbf{H} = -i\varepsilon_r\mathbf{E}$ in terms of the mixed field components $E_1$, $E^2$, $E_3$ and $H_1$, $H^2$, $H_3$, since these correspond to 'components' that are locally parallel and normal to the surface. They are defined by $E_1 = \mathbf{e}_1.\mathbf{E}$, $E^2 = \mathbf{e}^2.\mathbf{E}$, and $E_3 = \mathbf{e}_3.\mathbf{E}$, with similar relationships for the components of **H**. It should be noted that none of these **e**-vectors are normalised. Consequently, although it is convenient to formulate the equations in terms of $E_1$, $E_3$, $E^2$, and their magnetic counterparts, the actual field components of **E** in the directions defined by $\mathbf{e}_1$, $\mathbf{e}^2$, and $\mathbf{e}_3$ are given by $E_1\left(\mathrm{cosec}^2\eta + s_v^2\right)^{-1/2}$, $E^2\left(1 + s_v^2 + s_w^2 + 2s_vs_w\cos\eta\right)^{-1/2}$, and $E_3\left(\mathrm{cosec}^2\eta + s_w^2\right)^{-1/2}$. Similar relations hold for the field components of **H**.

I start by noting that the curl of a vector can be written as

$$Curl\mathbf{A} = \sin\eta\begin{vmatrix} \mathbf{e}_1 & \mathbf{e}_2 & \mathbf{e}_3 \\ \frac{\partial}{\partial v} & \frac{\partial}{\partial u} & \frac{\partial}{\partial w} \\ A_1 & A_2 & A_3 \end{vmatrix} \tag{9.4}$$

By taking the dot product of the two Maxwell equations with $\mathbf{e}^i$ ($i$=1,2,3) we arrive at six coupled equations

$$\sin\eta\left(\frac{\partial \mathrm{E}_3}{\partial \mathrm{u}} - \frac{\partial}{\partial w}\left(D_1E_1 + CE^2 + D_3E_3\right)\right) = i\mu_r\left(F_wH_1 - D_1H^2 + F_{vw}H_3\right) \tag{9.5}$$

$$\sin\eta\left(\frac{\partial E_1}{\partial \mathrm{w}} - \frac{\partial E_3}{\partial v}\right) = i\mu_rH^2 \tag{9.6}$$

$$\sin\eta\left(\frac{\partial}{\partial v}\left(D_1E_1+CE^2+D_3E_3\right)-\frac{\partial E_1}{\partial u}\right)=i\mu_r\left(F_{vw}H_1-D_3H^2+F_vH_3\right) \tag{9.7}$$

$$\sin\eta\left(\frac{\partial H_3}{\partial u}-\frac{\partial}{\partial w}\left(D_1H_1+CH^2+D_3H_3\right)\right)=-i\varepsilon_r\left(F_wE_1-D_1E^2+F_{vw}E_3\right) \tag{9.8}$$

$$\sin\eta\left(\frac{\partial H_1}{\partial w}-\frac{\partial H_3}{\partial v}\right)=-i\varepsilon_r E^2 \tag{9.9}$$

$$\sin\eta\left(\frac{\partial}{\partial v}\left(D_1H_1+CH^2+D_3H_3\right)-\frac{\partial H_1}{\partial u}\right)=-i\varepsilon_r\left(F_{vw}E_1-D_3E^2+F_vE_3\right) \tag{9.10}$$

Here unwanted components of the form $A^1$ , $A_2$ and $A^3$ have been eliminated using the relations

$$\begin{aligned} A^1 &= F_wA_1-D_1A^2+F_{vw}A_3 \\ A_2 &= D_1A_1+CA^2+D_3A_3 \\ A^3 &= F_{vw}A_1-D_3A^2+F_vA_3 \end{aligned} \tag{9.11}$$

where the following definitions have been made:

$$\begin{aligned} &C=\frac{1}{1+s_v^2+s_w^2+2s_vs_w\cos\eta} \\ &D_1=\left(s_v+s_w\cos\eta\right)C \quad D_3=\left(s_w+s_v\cos\eta\right)C \\ &F_v=\left(1+s_v^2\sin^2\eta\right)C \quad F_w=\left(1+s_w^2\sin^2\eta\right)C \quad F_{vw}=\left(\cos\eta-s_vs_w\sin^2\eta\right)C \end{aligned} \tag{9.12}$$

### *9.4 Maxwell's equations in the transformed space*

I am now in a position to reformulate the six equations (9.5-10) in terms of the field components $E_1$, $E_3$, $H_1$ and $H_3$ which are always tangential to the lower interface profile in any one medium. I do this, eliminating those field components perpendicular to the grating surface, thus reducing the six coupled equations to four.

$$\frac{\partial E_1}{\partial u}=\frac{\partial}{\partial v}\left(D_1E_1\right)+D_3\frac{\partial E_1}{\partial \omega}+\left(\frac{\partial D_3}{\partial v}\right)E_3+i\frac{\sin\eta}{\varepsilon_r}\frac{\partial}{\partial v}\left(C\left(\frac{\partial H_1}{\partial \omega}-\frac{\partial H_3}{\partial v}\right)\right)-i\frac{\mu_r}{\sin\eta}\left(F_{vw}H_1+F_vH_3\right) \tag{9.13}$$

$$\frac{\partial E_3}{\partial u}=\left(\frac{\partial D_1}{\partial \omega}\right)E_1+D_1\frac{\partial E_3}{\partial v}+\frac{\partial}{\partial \omega}\left(D_3E_3\right)+i\frac{\sin\eta}{\varepsilon_r}\frac{\partial}{\partial \omega}\left(C\left(\frac{\partial H_1}{\partial \omega}-\frac{\partial H_3}{\partial v}\right)\right)+i\frac{\mu_r}{\sin\eta}\left(F_wH_1+F_{vw}H_3\right) \tag{9.14}$$

$$\frac{\partial H_1}{\partial u}=-i\frac{\sin\eta}{\mu_r}\frac{\partial}{\partial v}\left(C\left(\frac{\partial E_1}{\partial \omega}-\frac{\partial E_3}{\partial v}\right)\right)+i\frac{\varepsilon_r}{\sin\eta}\left(F_{vw}E_1+F_vE_3\right)+\frac{\partial}{\partial v}\left(D_1H_1\right)+D_3\frac{\partial H_1}{\partial \omega}+\left(\frac{\partial D_3}{\partial v}\right)H_3 \tag{9.15}$$

$$\frac{\partial H_3}{\partial u}=-i\frac{\sin\eta}{\mu_r}\frac{\partial}{\partial \omega}\left(C\left(\frac{\partial E_1}{\partial \omega}-\frac{\partial E_3}{\partial v}\right)\right)-i\frac{\varepsilon_r}{\sin\eta}\left(F_wE_1+F_{vw}E_3\right)+\left(\frac{\partial D_1}{\partial \omega}\right)H_1+D_1\frac{\partial H_3}{\partial v}+\frac{\partial}{\partial \omega}\left(D_3H_3\right) \tag{9.16}$$

### *9.5 Formulation of the solution*

I now exploit the doubly-periodic nature of the system and write the field components in Fourier series assuming that radiation is incident in the $\theta$, $\phi$ direction as indicated in figure 9.1.

$$\Psi(v,u,w)=\sum_{m,n}\Psi_{m,n}(u)\exp i\left(\alpha_m v+\gamma_n w\right) \tag{9.17}$$

$$\text{with}\quad \left.\begin{aligned}\alpha_m &= \left(\varepsilon_r^{Q+1}\right)^{1/2}\sin\theta\left(\cos\phi-\sin\phi\cot\eta\right)+mK_v\\ \gamma_n &= \frac{\left(\varepsilon_r^{Q+1}\right)^{1/2}\sin\theta\sin\phi}{\sin\eta}+nK_w\end{aligned}\right\}\quad m,n=0,\ \pm1,\ \pm2,\ \ldots$$

where $\Psi$ represents any one of the four field components $E_1$, $E_3$, $H_1$ and $H_3$. Similarly the six shape functions $C$, $D_1$, $D_3$, $F_v$, $F_w$ and $F_{vw}$ are expanded in a double Fourier series

$$\Phi(v,w)=\sum_{p,q}\Phi_{p,q}\exp i\left(pK_vv+qK_ww\right)\qquad p,q=0,\ \pm1,\ \pm2,\ \ldots \tag{9.18}$$

where $\Phi$ represents any one of the functions $C$, $D_1$, $D_3$, $F_v$, $F_w$ and $F_{vw}$.

Introducing these expansions into equations (9.13-16) individual Fourier components of the fields may be singled out by using orthogonality with $\exp i(\alpha_m v \ +\gamma_n w)$ , leading to an infinite system of coupled differential equations, where for conciseness of notation $p\equiv a\text{-}m$ and $q\equiv b\text{-}n$ has been used.

$$-i\frac{\partial E_{1(a,b)}}{\partial u}=\sum_{m,n}\left\{\begin{array}{l}\left(\alpha_a D_{1(p,q)}+\gamma_n D_{3(p,q)}\right)E_{1(m,n)}+pK_v D_{3(p,q)}E_{3(m,n)}\\ -\left(\alpha_a\gamma_n\frac{\sin\eta}{\varepsilon_r}C_{(p,q)}+\frac{\mu_r}{\sin\eta}F_{vw(p,q)}\right)H_{1(m,n)}\\ +\left(\alpha_a\alpha_m\frac{\sin\eta}{\varepsilon_r}C_{(p,q)}-\frac{\mu_r}{\sin\eta}F_{v(p,q)}\right)H_{3(m,n)}\end{array}\right\} \tag{9.19}$$

$$-i\frac{\partial E_{3(a,b)}}{\partial u}=\sum_{m,n}\left\{\begin{array}{l}qK_\omega D_{1(p,q)}E_{1(m,n)}+\left(\alpha_m D_{1(p,q)}+\gamma_b D_{3(p,q)}\right)E_{3(m,n)}\\ -\left(\gamma_n\gamma_b\frac{\sin\eta}{\varepsilon_r}C_{(p,q)}+\frac{\mu_r}{\sin\eta}F_{w(p,q)}\right)H_{1(m,n)}\\ +\left(\alpha_m\gamma_b\frac{\sin\eta}{\varepsilon_r}C_{(p,q)}+\frac{\mu_r}{\sin\eta}F_{vw(p,q)}\right)H_{3(m,n)}\end{array}\right\} \tag{9.20}$$

$$-i\frac{\partial H_{1(a,b)}}{\partial u}=\sum_{m,n}\left\{\begin{array}{l}\left(\gamma_n\alpha_a\frac{\sin\eta}{\mu_r}C_{(p,q)}+\frac{\varepsilon_r}{\sin\eta}F_{vw(p,q)}\right)E_{1(m,n)}\\ +\left(-\alpha_a\alpha_m\frac{\sin\eta}{\mu_r}C_{(p,q)}+\frac{\varepsilon_r}{\sin\eta}F_{v(p,q)}\right)E_{3(m,n)}\\ +\left(\alpha_a D_{1(p,q)}+\gamma_n D_{3(p,q)}\right)H_{1(m,n)}+pK_v D_{3(p,q)}H_{3(m,n)}\end{array}\right\} \tag{9.21}$$

$$-i\frac{\partial H_{1(a,b)}}{\partial u}=\sum_{m,n}\left\{\begin{array}{l}\left(\gamma_n\gamma_b\frac{\sin\eta}{\mu_r}C_{(p,q)}-\frac{\varepsilon_r}{\sin\eta}F_{w(p,q)}\right)E_{1(m,n)}\\ -\left(\alpha_m\gamma_b\frac{\sin\eta}{\mu_r}C_{(p,q)}+\frac{\varepsilon_r}{\sin\eta}F_{vw(p,q)}\right)E_{3(m,n)}\\ +qK_\omega D_{1(p,q)}H_{1(m,n)}+\left(\alpha_m D_{1(p,q)}+\gamma_b D_{3(p,q)}\right)H_{3(m,n)}\end{array}\right\} \tag{9.22}$$

In preparation for the necessary numerical calculation I truncate these expansions, limiting them to the range $-M \leq m,a \leq M$, $-N \leq n,b \leq N$ and write the four equations in matrix form as

$$-i\frac{\partial \xi(u)}{\partial u} = \mathbf{T}\xi(u) \tag{9.23}$$

where $\xi(u) = \left(E_{1(m,n)}, E_{3(m,n)}, H_{1(m,n)}, H_{3(m,n)}\right)^{\mathrm{T}}$ and $\mathbf{T} = \begin{pmatrix} T_{11} & T_{12} & T_{13} & T_{14} \\ T_{21} & T_{22} & T_{23} & T_{24} \\ T_{31} & T_{32} & T_{33} & T_{34} \\ T_{41} & T_{42} & T_{43} & T_{44} \end{pmatrix}$

Each matrix $T_{ij}$ has dimension $(2M+1)(2N+1)$ and it's elements are conveniently labelled as $(\mathrm{T}_{ij})_{a,b;m,n}$. Using again for brevity the notation $p \equiv a-m$, $q \equiv b-n$, the elements have the form

$$T_{11}: \alpha_a D_{1(p,q)} + \gamma_n D_{3(p,q)} \qquad T_{21}: qK_\omega D_{1(p,q)}$$

$$T_{12}: pK_v D_{3(p,q)} \qquad T_{22}: \alpha_m D_{1(p,q)} + \gamma_b D_{3(p,q)}$$

$$T_{13}: -\alpha_a \gamma_n \frac{\sin\eta}{\varepsilon_r} C_{(p,q)} - \frac{\mu_r}{\sin\eta} F_{vw(p,q)} \qquad T_{23}: -\gamma_n \gamma_b \frac{\sin\eta}{\varepsilon_r} C_{(p,q)} + \frac{\mu_r}{\sin\eta} F_{w(p,q)}$$

$$T_{14}: \alpha_a \alpha_m \frac{\sin\eta}{\varepsilon_r} C_{(p,q)} - \frac{\mu_r}{\sin\eta} F_{v(p,q)} \qquad T_{24}: \alpha_m \gamma_b \frac{\sin\eta}{\varepsilon_r} C_{(p,q)} + \frac{\mu_r}{\sin\eta} F_{vw(p,q)}$$

$$T_{32}: \alpha_a \gamma_n \frac{\sin\eta}{\mu_r} C_{(p,q)} + \frac{\varepsilon_r}{\sin\eta} F_{vw(p,q)} \qquad T_{41}: \gamma_n \gamma_b \frac{\sin\eta}{\mu_r} C_{(p,q)} - \frac{\varepsilon_r}{\sin\eta} F_{w(p,q)}$$

$$T_{32}: -\alpha_a \alpha_m \frac{\sin\eta}{\mu_r} C_{(p,q)} + \frac{\varepsilon_r}{\sin\eta} F_{v(p,q)} \qquad T_{42}: -\alpha_m \gamma_b \frac{\sin\eta}{\mu_r} C_{(p,q)} - \frac{\varepsilon_r}{\sin\eta} F_{vw(p,q)}$$

$$T_{33} = T_{11} \qquad T_{43} = T_{21}$$

$$T_{34} = T_{12} \qquad T_{44} = T_{22} \tag{9.24}$$

This matrix is constant in each medium and so the truncated equations have eigensolutions of the form $\mathbf{V}^q \exp ir_q u$. The field vector may then be expanded as a linear combination of these

$$\xi(u) = \sum_{q=1}^{4(2M+1)(2N+1)} b_q \mathbf{V}^q \exp ir_q u \tag{9.25}$$

where $r_q$ are the eigenvalues of the matrix **T**, $\mathbf{V}^q$ the eigenvectors, and $b_q$ the amplitude associated with the $q^{\text{th}}$ eigenmode. Note that for a given eigenmode the corresponding eigenvector gives the relative field strengths while the eigenvalue gives us the spatial dependence. Finally using the above we may state the form of $\xi\,(u)$ in the $j^{\text{th}}$ medium.

$$\xi^j(u) = \mathbf{M}^j \phi^j(u)\mathbf{b}^j \tag{9.26}$$

where $\mathbf{M}^j$ is a matrix whose columns are the eigenvectors of $\mathbf{T}^j$, $\phi^j$ is a square matrix with elements $\phi^j_{qp} = \delta_{qp} \exp ir^j_q u$ , and $\mathbf{b}^j$ is a vector of amplitude coefficients which need to be determined in order to define the field in each medium. Although the co-ordinate transformation used in each medium is the same, the matrix **M** varies from medium to medium because of the form of **T**, and hence the eigensolution depends upon the changing values of $\varepsilon_r$ and $\mu_r$.

### *9.6 Internal boundary conditions*

The internal boundary conditions at each interface require that the tangential components of **E** and **H** are continuous, which is equivalent to the matching condition $\xi^{j-1}(d_j)=\xi^{j}(d_j)$ at the $j^{th}$ interface.

Using these boundary conditions it is possible to construct the transfer matrix or, as in this case, the scattering matrix [Ko and Sambles, 1988; Cotter *et. al.*, 1995], **S** that relates the amplitude of the eigenmodes in layer $j= Q+1$ to those in layer $j=0$. The procedure for doing this is exactly as outlined in *chapter* 5 (although all the matrices involved are of greater dimension) and has the advantage that it allows the inclusion of any number of arbitrarily thick overlayers without the onset of numerical instabilities.

### *9.7 External boundary conditions*

Having developed the Maxwell equations I now require the form of the incoming and scattered fields in the transformed frame, that is in terms of the co-ordinates $v$, $u$, and $w$. For the singly-periodic grating case these have previously been derived by Elston et al. [1991], and Li [1994].

For a Bragg plane wave with momentum components $\alpha_a$ and $\gamma_b$ in the directions of the grating vectors, the four associated field components are expanded in the common form

$\Psi^{a,b}(u,v,w)=\sum_{m,n}(\Psi)^{a,b}_{m,n}\exp i(\alpha_m v+\beta_{a,b}u+\gamma_n w)$ where $\beta_{a,b}$ takes the values

$$\text{Incident field:} \quad \beta_{0,0}=-\left(\mu_r^{Q+1}\varepsilon_r^{Q+1}-(\alpha_0+\gamma_0\cos\eta)^2-(\gamma_0\sin\eta)^2\right)^{1/2}$$

$$\text{Real reflected field:} \quad \beta_{a,b}=\left(\mu_r^{Q+1}\varepsilon_r^{Q+1}-(\alpha_a+\gamma_b\cos\eta)^2-(\gamma_b\sin\eta)^2\right)^{1/2} \qquad (9.27)$$

$$\text{Real transmitted field:} \quad \beta_{a,b}=-\left(\mu_r^{0}\varepsilon_r^{0}-(\alpha_a+\gamma_b\cos\eta)^2-(\gamma_b\sin\eta)^2\right)^{1/2}$$

The Fourier coefficients in the expansion of $E_1$, $E_3$, $H_1$, and $H_3$ associated with Bragg plane waves are not all independent since the plane wave is a solution of the equations (9.13-16) or alternatively (9.5-10).

If equations (9.5,7,8,10) of this latter system are written in terms of $E_i$ and $H_i$ using $A^1 = A_1 - (s_v + s_w \cos\eta)A_2 + \cos\eta A_3$ and $A^3 = A_3 - (s_w + s_v \cos\eta)A_2 + \cos\eta A_1$ then, after some algebraic manipulation, it is possible to express the amplitudes of the Fourier components of the fields $E_1$, $E_3$, $H_1$, and $H_3$ associated with the Bragg plane waves in terms of the associated fields $E_2$, and $H_2$.

Since for a plane wave solution $\frac{\partial E_i^{ab}}{\partial u} = i\beta_{ab} E_i^{ab}$ etc. this yields

$$E_1 = f\left(g_1 - g_3 \cos\eta - \frac{\beta_{ab}}{\varepsilon_r} h_3 \sin\eta\right) \tag{9.28}$$

$$E_3 = f\left(g_3 - g_1 \cos\eta + \frac{\beta_{ab}}{\varepsilon_r} h_1 \sin\eta\right) \tag{9.29}$$

$$H_1 = f\left(h_1 - h_3 \cos\eta + \frac{\beta_{ab}}{\mu_r} g_3 \sin\eta\right) \tag{9.30}$$

$$H_3 = f\left(h_3 - h_1 \cos\eta - \frac{\beta_{ab}}{\mu_r} g_1 \sin\eta\right) \tag{9.31}$$

where $f^{-1} = \sin^2\eta\left(1 - \frac{\beta_{ab}^2}{\mu_r \varepsilon_r}\right)$ and

$$g_1 = \frac{\sin\eta}{i\varepsilon_r}\frac{\partial H_2}{\partial w} + (s_v + s_w \cos\eta)E_2 \tag{9.32}$$

$$g_3 = -\frac{\sin\eta}{i\varepsilon_r}\frac{\partial H_2}{\partial v} + (s_w + s_v \cos\eta)E_2 \tag{9.33}$$

$$h_1 = -\frac{\sin\eta}{i\mu_r}\frac{\partial E_2}{\partial w} + (s_v + s_w \cos\eta)H_2 \tag{9.34}$$

$$h_3 = \frac{\sin\eta}{i\mu_r}\frac{\partial E_2}{\partial v} + (s_w + s_v \cos\eta)H_2 \tag{9.35}$$

$\mu_r$ and $\varepsilon_r$ being chosen appropriate to the medium in which the wave is propagating. Since $E_2 = \mathbf{e}_2.\mathbf{E} = \mathbf{j}.\mathbf{E}$ etc., the latter are the components of **E** (and **H**) normal to the plane of the bi-grating. A Bragg wave in the TM mode has $H_2$=0 and $E_2 = E^{TM}_{(a,b)} \sin\theta_{ab}$ whilst in the TE mode E$_2$=0 and $H_2 = H^{TM}_{(a,b)} \sin\theta_{ab}$ where $\theta_{ab}$ is the angle between the directions of diffracted radiation and the normal to the bi-grating.

Noting that

$$\frac{\partial\psi^{ab}}{\partial v} = i\left(\alpha_a + \beta_{a,b} s_v\right)\psi^{ab}$$

$$\frac{\partial\psi^{ab}}{\partial w} = i\left(\gamma_a + \beta_{a,b} s_w\right)\psi^{ab} \tag{9.36}$$

and that

$$\beta_{ab} s_v \psi^{ab} = \sum_{m,n} \psi^{a,b}_{m,n} (m-a) K_{g(v)} L_{m-a,n-b}\left(-\beta_{a,b}\right) \exp i\left(\alpha_m v + \beta_{a,b} u + \gamma_n w\right)$$

$$\beta_{ab} s_w \psi^{ab} = \sum_{m,n} \psi^{a,b}_{m,n} (n-b) K_{g(w)} L_{m-a,n-b}\left(-\beta_{a,b}\right) \exp i\left(\alpha_m v + \beta_{a,b} u + \gamma_n w\right) \tag{9.37}$$

the amplitudes of the Fourier components associated with the Bragg waves may be obtained:

$$\left(E_1\right)^{a,b}_{m,n} = \left\{ \frac{\gamma_b + \alpha_a \cos\eta}{\varepsilon \sin\eta \left(1 - \dfrac{\beta^2_{a,b}}{\mu_r \varepsilon_r}\right)} H_{2(a,b)} - \left( \frac{pK_v}{\beta_{a,b}} + \frac{\beta_{a,b}\alpha_a}{\mu_r \varepsilon_r \left(1 - \dfrac{\beta^2_{a,b}}{\mu_r \varepsilon_r}\right)} \right) E_{2(a,b)} \right\} L_{-p,-q}\left(-\beta_{a,b}\right) \tag{9.38}$$

$$\left(E_3\right)^{a,b}_{m,n} = \left\{ \frac{-\left(\alpha_a + \gamma_b \cos\eta\right)}{\varepsilon \sin\eta \left(1 - \frac{\beta^2_{a,b}}{\mu_r \varepsilon_r}\right)} H_{2(a,b)} - \left( \frac{qK_\omega}{\beta_{a,b}} + \frac{\gamma_b \beta_{a,b}}{\mu_r \varepsilon_r \left(1 - \frac{\beta^2_{a,b}}{\mu_r \varepsilon_r}\right)} \right) E_{2(a,b)} \right\} L_{-p,-q}\left(-\beta_{a,b}\right) \tag{9.39}$$

$$\left(H_1\right)^{a,b}_{m,n} = \left\{ -\left( \frac{pK_v}{\beta_{a,b}} + \frac{\beta_{a,b}\alpha_a}{\mu_r \varepsilon_r \left(1 - \frac{\beta^2_{a,b}}{\mu_r \varepsilon_r}\right)} \right) H_{2(a,b)} - \frac{\gamma_b + \alpha_a \cos\eta}{\mu_r \sin\eta \left(1 - \frac{\beta^2_{a,b}}{\mu_r \varepsilon_r}\right)} E_{2(a,b)} \right\} L_{-p,-q}\left(-\beta_{a,b}\right) \tag{9.40}$$

$$\left(H_3\right)^{a,b}_{m,n} = \left\{ -\left( \frac{qK_\omega}{\beta_{a,b}} + \frac{\beta_{a,b}\gamma_b}{\mu_r \varepsilon_r \left(1 - \frac{\beta^2_{a,b}}{\mu_r \varepsilon_r}\right)} \right) H_{2(a,b)} + \frac{\alpha_a + \gamma_b \cos\eta}{\mu_r \sin\eta \left(1 - \frac{\beta^2_{a,b}}{\mu_r \varepsilon_r}\right)} E_{2(a,b)} \right\} L_{-p,-q}\left(-\beta_{a,b}\right) \tag{9.41}$$

where $E_{2(a,b)} = E^{TM}_{(a,b)} \sin\theta_{\mathrm{a,b}}$ , $H_{2(a,b)} = H^{TE}_{(a,b)} \sin\theta_{a,b}$ , $p = a - m$ , $q = b - n$

and $L_{p,q}(t) = \dfrac{1}{\lambda_{g(v)}\lambda_{g(w)}} \displaystyle\int_0^{\lambda_{g(w)}} \int_0^{\lambda_{g(v)}} \exp - i\left(ts(v,w) + pK_v v + qK_w w\right) dv\, dw$

The incident wave expansions provide us with a vector describing the incident field in the transformed co-ordinates. By normalising the incident H field we may set values for $E^{TM}_{(0,0)}$ and $H^{TE}_{(0,0)}$ which provide our initial conditions. The total real reflected field and real transmitted field are then the summation of equations (9.28-31) over the subset of real diffracted waves $a,b \in P \Leftrightarrow \left|\left(\alpha_a + \gamma_b \cos\eta\right)^2 + \left(\gamma_b \sin\eta\right)^2\right| < \mu_r \varepsilon_r$ where the values of $\mu_r$ and $\varepsilon_r$ must be taken appropriate to the medium in which the wave is propagating. The field coefficients $E^{TM}_{(a,b)}$ and $H^{TE}_{(a,b)}$ are the unknowns we ultimately seek from which the TM-like and TE-like reflectivities for a given order $(a,b)$ can be determined.

### *9.8 Method of solution and final equations*

The mechanics of the final solution have been discussed previously for the singly-periodic grating case in *chapter* 5 and apply equally to our more general geometry with the understanding that all matrices are now much larger. I write the reflected wave amplitudes as

$$\begin{aligned}\hat{\mathbf{R}} = &\left[\hat{\mathbf{M}}_{11} - (\mathbf{M}_{11}\mathbf{S}_{12} + \mathbf{M}_{12})(\mathbf{M}_{21}\mathbf{S}_{12} + \mathbf{M}_{22})^{-1}\hat{\mathbf{M}}_{21}\right]^{-1} \cdot \\ &\cdot\left[(\mathbf{M}_{11}\mathbf{S}_{12} + \mathbf{M}_{12})(\mathbf{M}_{21}\mathbf{S}_{12} + \mathbf{M}_{22})^{-1}\mathbf{L}'' - \mathbf{L}'\right]\end{aligned} \tag{9.32}$$

in which $\hat{\mathbf{M}}^{Q+1}$ is the same as $\mathbf{M}^{Q+1}$ with those columns representing the eigenvectors of the real upward propagating modes replaced by the appropriate Fourier components of (9.28-31). Similarly $\mathbf{L} = (\mathbf{L}', \mathbf{L}'')^{\mathrm{T}}$ is a column vector containing the incident wave components. A related calculation gives the transmitted wave amplitudes

$$\hat{\mathbf{T}} = \mathbf{Q}\mathbf{S}_{22}(\mathbf{M}_{21}\mathbf{S}_{12} + \mathbf{M}_{22})^{-1}\left(\hat{\mathbf{M}}_{21}\hat{\mathbf{R}} + \mathbf{L}''\right) \tag{9.33}$$

where the matrix **Q** is defined by

$$\begin{pmatrix} \hat{\mathbf{M}}^{0}_{11} & \hat{\mathbf{M}}^{0}_{12} \\ \hat{\mathbf{M}}^{0}_{21} & \hat{\mathbf{M}}^{0}_{22} \end{pmatrix}^{-1} \begin{pmatrix} \mathbf{M}_{11} & \mathbf{M}_{12} \\ \mathbf{M}_{21} & \mathbf{M}_{22} \end{pmatrix} = \begin{pmatrix} \mathbf{I} & \mathbf{0} \\ \mathbf{0} & \mathbf{Q} \end{pmatrix} \tag{9.34}$$

Here $\hat{\mathbf{M}}^{0}$ is the substrate medium equivalent of $\hat{\mathbf{M}}^{Q+1}$ with the eigenvectors associated with the real modes replaced by the appropriate Fourier components as defined in (9.28-31).

### *9.9. Numerical Results*

Here I will describe the numerical solution of equation (9.23) and show some examples of our theoretical calculation along with fits to experimental data.

### *9.9.1 Scale of the calculation*

The numerical solution of the eigen-equation (9.23) is obtained via a knowledge of the eigenvalues and eigenvectors of the matrix **T**. Being a general complex matrix the eigen problem is time consuming, amounting to some 70-90% of the total computation time. Both this and the 2D Fourier integrals required by (9.23) are computed using NAG library routines for Fortran 90. In general as we include more and more terms in the expansion of our coupled equations so these routines dominate the computational requirements of our Fortran code, and limit it's use with personal computers. To appreciate the scale of the calculation one need only recall that the size of the matrix **T** is $4(2M+1)(2N+1)=1936$ for $M=N=10$. For a more efficient approach Granet [1995] describes a simple transformation to block diagonalise **T**. Equation (9.23) then tells us that the field has effectively been split into two independent states of polarisation, satisfying separate eigenequations half the size of the original equation (9.23). The complete eigensolution may then be obtained by appealing to each in turn, before combining the two so as to reconstruct the original field vector $\xi$. The time spent solving an eigenequation of size $T$ is proportional to $T^3$ so we can expect this method to be some four times faster than the original approach.

### *9.9.2 Testing the computer code*

First and foremost, in the limit of one grating amplitude tending to zero, our code must agree with a previously developed code designed to model singly-periodic gratings in the conical mount. With this condition satisfied we can perform an approximate test on a general, doubly-periodic grating as follows: first we use our bi-grating code to model a grating surface that is the sum of two sine series $s(v,w)=s_1(v)+s_2(w)=\sum_i a_{v(i)}\sin\left(iK_{g(v)}v+\chi_{v(i)}\right)+\sum_j a_{w(j)}\sin\left(jK_{g(w)}w+\chi_{w(j)}\right)$ and obtain an efficiency $R_{mn}(s(v,w))$. For comparison we use our single-grating code to model the optical responses of each of those individual gratings, producing reflection efficiencies $R_m(s_1(v)),\ R_n(s_2(w))$. For shallow gratings we expect that $R_{mn}(s)\approx\frac{R_m(s_1(v))R_n(s_2(w))}{R(0)}$ where $R(0)$ is the reflection efficiency of the planar surface. This expression, given by McPhedran in *The electromagnetic theory of gratings* [Petit, 1972], is the analogue of the impulse approximation in scattering theory, including repeated scattering of each grating components but omitting sequences involving alternate scattering off both gratings.

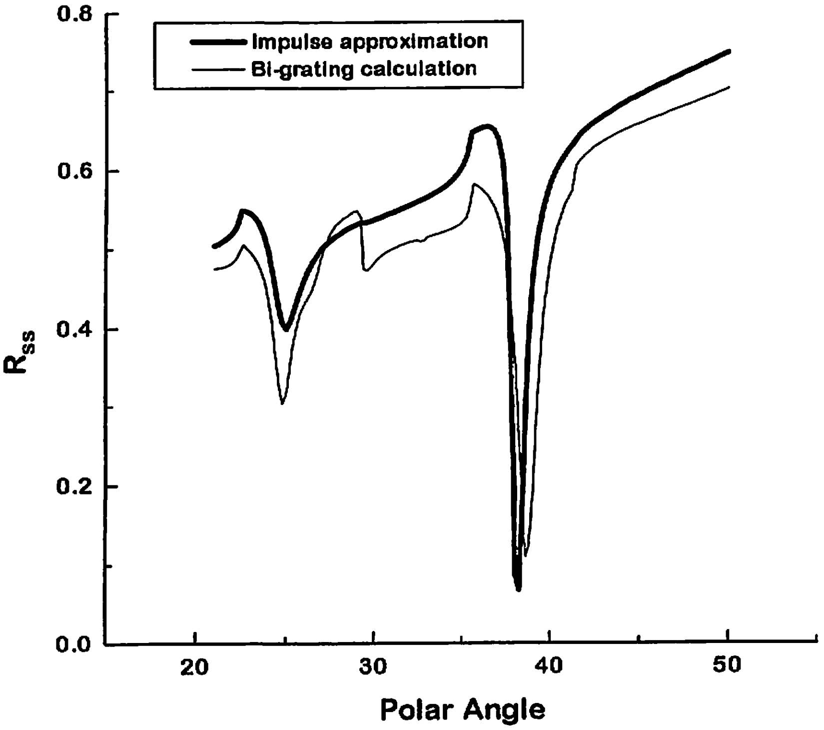

**Figure 9.2:** Comparison of the product of efficiencies calculated with a previous code for two separate gratings of profile $s_1(v)$ and $s_2(w)$, with the efficiency calculated for a bi-grating of profile $s_1(v)$ + $s_2(w)$. The overall agreement between the two obtained using the parameters in table 9.1 can be regarded as a first order test of our code.

This approximation can be used to make an approximate test of the code. Figure 9.2 shows an example of one such comparison for an uncoated, sinusoidal, silver grating illuminated at 632.8*nm*, with azimuthal angle 30°: The 'impulse' approximation reproduces the general features of zeroth order reflection as a function of angle of incidence but the bi-grating calculation contains two additional features: a minimum at ~ 30° corresponding to the excitation of a surface plasmon resonance; and an edge at ~ 41°. Both of these features are connected with double scattering events from first one and then the other grating and can be modelled only when both gratings are considered simultaneously. The grating parameters are given in table 9.1, while a selection of the calculated zeroth order efficiencies are shown in table 9.2.

| $\lambda = 632.8nm$ | |
|---|---|
| $\lambda_{g(v)} = 1000nm$<br>$a_{v(1)} = 60nm,\ a_{v(2)} = 15nm,\ \chi_{v(2)} = 90^o$<br>$\eta = 80^o$ , $\phi = 20^o$<br>$\varepsilon^1 = (1,0),\ \varepsilon^0 = (-17.5, 0.7)$ | $\lambda_{g(w)} = 1100nm$<br>$a_{w(1)} = 40nm,\ a_{w(2)} = 10nm,\ \chi_{w(2)} = 90^o$ |

**Table 9.1:** Bi-grating parameters used to calculate the theoretical curves in figure 9.2 and the efficiencies shown in table 9.2.

| Polar angle | Zeroth order efficiencies | | | |
|---|---|---|---|---|
| | $R_{pp}$ | $R_{ps}$ | $R_{ss}$ | $R_{sp}$ |
| 20.0 | 0.25815 | 0.00755 | 0.48130 | 0.00781 |
| 25.0 | 0.54351 | 0.20244 | 0.31669 | 0.26701 |
| 30.0 | 0.45373 | 0.01369 | 0.48317 | 0.01634 |
| 35.0 | 0.48363 | 0.00743 | 0.53367 | 0.00820 |
| 40.0 | 0.44843 | 0.01526 | 0.48748 | 0.01793 |
| 45.0 | 0.54187 | 0.00070 | 0.65807 | 0.00095 |
| 45.0 | 0.56583 | 0.00064 | 0.70252 | 0.00083 |

**Table 9.2:** A selection of zero-order efficiencies calculated using the parameters shown in table 9.1.

The perfectly conducting, symmetric, rectangular form of this crossed grating corresponds to one considered by Granet [1995]: $s(v,w) = \frac{h}{4}\left[\sin\left(\frac{2\pi v}{\lambda_g}\right) + \sin\left(\frac{2\pi w}{\lambda_g}\right)\right]$

with $\frac{\lambda}{\lambda_g} = 0.83$ at normal incidence $(\theta = \phi = 0^{o})$. Either TM or TE polarisation may be chosen as both are equivalent in this symmetric geometry. Table 9.3 shows a comparison between efficiencies calculated by Granet and those from our own code for a number of grating depth to pitch ratios $\frac{h}{\lambda_g}$, where we find near perfect agreement between the output of the two computer codes.

| Grating depth/pitch ratio | M | Efficiencies | | | | | |
|---|---|---|---|---|---|---|---|
| | | -1,0 | | 0,-1 | | 0,0 | |
| | | Granet | The author | Granet | The author | Granet | The author |
| 0.8 | 5 | 0.03533 | 0.03533 | 0.03387 | 0.03387 | 0.86160 | 0.86160 |
| 0.9 | 5 | 0.09789 | 0.09790 | 0.03999 | 0.03999 | 0.72422 | 0.72420 |
| 1.0 | 5 | 0.18330 | 0.18312 | 0.04437 | 0.04412 | 0.54483 | 0.54487 |
| 1.2 | 5 | - | - | - | - | 0.32145 | 0.32144 |
| 1.6 | 5 | - | - | - | - | 0.05719 | 0.05720 |
| 2.0 | 7 | - | - | - | - | 0.03648 | 0.03647 |

**Table 9.3:** Comparison of efficiencies calculated by Granet [1995] and those calculated by the author.

### *9.9.3 Comparison with experimental data*

The surface chosen for this study was composed of two near sinusoids crossed at ~60°. A crossing angle other than 90° was chosen so as to avoid the degeneracy which arises between the two polarisations on a 90° crossed grating surface, and thus provide us with a more general test of our theory. Hence a 60° bi-grating was chosen as this provides us with the interesting case of a reciprocal lattice with near hexagonal symmetry. The bi-gratings were manufactured by spin coating a silica (fused quartz) substrate with 0.2 micron filtered Shipley S1805 photoresist which was then placed in a drying cabinet at 60°C for 30 minutes in order to fully drive any remaining solvent from the resist.

The substrate was then pre-exposed to a diffuse, expanded, collimated beam of 457.9*nm* radiation from an argon ion laser, in order to move the response of the photoresist into the regime where its response to light varies approximately linearly with exposure time. This step is essential as two separate exposures are required to write the bi-grating and the response of the resist to light exposure should remain linear during this process.

A single grating was written into the surface of the photoresist by holographic exposure to the interference fringes generated by two diffuse, expanded, collimated beams of 457.9*nm* radiation. The second corrugation was written for the same exposure time as the first, but after rotating the substrate through 60°. Exposure to light at the blue end of the optical spectrum renders the photoactive compound suspended in the photoresist resin about a thousand times more soluble in a solution of dilute alkali. This variation in solubility is converted into a spatial profile by washing off exposed resist in such a solution. The developed crossed grating was placed in a drying cabinet overnight at a temperature of 60° C, and then coated with an optically thick (~300*nm*) layer of gold by thermal evaporation. For our purposes gold was chosen over silver (which gives a sharper plasmon resonance in the visible region of the electromagnetic spectrum) because of its inert nature which means that the metal's dielectric function will not vary over the timescale of the experiment.

As mentioned previously we aim to expose our photoresist in the regime where its response to light varies approximately linearly with exposure time. In practice we are likely to encounter some non-linearity which gives rise to a grating whose surface cannot be described by the simple sum of two sine series as given in section 9.9.2 Consider the effect of exposing a surface of photoresist, defined to be the *v*,*w* plane, to light of intensity $I = \sum_i A_i \sin\left(iK_{g(v)}v\right) + \sum_j B_j \sin\left(jK_{g(w)}w\right)$. Suppose the response of the resist may be approximated by a polynomial of order n in the intensity *I*. Then the final grating will have a profile $s(v,w) = \sum_n p_n I^n$ - thus the cross scattering terms may be quite strong. This will need to be borne in mind when fitting the theory to data.

The separate angle dependent specular reflectivities of both *p* and *s*-polarised 632.8*nm* electromagnetic radiation were measured from the grating surface. By attaching a polariser to the detector, it is possible to specify the polarisation of the light detected thus allowing us to measure the $R_{pp}$ and $R_{ss}$ reflectivities, where the subscripts refer to the setting of the input and output polarisers in that order. In addition $R_{ps}$ or $R_{sp}$ can be detected, permitting the measurement of the polarisation mixing that occurs when a plasmon resonance is coupled to via one of the gratings that form the surface, if that grating is oriented so that $\phi \neq 0^\circ$ or $90^\circ$. Reflectivity scans were recorded for fixed $\phi$, with $\theta$ being scanned from 10° to 80° in 0.02° steps, for all four observable reflectivities.

A theoretical fit was obtained for the data taken at $\phi = 90^\circ$ so that the surface plasmon resonances associated with the two independent gratings are well separated in excitation angle. Thus a fit over a limited angle range is largely dictated by one of the gratings allowing us to establish it's harmonic content. Likewise a fit over a second angle range, for example 55°-70° in figure (9.3) gives the other grating parameters. Figures (9.3,4) show fits to the $R_{ss}$ and $R_{pp}$ data respectively.

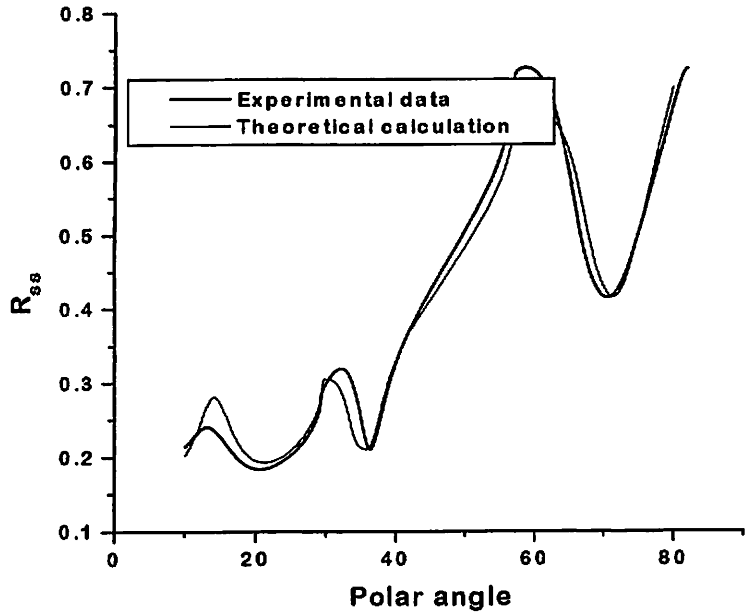

**Figure 9.3:** Fit to experimental data of zero-order efficiencies taken at azimuthal angle $\phi=90^\circ$ from a gold bi-grating of crossing angle 60° $R_{pp}$ polarisation. The parameters used in calculating the theoretical curves are given in table 9.4.

The theoretical calculation used to produce these fits assumes that the bi-grating surface is simply a linear superposition of the two surfaces $s(v,w)=s_1(v)+s_2(w)$ generating reflection coefficients $R_{mn}(s_1(v)+s_2(w))$. These differ from the impulse approximation in that the computation allows sequences of scattering involving both grating components. The parameters used to obtain these fits are given in table 9.3. The agreement with the data is extremely encouraging and could be improved by using fitting routines but this would take considerable computing time. This would not however lead to complete agreement since there are features in the data that can only be effected by the inclusion of additional terms in the surface description.

In general a surface $s(v,w)$ can be expressed in the form $s(v,w)=\sum_m\sum_n s_{mn}\exp i(mK_v v+nK_w w)$. The approximation to the surface used previously includes only components of type $s_{mo}$ and $s_{On}$. However we are aware that the non linearities associated with the process of production of the bi-gratings do yield other components with small but not negligible amplitudes. We are currently investigating ways of modelling the production process to obtain estimates of the size of these contributions to the bi-grating surface. If a satisfactory model can be defined then one can expect that the inclusion of the additional components will lead to a further improvement between theory and experiment.

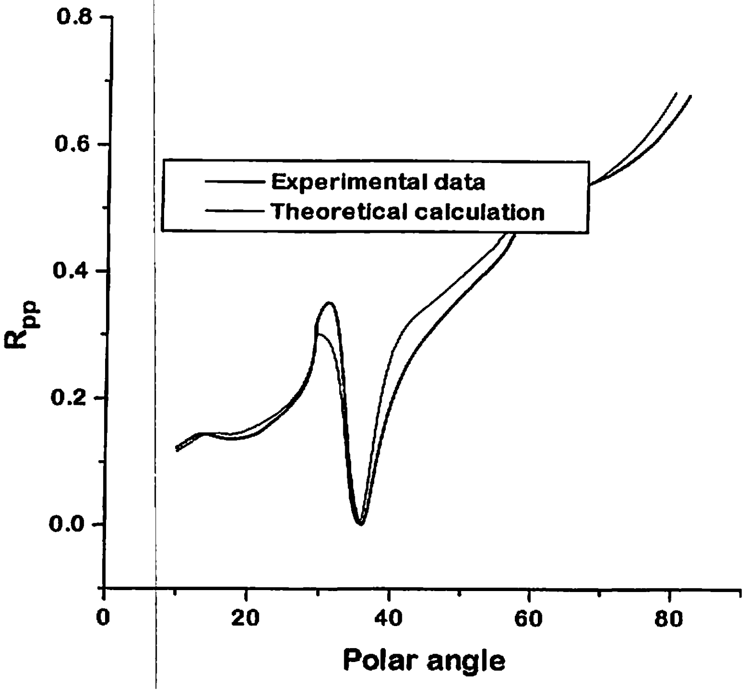

**Figure 9.4:** Fit to experimental data of zero-order efficiencies taken at azimuthal angle ϕ=90° from a gold bi-grating of crossing angle 60° $R_{ss}$ polarisation. The parameters used in calculating the theoretical curves are given in table 9.4.

| $\lambda = 632.8nm$ | |
|---|---|
| $\lambda_{g(v)} = 1166.58nm$<br>$a_{v(1)} = 50nm,\ a_{v(2)} = 10nm,\ \chi_{v(2)} = 90''$<br>$\eta = 60.4''$ , $\phi = 90^\circ$<br>$\varepsilon^1 = (1,0),\ \varepsilon^0 = (-8.2,1.35)$ | $\lambda_{g(w)} = 1166.58nm$<br>$a_{w(1)} = 80nm,\ a_{w(2)} = -10nm,\ \chi_{w(2)} = 90''$ |

**Table 9.4:** Parameters determined in comparing theory to experimental data in figures (9.3,4).

### *9.10 Conclusion*

By developing the formalism of Chandezon I have produced a theoretical framework for modelling bi-grating structures that is conceptually and numerically simple, leading to a computer code that is capable of modelling a wide variety of bi-grating structures. I have shown fits to experimental data and introductory calculations of some interesting doubly-periodic structures. In view of the potential applications of such bi-gratings in improving the efficiency of optical coupling, or in the exploration of photonic surfaces, this approach with its ability to satisfactorily model real systems has much to offer. The reader should of course appreciate that any comparison with real experimental data or attempt to characterise an experimental system by fitting theory to such data involves a vast amount of computation, far in excess of point for point comparisons like table 9.3.

Further work is currently underway to explore surface plasmon band-gaps on bi-gratings as well as deeper zero-order gratings.

In addition, extension of this two dimensional grating surface calculation paves the way for the exploration of the optical response of three dimensional photonic solids. While much has been said of the potential of photonic solids as regards zero threshold lasers, new optical gain media etc., the potential realisation will be more than likely multilayered, or at best relatively thin three dimensional structures, to which the infinite lattice calculations are only approximations. The modelling presented here may obviously be applied to this problem, thus providing a direct route to modelling the optical response of few-layer repeat units of two dimensional photonic surfaces.

At present the computer codes are relatively slow and before implementing a three dimensional calculation it will be necessary to explore avenues for improving computational speed, since at the time, although the principles of the three dimensional calculation are clear, the practical realisation will be considerable except on very high power machines.

# 10. Conclusions

## *10.1 Summary of this thesis*

The work presented in this thesis stems from a desire to model multilayered gratings having sinusoidal like interface profiles. In particular my aim was to model such structures when made with uniaxial materials.

With integral methods the diffracted field is evaluated ultimately by an integral along the grating surface, whereas differential methods expand the field in Bloch waves and thus need to Fourier analyse the grating surface. As a consequence integral methods are best suited to square type gratings where the necessary surface integral is much simplified. Conversely differential methods lend themselves to sinusoidal type gratings which when Fourier analysed produce no high order harmonics and only a small number of Bloch waves need be considered. Given this, the differential method of Chandezon was chosen as a suitable formalism on which to base this work. Despite being both conceptually simple and easy to implement as a computer code, the method is rigorous for all but the most extreme grating geometries, while retaining fast computation times.

Chapter 2 provides a detailed look at the method as it was first described by J. Chandezon *et. al.* In their 1982 paper - formulated to model a singly - periodic, bare grating, illuminated so that the plane of incidence contains the grating vector.

Chapter 3 uses Chandezon's method to look at electromagnetic field amplitudes as a function of position. In particular it is shown that, for deep gratings, the structure of the near field can be used to explain some interesting reflectivity features.

From here on the remaining chapters progressively generalise Chandezon's theory to more and more complex grating structures. Chapter 4 introduces multilayer gratings, while chapter 5 generalises the problem to the conical mount and shows fits to experimental data.

Chapter 6 considers a 'Rayleigh limited' approach for modelling multilayered gratings having interfaces of different profile, but sharing the same periodicity. While this method suffers convergence problems for adjacent interfaces with significantly different profiles, it is nonetheless able to model most experimental cell geometries involving layers bounded on one side by a shallow grating, and on the other by a planar surface.

Chapter 7 introduces uniaxial layers, while chapter 8 brings together all the features described so far, characterising two grating - coupled liquid crystal cells with excellent results.

Finally chapter 9 extends the isotropic analysis to doubly - periodic structures, showing some pleasing comparisons with experimental data.

### *10.2 Future work*

There are many areas of work, both in the fields of 1 dimensional and 2 dimensional surface relief - gratings, that the Chandezon technique could be usefully applied to.

For 1 dimensional gratings, chapter 3 showed how the spatial distribution of field vectors near to a bare grating surface can give valuable insight into the behaviour of the far field and hence the reflectivity characteristics of that grating. It would be interesting to look at multilayered gratings, containing both isotropic and anisotropic overlayers investigating field amplitudes within them.

Another potentially rewarding area is the study of photonic solids using the Chandezon technique. Clearly the analysis presented in chapter 6, is inadequate for this task because of it's inability to deal with substantially different adjacent interface profiles. An alternative approach in the light of work by Granet *et. al.* [1995] could facilitate the modelling of these structures in two dimensions. While much has been said of the potential of photonic solids as regards zero threshold lasers, new optical gain media etc., the potential realisation will be more than likely multilayered, or at best relatively thin three dimensional structures, to which the infinite lattice calculations are only approximations. The modelling presented in chapter 9 could obviously be applied to this problem, thus providing a direct route to modelling the optical response of few-layer repeat units of two dimensional photonic surfaces.

Also much is left to be done in the area of anisotropic materials. The work of chapter 7 has yet to be generalised to doubly - periodic gratings, and there is plenty of scope for investigating liquid crystal alignment near periodic surfaces via the techniques applied in chapter 8.

Finally in light of recent experimental work an interesting variation on the usual grating geometries considered is the inclusion of layers of dye molecules. When stimulated to fluoresce these add a new source of radiation with potentially interesting implications for the optical response of such structures, which have yet to be modelled theoretically.

## *10.3 Publications*

- *A differential formalism for multilayer diffraction gratings made with uniaxial materials*

  J. B. Harris, T. W. Preist, and J. R. Sambles

  Journal of the optical society of America A. **12**, 1965-1973, (1995).

- *Conical diffraction from multicoated gratings containing uniaxial materials*

  J. B. Harris, T. W. Preist, E. L. Wood, and J. R. Sambles

  Journal of the optical society of America A. **13**, 803-810, (1995).

- *Characterisation of a grating - coupled liquid crystal cell using a rigorous theoretical model*

  J. B. Harris, E. L. Wood, T. W. Preist, and J. R. Sambles

  Journal of modern optics **12**, 1965-1973, (1995).

- *The optical response of bi - gratings*

  J. B. Harris, T. W. Preist, J. R. Sambles, R. N. Thorpe, and R. A. Watts

  Journal of the optical society of America A. **13**, (to be published 1995).

- *Differential formalism for predicting the electromagnetic response of textured surfaces from visible to millimetre wavelengths*

  C. R. Lawrence, J. B. Harris, R. A. Watts, T. W. Preist, S. G. Appleton, and J. R. Sambles

  Digest of the 20th international conference on infrared and millimetre waves 499-500, (Dec. 1995).

- *Optical excitation of surface plasmon - polaritons on $90^o$ and $60^o$ bi - gratings*
  R. A. Watts, J. B. Harris, A. P. Hibbins, T. W. Preist, and J. R. Sambles
  Journal of the optical society of America A. (To be published).

- *An experimental test of conical diffraction theory*
  R. A. Watts, J. R. Sambles, and J. B. Harris
  (To be published).

## Appendix: computer code flow diagrams

Before any application can be coded it is necessary to identify major areas of common functionality or modules. For the general multilayer Chandezon problem these are:

1. Calculate eigenvalues and vectors for each medium
2. Using these to generate the full scattering matrix
3. Use plane wave expansions in the input medium to generate $\mathbf{L}$ and $\hat{\mathbf{M}}$ (chapter 2)
4. Evaluate $\mathbf{R}$ and hence the reflected efficiencies from equation 5.31

Certain data structures are shared by all of these modules, such as the Bragg momenta $\alpha$, $\beta$, and $\gamma$. For each of these structures a new module should be created, since they need only be determined once, after which they can be passed to the various other modules that require them.

By identifying these common structures, we arrive at the schematic representation of figure A.1 which shows all the major steps in the numerical solution of the general uniaxial problem exemplified in chapter 8. It is assumed that we want to calculate the reflective efficiency as a function of the incident wavelength $\lambda$ and orientational angles $\theta$ and $\phi$.

Enquiries regarding the codes used in this thesis should be addressed to:

Professor J. R. Sambles
Thin Film Photonics Group
Department of Physics
University of Exeter
Stocker Road
Exeter. EX4 4QL

```
Start wavelength ($\lambda$) loop ------------------------------------------------------------>
Fourier analyse surface functions $C$, $D$, and those $X_i$ which do not depend on $\phi$

Start azimuthal angle ($\phi$) loop ---------------------------------------------------------->
Start polar angle ($\theta$) loop ----------------------------------------------------- ------>
Fourier analyse angle dependent surface functions $X_i$
Define Bragg momenta $\alpha$, $\beta$, and $\gamma$

Start layer loop ----------------------------------------------------------------------------->
        Calculate eigenvalues & vectors
<-------------------------------------------------------------------------------close layer loop
Make scattering matrix

Start polarisation loop (TM or TE)----------- -------------------------------------->
        Use plane wave expansions in the input medium to generate L and $\hat{M}$
        Evaluate R from equation 5.31
        Calculate efficiencies
<-----------------------------------------------------------------------close polarisation loop

Write efficiencies for both polarisations to screen

<--------------------------------------------------------------- close polar angle ($\theta$) loop
<---------------------------------------------------------- close azimuthal angle ($\phi$) loop
<-------------------------------------------------------- close wavelength angle ($\lambda$) loop
```

**Figure A.1:** Flow diagram for the numerical solution of the multilayer uniaxial problem

# REFERENCES

| | | |
|---|---|---|
| Azzam, R. M. A., and Bashara, N. M. | 1979 | *Ellipsometry and Polarised Light* (North Holland, Amsterdam) |
| Berreman, D. W. | 1972 | Phys. Rev. Lett. **28**, 1683-1686 |
| Bryan-Brown, G. P., Elston, S. J., and Sambles, J. R. | 1991 | J. Mod. Opt. **38**, 1181-1187 |
| Bryan-Brown, G. P., Elston, S. J., and Sambles, J. R. | 1991 | SPIE **1545**, 167-178 |
| Born, M. And Wolf, E. | 1975 | *Priciples of Optics* (Pergamon Press) |
| Chandezon, J., Dupuis, M. T., Cornet, G., and Maystre, D. | 1982 | J. Opt. Soc. Am. A. **72**, 839-846 |
| Cotter, N. P. K., Preist, T. W. P., and Sambles, J. R. | 1995 | J. Opt. Soc. Am. A. **12**, 1097-1103 |
| De Gennes, P. G., and Prost, J. | 1993 | *The physics of liquid crystals* (Clarendon press, Oxford) |
| Derrick, G. H., McPhedran, R. C., Maystre, D., and Nevière, M. | 1979 | Appl. Phys. **18**, 39-52 |
| Derrick, G. H., and McPhedran, R. C., | 1984 | J. Opt. Paris. **15**, 69-81 |
| Elston, S. J., and Sambles, J. R. | 1989 | Appl. Phys. Lett. **55**, 1621-1623 |

| | | |
|---|---|---|
| Elston, S. J., and Sambles, J. R. | 1991 | Mol. Liq. Cryst. **200**, 167-186 |
| Glass, N. E., Maradudin, A. A., and Celli, V. | 1983 | J. Opt. Soc. Am. **73**, 1240-1248 |
| Granet, G. | 1995 | Pure Appl. Opt. **4**, 777-793 |
| Greffet, J., Baylard, C., and Versaevel, P. | 1992 | Optics Letters **17**, 1740-1742 |
| Inchaussandague, M. E., and Depine, R. A. | 1994 | J. Opt. Soc. Am. A. **12**, 1261-1270 |
| Inchaussandague, M. E., and Depine, R. A. | 1996 | To be published |
| Jory, M. J., Bradberry, G. W., Cann, P. S., and Sambles, J. R. | 1995 | J. Phys. E: Meas. Sci. Technol. **6**, 1193-1200 |
| Kawatsuki, N., and Uetsuki, M. | 1990 | Jap. J. Appl. Phys. **29**, 2420-2423 |
| Ko, D. Y. K., and Sambles, J. R. | 1988 | J. Opt. Soc. Am. A. **5**, 1863-1866 |
| Laks, B., Mills, D. L., and Maradudin, A. A. | 1981 | Phys. Rev. B **23**, 4965-4976 |
| Li, L. | 1994 | J. Opt. Soc. Am. A. **11**, 2816-2828 |
| Maystre, D. | 1984 | chap1, 'Rigorous vector theories of diffraction gratings', in E.Wolf, Progress in optics XXI (Elsevier) |
| Moaveni, M. K., Kalhor, H. A., and Afrashteh, A. | 1975 | Comput. Elect. Eng. **2**, 265-271 |

| | | |
|---|---|---|
| Nevière, M., Cerutti-Maori, G., and Cadilhac, M. | 1971 | Opt. Commun. **3**, 48 |
| Nevière, M., Cadilhac, M., and Petit, R. | 1973 | IEEE Trans. AP-**21**, 37 |
| Petit, R. | 1966 | Rev. Opt. **8**, 353-370 |
| Petit, R. | 1972 | *The electromagnetic theory of gratings*<br>(Springer Verlag, Berlin) |
| Petit, R., and Cadilhac, M. | 1964 | C. R. Acad. Sci. Paris **259**, 2077 |
| Petit, R., and Cadilhac, M. | 1966 | C. R. Acad. Sci. AB **262**, 468 |
| Popov, E., Tsonev, L., and Maystre, D. | 1989 | J. Mod. Opt. **37**, 379-387 |
| Popov, E., and Mashev, L. | 1986 | J. Opt. Paris **17**, 175-180 |
| Popov, E., Tsonev, L., and Maystre, D. | 1994 | J. Appl. Opt. **33**, 5214-5219 |
| Preist, T. W., Cotter, N. P. K., and Sambles, J. R. | 1995 | J. Opt. Soc. Am. A. **12**, 1740-1748 |
| Raether, H. | 1988 | *Surface Plasmons*<br>(Springer-Verlag, Berlin) |
| Rayleigh, Lord | 1907 | Proc. Roy. Soc. **A79**, 399 |
| Wood, E. L., Sambles, J. R., Cotter, N. P., and Kitson, S. C. | 1994 | J. Mod. Opt. **42**, 1343-1349 |

Yang, F., and Sambles, J. R. 1993 J. Opt. Soc. Am. B. **10**, 858-866